Computer aided development and optimization of chromatographic separations

Frederiksen, Søren Søndergaard

Publication date:
2004

Document Version
Publisher's PDF, also known as Version of record

Computer Aided Development and Optimization of Chromatographic Separations

by

Søren Søndergaard Frederiksen

Ph.D. Thesis

IVC-SEP, Department of Chemical Engineering, Technical University of Denmark

Preface

This thesis is submitted in partial fulfilment of the requirements for admission to the candidacy for the degree of philosophy, Ph.D., at the Technical University of Denmark.

The project, funded by DTU, has been carried out from March 2001 to February 2004 at the Center for Phase Equilibria and Separation Processes – IVC-SEP, at the Technical University of Denmark, DTU.

I would like to thank my two supervisors at DTU Michael L. Michelsen who has been very helpful when I ran into mathematical problems or problems with Fortran programming and my main supervisor Jørgen M. Mollerup who has been very helpful and with whom I have had many fruitful discussions. I have found it very inspiring to work with both in the past three years.

Further more I would like to thank Klaus Wekenborg, Prof. Henne Schmidt-Traub, and the group “Lehrstuhl für Anlagentechnik” from Universität Dortmund, where I worked six months with SMB chromatography. They all contributed to a good atmosphere and I felt very welcome. I really enjoyed my stay.

Lyngby, February 2004

Søren Søndergaard Frederiksen

Abstract

The thesis deals with the chromatographic separation of proteins by ion exchange. Ion exchange chromatography has for many years been used for separation of proteins. The development of the chromatographic separation, however, is often done by systematic experiments and statistical methods. During the development phase modelling can be used as a valuable tool, both for process optimization and to get a better understanding of the process. Modelling has previously been used extensively for chromatography of smaller molecules. Proteins are, however, large molecules, which must be accounted for in the model.

For modelling to be a valuable tool, close interaction between interpretation of laboratory results and modelling is required. Therefore emphasis has been put on comparing experimental results with results from modelling and discussion of the results.

Whey proteins have been used as model system. The used whey proteins are Bovine Serum Albumin (BSA), α-lactalbumin, and β-lactoglobulin A and B. A few experiments are using aprotinin and the amino acid tyrosine. All experiments are performed using the strong anion exchangers: Source 30 Q, Q Sepharose XL, Ceramic Q-HyperD F and Fractogel EMD TMAE 650(S).

The Steric Mass Action formalism (SMA-formalism) is used to describe the equilibrium. This isotherm is capable of taking the influence of salt into account. Two modifications of the SMA-formalism has been suggested: One modification which is able to handle negative protein concentrations and a method for solving small system of equations, e.g. the Craig model.

It is shown that both axial dispersion and mass transfer resistance needs to be taken into account to describe experimental results. A model has been suggested, which takes mass transfer resistance in the film layer around the particles, in the pores, and surface diffusion inside the particles into account. Both a model with diffusion inside the particles, and a linear driving force approximation for the particle side mass transfer has been derived.

To avoid a double boundary value problem adding the axial dispersion with the mass transfer coefficient for the film layer has been suggested. Alternatively a double boundary value problem can be avoided by using open boundary condition at the column exit, this model has also been used. The models have been solved using orthogonal collocation on finite elements (OCFE), which allows a fast solution of the equations. The suggested method has been compared with the solution using global orthogonal collocation.

The mass transfer coefficient for the film layer has been determined from a correlation. Correlations for the film layer mass transfer coefficients in packed columns at low Reynolds numbers are compared.

Equilibrium and mass transfer coefficient inside the particles for a number of proteins and anion exchangers have been determined. It is also demonstrated how the equilibrium parameters can be used to determine the gradient elution volume.

A detailed example using theory and experimental results to determine equilibrium and mass transfer parameters are given for the system α-Lactalbumin and Q Sepharose XL. The example also compares modelled and experimental data.

Methods to determine the non-linear part of the isotherm has been evaluated. These are batch experiments and breakthrough experiments. The batch experiments turned out to be sensitive to impurities in the protein solutions. Additionally the resin gradually lost its capacity when reusing the resin from one batch experiments to the following. Breakthrough experiments are evaluated, too, and have been used to determine the isotherms for BSA and β-Lactoglobulin A and B with Source 30Q. Both successful and less successful experiments are presented, since this forms the basis of discussion for interpretation of the results.

Due to the large amount of experimental data, a prototype of a program has been made. The program fits the experimental chromatograms, and stores these in a number of databases. Hereafter desired data can be retrieved from the databases and parameters can be fitted from these. The program is also able to simulate experiments and compare modelled and experimental data.

The last part of the thesis deals with the separation of β-lactoglobulin A and B by Simulated Moving Bed chromatography (SMB-chromatography). SMB-chromatography is a continuous countercurrent process. The anion exchanger used is Source 30Q.

The first part of the thesis mainly describes modelling and experiments in the linear part of the isotherm. In a SMB-plant protein concentration is normally not in the linear part of the isotherm and it is necessary to take the non-linear part of the isotherm into account. In the SMB-chapter the simultaneous use of theory and experimental work is emphasised, too. The equilibrium parameters for β-Lactoglobulin A and B are determined from pulse experiments and from breakthrough experiments on a single column. This forms the basis for a simulation of a gradient experiment in the SMB-process. An excellent agreement between simulated and experimental results from a gradient experiment has been found.

A difficult method to determine the area of complete separation for components with non-constant selectivity has previously been suggested. An alternative and easier method to calculate this is suggested.

Resumé

Afhandlingen omhandler kromatografisk oprensningning af proteiner vha. ionbytningskromatografi. Ionbytningskromatografi har i mange år været anvendt til oprensning af proteiner men udviklingen af den kromatografiske oprensing foregår i høj grad ved faktorforsøg. Modellering kan her være et vigtigt værktøj under udviklingsprocessen, både til procesoptimering samt til at at få en bedre forståelse af processen.
Meget modellering er lavet på kromatografi af mindre molekyler: Proteiner er dog store molekyler, hvilket er nødvendigt at tage højde for ved modellering.
Modellering kan dog ikke stå alene i en udviklingsproces, men må være tæt knyttet til observationer fra laboratoriet. Der er derfor lagt vægt på at sammenholde resultater fra modellering og fra laboratoriet og diskutere, hvorledes disse behandles.
Som model er anvendt valleproteinerne bovin serum albumin (BSA), α-lactalbumin samt β-lactoglobulin A og B. Ud over disse er enkelte forsøg lavet med aprotinin og med aminosyren tyrosin. Alle forsøg er foretaget på stærke anionbyttere disse er Source 30 Q, Q Sepharose XL, Ceramic Q-HyperD F og Fractogel EMD TMAE 650(S).
Til beskrivelse af ligevægten er anvendt massevirkningsloven, da denne er i stand til at tage højde for saltets indflydelse på isothermen. To modifikationer af massevirkningsloven er foreslået til løsning af denne: En til løsning af negative proteinkoncentration samt en for små ligningssystemer, der opnås ved anvendelse af f.eks. en Craig Model.
Det er vist, at det er nødvendigt at tage højde for både aksial dispersion og stoftransportmodstand for at beskrive de i laboratoriet observerede resultater.
En model er opstillet, der tager højde for stoftransportmodstand i filmlaget omkring partiklen samt ved pore og overfladediffusion i partiklen. Modeller er opstillet både for diffusion i partiklen og for en lineær drivende kraft i partiklen.
For at undgå et dobbelt randværdiproblem addition af den aksiale dispersion og modstanden mod stoftransport i filmlaget er foreslået. Alternativt kan et dobbelt randværdiproblem også undgås ved anvendelse af åbne randbetingelser, hvilket også er anvendt. En formulering af problemet, der bruger orthogonal kollokation på endelige elementer og tillader en hurtig løsning af lignigssystemet er foreslået. Denne løsning er sammenlignet med løsningen fra global orthogonal kollokation.
Korrelationer for stoftransport i pakkede kolonner for lave Reynolds tal er sammenlignet.
Ligevægtene og stoftransporten i partiklerne for en række kombinationer af protein og

anionbyttere er bestemt. Anvendelsen af ligevægtsparametrene til bestemmelse af elueringsvolumenet ved gradienteluering er vist.

Et detaljeret eksemple med anvendelse af teori og eksperimentelle resultater til bestemmelse af ligevægts- og stofovergangsparametre er givet for systemet α-Lactalbumin og Q Sepharose XL. Eksemplet giver også, en sammenligning mellem modellerede og eksperimentelle data, og fordelen af modellering ses.

Metoder til bestemmelse af den ikke lineære del af isotermen er evalueret for både batch forsøg og gennembrudsforsøg. Batchforsøgene har vist sig at være meget påvirkelige af urenheder i proteinerne. Endvidere har genbrug af resin ved batchforsøg vist sig at ødelægge resinen. Gennembrudsforsøg er også evalueret og disse er brugt til at bestemme isotermer for BSA og β-Lactoglobuling A og B på Source 30Q. Både succesfulde og mindre succesfulde eksperimenter er præsenteret, da disse danner en basis for diskussion af resultaterne.

Da datamaterialet hurtigt bliver meget stort, er lavet et prototype på et program. Programmet muliggører at fitte chromatogrammer, gemme disse i databaser. Herefter kan ønskede data findes og modelparametre kan bestemmes herudfra. Programmet giver også mulighed for at simulere forsøgene og sammenligene modellerede og eksperimentelle data.

Afhandlingens sidste del omhandler separation af β-lactoglobulin A og B vha. Simulated Moving Bed kromatografi (SMB-kromatografi). SMB-kromatografi er en kontinuerlig modstrømsproces, til separation af f.eks. proteiner. Som ionbytter er anvendt Source 30Q. Hvor afhandlingens tidligere arbejde i høj grad beskriver isothermens lineære del, er proteinkoncentrationen i et SMB-anlæg ofte i den ikke lineære del af isotermen og det er derfor nødvendigt også at tage den ikke lineære del af isotermen i betragtning. Også i SMB-afsnittet er der lagt vægt på anvendelse af teori og eksperimentelt arbejde i et tæt samspil. Til modellering af forsøgene er ligevægtsparametrene for β-Lactoglobulin A og B bestemt ud fra pulsforsøg og gennembrudsforsøg på en enkelt kolonne. Dette danner baggrunden for en simulering af et gradientforsøg i et SMB-anlæg. En god overensstemmelse mellem simulerede og eksperimentelle resultater fra gradientforsøg er fundet.

Til at bestemme området for fuldstændig seperation for isotermer med en ikke konstant selektivitet er tidligere anvendt en vanskelig numerisk metode. En alternativ og lettere metode til bestemmelse af dette område er forslået.

Table of Contents

Notation

All units refer to the units used as standard units in the program.

	page	unit	
A	24	[ ]	A=Q/C
A_{col}	2	[m^2]	Column cross section area, $A_{col}=\pi/4\cdot d_{col}^2$
a_p	16	[m^{-1}]	Specific area of the particle (for spheres $a_p=6/d_p$)
B	71	[m^3]	$B=V_{col}(1-\varepsilon)\varepsilon_p\cdot K_D\cdot K_{eq}\cdot$
Bi	19	[ ]	Biot number, $Bi=R\cdot k_f/D$
C	3	[mole/m^3]	Concentration, alternative unit [kg/m^3]
d_{col}	2	[m]	Column diameter
d_p	2	[m]	Particle diameter
C_{D0}	40	[ ]	Drag coefficient
D	4	[m^2/s]	Diffusion coefficient
D_m	4	[m^2/s]	Diffusion coefficient in mobile phase
DV	6	[m^3]	Dead volume
E	40	[m^2/s^3]	Energy dissipation rate per unit mass of fluid
E_D	16	[m^2/s]	Eddy diffusion coefficient
G	71	[mole/m^6]	Gradient slop
h	26	[ ]	Reduced plate height
K	45	[ ]	Selectivity
K_{ads}	18	[ ]	Adsorption rate
K_D	3	[ ]	Steric exclusion factor
K_{eq}	9	[ ]	Equilibrium constant
k_f	16	[m/s]	Film layer mass transfer coefficient. The surface refers to the entire particle surface area.
L	2	[m]	Column length
m	43	[kg]	Mass
m	121	[ ]	Dimensionless flow rate in SMB plant
M	56	[ ]	Moment of a peak
MW	4	[kg/mole]	Molecular weight
Pe_d	22	[ ]	Peclet number made dimensionless with the particle diameter
Pe_L	16	[ ]	Peclet number made dimensionless with the column length

q	9	[ ]	Dimensionless concentration of bound protein
Q	2	[m^3/s]	Volumetric flow rate
Q	3	[$mole/m^3$]	Concentration of bound component, the volume is referring to the pore phase, alternative unit [kg/m^3]
Q_r	121	[m^3/s]	Resin flow rate in SMB-plant
r	18	[m]	Radial position in particle
R	9	[J/mole K]	Gas constant, R=8.314472(15) J/mole K
R_p	18	[m]	Particle radius
Re	27	[ ]	Reynolds number based on superficial velocity
S_k	120	[ ]	Split outlet section k
Sc	27	[ ]	Schmidt number
Sh	27	[ ]	Sherwood number
St_f	16	[ ]	Stanton number for the film layer
St_p	21	[ ]	Stanton number for mass transport in the pore phase
St_q	21	[ ]	Stanton number for surface diffusion mass transport
t	16	[s]	Time
T	4	[K]	Temperature
u	18	[ ]	Dimensionless position in particle
v	28	[m^3/kg]	Specific volume (appendix p. 28)
v_i	2	[m/s]	Interstitial velocity (velocity between the particles)
v_r	121	[m/s]	Resin velocity
v_s	2	[m/s]	Superficial velocity (based on empty column)
V	43	[m^3]	Volume
V_{col}	43	[m^3]	Column volume
V_m	71	[m^3]	Volume the gradient travels before it reach the detector
V_{MC}	71	[m^3]	Volume from mixer to column inlet
V_t	71	[m^3]	Total liquid volume in the column, $V_t=V_{col}[\varepsilon+(1-\varepsilon)\varepsilon_p]$
x	16	[ ]	Dimensionless axial position
x	102	[ ]	Fraction
$x_{p,0}$	71	[ ]	Dimensionless axial position of the protein
y	9	[ ]	Dimensionless concentration
z	8	[ ]	Binding charge

z	16	[m]	Axial position

Greek

α	128	[ ]	Fraction of feed from the previous column
ε	2	[ ]	Interstitial porosity
ε_p	3	[ ]	Particle porosity
ε_t	3	[ ]	Total porosity, $\varepsilon_t=\varepsilon+(1-\varepsilon)\varepsilon_p$
ϕ	3	[ ]	Overall phase ratio, $\phi=(1-\varepsilon)/\varepsilon$
γ	121	[ ]	Dimensionless flow in SMB plant
η	4	[Pa·s]	Dynamic viscosity
λ	6	[mole]	Total number of binding charges in the column
ν	9	[ ]	Dimensionless binding charge
ν	38	[ ]	Reduced velocity
ψ	3	[ ]	Phase ratio for protein, $\psi=(1-\varepsilon)/\varepsilon\cdot\varepsilon_p K_d$
ρ	43	[kg/m^3]	Density
σ	9	[ ]	Dimensionless shielding parameter
τ	16	[ ]	Dimensionless time, $\tau=tv_i/L$, (SMB $\tau=t\cdot v_r/L$, p. 121)
ζ	9	[ ]	Shielding parameter
Λ	8	[M]	Concentration of binding charge of the ion exchanger
Θ	19	[ ]	Fraction of particle volume used for surface mass balance

Index

0	Salt
an	Anion
avg	Average
cat	Cation
in	Inlet
init	Initial condition
f	Feed
m	Mobile phase
min	Minimum

max	Maximum
NA	Non-Adsorbed
out	Outlet
p	Pore phase
p	Protein
p	Product
q	Bound protein
R	Retention (retention volume or time)
s	Surface
sft	Shifting period in SMB plant
SMB	Simulated moving bed
TCC	True counter current
'	Modified value
'	Normal moment

1. Introduction

The chapter gives a very short introduction to chromatography, where a number of model parameters are defined, and gives also a short description of the chosen model with some of the considerations built into this model. Hereafter follows the properties of the proteins and salts and finally the properties of the columns.

1.1 Basic Set-up

A basic chromatographic set-up consists of a vessel containing the buffer, a pump, an injection loop, and the chromatographic column. A UV-detector connected to a computer is located at the outlet of the column, figure 1.1.

In a chromatographic run the column is first equilibrated. After the equilibration the protein mixture is introduced into the injection loop. Buffer solution is pumped through the injection loop and the protein mixture is washed out of the injection loop and into the column.

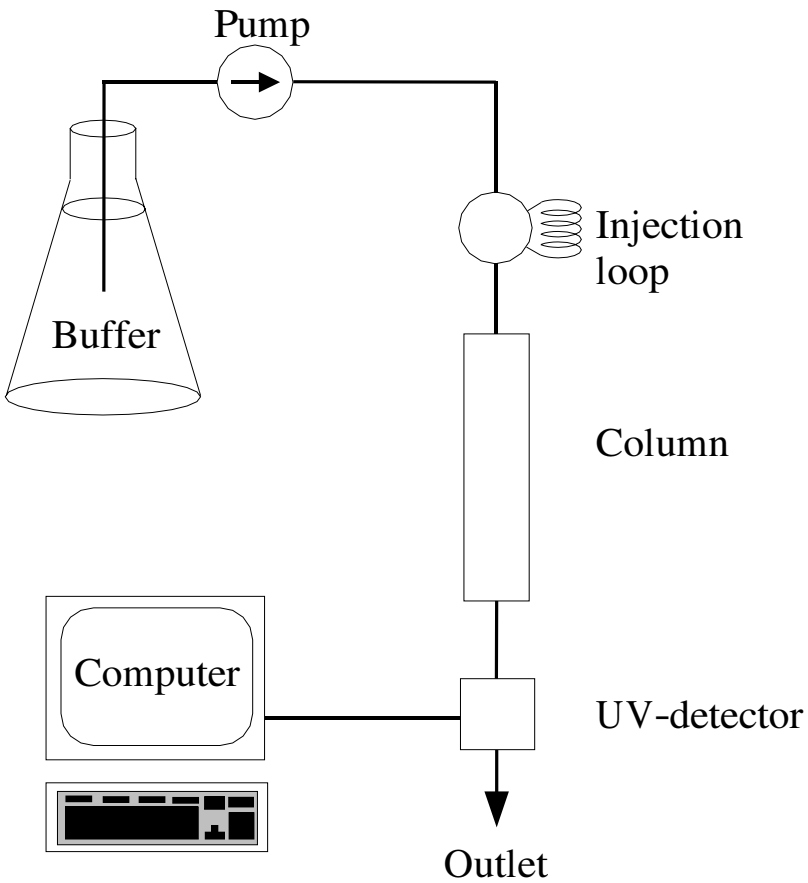

Figure 1.1 Basic chromatographic set-up.

Depending on how strong the proteins bind to the material inside the column, the proteins will elute at different times. The proteins have UV-absorbance and the protein peaks can be detected with the UV-detector at the column outlet.

The chromatographic column is packed with porous particles, a schematic drawing is given in figure 1.2.

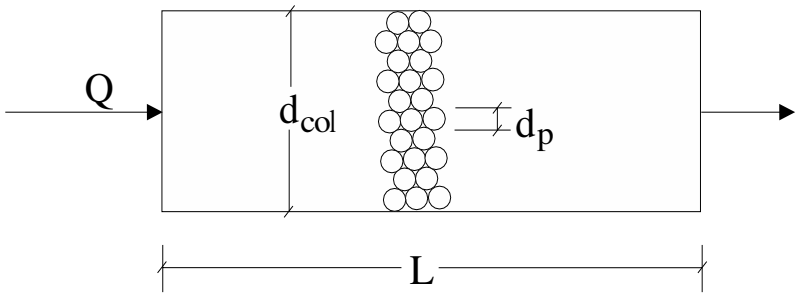

Figure 1.2 Schematic illustration of a packed column. L Column length, d_{col} column diameter d_p particle diameter, and Q volumetric flow rate.

The superficial velocity, v_s, is the velocity based on the empty column

$$v_s = \frac{Q}{A_{col}} \tag{1-1}$$

where Q is the inlet flow and A_{col} is the cross section area of the column.

The interstitial velocity, v_i, is the velocity in the packed column

$$v_i = \frac{Q}{\epsilon A_{col}} = \frac{v_s}{\epsilon} \tag{1-2}$$

Where ε is the interstitial porosity.

In the most basic form the column consists of two phases, one liquid phase and a phase where the components are bound. This is very common for chromatographic models, however, a large variation is seen in how these phases are described in the models. With the model suggested here the packed column is divided into five different sections given in the table 1.1, and shown in figure 1.3.

The total porosity of the particles is ε_p and the pores are divided into pores sufficiently large for the protein to enter and pores too small for the proteins to enter. The fraction of the pores which are sufficiently large for the proteins to enter is K_D. This distinction allows the modelling of size exclusion chromatography of proteins of various sizes.

The overall phase ratio is defined as the ratio between the particle volume and the mobile phase volume

$$\phi = \frac{1-\epsilon}{\epsilon} \tag{1-3}$$

The protein concentration in the resin refers to the available pore phase. Since proteins are large molecules, only a fraction of the pores are available for a protein to enter. This gives the phase ratio of the accessible pores for the proteins

$$\psi = \frac{1-\epsilon}{\epsilon}\epsilon_p K_D \tag{1-4}$$

The total porosity of a column is the interstitial porosity and the particle porosities, from table 1.1 is seen that this is equivalent to

$$\epsilon_t = \epsilon + (1-\epsilon)\epsilon_p \tag{1-5}$$

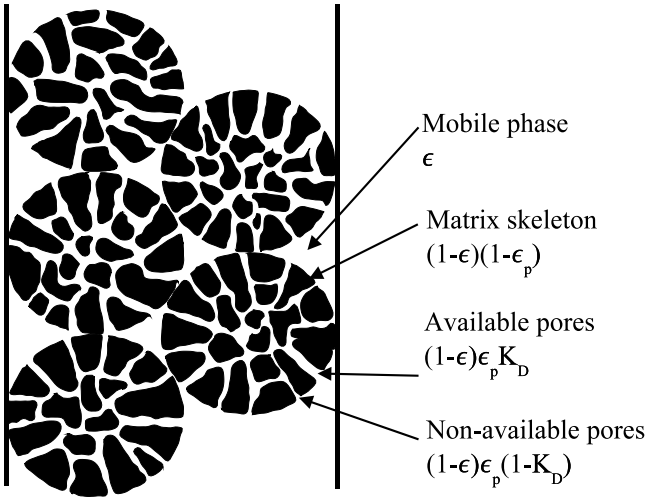

Figure 1.3 Column packing and column fractions.

Phase	***Fraction***	***Concentration***
Mobile	ϵ	C
Available pores	$(1-\epsilon)\epsilon_p \cdot K_D$	C_p, Q_p
Non-available pores	$(1-\epsilon)\epsilon_p(1-K_D)$	0
Matrix	$(1-\epsilon)(1-\epsilon_p)$	0
Particle surface	0	C_s, Q_s

Table 1.1 The different phases in the column with the volume fraction of the sections and the concentrations in the corresponding sections.

1.2 Component Properties

Proteins can contain a number of surface charges. The point where the net charge of the protein is zero is known as the isoelectric point. When the pH moves away from the isoelectric point, the absolute value of the charge increases.

Mass transfer parameters are to a large extent based on the size of the molecules and the diffusion coefficients.

Tables containing these data can be found in literature. Two large tables containing molecular weights and isoelectric points are given by Righetti *et al.* (1976) and Righetti *et al.* (1981). The molecular weights are also given by Sober (1968) together with the diffusion coefficients. For globular proteins the protein diffusion coefficient can be estimated from the correlation suggested by Young *et al.* (1980)

$$\frac{D_m \eta}{T} = 8.34 \cdot 10^{-16} \cdot MW^{-1/3} \tag{1-6}$$

Where D_m is the diffusion coefficient in m^2/s for the protein, η is the viscosity of the liquid in Pa·s, T is the temperature in K and MW is the molecular weight in kg/mole. For pure water at 20°C the viscosity is $\eta = 1.002 \cdot 10^{-3}$ Pa·s. This correlation together with tabulated values for the proteins from table 1.2 are plotted in figure 1.4 below[1].

Component	*MW* [kg/mole]	*pI*	D_m [m^2/s]	*Reference*
β-Lactoglobulin A	18.3	5.13	$73.4 \cdot 10^{-12}$	Sober (1968) p. C-14, Righetti *et al.* (1976), p. 15
β-Lactoglobulin B	18.3	5.23	$73.4 \cdot 10^{-12}$	Sober (1968) p. C-14, Righetti *et al.* (1976), p. 15
Bovine Serum Albumin	65.4	4.8	$61.5 \cdot 10^{-12}$	Sober (1968) p. C-16, Molekylærbiologisk Institut (2001), p. 24
α-Lactalbumin	14.15	4.4	$106 \cdot 10^{-12}$	Molekylærbiologisk Institut (2001) p. 24
Tyrosine	0.181	5.66	10^{-9}	Hansen (2000) paper 2 p. 17
Aprotinin	6.5	10.5	$130 \cdot 10^{-12}$	Roche (2003), Hansen (2000) paper 2 p. 17

Table 1.2 Properties of the proteins in the database.

1 The diffusion coefficients for β-Lactoglobulin A and B are probably for the dimer, Yamamoto (1988) p. 360.

The diffusion coefficient of a salt can be calculated from the diffusion coefficients of the individual ions, Lide (1998) p. 5-95.

$$D_{salt} = \frac{\left(z_{cat} + |z_{an}|\right) D_{an} D_{cat}}{z_{cat} D_{cat} + |z_{an}| D_{an}} \tag{1-7}$$

Beside the proteins and salt also a buffer is used. For all the experiments bis-tris propane is used as buffer[2].

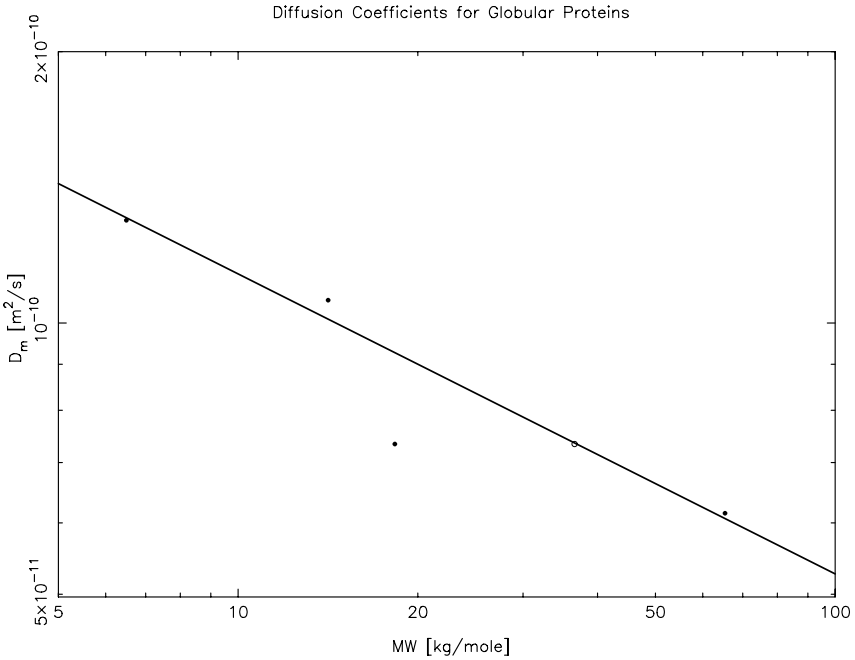

Figure 1.4 Tabulated diffusion coefficients and diffusion coefficients calculated at 20°C from the correlation suggested by Young (1980). The diffusion for β-Lactoglobulin A and B as a dimer is inserted as and open circle.

Salt	***MW*** [g/mole]	z_{an}	z_{cat}	D_{an} [m²/s]	D_{cat} [m²/s]	***Reference***
NaCl	58.4	-1	1	$2.032 \cdot 10^{-9}$	$1.334 \cdot 10^{-9}$	Lide (1998) p. 5-95
KNO_3	101.1	-1	1	$1.957 \cdot 10^{-9}$	$1.902 \cdot 10^{-9}$	Lide (1998) p. 5-95

Table 1.3 Component properties of the salts.

2 1,3-bis[tris(hydroxymethyl)-methylamino]propane, $C_{11}H_{26}N_2O_6$, MW=282.3 g/mole, pKa_1=6.8, pKa_2=9.0.

1.3 Ion Exchangers and Column Properties

The ion exchangers for all the experiments are strong anion exchangers. Four different ion exchangers have been used, these are Source 30Q and Q Sepharose XL from Amersham Biosciences, Ceramic Q-HyperD F from BioSepra and Fractogel EMD TMAE 650(S) from Merck. These have been packed in the columns given in table 1.4. In chapter 5 "Determination of Model Parameters" it is described how the parameters are determined. The majority of the experiments have been made using Source30Q and BSA.
The breakthrough experiments and the investigation of the column capacity have used the columns in table 1.5.

	Unit	*Source 30Q*	*Q-Sepharose*	*Fractogel*	*Q-HyperD F*
V_{col}	[ml]	8.07	7.56	3.93	7.56
d_{col}	[cm]	1	1.6	1	1
d_p	[μm]	28.7-32.8 (30 avg)	45-165 (90 avg)	20-40	50 avg.
ε_t	[ ]	0.74	0.93	0.75	0.81
ε_p	[ ]	0.57	0.91	0.58	0.68
ε	[ ]	0.40	0.30	0.40	0.40
$V_{NA,\beta\text{-Lactoglobulin}}$	[ml]	5.17	3.52	2.34	3.58
$V_{NA,BSA}$	[ml]	4.93	2.80	2.19	3.53
$V_{NA,\alpha\text{-Lactalbumin}}$	[ml]	5.28	4.46	2.73	3.64
$K_{D,\beta\text{-Lactoglobulin}}$	[ ]	0.70	0.26	0.56	0.181
$K_{D,BSA}$	[ ]	0.61	0.11	0.45	0.165
$K_{D,\alpha\text{-Lactalbumin}}$	[ ]	0.74	0.46	0.85	0.201
λ_{NO3-}	[mmole]	0.843	2.15	0.112	2.38
Λ_{NO3-}	[M]	308	448	82.5	777
DV_{col}	[ml]	0.547	0.946	0.690	0.547

Table 1.4 Column data from Pedersen (2003).

		Source 30Q	*Cer. Q-HyperD F*	*Source 30Q*	*Source 30Q*
V_{col}	[ml]	1.35	1.34	10 drops	20 drops
d_{col}	[cm]	1.6	1.6	1.6	1.6
d_p	[μm]	30	50	30	30
ε_t	[ ]	0.74	-	-	-
ε_p	[ ]	0.57	-	-	-
ε	[ ]	0.4	-	-	-
$V_{NA,BSA}$	[ml]	0.82	-	-	-
$K_{D,BSA}$	[ ]	0.62	-	-	-
λ_{NO3-}	[mmole]	0.114	-	-	-
Λ_{NO3-}	[M]	0.246	-	-	-
DV_{col}	[ml]	0.600	-	-	-

Table 1.5 Column properties for the column used to measure the breakthrough curves. The two last columns were differential columns where 10 and 20 drops of resin slurry was used to pack the columns. The Ceramic Q-HyperD F was the column used for the nitrate capacity measurements, as described in chapter 5 "Determination of Model Parameters". The first column packed with Source 30 Q is previously used by Pedersen (2003).

1.4 Summary

The properties given here are the pure component properties. For a chromatographic separation process it is, however, the distribution between the the liquid phase and the particle phase that is the most interesting. This is described by an appropriate equilibrium expression.

2. SMA-formalism

For any chemical separation process the knowledge of equilibrium is of outmost importance. In chemical engineering thermodynamic models have been developed for many systems. But in the chromatography of proteins thermodynamic models are normally not applied and the equilibrium is described by an isotherm. Very often a Langmuir or a multicomponent Langmuir isotherm is applied, although a lot of other isotherms have also been suggested, Perry (1997) p. 16-11.

The Langmuir isotherm is, however, not able to take the influence of salt into account and salt is known to have a large impact on the binding of the protein. Brooks *et al.* (1992) have suggested to use the Steric Mass Action formalism (SMA-formalism).

Calculating the chromatographic separation of proteins involves a lot of equilibrium calculations. It is therefore import that this is done in an optimal way to reduce calculation time. A method for solving this is suggested.

Some numerical methods can lead to negative concentrations and the SMA-formalism is in the original form not able to handle negative salt concentrations. A method for handling negative concentrations is therefore also required.

The mobile phase concentration is a natural choice when calculating an isotherm. By calculating the SMA-isotherm using the mobile phase concentrations the equations are implicitly given. Using other independent variables an explicit method can be used and this is advantageous in some situations.

2.1 Ion Exchange

In ion exchange chromatography the pores inside the particle phase are charged. The concentration of the surface charges is Λ, where the volume refers to the pore volume.

Both salt and proteins bind to the surface according to the exchange reaction

$$z_0 C_p + z_p \bar{Q}_0 \Leftrightarrow z_0 Q_p + z_p C_0 \qquad (2\text{-}1)$$

where z is the charge of the component and the indices 0 is for salt and p is for the protein. C is the concentration in the liquid phase and Q is the concentration of bound protein. The bar above Q_0 indicates that only “free” salt is involved in the equilibrium.

Proteins are normally large molecules and in the SMA-formalism a number of salt ions bound to the surface of the ion exchanger, is considered to be hidden below the proteins, figure 2.1. These salt molecules will not participate in the ion exchange. The “free” salt molecules are hence the salt molecules that are not covered by the protein. The number of surface charges

covered by the protein is denoted ζ.

The equilibrium constant for the reaction given in (2-1) is given by

$$K_{eq,i} = \frac{Q_i}{C_i}\left(\frac{C_0}{\bar{Q}_0}\right)^{\frac{z_p}{z_0}} \tag{2-2}$$

Where the free salt is given as

$$\bar{Q}_0 = \Lambda - \sum_{j=1}^{NP} (\zeta_j + z_j) Q_j \tag{2-3}$$

where NP is the number of proteins.

After some manipulations and by introducing the dimensionless variables

$$y_i = \frac{C_i z_0}{\Lambda} \qquad q_i = \frac{Q_i z_0}{\Lambda} \qquad \nu_i = \frac{z_i}{z_0} \qquad \sigma_i = \frac{\zeta_i}{z_0} \tag{2-4}$$

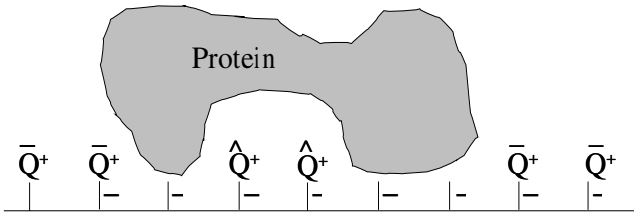

Figure 2.1 Bound protein to the surface of the ion exchanger. Only "free" salt (indicated with a bar) contributes to the ion exchange.

the concentration of the bound protein i is given as

$$q_i = \frac{K_{eq,i}\left(\frac{\bar{q}_0}{y_0}\right)^{\nu_i - 1} y_i}{y_0 + \sum_{j=1}^{NP} (\sigma_j + \nu_j) K_{eq,j}\left(\frac{\bar{q}_0}{y_0}\right)^{\nu_j - 1} y_j} \qquad \text{i=0,NP} \tag{2-5}$$

where index 0 is for the salt. A more detailed of this derivation is given in Brooks *et al.* (1992).

As suggested by Gerstner *et al.* (1994), the equilibrium constant can be calculated from the change in Gibbs energy , ΔG, as

$$K_{eq,i} = \exp\left(-\frac{\Delta G_i}{RT} + \nu_i \frac{\Delta G_0}{RT}\right) \qquad \text{i=1,NP} \tag{2-6}$$

where R is the gas constant and T is the temperature. The equilibrium constant depends on the protein binding charge which depends on the pH.

2.2 SMA-formalism for Positive Concentrations

From the SMA-formalism it is seen that the ratio between the free salt and the salt concentration is raised to the power of $\nu-1$, where ν is normally a non-integer. It must therefore be ensured that this ratio is always positive.

The bound concentrations are implicitly given and a iterative procedure is needed. The fastest way to solve these equations is to determine the free amount of salt first, since this is only one implicit equation with one variable. For salt eq. (2-5) reads

$$F_1 = -y_0 + \bar{q}_0\left(y_0 + \sum_{j=1}^{NP}(\sigma_j+\nu_j)K_{eq,j}\left(\frac{\bar{q}_0}{y_0}\right)^{\nu_j-1}y_j\right)=0 \qquad (2\text{-}7)$$

For positive protein concentrations the function is monotonically increasing in $\bar{q}_0$ and only one solution exist. For negative protein concentrations multiple solutions can be found.

A large number of equilibrium calculations are needed in each simulation, and it is therefore important that the calculations are optimised. A method for solving the SMA-formalism is given in appendix A.I “SMA-Formalism for Positive Concentrations”.

2.3 SMA-formalism Handling Negative Concentrations

In some numerical methods, e.g. orthogonal collocation, negative concentrations can occur. As described above negative concentrations can cause two problems: Multiple solutions of $\bar{q}_0$ and negative numbers raised to a non-integer number. Both these problems must be handled by the equilibrium calculation and another approach is needed.

Replacing the denominator in the equilibrium expression with a polynomial for low concentrations gives

$$q_i = \frac{K_{eq,i}\left(\frac{\bar{q}_0}{y_0}\right)^{\nu_i-1}y_i}{y_0 + \sum_{y\geq y_{c,j}}(\sigma_j+\nu_j)K_{eq,j}\left(\frac{\bar{q}_0}{y_0}\right)^{\nu_j-1}y_j + \sum_{0<y<y_{c,j}}P_j(\boldsymbol{y})} \qquad \text{i=0,NP} \qquad (2\text{-}8)$$

Below a critical proteins concentration, $y_{c,i}$

$$y_{c,j} = \frac{\beta\, y_0}{(\sigma_j+\nu_j)K_{eq}\left(\frac{\bar{q}_0}{y_0}\right)^{\nu_j-1}} \qquad \text{j=1,NP} \qquad (2\text{-}9)$$

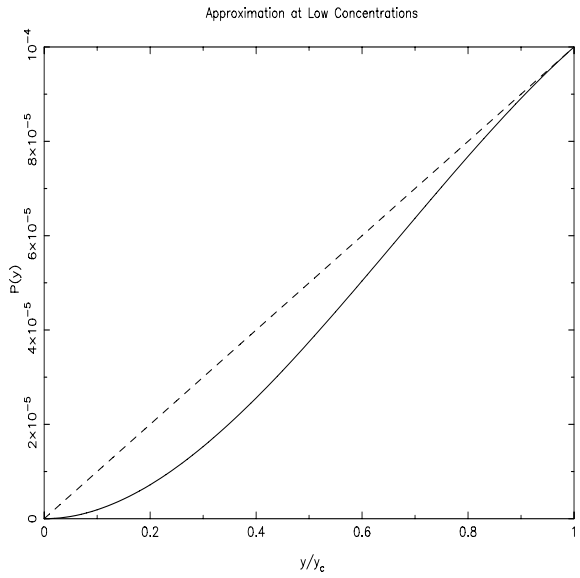

Figure 2.2 Comparison of true term (- - -) and approximated polynomial (——). Parameter $\beta y_0=10^{-4}$.

where β is a small number. The term in the denominator is replaced by a polynomial approximation

$$P_j(\boldsymbol{y}) = \beta\, y_0 \left[2 - \left(\frac{y_j}{y_{c,j}} \right) \right] \left(\frac{y_j}{y_{c,j}} \right)^2 \qquad \text{j=1,NP} \qquad (2\text{-}10)$$

The approximation together with the SMA-isotherm at low concentrations is given in figure 2.2. A detailed description of this is given in appendix A.II “Handling Negative Concentrations”.

2.4 SMA with Alternative Independent Variables

In the general case the most obvious set of variables is the mobile phase concentrations since these are easy to measure, compared to concentrations in the resin phase. This is also the variables used in the two approaches suggested above. This, however, leads to an implicit system of equations to be solved.

When solving large systems of equations the time consuming part is often the LU-factorisation, and the increased calculation time from solving the implicit version of SMA-formalism is small.

A Craig model, see chapter 3.9 “Craig Model”, is usually a small set of equations since this model only has one variable per component in each cell. For a small system of equations the time consuming step is no longer the LU-factorisation and the calculation time of the SMA-

formalism is relative larger.

For the Craig model it is too time consuming to have an iteration for the equilibrium inside an iteration for the mass balance. In this case an explicit formulation of the SMA-formalism is a better choice. This can be done if y_0 and q_p are used as variables.

As in the methods above it is most advantageous first to calculate the free amount of salt

$$\hat{q}_0 = q_0 - \sum_{i=1}^{NP} (\sigma_i + \nu_i) q_{p,i} \tag{2-11}$$

To avoid negative concentrations $\hat{q}_0$ is introduced. From this the free salt is given as

$$\bar{q}_0 = \hat{q}_0 \quad \text{for} \quad \hat{q}_0 \geq \beta \tag{2-12}$$

and

$$\bar{q}_0 = \beta \exp\left(\frac{\hat{q}_0}{\beta} - 1\right) \quad \text{for} \quad \hat{q}_0 < \beta \tag{2-13}$$

This ensures that the function is continuous and has continuous derivatives in the point

$$\hat{q}_0 = \bar{q}_0$$

Using this approach the isotherm is modified at high concentrations, whereas the approach described in the chapter above modified the isotherm at low concentrations.

A detailed derivation of this is given i appendix A.III “Alternative Variables”.

2.5 Summary

Different methods to solve the SMA-formalism have been suggested. Which method to use depends on the problem to be solved and the numerical method which is used. In a generalised routine for solving the chromatographic separation of proteins the most logical choice will be using the mobile phase concentration as independent variables. In these cases the appropriate method depends on whether the concentrations can be guaranteed to be positive or not.

The fastest method to solve the SMA-formalism is by using y_0 and q_p as independent variables since $\bar{q}_0$ is explicitly given and no iterations are required. If the calculation time depends strongly on the calculation of the SMA-formalism, this method is an excellent choice.

After an appropriate equilibrium expression is chosen the next thing to consider is what a good model for ion exchange chromatography should contain. A good model is able to predict the behaviour of the system without taking unnecessary effects into account, which increases the calculation time and makes the results difficult to analyse.

3. Modelling

In order for modelling to be a good tool for optimization the model must of course be able to describe what is observed in the laboratory. To validate a model it is therefore important to compare results from the laboratory with the corresponding model. The model must be able to describe the equilibrium and zone spreading mechanisms.

In chromatography zone spreading can origin from axial dispersion, mass transfer resistance, adsorption kinetics, and when the isotherm is not in the linear range of the isotherm, equilibrium can be a major contributor to zone spreading. To avoid the effect of equilibrium when determining the other zone spreading mechanisms these are obtained from pulse experiments in the linear range, which is easy to determine. For the non-linear case Guiochon *et al.* (1994) p. 218 says *"For single-component systems, the theoretical solutions obtained are easy to compare to experimental profiles. They differ only by the smoothing effect due to axial dispersion and to the finite mass transfers in actual columns. In many cases, because of the stationary phases currently available, these effects appear to be secondary compared to the major role of thermodynamics in controlling the band profiles in overloaded elution.*". In other words the zone spreading mechanisms will have a minor impact compared to the equilibrium effect on the resulting chromatogram at preparative load.

Often in chromatographic literature the model for the calculation of the chromatographic column only takes axial dispersion into account, e.g. Migliorini *et al.* (1999), Schramm *et al.* (2003), Guiochon *et al.* (1994) p. 34. All zone spreading comes from the axial dispersion and the Pe-number is modified to match the zone spreading.

However, proteins are large molecules with small diffusion coefficients and the main contributor to zone spreading can be mass transfer resistance. The van Deemter equation (van Deemter *et al.*, 1956), is sometimes written as

$$H = A_H + \frac{B_H}{v_i} + C_H \cdot v_i \qquad (3\text{-}1)$$

where H is the plate height, and A_H, B_H, and C_H are constants and v_i is the interstitial velocity, Mollerup *et al.* (2000).

The constant A_H comes from axial dispersion, B_H comes from the molecules self diffusion and C_H comes from mass transfer resistance.

From the van Deemter equation it is seen that axial dispersion will contribute to the plate height by a constant whereas mass transfer resistance will lead to a plate height that is almost

a linear function of the velocity (k_f is a function of v_s), in liquid chromatography the self diffusion is normally neglectable.

In figure 3.1 the reduced plate height is plotted vs. the superficial velocity, which has been measured by pulse experiments at non-binding conditions. From the plot is seen that the reduced plate height is almost a linear function of the superficial velocity as predicted by the van Deemter equation. Even for a small molecule like tyrosine a slight increase in the plate height is observed when the flow rate is increased. An intercept with the y-axis which can origin from the axial dispersion is also seen in the figure.

The figure shows that the molecules with the lowest diffusion coefficients are also the molecules with the highest slope. This is also an indication of that mass transport resistance is contributing to the zone spreading. Kinetic effects from the adsorption/desorption of the proteins can not be observed in this plot due to the high salt concentration, which corresponds to non-adsorbing conditions.

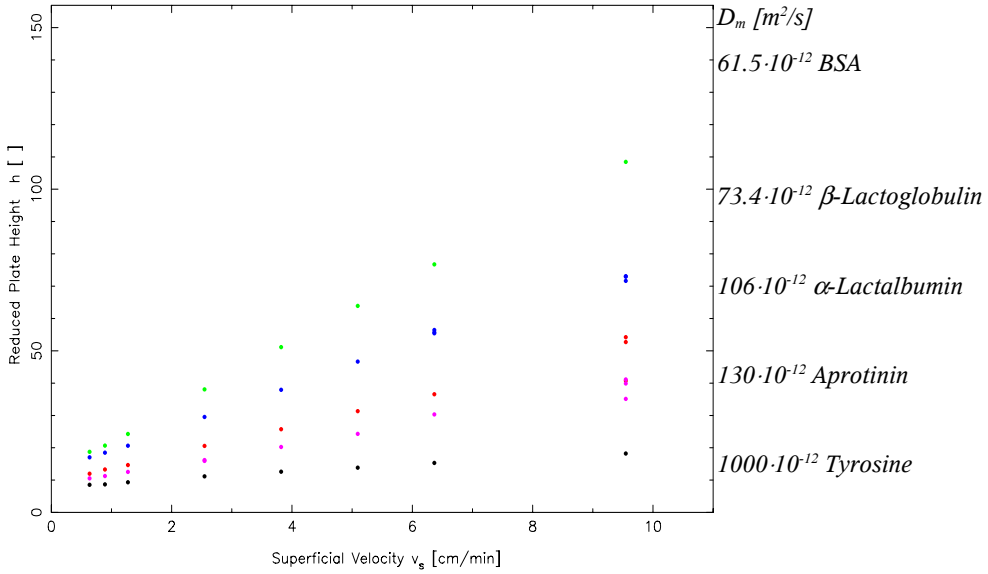

Figure 3.1 Reduced plate height, eq. (3-56), at various superficial velocities. The diffusion coefficients of the different components are given to the right. The experiments were performed at non-binding conditions at pH 7 and C_0=1 M on a column packed with Source 30Q with d_{col}=1 cm and V_{col}=7.4 ml.

Helfferich (1995) writes in the chapter "Kinetics", p. 251 "*In all cases which have been studied so far, the rate-determining step of the process was established to be diffusion of counter ions rather that an actual "chemical" exchange reaction at the fixed ionic groups, an alternative that cannot be ruled out a priori. This shows that ion exchange, as a rule, is purely a diffusion phenomenon. Reaction rate constants may be defined formally, but in their*

physical interpretation they have little in common with rate constants of actual chemical reactions.”.

From this it seems reasonable that the suggested model takes mass transport resistance and axial dispersion into account, but not adsorption/desorption. A model taking only axial dispersion into account would not be adequate to describe the zone spreading. However, for smaller molecules a model only taking axial dispersion into account might be adequate.

3.1 Assumptions

- Thermodynamic ideality is assumed in the column wherefore the activities are replaced by the concentrations.
- The fluid is incompressible and the flow is steady.
- The mean linear velocity is uniform.
- The dispersive effect is given by an effective axial diffusion coefficient.
- The film layer theory describes mass transfer at the particle surface.
- The diffusion obeys Fick's law in the particle or one mass transfer coefficient per phase can describe the flow inside the particle.

The first assumption is a very rough approximation, however, taking non-ideality into consideration is outside the scope of this thesis. As such the SMA-formalism should be considered as a convenient fitting function, capable of taking the influence of salt on the isotherm into consideration.

Neglecting the compressibility of a liquid is a normal assumption and a uniform flow can normally be assumed when $d_{col}>200d_p$, Yamamoto (1988) p. 315[3].

The film layer theory and Fick's law are the usual assumptions for the mass transport in the film layer and inside a particle.

3.2 Mobile Phase

The mobile phase mass balance usually contains a diffusion term with a first order derivative in the axial dimension. When setting up the differential mass balance, this term creates a second order derivative in the axial dimension requiring two boundary conditions. As seen in figure 3.1 the axial term might be small compared to the mass transfer term and in some cases this can be neglected and a double boundary value problem is avoided. This simplifies the solution of the equations and this mass balance is also set up.

3 This is in contradiction to what Yamamoto says on p. 168 “*They found that the column diameter should be 50-100 times the particle diameter to obtain a practically uniform velocity profile across the cross section of a column.*”

3.2.1 Including Axial Dispersion

The mass balance for the mobile phase taking both mass transport resistance in the film layer around the particle and axial dispersion into account reads

$$\epsilon \frac{\partial C}{\partial t} + \epsilon \cdot v_i \frac{\partial C}{\partial z} + (1-\epsilon) a_p k_f (C - C_s) - \epsilon (D_m + E_D) \frac{\partial^2 C}{\partial z^2} = 0 \tag{3-2}$$

where t is the time and z is the axial position. The film layer coefficient, k_f, is referring to the entire particle surface, a_p. D_m is the diffusion coefficient of the component and E_D is the eddy diffusion coefficient.

With the insertion of the dimensionless concentrations, eq. (2-4), time, and position

$$\tau = \frac{t \cdot v_i}{L} \tag{3-3}$$

$$x = \frac{z}{L} \tag{3-4}$$

the mobile phase mass balance reads

$$\frac{\partial y}{\partial \tau} + \frac{\partial y}{\partial x} + St_f \Phi (y - y_s) - \frac{1}{Pe_L} \frac{\partial^2 y}{\partial x^2} = 0 \tag{3-5}$$

The introduced dimensionless groups are the Stanton number for the film layer, St_f, and the Peclet number, Pe_L for the column.

$$St_f = \frac{6 \cdot L \cdot k_f}{d_p v_i} \tag{3-6}$$

$$Pe_L = \frac{L v_i}{D_m + E_D} \tag{3-7}$$

The mass balance at x=0 gives one of the boundary conditions

$$y_{in}(\tau) - y(\tau, x=0) = -\frac{1}{Pe_L} \frac{\partial y}{\partial x}\bigg|_{x=0} \tag{3-8}$$

where $y_{in}(\tau)$ is the specified inlet concentration.

Sometimes the dispersive term is omitted at the inlet and the inlet condition reads

$$y(\tau, x=0) = y_{in}(\tau) \tag{3-9}$$

As the second boundary condition the Danckwerts boundary conditions is often used (Danckwerts, 1953).

$$\frac{\partial y}{\partial x}\bigg|_{x=1} = 0 \tag{3-10}$$

However, the open boundary condition previously used by Guiochon *et al.* (1994) p. 181 and

Michelsen (1994) will in general be used here to avoid a double boundary problem.

$$y \text{ is finite for } x \to \infty \tag{3-11}$$

Normally, the boundary conditions do not influence the resulting chromatogram significantly. A discussion of the boundary conditions impact on the solution is given by Guiochon *et al.* (1994) p.178-183.

The initial condition is specified by the user.

$$y(\tau = 0, x) = y_{init} \tag{3-12}$$

3.2.2 Excluding Axial Dispersion

The diffusion coefficients for the proteins are in general low and axial dispersion is often also low and mass transport is then the major zone spreading mechanism. Neglecting the axial dispersion the mobile phase mass balance reads

$$\frac{\partial y}{\partial \tau} + \frac{\partial y}{\partial x} + St_f \phi (y - y_s) = 0 \tag{3-13}$$

Where the inlet condition is given by eq. (3-9) and the initial conditions are the same as above, eq. (3-12). This turns the problem into a first order partial differential equation. Rhee *et. al.* (2001a), (2001b) have made an extensive work for chromatography on coupled first order partial differential equations.

3.3 Particle Phase

A mass balance for the particle phase is normally adding one extra dimension to the problem. There will then be derivatives in t, z, and r and the number of variables will increase very rapidly. The derivatives in r can, however, be avoided by using a linear driving force approximation as previously suggested by Glueckauf (1955), see p. 20. The linear driving force approximation for the particle phase models the mass transfer in the particle with a term similar to the film layer term for the particle surface. Other approximations for modelling the mass transfer inside the particle has also been suggested (Carta *et al.*, 1998).

In this section it is important to distinguish between particle surface, the exterior surface of the particle, and the pore surface which is the surface of the pores inside the particle.

The mass balance for the particle phase takes both pore phase and surface phase diffusion into account, Do *et al.* (1987) Yoshida *et al.* (1994). This is necessary with the suggested model to be able to model the bell-shaped curves previously found by Hansen (2000).

3.3.1 Diffusion Model

Using Fick's diffusion for mass transport in the particles the mass balance for the particles reads

$$\frac{\partial Q_p}{\partial t}+\frac{\partial C_p}{\partial t}=\frac{1}{r^2}\frac{\partial}{\partial r}\left(r^2 D_q \frac{\partial Q_p}{\partial r}\right)+\frac{1}{r^2}\frac{\partial}{\partial r}\left(r^2 D_p \frac{\partial C_p}{\partial r}\right) \tag{3-14}$$

Where r is the radial position, D_p and D_q are the diffusion coefficients for the protein in the pore phase and for the bound protein.

Q_p is a function of C_p, and the time derivative in equation (3-30) is implicitly given. The particle phase mass balances for the different components must then be solved simultaneously in each iteration step. The Jacobian for this system will be difficult to calculate, too. To avoid this the pore phase is divided into two balances, a pore phase and a pore surface phase, with a finite mass transfer rate between. The pore phase mass balance reads

$$\frac{\partial C_p}{\partial t}=-K_{ads}\left(Q_{SMA}(C_p)-Q_p\right)+\frac{1}{r^2}\frac{\partial}{\partial r}\left(r^2 D_p \frac{\partial C_p}{\partial r}\right) \tag{3-15}$$

and the pore surface mass balance reads

$$\frac{\partial Q_p}{\partial t}=K_{ads}\left(Q_{SMA}(C_p)-Q_p\right)+\frac{1}{r^2}\frac{\partial}{\partial r}\left(r^2 D_q \frac{\partial C_q}{\partial r}\right) \tag{3-16}$$

where K_{ads} is the adsorption rate. Addition of these two equations gives eq. (3-14).

With the dimensionless variables given above and

$$u=\frac{r^2}{R_p^2} \tag{3-17}$$

where R_p is the particle radius, the dimensionless pore phase mass balance reads

$$\frac{\partial y_p}{\partial \tau}=-\frac{L K_{ads}}{v_i}(q_{SMA}-q_p)+2\frac{St_f}{Bi_p}\frac{\partial y_p}{\partial u}+\frac{4}{3}\frac{St_f}{Bi_p}u\frac{\partial^2 y_p}{\partial u^2} \tag{3-18}$$

and the corresponding pore surface mass balance reads

$$\frac{\partial q_p}{\partial \tau}=\frac{L K_{ads}}{v_i}(q_{SMA}-q_p)+2\frac{St_f}{Bi_q}\frac{\partial y_q}{\partial u}+\frac{4}{3}\frac{St_f}{Bi_q}u\frac{\partial^2 q_p}{\partial u^2} \tag{3-19}$$

The boundary conditions are

$$\left(\frac{\partial C_p}{\partial r}\right)_{r=0}=\left(\frac{\partial Q_p}{\partial r}\right)_{r=0}=0 \tag{3-20}$$

due to symmetry. With the dimensionless variables, eq. (3-17), this is automatically fulfilled and replaced by

$$y_p \text{ is finite for } u \to 0 \quad \text{and} \quad q_p \text{ is finite for } u \to 0 \tag{3-21}$$

and a mass balance equation at r=R_p. Neglecting adsorbed material on the surface, the surface mass balance becomes

$$k_f(C-C_s) = K_D \epsilon_p D_p \left(\frac{\partial C_p}{\partial r}\right)_{r=R_p} + K_D \epsilon_p D_q \left(\frac{\partial Q_p}{\partial r}\right)_{r=R_p} \tag{3-22}$$

which in dimensionless variables becomes

$$\phi(y-y_s) = \psi \frac{2}{Bi_p}\left(\frac{\partial y_p}{\partial u}\right)_{u=1} + \psi \frac{2}{Bi_q}\left(\frac{\partial q_p}{\partial u}\right)_{u=1} \tag{3-23}$$

Equilibrium is assumed for the particle surface.

In the film layer around the particle the entire surface area of the particle is active in the mass transport, where k_f is calculated from a correlation. Inside the particles only a fraction corresponding to $K_D \cdot \epsilon_p$ is active in the mass transport, and from this the parameters D_p and D_q are fitted.

The initial conditions are

$$y_p(t=0,r) = y_{p,init} \tag{3-24}$$

$$q_p(t=0,r) = q_{p,init} \tag{3-25}$$

The dimensionless groups are the Biot numbers

$$Bi_p = \frac{R_p k_f}{D_p} \tag{3-26}$$

$$Bi_q = \frac{R_p k_f}{D_q} \tag{3-27}$$

It will be advantageous in some situations to have the surface phase mass balance rewritten to include a time derivative. Then all equations will have first order derivatives in τ. This can be done by setting up a differential mass balance up over a surface layer with thickness Δr.

$$4\pi R_p^2 \Delta r = \frac{4}{3}\pi R_p^3 \Theta \frac{\epsilon}{1-\epsilon} \tag{3-28}$$

Where Θ is the volume fraction (e.g. $\Theta=10^{-3}$) of the particle used for the surface mass balance (the factor ε/(1-ε) has been included to make use of dimensionless groups).

From this

$$\Delta r = \frac{d_p}{6}\Theta \frac{\epsilon}{1-\epsilon} \tag{3-29}$$

and a mass balance for the surface in dimensionless units gives

$$\frac{\partial y_s}{\partial \tau} = \frac{St_f}{\Theta}\left(\phi(y - y_s) - \psi \frac{2}{Bi_p}\left(\frac{\partial y_p}{\partial u}\right)_{u=1} - \psi \frac{2}{Bi_q}\left(\frac{\partial q_p}{\partial u}\right)_{u=1} \right) \tag{3-30}$$

3.3.2 Film Layer Model

As previously mentioned the system of equations rapidly becomes a very large. It is therefore desirable to reduce this system by one dimension if possible. This can be done by using a film layer model for the mass transfer inside the particle similar to the film layer for the particle surface.

The average concentration in the pore phase is given by

$$C_{p,avg} = \frac{\int_0^{R_p} 4\pi r^2 C_p \, dr}{\int_0^{R_p} 4\pi r^2 \, dr} \tag{3-31}$$

and correspondingly for $Q_{p,avg}$. Multiplication with r^2dr and integration from 0 to R_p in equation (3-14) gives

$$\frac{R_p^3}{3}\left(\frac{\partial C_{p,avg}}{\partial t} + \frac{\partial Q_{p,avg}}{\partial t} \right) = R_p^2 D_p \left(\frac{\partial C_p}{\partial r}\right)_{r=R_p} + R_p^2 D_q \left(\frac{\partial Q_p}{\partial r}\right)_{r=R_p} \tag{3-32}$$

A linear approximation of the two concentration gradients at the particle surface as previously used by Hansen (2000) gives

$$\frac{dC_{p,avg}}{dt} + \frac{dQ_{p,avg}}{dt} = a_p k_p \left(C_s - C_{p,avg}\right) + a_p k_q \left(Q_s - Q_{p,avg}\right) \tag{3-33}$$

Again this is split into two phases with a finite mass transfer rate between these

$$\frac{\partial y_p}{\partial \tau} = -\frac{L K_{ads}}{v_i}\left(q_{SMA}(y_p) - q_p\right) + St_p\left(y_s - y_p\right) \tag{3-34}$$

and the pore surface mass balance reads

$$\frac{\partial q_p}{\partial \tau} = \frac{L K_{ads}}{v_i}\left(q_{SMA}(y_p) - q_p\right) + St_q\left(q_s - q_p\right) \tag{3-35}$$

By this the derivatives with respect to r have been removed and the system has been reduced by one dimension.

The flux between the mobile phase and the particle phase is

$$St_f \phi(y - y_s) = St_p \cdot \psi(y_s - y_p) + St_q \cdot \psi\left(q_s(y_s) - q(y_p)\right) \tag{3-36}$$

Again a balance over the surface of the particle can be set up and this gives

$$\frac{\partial y_s}{\partial \tau} = \frac{St_f}{\Theta}\phi(y - y_s) - \frac{St_p}{\Theta}\psi(y_s - y_p) - \frac{St_q}{\Theta}\psi(q_s - q_p) \tag{3-37}$$

The initial conditions for these equation are given by

$$y_p(\tau = 0) = y_{p,init} \tag{3-38}$$

$$q_p(\tau = 0) = q_{p,init} \tag{3-39}$$

with the Stanton numbers for the pore phase and pore surface as dimensionless groups

$$St_p = \frac{6 \cdot L \cdot k_p}{d_p \cdot v_i} \tag{3-40}$$

$$St_q = \frac{6 \cdot L \cdot k_q}{d_p \cdot v_i} \tag{3-41}$$

3.4 Dispersive Model

If mass transport is fast, the dispersive effects are the main contributors to the zone spreading. The dispersive model can be found by addition of the mobile phase mass balance, eq. (3-5), with the pore phase balances, eq. (3-34-3-35), and the flux equation, eq. (3-36). The concentrations will be the same in the mobile phase at the particle surface and inside the particles. This leads to

$$(1 + \psi)\frac{\partial y}{\partial \tau} + \psi\frac{\partial q}{\partial \tau} + \frac{\partial y}{\partial x} - \frac{1}{Pe_L}\frac{\partial^2 y}{\partial x^2} = 0 \tag{3-42}$$

The initial and boundary conditions of this will be the same as for the mobile phase. This model reduces the number of variables to ¼ (y_s, y_p, and q_p disappear) and leads to a smaller system. For proteins this model is inadequate since it is unable to model the slope of the van Deemter equation, figure 3.1.

3.5 Ideal Chromatography

Ideal chromatography is a purely equilibrium model taken no zone spreading effects from mass transport and axial dispersion into account. This simplifies the system even further to

$$(1 + \psi)\frac{\partial y}{\partial \tau} + \psi\frac{\partial q}{\partial \tau} + \frac{\partial y}{\partial x} = 0 \tag{3-43}$$

An example of ideal chromatography can be found in Guiochon *et al.* (1994) pp. 248-266 for the Langmuir isotherm with two components.

The retention time and the breakthrough time can also be calculated from this model, Mollerup *et al.* (2000) p. 33 and p. 35. The retention time is given as

$$t_R = \frac{L}{v_i}\left(1+\psi(1+A)\right) \tag{3-44}$$

and the breakthrough time is given as

$$t_{ch} = \frac{L}{v_i}\left(1+\psi\left(1+\frac{\Delta q}{\Delta c}\right)\right) \tag{3-45}$$

3.6 Calculation Considerations

Before starting to solve the system a number of considerations will be addressed. These involve both mathematical and process considerations.

3.6.1 Boundary Conditions

Using the Danckwerts boundary condition at the column exit, eq. (3-10), leads to a double boundary value problem with the complications usually associated with solving these. Global orthogonal collocation would lead to a full matrix that has to be inverted at every time step. In order to reduce the calculation time the column can be subdivided into a number of elements and the requirements between each element is continuity and a continuous first derivative, Rice *et al.* (1995) pp. 603-615. The matrix is then a banded matrix requiring less resources to invert.

As discussed by Guiochon *et al.* (1994) pp. 178-183 the boundary conditions do normally not play a major role in the resulting chromatogram. To avoid the problems associated with the Danckwerts boundary condition at the column exit, eq. (3-10), the open boundary condition, eq. (3-11), is used instead.

The problem is then converted to an initial value problem in x and each element can be solved individually as previously suggested by Michelsen (1994), using the outlet concentration from one element as the inlet concentration to the following element. This has two advantages: The matrix is significantly reduced in size reducing the time for the matrix inversion. The second advantage is that the time step length can be increased when this is allowed for the individual element. The time step length is hence not reduced by other elements in the column.

3.6.2 Pooling Axial Dispersion and Mass Transfer Resistance

The Pe_d number is usually in the order ½-1, Yamamoto *et al.* (1988) p. 170. For a 10 cm Source 30Q column this gives

$$Pe_L = Pe_d \frac{L}{d_p} \approx 0.75 \frac{0.1\,m}{30\cdot 10^{-6}\,m} \approx 2500 \tag{3-46}$$

The factor before the second order term in x in the mobile phase mass balance is therefore small. This in line with the observations from figure 3.1 where mass transfer resistance is a major contributor to the zone spreading.
Another way to avoid a double boundary value problem in x is neglecting the second order term, leading to equation (3-13). If the second order term was eliminated the problem would be an initial value problem in x. The discussion about which boundary conditions to use would then vanish. Neglecting axial dispersion would lead to a model simplification, but would introduce an error. This error can be reduced by modifying the film layer mass transfer resistance to match the reduced plate height of the model including axial dispersion. The effect of this simplification is described below in chapter 3.7.2 “Laplace Transform”.

3.6.3 Solution of the System

Taking only an initial value problem in τ and x into consideration this can be solved in different ways. The system can be solved using Finite Difference Time Domain-methods (FDTD). These methods are, however, of low order and numerical dispersion is introduced. For a linear isotherm the numerical dispersion can be set to match the axial dispersion by a proper selection of elements (Guiochon *et al.*, 1994, pp. 348-351). Unfortunately, this is no longer possible when the isotherm is not linear.
A better method for solving the system is to use Orthogonal Collocation on Finite Elements (OCFE), this has previously been done by Ma *et al.* (1991). This has the advantage of high order methods. However, the drawback of this method is that negative concentrations can occur and the equations must be able to handle these.
A comparison of the resulting chromatograms using OCFE and FDTD-method is given by Guiochon *et al.* (1994) p. 367.

3.6.4 Salt

Beside the proteins in the calculation, salt must also be taken into account, due to the strong influence of the salt on the protein adsorption. From the SMA-formalism it is seen that the salt concentration must be positive, since the concentration is raised to a non-integer power.
The properties of salt is significantly different from the properties of protein, salt is a much smaller molecule with a correspondingly larger diffusion coefficient, and often the molar concentration of salt is significantly larger than the concentration of the proteins.
With a fast mass transfer of salt the same salt concentration in the mobile phase and the pore phase can be assumed, and a high salt concentration will only be marginally influenced by the

change in salt concentration from the adsorption/desorption of the proteins. Neglecting axial dispersion of the salt the concentration can be calculated as an explicit function of x and τ, eliminating this from the mass balances and guaranteeing that the salt concentration will always be positive.

3.7 Linear Isotherm

At high salt concentrations and low protein concentrations the isotherm can normally be considered to be linear. With a linear isotherm the particle phase differential mass balance can be simplified and the equations given above can be solved using Laplace transform or Fast Fourier Transform.

For a linear isotherm the ratio Q/C can be written

$$A=\frac{Q}{C}=K_{eq}\left(\frac{\Lambda}{C_0}\right)^{\nu}=K_{eq}\left(\frac{z_0}{y_0}\right)^{\nu} \tag{3-47}$$

Where the index 0 refers to salt

3.7.1 Film Layer Model

Inserting A=Q/C in the flux equation for the film layer model, eq. (3-36), and isolating the surface concentration, y_s, gives

$$y_s=\frac{\phi\, St_f\cdot y+\psi\cdot(St_p+A\cdot St_q)\, y_p}{\phi\, St_f+\psi\,(St_p+A\cdot St_q)} \tag{3-48}$$

The mobile phase balance equation (3-5) can then be written as

$$\frac{\partial y}{\partial \tau}=\frac{1}{Pe_L}\frac{\partial^2 y}{\partial x^2}-\frac{\partial y}{\partial x}-\gamma\cdot\psi\cdot y+\gamma\cdot\psi\cdot y_p \tag{3-49}$$

and the particle phase, eq. (3-34 added with 3-35) as

$$\frac{\partial y_p}{\partial \tau}=\frac{1}{(1+A)}\cdot\gamma\cdot y-\frac{1}{(1+A)}\cdot\gamma\cdot y_p \tag{3-50}$$

where

$$\gamma=\frac{\phi\, St_f(St_p+A\cdot St_q)}{\phi\, St_f+\psi\,(St_p+A\cdot St_q)} \tag{3-51}$$

The initial conditions used here will be (3-12) and (3-38) and the boundary conditions are (3-9) and (3-11).

This system can be analysed in a number of ways. A Laplace analysis will give valuable insight into the retention time and central moments of the peaks, and the resulting chromatogram can be calculated using Fast Fourier Transform.

3.7.2 Laplace Transform

The set of linear partial differential equations is an initial value problem and can be solved using Laplace transform and a moment analysis can be performed in the Laplace domain, Rhee *et. al.* (2001a) pp. 161-166 or Østergaard *et al.* (1969). The derivation of these equations can be found in appendix B “Laplace Transform”.

When injecting a small pulse (corresponding to a Dirac's delta) into the column the first normal[4] and higher central moments can be determined from the resulting chromatogram, chapter 6 “Pulse Experiments”. These can be used to determine the axial dispersion and mass transport parameters.

From the first normal moment the retention time is found as

$$t_R = \frac{L}{v_i}\left(1+\frac{1-\epsilon}{\epsilon}\epsilon_p K_D(1+A)\right) \tag{3-52}$$

This result is identical to the result found from ideal chromatography, eq. (3-44). It is seen that the retention time does not depend on the axial dispersion or the mass transfer coefficients.

The reduced plate height is given as

$$h = \frac{2}{Pe_d} + 2\left(\frac{1+A}{\frac{1}{\psi}+1+A}\right)^2 \frac{\epsilon v_i}{6(1-\epsilon)}\cdot\left(\frac{1}{k_f}+\frac{1}{\epsilon_p K_D(k_p + A k_q)}\right) \tag{3-53}$$

where Pe_d is defined as

$$Pe_d = \frac{v_i d_p}{D_m + E_D} = \frac{d_p}{L} Pe_L \tag{3-54}$$

and the number of stages in the column is defined as the ratio between the second central moment, eq. (6-2), and the first normal moment squared

$$N_{stg} = \frac{M'^2_1}{M_2} \tag{3-55}$$

M'_1 is the first normal moment and M_2 is the second central moment.

From the column length, L, the reduced plate height can then be calculated as

4 The first normal moment is called so to distinguish it from the central moments.

$$h=\frac{L}{d_p \cdot N_{stg}} \tag{3-56}$$

Equation (3-53) is also known as the van Deemter equation for the current model. It can be seen that the different zone spreading mechanism (axial dispersion, film layer resistance and particle phase resistance) are additive. Hence it is not possible to determine which factor causes the zone spreading.

The skewness of the peak is given as the third central moment over the second central moment raised to the power of 3/2. The skewness is not used in evaluating the parameters since the third central moment is difficult to determine accurately enough (Lode *et al.*, (1998). The skewness for the model is derived in appendix B "Laplace Transform". Here it should only be noted that the skewness is positive meaning that the peaks will always be tailing.

The van Deemter equation is also derived for the diffusion model in appendix B "Laplace Transform" and is given as

$$h=\frac{2}{Pe_d}+2\left(\frac{1+A}{\frac{1}{\psi}+1+A}\right)^2\frac{\epsilon v_i}{6(1-\epsilon)}\cdot\left(\frac{1}{k_f}+\frac{1}{5}\cdot\frac{R_p}{\epsilon_p K_D(D_p+A D_q)}\right) \tag{3-57}$$

3.7.3 Eliminating Axial Dispersion

The model including axial dispersion will create a double boundary value problem with the boundary condition (3-8) or (3-9) and (3-10). The model could be simplified if the second order term is omitted as described in chapter 3.6.2 "Pooling Axial Dispersion and Mass Transfer Resistance".

Instead of neglecting axial dispersion and setting the Peclet number equal to infinity, a better strategy would be to demand that the second central moment is the same for the model including axial dispersion and the model without. For a plate model this would lead to the same plate height, since the first moment only depends on equilibrium parameters, eq. (3-52). The modified mass transfer coefficient, k'_f, is then calculated from the original mass transfer coefficient, k_f, by setting the axial dispersion equal to 0 and demanding that the second central moment is the same for the two cases, $M'_2=M_2$. These central moments are found in the Laplace domain, eq. (B-35), and gives

$$\frac{2}{Pe_L}\big(1+\psi(1+A)\big)^2+2\frac{\psi}{\gamma}(1+A)^2=2\frac{\psi}{\gamma'}(1+A)^2\Leftrightarrow\gamma'=\frac{1}{\frac{1}{\gamma}+\frac{1}{Pe_L}\frac{(1+\psi(1+A))^2}{\psi(1+A)^2}} \tag{3-58}$$

From this γ' a new St' and k'_f can be calculated.

The skewness of the peak is allowed to vary, however, the skewness between the two different approaches can be compared by insertion of (B-39) into (B-40) this gives

$$\frac{skew}{skew'}=\frac{\frac{12}{Pe_L^2}\left(\frac{1+\psi(1+A)}{1+A}\right)^3+\frac{12}{Pe_L}\frac{\psi}{\gamma}\left(\frac{1+\psi(1+A)}{1+A}\right)+6\frac{\psi}{\gamma^2}}{\frac{6}{Pe_L^2}\frac{1}{\psi}\left(\frac{1+\psi(1+A)}{1+A}\right)^4+\frac{12}{Pe_L}\frac{1}{\gamma}\left(\frac{1+\psi(1+A)}{1+A}\right)^2+6\frac{\psi}{\gamma^2}} \tag{3-59}$$

The numerator and denominator is seen to be somehow similar and the difference between the two terms containing the Peclet number only depends on the phase ratio for the protein, ψ, and the term inside the parenthesis.

The last term in the numerator and denominator are identical and the first term is proportional to Pe_L^{-2} which rapidly goes to 0 for large Pe_L-numbers, eq. (3-46).

The largest deviations between the skewness between the two approaches must be expected when the contribution to zone spreading from the pore phase can be neglected. In this case $St_p+A\cdot St_q>>St_f$ and γ will reach its maximum value

$$\gamma_{max}=\frac{\phi}{\psi}St_f=\frac{\phi}{\psi}\frac{6Lk_f}{v_i d_p}=\frac{\phi}{\psi}\frac{6Lk_f}{\epsilon Re\,Sc\,D_m} \tag{3-60}$$

The value of γ_{max} can be estimated by use of the correlation suggested by Kataoka *et al.* (1972), eq. (4-5).

$$Sh=1.85\phi^{1/3}Re^{1/3}Sc^{1/3} \qquad Re<40 \tag{3-61}$$

Isolating Re·Sc in this and inserting into γ_{max} gives

$$\gamma_{max}\approx\frac{\phi}{\psi}6L\frac{1.85^3\phi k_f}{\epsilon Sh^3 D_m}=\frac{6}{\psi}\frac{L}{d_p}\frac{1.85^3\phi^2}{\epsilon Sh^2} \tag{3-62}$$

For a column packed with Source 30Q and BSA $\psi\approx$½, ϕ=3/2, and ε=0.4, Pedersen (2003) p. 26. With a Sherwood number of 10, $\gamma_{max}\approx 4\cdot L/d_p$, and the last term in equation (3-53) will be small. This, however, is under the assumption that mass transfer resistance inside the particle is negligible, in this case

$$\frac{skew}{skew'}\approx\frac{\psi(1+A)}{1+\psi(1+A)} \tag{3-63}$$

It is seen that for $A\rightarrow\infty$ the skewness ratio will approach unity and for A=0 the skewness ratio will approximately be $\psi/(1+\psi)$. The other extreme case is that $St_p+A\cdot St_q<<St_f$ in this case

$\gamma_{min}=St_p+A\cdot St_q$.

When the mass transfer resistance inside the particle also contributes to the zone spreading, γ is reduced and the difference between the two approaches will be smaller.

With this approach it is ensured that the first normal moment and the second central moment will be the same, and as A increases the third central moment will also be approximately the same.

The best way to compare the importance of this simplification is to compare the calculated peaks with experimental peaks. The resulting peaks can be calculated by Fast Fourier Transform. This comparison is found in chapter 7 “Lactalbumin and Q-Sepharose XL".

3.7.4 Fast Fourier Transform

For a linear isotherm the two mass balances and the flux equation can also be solved using Fast Fourier Transform (FFT). FFT is an extremely fast and accurate method to solve linear partial differential equations, Iserles (1996) p.249 (a more general description of the Fourier transform can be found in Kreyszig (1999) pp. 569-578).

Neglecting axial dispersion, eq. (3-13), and using the linear driving force approximation the solution is

$$\hat{y}_m(x)=C_m\exp\left(-\left(\frac{L}{v_i}\frac{2\pi}{t_{end}}im+\psi\gamma-\psi\frac{\gamma^2}{\gamma+(1+A)\frac{L}{v_i}\frac{2\pi}{t_{end}}im}\right)x\right) \tag{3-64}$$

Where $\hat{y}_m$ is the m'th concentration in the Fourier domain and t_{end} is the run time for an experiment.

The model including axial dispersion gives

$$\hat{y}_m(x)=C_m\exp\left(\frac{Pe_L}{2}\left(1-\sqrt{1+\frac{4}{Pe_L}\left(\frac{L}{v_i}\frac{2\pi}{t_{end}}im+\psi\gamma-\psi\frac{\gamma^2}{\gamma+(1+A)\frac{L}{v_i}\frac{2\pi}{t_{end}}im}\right)}\right)x\right) \tag{3-65}$$

The derivations of equation (3-64) and (3-65) are given in appendix C “Fast Fourier Transform”, together with the derivations of the equations with the pore phase diffusion model.

A comparison between the two calculated chromatograms are given in chapter 7 “Lactalbumin and Q Sepharose XL”.

3.8 Non-Linear Isotherm

When the isotherm is no longer linear, the equations cannot be solved by Laplace transform and Fourier transform, instead orthogonal collocation on finite elements, OCFE, is used to solve the equations. Using OCFE the column is subdivided into a number of elements, NE, and each element is solved by orthogonal collocation, Ma *et al.* (1991). The orthogonal collocation discretizes the derivatives in x (and u) and a set of coupled first order ordinary differential equations in τ remains.

From ideal chromatography is known that shock-waves can occur in chromatography, a shock wave travelling through the column is very demanding to calculate and this will reduce the time step length significantly.

An initial value problem with coupled ordinary differential equations is normally solved by either predictor corrector methods or by Runke-Kutta methods, Lambert (1991). The advantage of predictor corrector methods is that high order can be obtained without the Jacobian, however, if the local error becomes too large the calculating has to be redone from τ=0 with a reduced step length. Runge-Kutta methods does not use information from previous steps to calculate the present step and the local error can be controlled by changing only the current step length. This is a major advantage of the Runge-Kutta methods especially when calculating chromatography where sometimes shock waves are travelling through a column element (requiring a short step length) and at other times nothing is passing through the column element (allowing large time steps). Explicit Runge-Kutta methods are normally not very efficient to handle stiff systems and in these cases a semi-implicit Runge-Kutta method is used. These can be designed with a step length control to vary the step length during the calculation.

3.8.1 Orthogonal Collocation on Finite Elements

The column is subdivided into a number of elements, NE, and each element is solved individually, where the outlet concentration from one element is used as the inlet concentration to the following element as suggested by Michelsen (1994). Each element is solved by orthogonal collocation in the x-direction, Villadsen and Michelsen (1978).

The methods for the two mobile phase mass balances, with/without axial dispersion, can be generalised and also the two particle phase mass balances can be generalised as shown in appendix D “Orthogonal Collocation”.

The easiest way to compare the different approaches are to make a number of simulations and

compare the results.

The column parameters for all these simulations are L=3.76 cm, d_{col}=1.6 cm, ε=0.4, ε_p=0.68, d_p=90 μm, Λ=777 M, and Pe_d=0.6. The parameters for the salt are $D=D_p=10\cdot D_q=1.611\cdot 10^{-9}$ m^2/s, z=1, $\Delta G_0/RT=0.62$, $k_p=10\cdot k_q=76.7\cdot 10^{-6}$ m/s, and $K_D=1$. For the protein the parameters are MW=18.3 kg/mole, $D=73.4\cdot 10^{-12}$ m^2/s, $D_p=39.096\cdot 10^{-12}$ m^2/s, $D_q=16.776\cdot 10^{-12}$ m^2/s, z=2.723, $\Delta G/RT=3.2$, ζ=0, $k_p=2.172\cdot 10^{-6}$m/s, $k_q=0.932\cdot 10^{-6}$ m/s, $K_D=0.165$ and k_f is calculated using the correlation suggested by Ohashi. The flow rate is Q=1 ml/min and the column is equilibrated at c_0=39 mM. 1 g/l of protein is added for 6 seconds with c_0=39 mM and eluted to t=6000 s with c_0=79 mM. All the calculations use the model incl. axial dispersion. These conditions corresponds to the conditions for experiment 200110160941 given in chapter 7 “Lactalbumin and Q Sepharose XL”, with the exception that the the column is equilibrated at a lower salt concentration. The tolerance for the RK method is set to 10^{-6}. The diffusion coefficients inside the particles are calculated using the van Deemter equations for the two models (3-53) and (3-57) as

$$D_p = \frac{k_p R_p}{5} \tag{3-66}$$

The results of the simulations are summarised in table 3.1, and the calculated chromatograms are given in figure 3.2 to 3.8. As seen from table 3.1 using global orthogonal collocation including salt in the calculation and a diffusion model for the particle phase the number of variables rapidly becomes very large, leading to excessive calculation time. The resulting chromatogram for this calculation is given in figure 3.2. From the figure is seen that at large number of steps are required at the start of the calculation, here the protein and salt concentrations are steep leading to the short step length. When the protein gets further into the column, the zone spreading mechanisms make the profile less steep and the step length is increased. Calculating the salt concentration as plug flow reduces the calculation time to app. 1/5 of the previous calculation time, no. 2. The system of equations is, however, still large and also in this calculation a short step length at the calculation start is required. When the system is solved each element at a time, no. 3, the number of variables is significantly reduced and the calculation time is reduced significantly too. In figure 3.4 is seen that the step length from the last element has got another structure than for global collocation, the steps are here located around the peak. The reason for this is that the salt is not included in the mass balances, and initially no protein enters the last element, the step length is therefore increased. When protein

enters the last element, the step length is reduced, and when the protein leaves, the element the step length is increased again. This is not possible with an OCFE-method where the matrix in on diagonal form, as suggested by Rice *et al.* (1995) p. 603-615.

The same calculations have been made for the linear driving force approximation and are also given in table 3.1. Due to the smaller system of equations this is faster to solve, but similar results are seen. Reducing the tolerance to 1/10 approximately doubles the calculation time. The calculation time may seem to be insignificant since this is only taking a few minutes. However, it should be kept in mind that the calculations here only includes one protein. Secondly, a SMB-plant with 8 columns and 3 cycles required $3 \cdot 8^2 = 192$ column calculations. With a calculation time of 204 s/column, for one component, this will require 11 h, whereas the OCFE method with linear driving force approximation and no salt included only requires 1½ min.

No.	***NE***	***N***	***LDF/DIF***	***NP***	***salt***	n_{var}	n_{steps}	t_{calc} [s]
1	1	30	DIF	3	Incl.	497	2156	204
2	1	30	DIF	3	Excl.	249	2462	37
3	10	3	DIF	3	Excl.	33	544	2
4	1	30	LDF	-	Incl.	249	1994	26
5	1	30	LDF	-	Excl.	125	1767	5
6	10	3	LDF	-	Excl.	17	315	½

Table 3.1 Comparison of calculations. NE is the number of elements in the column, N, is the number of inner collocation points in each element, LDF=linear driving force approximation, DIF=Diffusion model, NP is the number of inner collocation points in the particle. The column salt indicates if salt is included in the differential mass balance (incl.) or calculated as plug flow (excl.), n_{var} is the number of variables, n_{steps} is the number of time steps taken, and t_{calc} is the calculation time. When OCFE is used the number of steps refers to the number of steps for the last element.

Figure 3.8 shows a comparison of the calculated chromatograms from table 3.1. All the peaks using the diffusion model coincides, and all the peaks using the linear driving force approximation also coincides. Solving each element at a time therefore reduces the calculation time significantly but will only influence the results insignificantly.

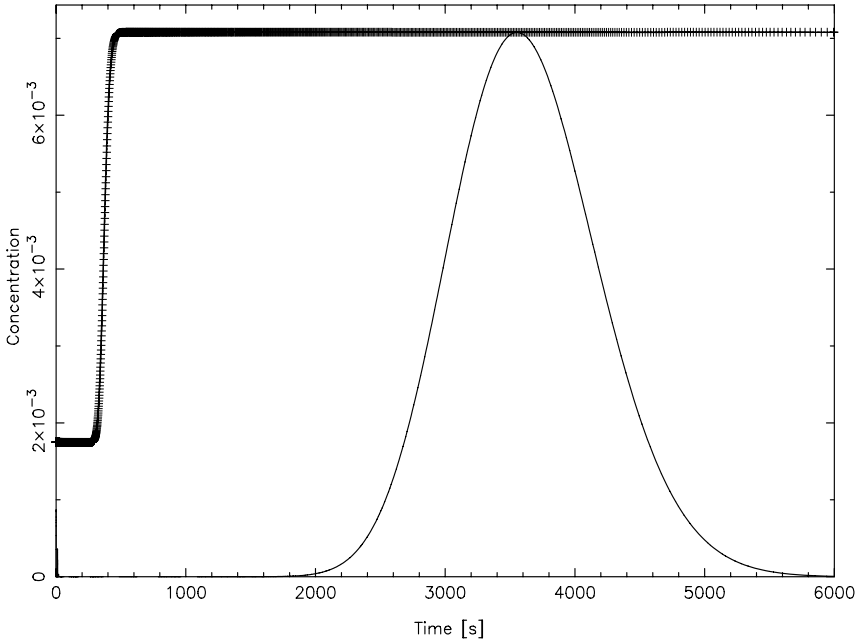

Figure 3.2 Simulation no. 1. Global orthogonal collocation incl. mass balance for salt and with diffusion model in the particles. The salt profile is given as the line with +. Each + on the salt profile indicates a step, and the step length can be seen from this.

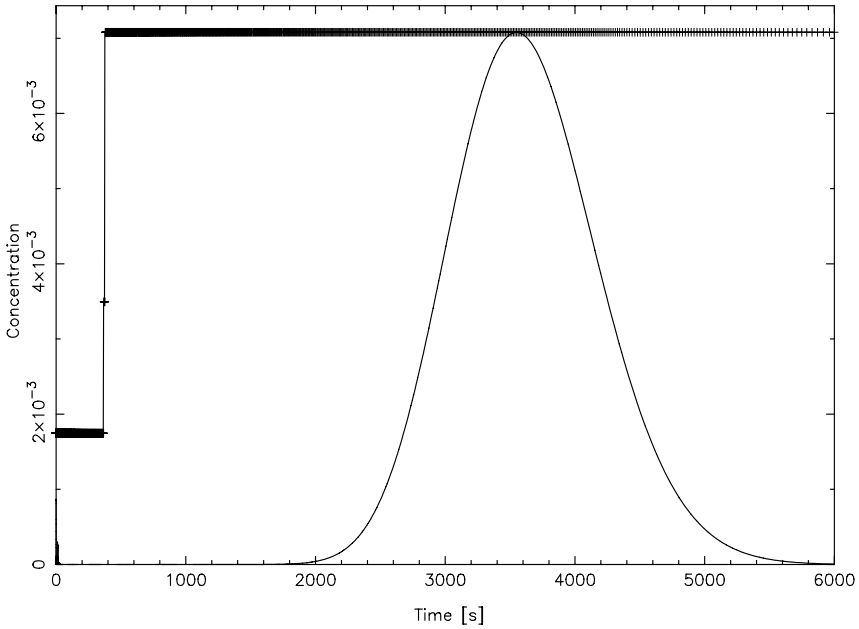

Figure 3.3 Simulation no. 2. Global orthogonal collocation excl. mass balance for salt and with diffusion model in the particles.

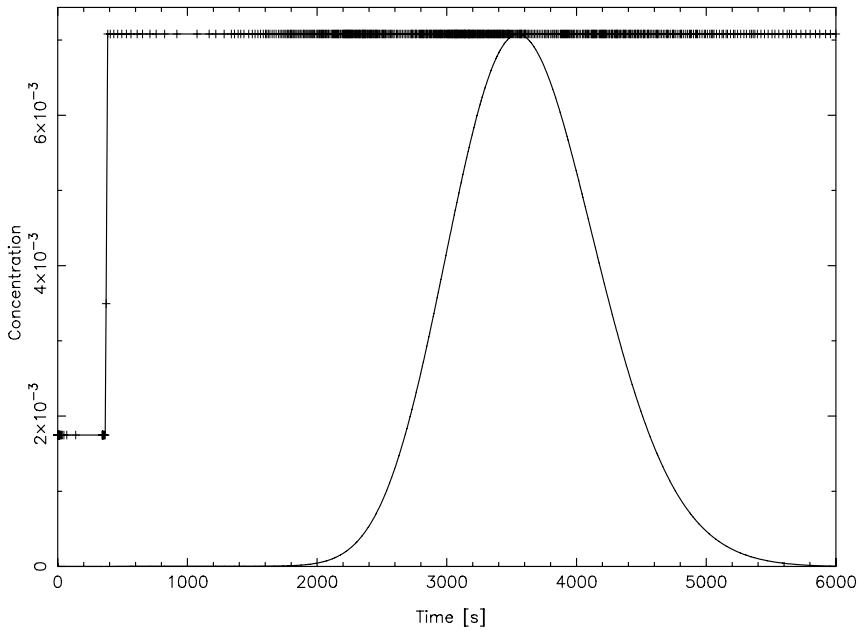

Figure 3.4 Simulation no. 3. OCFE excl. mass balance for salt and with diffusion model in the particles.

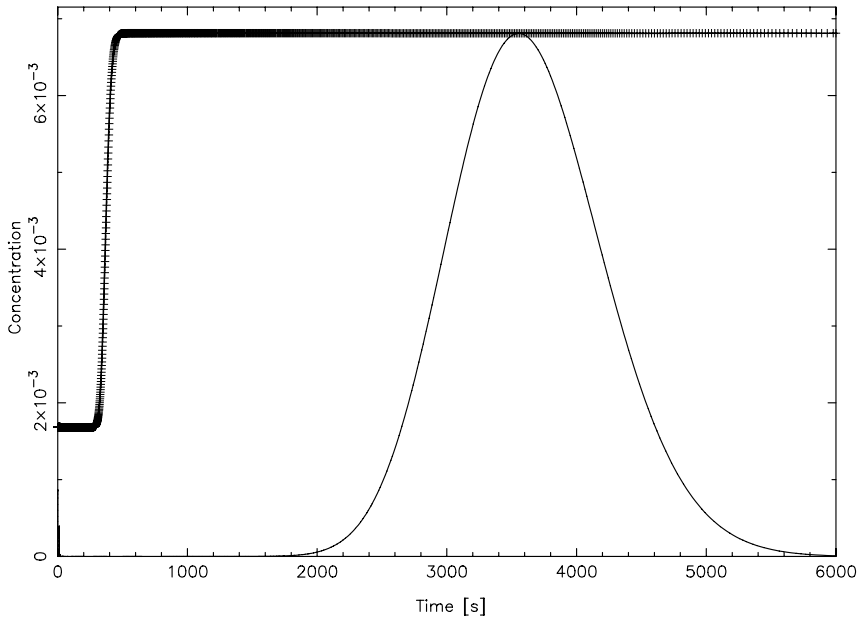

Figure 3.5 Simulation no. 4. Global orthogonal collocation incl. mass balance for salt and with linear driving force model in the particles.

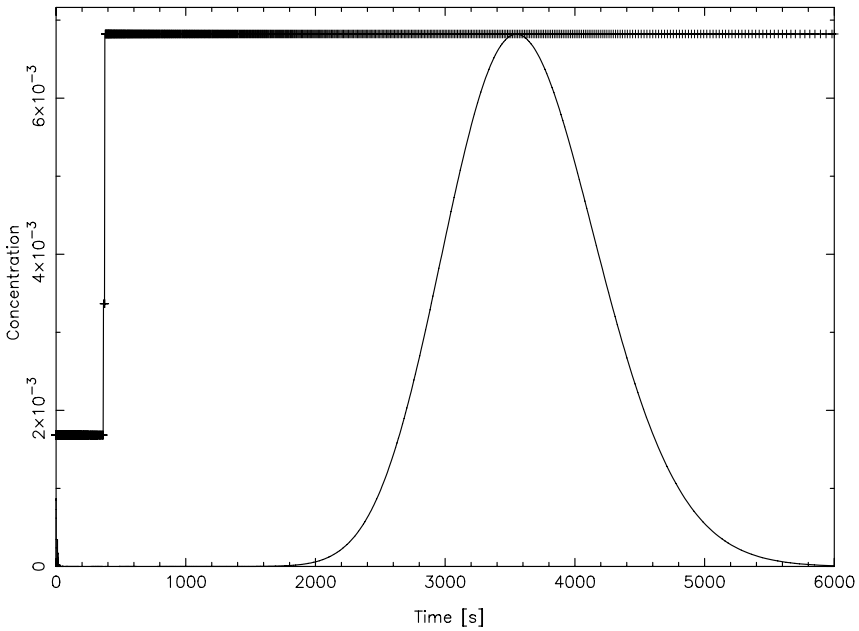

Figure 3.6 Simulation no. 5. OCFE excl. mass balance for salt and with linear driving force model in the particles.

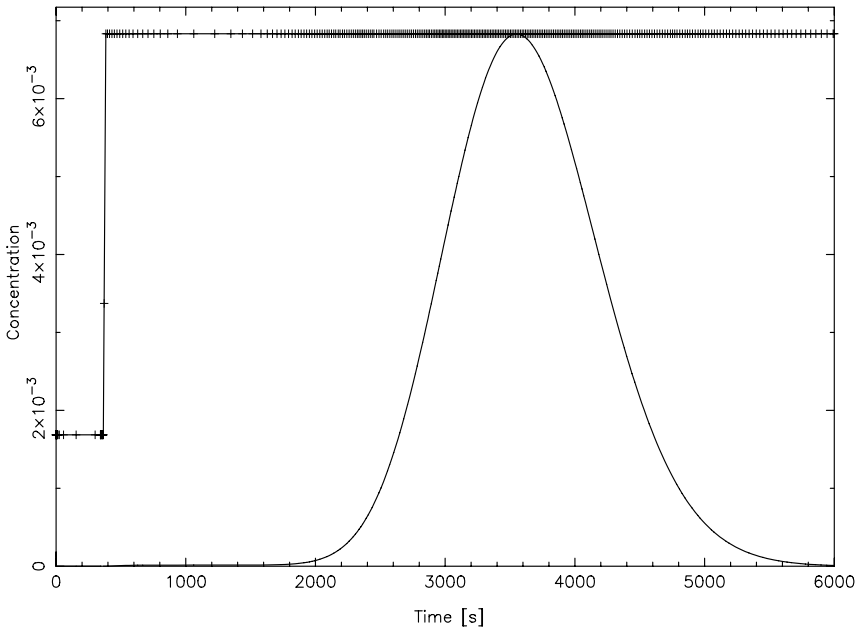

Figure 3.7 Simulation no. 6 OCFE excl. mass balance for salt and with linear driving force model in the particles.

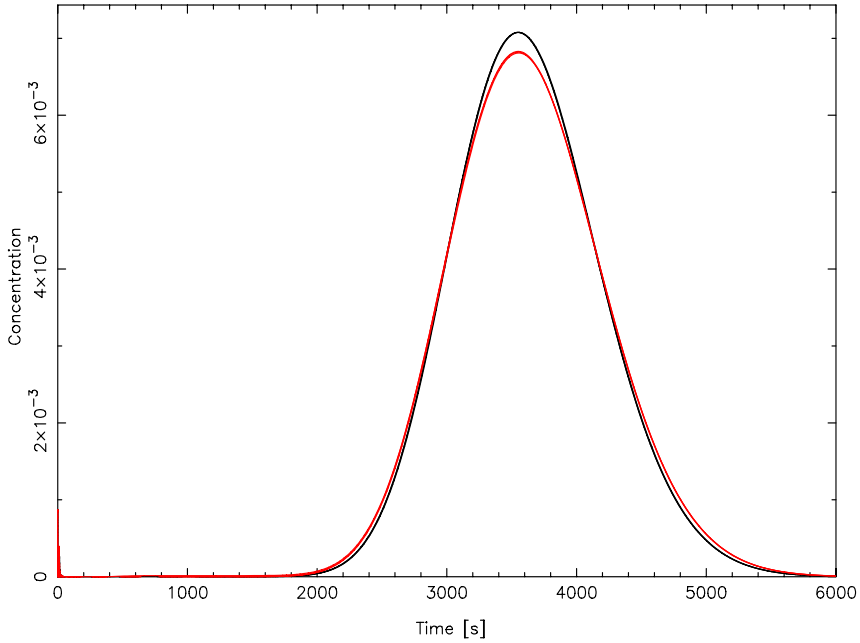

Figure 3.8 Comparison of resulting peaks from the simulations in table 3.1. The three models using a diffusion model inside the particles lie on top of each other and are the highest/black peak. The lower/red peak are the results using the LDF approximation.

3.9 Craig Model

Instead of solving the system of partial differential equation, a plate model is sometimes used. The Craig model is a stage model where the column is divided into a number of elements with equilibrium in each element. This approach is comparable to stage models in distillation/extraction. The Craig model can be considered as a number of glasses each containing resin and mobile phase. The mobile phase from the last element is collected as the outlet stream. Hereafter the mobile phase in the second last element is poured into the last element and equilibrium is established in the last element. This is repeated for all the elements in the column and finally the first element is fed with the feed stream and equilibrium is also established here. This is repeated until the entire feed stream has been fed to the column and a resulting chromatogram is obtained from the outlet stream.

Since the Craig model is a stage model, mass transfer resistance and axial dispersion does not enter the model directly but influence the number of stages in the column. In a stage model equilibrium is assumed and the number of variables (and equations) corresponds to the number of components. The equations to be solved is the mass balance for each element which must be iterated until convergence.

$$n_{tot}=\left(\epsilon+(1-\epsilon)\epsilon_p K_D\right)c+(1-\epsilon)\epsilon_p K_D q \tag{3-67}$$

Where n_{tot} is the total amount of protein in the element. n_{tot} for element no. i can be calculated from the total amount in on the stage before equilibration.

$$n_{tot}=\epsilon\, c^{i-1}+(1-\epsilon)\epsilon_p K_D(c^i+q^i) \tag{3-68}$$

The system of equations is small and the LU-factorisation is most likely not the time consuming step in the calculation.

With the SMA-formalism using C as the independent variables Q is found by iterations. In this way two iteration inside each other (SMA inside the mass balance) is obtained which is normally not desirable. A better choice is then to formulate the SMA-formalism by C for the salt and Q for the proteins, in this way the SMA-formalism is explicitly given, leading to faster convergence, see chapter 2.4 “SMA with Alternative Independent Variables”.

The SMA-formalism has a number of drawbacks like other stage models, e.g. will the plate height for different components not necessarily be the same, which cannot be taken into account by the Craig model.

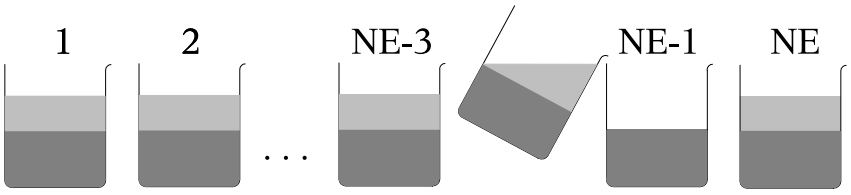

Figure 3.9 The Craig model can be considered as a number of glasses/stages where the mobile phase is poured from one glass to the following.

3.1 Summary

A number of different models have been made, these take axial dispersion, mass transfer resistance in the film layer around the particle, and mass transfer resistance inside the particles into account. This is necessary since proteins are large molecules with low diffusion coefficients. All the models assume ideal solutions.

Two models for the pore phase have been suggested these are Fick's diffusion and a linear driving force approximation.

The van Deemter equation for the different models have been derived, these can be used to determine parameters for the models. From the van Deemter equation is also suggested a method to eliminate the axial dispersion term for the linear driving force approximation.
For the linear isotherm the fastest method to solve the equations are by Fast Fourier Transform, which has been implemented. The Fast Fourier Transform can be used to calculate the resulting chromatogram, and this method can be used to compare the results of the model simplifications.
For a non-linear isotherm the models can be solved by using orthogonal collocation on finite elements, this is more accurate than finite difference time domain methods. With an open boundary condition the elements can be solved one at a time and the calculation time can be reduced significantly.

4. Zone Spreading Mechanisms

After having set up the model the parameters have to be determined. Some of the zone spreading parameters are taken from correlations whereas others are fitted parameters.
Many unit operations involve flow in packed beds and intensive investigations have been made for these processes. Correlations have been developed and some of the parameters can be determined from these correlations. In this way the parameters will be in line with previous investigations and reduce the number of fitted parameters.
With the current model the zone spreading mechanisms has two different origins, the axial dispersion and the mass transfer resistance.
In previous work the axial dispersion has been set to a constant (Pedersen, 2003, p. 92), and all mass transfer coefficients have been determined by fitting these. However, some parameters found by this approach varies by more than a factor of 100 for proteins of similar size, Pedersen p. 97. The film layer mass transfer coefficient, k_f, varies up to a factor 8.000 by changing the fit, Pedersen p. 98. This huge variation of the fitted parameters can be caused by a strong correlation of the different parameters or fitting of parameters with little or no impact of the resulting peak width.

4.1 Axial Dispersion

From the van Deemter equation (3-53), the axial dispersion term is seen to be independent of the flow rate, whereas the second term increases with increasing flow rate. The intercept at $v_i=0$ is equal to $2/Pe_d$.
Cluff *et.al.* (1976) collected more than 750 data points and plotted these against the reduced velocity, ν, given as

$$\nu = \frac{v_i d_p}{D_m} = Re_i \cdot Sc \tag{4-1}$$

These data, however scattered, seems to be a weak function of the reduced flow rate. From these investigations Yamamoto (1988) p. 165, concluded that the Pe_d-number is in the order of 1-2. However, on p. 170 Yamamoto also concludes "*...; in other words, 0.5-1 can be used as the Pe_d number under the usual conditions of ion exchange chromatography of proteins.*" which is not in line with the first statement.
Guiochon *et al.* (1994), p. 148, suggests the correlation by Chung *et al.* (1968)

$$Pe_L = \frac{L}{\epsilon d_p}\left(0.2 + 0.011\left(Re\,\epsilon\right)^{0.48}\right) \tag{4-2}$$

Corresponding to

$$Pe_d = Pe_L \frac{d_p}{L} = \frac{0.2}{\epsilon} + \frac{0.011}{\epsilon}(Re\,\epsilon)^{0.48} \qquad (4\text{-}3)$$

The Reynolds number is usually low for chromatography (Re<0.1, Guiochon *et al.*, 1994, p. 149) and the first term is the dominating leading to a Pe_d-number almost independent of flow rate and in the order of 0.5.

Carta (Perry, 1997), p. 16-22 recommends "*... As such, the axial dispersion coefficient is best determined experimentally for each specific contactor*". This approach will be used in the present work since the intersect at v_i=0 can easily be found. Bearing in mind that a value around 0.5 is expected.

4.2 Correlations for Film Layer Mass Transfer

The mass transfer coefficient for the film layer has been extensively investigated, and a large number of correlations have been suggested. An overview of these can be found in Perry's Chemical Engineer's Handbook (1997) p. 5-72 – 5-73. Obtaining k_f from a correlation rather than a fitted value is preferred to reduce the number of fitted parameters. It can be shown that for a single particle in a stagnant liquid the lower limit of the Sherwood number is 2. It is hard to believe a Sherwood number below this limit in a packed column with forced convection.

4.2.1 Wilson and Geankoplis

One of the most widely used correlations (Guiochon *et al.* (1994) p.147, Yamamoto *et al.* (1998) p. 68, Hansen (2000) p. 23, and Jansen *et al.* (1996)) for ion exchange chromatography is the correlation suggested by Wilson and Geankoplis, (1996).

$$Sh = \frac{1.09}{\epsilon} Re^{1/3} \cdot Sc^{1/3} \qquad 0.0015 < \mathrm{Re} < 55 \qquad (4\text{-}4)$$

Where Sh is Sherwood number $Sh = \frac{k_f d_p}{D_m}$, Sc is Schmidt number $Sc = \frac{\mu}{\rho D_m}$ and Re is

Reynolds number based on superficial velocity $Re = \frac{\rho v_s d_p}{\mu}$

4.2.2 Kataoka

Kataoka *et al.* (1972) has suggested an equation very similar to the Wilson and Geankoplis equation. However, using a larger set of experimental data.

$$Sh = 1.85\left(\frac{1-\epsilon}{\epsilon}\right)^{1/3} Re^{1/3} Sc^{1/3} \qquad \text{Re}<40 \tag{4-5}$$

4.2.3 Carberry

Hansen (2000) p. 22 has previously used the correlation suggested by Carberry (1960)

$$k_f = 1.15\, v_i\, Re_i^{-1/2} Sc^{-2/3} \tag{4-6}$$

Re_i is Reynolds number based on the interstitial velocity

$$Re_i = \frac{\rho v_i d_p}{\mu} \qquad \text{Re}_i<1000 \tag{4-7}$$

This expression can be rewritten to

$$Sh = 1.15\left(\frac{Re}{\epsilon}\right)^{1/2} \cdot Sc^{1/3} \tag{4-8}$$

4.2.4 Ohashi

Ohashi *et. al.* (1981) have in a work investigated the mass transfer for single particles and packed beds. This work was sponsored by Mitsubishi Chemical Industries Ltd., who also supplied ion exchange resin. The work was therefore possibly aiming at chromatography.
A large number of experimental values was compared with the correlation

$$Sh = 2 + 0.51\left(\frac{E^{1/3} d_p^{4/3} \rho}{\mu}\right)^{0.60} Sc^{1/3} \tag{4-9}$$

where E is the energy dissipation rate per unit mass of fluid [m^2/s^3]

$$E = \left[\frac{50(1-\epsilon) C_{D0}}{\epsilon}\right]\left(\frac{v_s^3}{d_p}\right) \tag{4-10}$$

For various Reynolds number the drag coefficient, C_{D0}, for a single particle can be calculated from

$$C_{D0} = A \cdot Re^{-m} \tag{4-11}$$

where the values for A and m are given in table 4.1 below
The correlation is valid for Reynolds numbers in the range $10^{-3} < Re < 10^3$, for Schmidt numbers in the range $505 < Sc < 70600$ and for $0.2 < \frac{E^{1/3} d_p^{4/3} \rho}{\mu} < 4600$

Re	*A*	*m*
10^{-3} to 5.8	24	1
5.8 to 500	10	0.5
500 to 1000	0.44	0

Table 4.1 Parameter for calculating single particle drag coefficient.

4.2.5 Comparison of Correlations

The correlations above have been compared. The parameters for the calculations are given in figure 4.1. The parameters are typical parameters from previous experiments with the Source 30Q resin (Pedersen, 2003).

Under these conditions the Reynolds number is in the range from $3 \cdot 10^{-3}$ to $7 \cdot 10^{-3}$. This applies well with Re<0.1 as previously mentioned. The results from the calculations are given in figure 4.1.

As seen from the figure there is a reasonable agreement with the two correlations by Wilson and Geankoplis and the one by Ohashi. However, the correlation by Carberry gives significantly lower results, in addition it is seen that the Sherwood number approaches 2 (the limit in a stagnant liquid) at Q=0.5 ml/min. The slope of the two curves for Wilson and Geankoplis and Ohashi are both 1/3 whereas the slope for the Carberry correlation is ½. A closer look at the Carberry correlation shown that no data points exist below Re_i<0.1, and only a few values with Re<0.5. Carta (Perry, 1997, p. 16-21) recommends only to use this correlation for Re>1. Kataoka further writes "*However, in the low Reynolds number region, it has been reported that previous experimental data deviate from Carberry's equation.*".

From this it is concluded that the Carberry correlation is not well suited for ion exchange chromatography.

An excellent agreement between the Ohashi and the Kataoka correlations are also found. Whereas the Wilson/Geankoplis gives slightly higher values of k_f. Both the Ohashi and the Kataoka correlations are based on much larger data sets than the Willson/Geankopolis correlation.

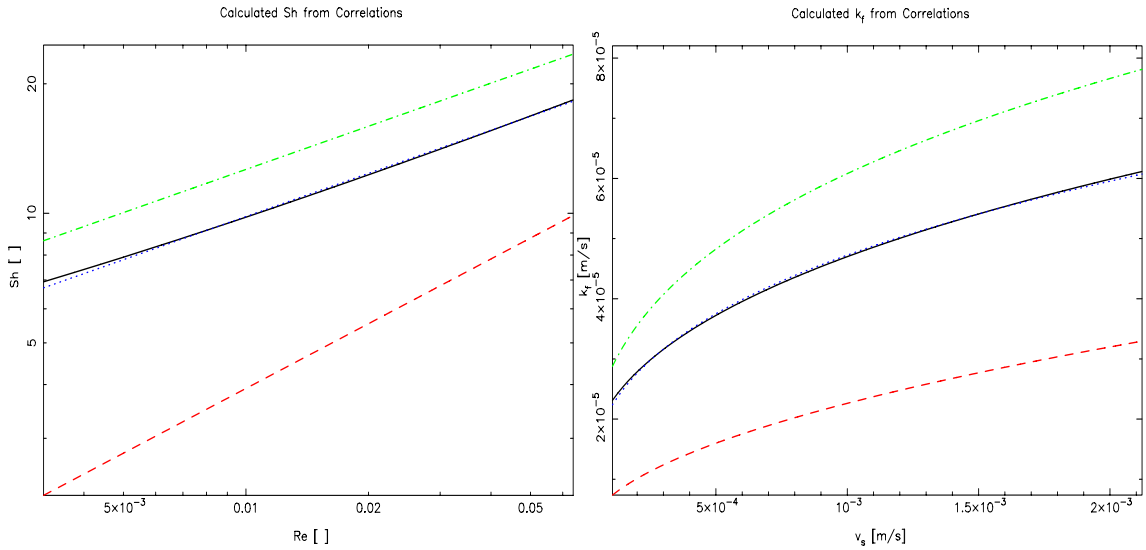

Figure 4.1 Sherwood number as a function of Reynolds number and the calculated mass transfer coefficient for the film layer as a function of the linear velocity. Legends (green dash dot) Wilson and Geankoplis, (full black) Ohashi, (red dashed) Carberry, and (blue dot) Kataoka. Parameters for the calculations ε=0.4, $\mu=10^{-3}$ Pa s, $\rho=10^{3}$ kg/m^3, $d_p=30\cdot10^{-6}$ m, $D_m=10^{-10}$ m^2/s and with a flow rate from 0.5 ml/min to 10 ml/min, d_{col}=1cm.

4.3 Particle Side Mass Transfer Parameters

Having determined the Pe_d-number and k_f only the internal mass transfer coefficients k_p and k_q have to be determined. These parameters are fitted to the experimental values.

From the van Deemter equation (3-53) it is seen that k_p is dominating when $k_p > A\cdot k_q$ and k_q is dominating when $k_p < A\cdot k_q$. The two values to be determined are dominating in two different regimes and it is unlikely that they are strongly correlated.

4.4 Summary

The Pe_d-number is preferably determined from each column experimentally. If an experimental value of Pe_d is not available, a value of 0.5 seems reasonable.

The correlation suggested by Carberry is not recommended for ion exchange chromatography, due to the low Reynolds number. The preferred correlations are those suggested by Kataoka or Ohashi and the Willson and Geankoplis correlation. The Willson and Geankoplis correlation gives somehow higher results but is widely used in ion exchange chromatography.

The two remaining parameters for mass transport inside the particle k_p and k_q or D_p and D_q will have to be determined experimentally. These can be determined from pulse experiments using the van Deemter equation.

5. Determination of Model Parameters

The current model contains a number of parameters to be determined, beside the equilibrium, mass transfer, and axial dispersion parameters, these are the column volume, V_{col}, the interstitial porosity, ε, the particle porosity, ε_p, the concentration of the binding charges, Λ, and the steric exclusion factors for the different proteins, K_D.

The column volume is easily determined from the diameter and the height of the column, for pre-packed columns these informations are specified by the vendor.

The first two parameters to determine are the column parameters, the total porosity, and the binding concentration, hereafter follows the parameters for the proteins at non-binding conditions. The equilibrium and mass transfer parameters are determined as described in the following chapters.

5.1 Total Porosity

The total column porosity can be calculated if the density of the dry resin, ρ_{res}, and the amount of dry resin in the column, m_{res}, is known

$$\epsilon_t = \epsilon + (1-\epsilon)\epsilon_p = 1 - \frac{m_{res}}{\rho_{res} \cdot V_{col}} \tag{5-1}$$

The total porosity can also be found from a pulse experiment at non-binding conditions (A=0) and with a molecule sufficiently small to enter all the pores (K_D=1). This results in

$$\epsilon_t = \frac{V_r}{V_{col}} \tag{5-2}$$

Where the V_r is the retention volume corrected with the dead volume ($V_r = M'_1 - DV_{col}$).

From eq. (5-1) and (5-2) is seen that the particle and interstitial porosity cannot be individually determined from these experiments. One of the porosities must be specified and the other can be calculated from this. An experimental procedure to determine the total porosity is given in appendix E “Determination of Total Column Porosity”.

5.2 Total Binding Capacity

The columns total ion exchange capacity, λ, is used to calculate the concentration of charges in the pores, Λ. Additionally, it can be used to scale the amount of resin in a column.

Often the resins are compressible, and this is not taken into account by scaling on basis of the column volume. The columns used for breakthrough experiments are often very small and the relative error on the column height correspondingly large. A better way of scaling experiments could be to scale these on the total column binding capacity.

From previous studies (Pedersen 2003, Kidal 2001) the total column binding capacity have been determined in two different ways, from nitrate determinations or from titrations. In both methods the resin is in a packed column.

In addition to these two methods a third method using batch titration has been tested by Pedersen.

Batch experiments have also been described by Helfferich (1995), p.81-84. The titrations have been made both with and without salt in the solution. In batch experiments competing ions can be present at the same time and the influence of competing ions can have an effect on the determined capacity, Helfferich (1995). In a packed column the desorbed ions will be washed out of the column, and the effect of competing ions can be avoided. Therefore only packed bed experiments are considered here.

The total capacity of an ion exchanger can according to Helfferich (1995, p.78) be divided into two different capacities the "ion exchange capacity" and the "sorption capacity". The sum of these two capacities is also called the "overall sorption capacity". The ion exchange capacity is the number of charged groups in the ion exchanger. The sorption capacity is the capacity of ions bound by other means than ion exchange and the ions in the pores. Sorbed molecules can be washed out of the pores by washing the column with pure water (Helfferich 1995 p. 91). The ion exchange capacity is given by the amount of fixed charges and must be balanced by counter ions. This is "*essentially constant, i.e., independent of the particle size and shape and of the nature of the counter ion.*" (Helfferich, 1995, p. 72).

This is in contradiction to the previous findings of Pedersen (2003, p. 26) who found that the nitrate capacity usually is higher than the capacity found by titration. Helfferich describes how titration experiments are made for a cation exchanger and that similar results will be obtained for the conversion of the ion exchanger from H^+ form to Na^+ form and from Na^+ form to H^+ form, Helfferich p. 91. Helfferich p. 91, further writes for a strong anion exchanger that "*Capacity determinations by reconversion to the OH^- form are impractical because an inconveniently large excess of NaOH would be required.*". The differences between a strong cation and anion exchanger should be stressed.

How strong competing ions bind to the resin is given by the selectivity. The selectivity is defined as

$$K_{a,b} = \frac{q_a \, y_b}{q_b \, y_a} \tag{5-3}$$

The selectivity depends on the concentration of the components and is usually given for dilute solutions.

Anderson (Schweitzer, 1979, p. 1-369) gives the following selectivity for a strong cation exchanger $K_{H,Li}$ =1.3 and $K_{Na,Li}$ =2. The selectivity $K_{Na,H}$ is in the order of one and that the conversion from the Na^+-form to the H^+-form and back gives identical results as described by Helfferich seems likely.

Helfferich, p. 168, gives the following selectivity sequence for anion exchangers

Citrate > SO_4^{2-} > oxalate > I^- > NO_3^- > CrO_4^{2-} > Br^- > SCN^- > Cl^- > formate > acetate > F^- (5-4)

Hydroxide falls between acetate and fluoride for strong-base resin and farther to the left for weak-base resins.

Anderson (Schweitzer, 1979, p. 1-370) gives the following selectivity of $K_{NO3,\,Cl}$=4 and $K_{OH,\,Cl}$=0.05-0.07 (type I) and $K_{OH,Cl}$=0.65 (type II). Type I and type II are both strong anion exchangers containing quartenary ammonium groups, figure 5.1. As can be seen from the selectivities these depend strongly on the structure of the quartinary ammonium group. It is seen that the Cl^-/OH^--selectivity can be significantly larger for the anion exchangers compared to H^+/Na^+-selectivity for the cations exchangers, leading to an impractical large excess of hydroxide to replace nitrate as concluded by Helfferich.

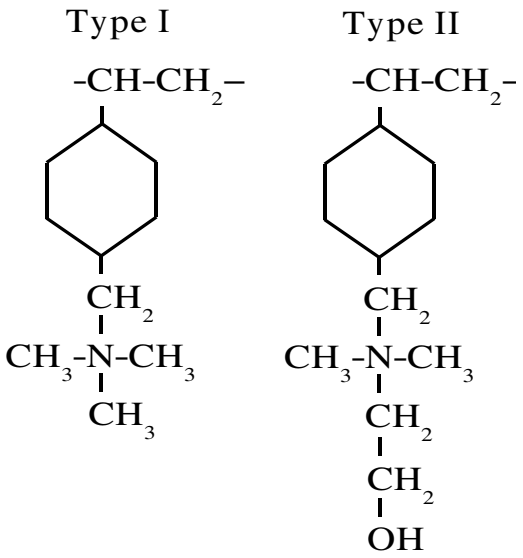

Figure 5.1 Active groups of type I and type II resins. ref: Anderson (Schweitzer, p. 1-387).

For all the experiments described below a column packed with Ceramic Q Hyper D, with d_{col}=16 mm and approximately L≈7 mm is used.

5.2.1 Hydroxide Capacity

To investigate why the capacity from titration is lower than the nitrate capacity four experiments were made. The main purpose of the experiments was to follow the displacement of nitrate in the column with hydroxide. Normally, it is the displacement of chloride with hydroxide that is interesting. However, nitrate can be detected with an UV-detector. This can be considered to be a conservative approach, if hydroxide can replace nitrate it will also be able to replace chloride.

In the experiments the column was fed with chloride and the UV-detector was reset. Hereafter the column was fed with nitrate to saturate the column with nitrate. The column was washed with water before the 1 M NaOH was fed to the column to displace the nitrate. Finally 1 M NaCl was fed to the column to see if all nitrate was washed out of the column. An example of the program is given in program F.1 in appendix F “Column Capacity”.

If a UV-signal appears when chloride is added at the end of the run, nitrate has been displaced with chloride, indicating that hydroxide was unable to replace nitrate.

A summary of the experiments are given in table 5.1.

rundate	***Q***	***Col in/off***	V_{OH^-}
YYYYMMDDhhmm	[ml/min]		[ml]
200301061435	1	+	100
200301061832	0.5	-	100
200301062302	1	+	50
200301070208	1	+	25

Table 5.1 Experiments to determine the displacement of nitrate with hydroxide. The following volumes were used for all the experiments V_{Cl}=35 ml, V_{NO3}=10 ml, V_{H2O}=10 ml, V_{Cl}=10 ml (volumes with column in line). The "col in/off" column indicates if the column was bypassed (+) or not (-) when introducing a new feed.

With a column volume of 1.34 ml the hydroxide volumes are almost 100 times the column volume. In addition to this the flow rate is low, to have sufficiently time for mass transport. Even under these conditions it is seen that the resulting chromatograms have a nitrate peak when chloride is fed to the column. From this it is concluded that hydroxide is not capable of replacing all the nitrate bound to the ion exchanger. It is doubtful whether hydroxide will be able to replace chloride, and the column is on hydroxide form in the titration experiments. This may explain the discrepancy between the nitrate and hydroxide capacity, where the latter is always found to be the lowest.

The resulting chromatograms for the two experiments with a hydroxide feed volume of 100 ml is given in figure 5.2.

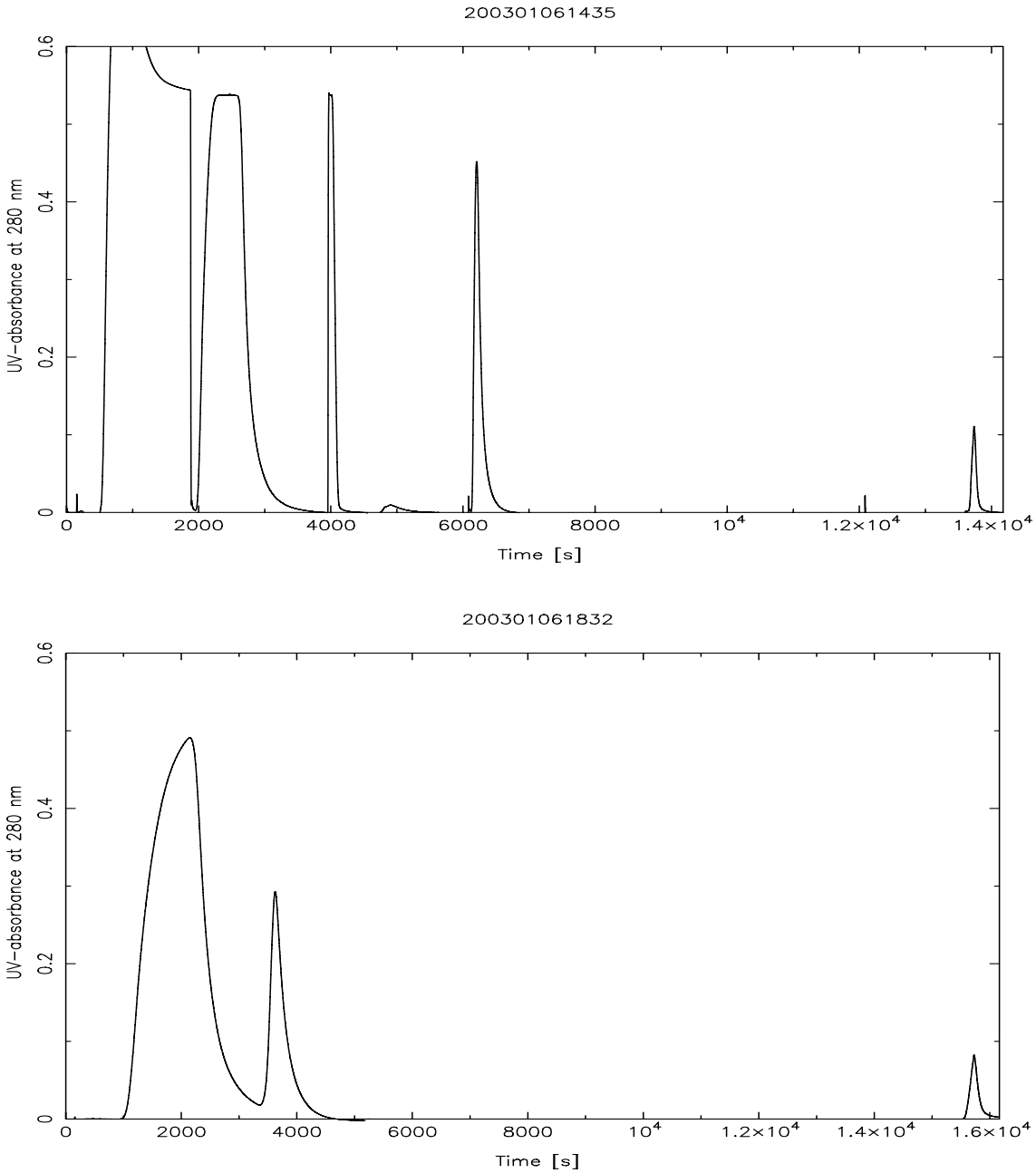

Figure 5.2 Resulting chromatograms. Top: The first peak (t=4000 s) after the wide nitrate feed peaks is the washing peak. The second peak (t=6000s) is the displacement peak where OH^- displace NO_3^-. The last peak (t=14000 s) is the displacement of the remaining NO_3^- with Cl^-.

Bottom: The column has been in-line for the entire experiment, due to the low flow rate. Therefore the nitrate feed peak and the washing peak cannot be separated. The peak at t=4000 s is the displacement of NO_3^- with OH^- and the peak at t=16000 s is the displacement of the remaining NO_3^- with Cl^-.

Comment: The nitrate was changed before the first experiment and the tubing was not purged properly with the new nitrate, this causes the "overshoot" of the first nitrate peak (t=1000 s) in experiment 200301061435 . The column was bypassed and this has no impact on the results.

5.2.2 Nitrate Capacity

The ion exchange capacity measured using hydroxide is difficult to measure, and the nitrate capacity is preferred since the nitrate/chloride selectivity is closer to one and the same problems as above would not be expected.

Some problems still need to be addressed. As mentioned above the total uptake of ions is the ion exchange capacity and the sorption capacity. The ion exchange capacity is essentially constant and the sorption capacity can be washed out. In the first series the nitrate concentration was changed to see how this influenced the measured capacity, table 5.2. The purpose of the second series was to investigate the washout of the sorption capacity, table 5.3. The experiments are performed in the same way as the breakthrough curves with proteins, appendix I "Breakthrough Experiments". The nitrate is fed to the column, the nitrate from the mobile phase is washed out and the bound nitrate is displaced with salt. The program for these experiments are given in program F.2 in appendix F "Column Capacity". 12 experiments were made in total and these are listed in table 5.2. In the first six experiments the washing volume was 15 ml and this was doubled for the last six experiments.

Rundate [YYYYMMDDhhmm]	C_{KNO3} [M]	***UV-280 nm***	***Adsorption*** [mmole]	***Wash*** [mmole]	***Desorption*** [mmole]
200212171628	0.0465	0.085	0.600	0.106	0.521
200212171706	0.1380	0.255	0.843	0.260	0.547
200212171744	0.2295	0.430	0.929	0.440	0.552
200212171822	0.3210	0.594	1.093	0.609	0.556
200212171900	0.4125	0.756	1.251	0.783	0.558
200212171938	0.5000	0.906	1.399	0.942	0.558
200212191703	0.0465	0.083	0.589	0.094	0.527
200212191756	0.1380	0.257	0.798	0.278	0.559
200212200943	0.2295	0.409	0.981	0.435	0.540
200212201036	0.3210	0.572	1.119	0.635	0.562
200212201129	0.4125	0.748	1.242	0.807	0.563
200212201222	0.5000	0.904	1.382	0.977	0.568

Table 5.2 Measured data for determination of total column capacity using nitrate. The values are plotted in figure 5.4. The first six data sets use 15 ml washing volume and the last six use 30 ml washing volume. The first column is the rundate for the experiment, the second column contains the nitrate concentration, the third the UV-absorbance when the column is bypassed. The three last column contains the adsorbed amount, the amount washed out of the column and the desorbed amount of nitrate. The adsorbed amount ought to be equal to sum of the washed and the desorbed amount.

It has previously been showed (Kidal, 2001) that the area of the washout peak is a linear function of the concentration in the column. The area of the washing peak is shown in figure 5.3. The slope of the fitted line is 1.895 ml, this volume corresponds to the dead volume, the interstitial volume, and if nitrate is washed out of the pores also the pore volume. In figure 5.4 is shown the desorbed amount of the nitrate as a function of the nitrate concentration. It is seen that at low nitrate concentrations the desorbed amount seems to be lower, the reason for this has not been found. When the experiments were repeated with a higher washing volume, the capacity were a little higher that whan was observed in the first six experiments.
For the differential columns, see chapter 8.1 “Differential Column Breakthrough Curves”, it turned out to be impossible to determine the nitrate capacity. To investigate if nitrate could be washed out of the column a series of washing experiments were made where the column was saturated with nitrate and hereafter washed with 100 ml of ultra pure water to see if the nitrate could be washed out of the column. The experiments are tabulated in table 5.3. An exponential washout of the column was assumed

$$C_{out}(V) = C_0 \cdot 10^{-\alpha V} \tag{5-5}$$

Where C_{out} is the outlet nitrate concentration from the column and C_0 is the pre-exponential factor.

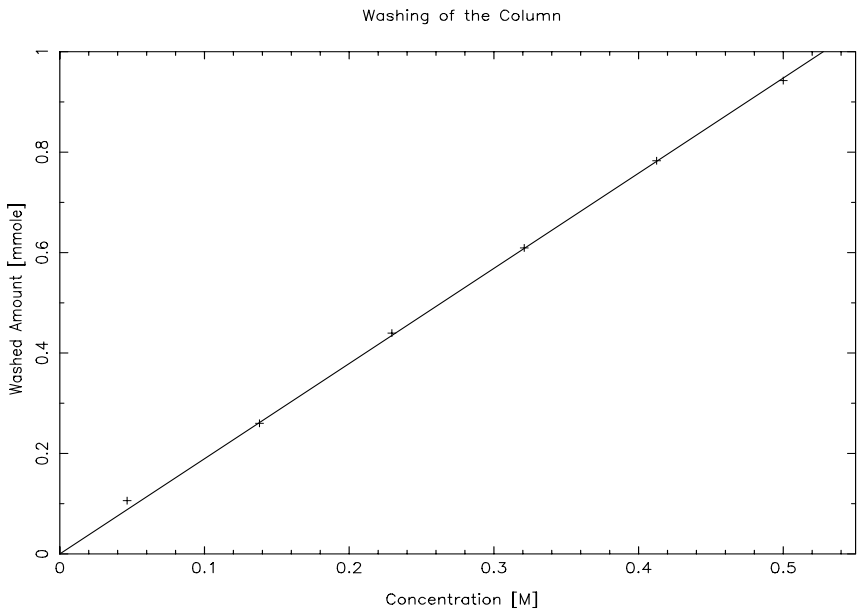

Figure 5.3 The area of the washing peak is a linear function of the nitrate concentration for the first six experiments in table 5.2. The slope of the fitted line is 1.895 ml.

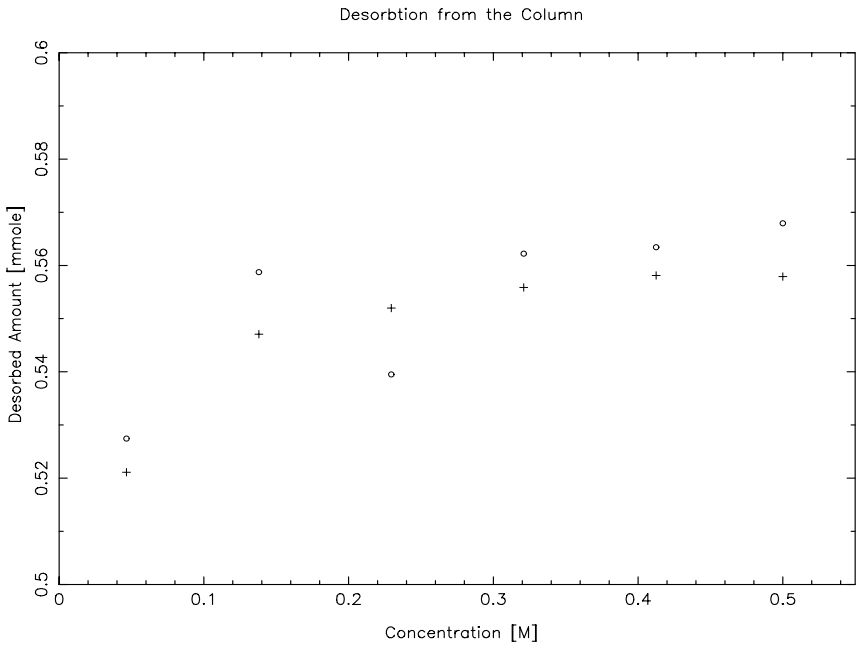

Figure 5.4 Desorbed amount of nitrate, as a function of the nitrate concentration. It is seen that at higher nitrate concentrations, the nitrate capacity increases. Legends + 15 ml washing volume, o 30 ml washing volume.

The remaining nitrate in the column is then given as

$$n(V)=\int_{V}^{\infty} C_{out}(v)\,dv=\frac{C_0}{\ln(10)\cdot\alpha}\cdot 10^{-\alpha V}=n_0\cdot 10^{-\alpha V} \tag{5-6}$$

The concentrations are very low during the washout and it is difficult to distinguish these from the the baseline. The outlet nitrate concentration is shown in figure 5.5, from this it is clearly seen that the nitrate concentration decreases. The correlation coefficient for UV-signal in the last 5 ml of the washing period also showed that the UV-signal is decreasing, table 5.3, indicating that nitrate is washed out of the column (a few correlation coefficients are close to zero).

Subtracting the baseline (the baseline is calculated as the average UV-signal in the last minute of the washing period) from the outlet concentration an exponential decay is clearly seen, figure 5.6. Since nitrate is still washed out of the column after a 100 ml washing volume the baseline will be lower and only a small modification of the baseline will change the remaining nitrate content to an exponential decay in the entire interval, figure 5.7. The outlet concentration will have the same exponential decay, figure 5.8.

The baseline offset, c_{b0} in table 5.3, is calculated as the average in the last minute of the washing period. However, if the concentration is still decreasing at the end of the washing period, the outlet concentration would be expected to be c_{end}, eq. (5-8), this value must be

subtracted from c_{b0} to give the true offset

$$c_{off} = c_{b0} - c_{end} \tag{5-7}$$

Where c_{end} is calculated as

$$c_{end} = c_{out}(20\,ml) \cdot 10^{\alpha(20\,ml - 100\,ml)} \tag{5-8}$$

hereafter the measured concentrations, $c_m(V)$, are corrected by subtracting the baseline.

$$c_{out}(V) = c_m(V) - c_{off} \tag{5-9}$$

In table 5.3 is seen that n_0 is up to almost 15% of the nitrate washed out of the column, table 5.2, and it must be expected that the determined nitrate capacity is sensitive to the washing volume.

The sorption capacity of a strong electrolyte is usually small, (Helfferich, 1995, p. 134) due to the Donnan exclusion of the counter ion. The reason for this large wash out has not been investigated further. It should here only be stated that the large deviation makes it doubtful if scaling on the nitrate capacity rather than on the column dimension gives better results. Additionally any error introduced on the columns total capacity will influence the charge density of the column, Λ, which is raised to the power of ν and any error is therefore amplified.

$$\Lambda = \frac{\lambda}{V_{col}(1-\epsilon)\epsilon_p} \tag{5-10}$$

runDate	***Q***	***Corr***	n_0	α	c_0	c_{b0}	c_{off}
	[ml/min]		[10^{-6} mole]	[ml^{-1}]	[mM]	[mM]	[mM]
200301081620	1	-0.75	82.18	0.0089	1.751	-0.287	-0.5127
200301081925	2	-0.766	69.04	0.0093	1.502	-0.040	-0.2182
200301082104	3	-0.236	74.20	0.0094	1.725	0.135	-0.0617
200301082215	5	-0.817	44.12	0.0157	1.750	0.258	0.2119
200301082303	7	-0.461	44.78	0.0118	1.246	0.531	0.4476
200301082341	10	-0.095	35.56	0.0160	1.338	0.457	0.4237
200301090012	15	-0.684	43.98	0.0140	1.467	0.151	0.094

Table 5.3 Summary of washing experiments. Corr is the correlation coefficient calculated for the last 5 ml of the washing period, in the time interval all the UV-signals are decreasing. n_0 is the pre-exponential factor for the total amount of nitrate in the column, α is the exponent, c_0 is the pre-exponential factor for the concentration, $c_{b,0}$ is the concentration in the last minute of the washing period and and c_{off} is offset required to get an exponential decay in the entire washing period, $c_{off} < c_{b,0}$.

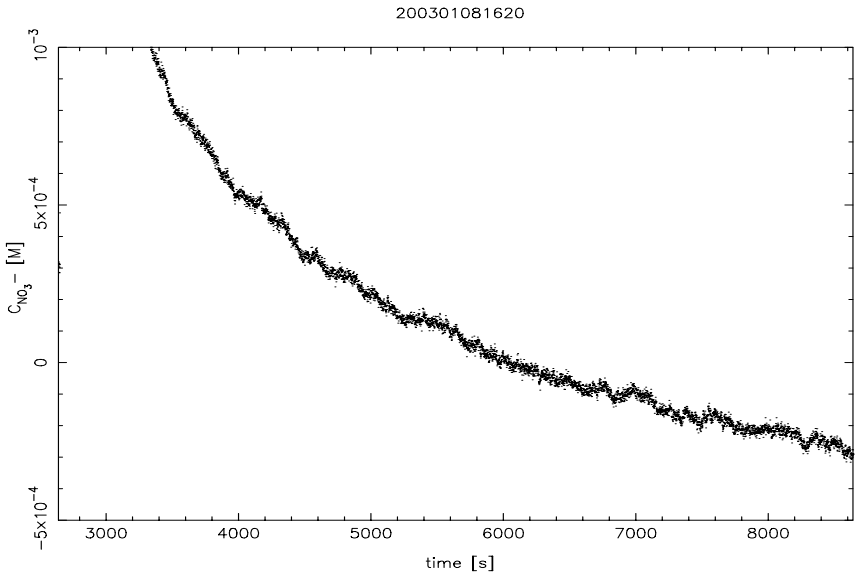

Figure 5.5 Outlet nitrate concentration from the column in the washing period. The washing period starts at 2640 sec. and ends at 8640 sec.

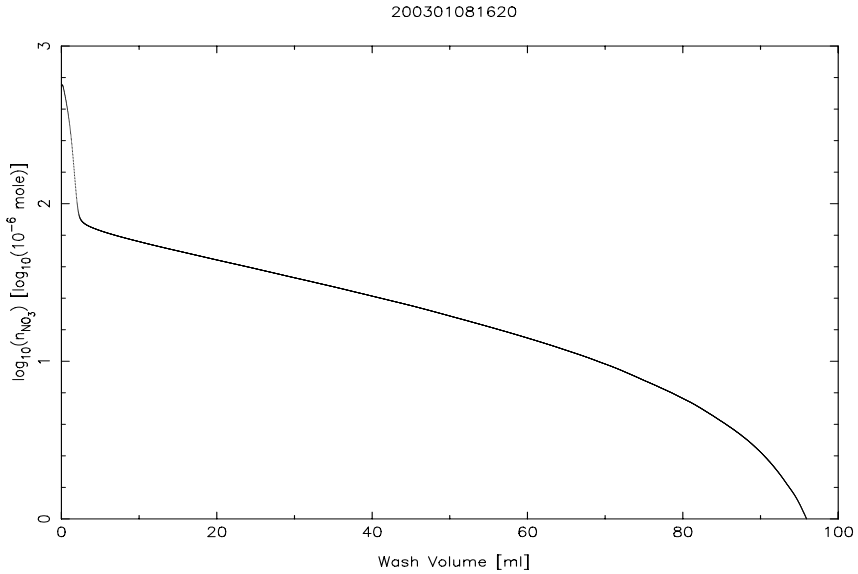

Figure 5.6 Non-bound nitrate in the column, as a function of the washing volume at Q=1 ml/min. The first peak is the washing peak removing the nitrate in the tubing and between the particles in the column. The data are only corrected by subtracting the baseline $c_{b,0}$.

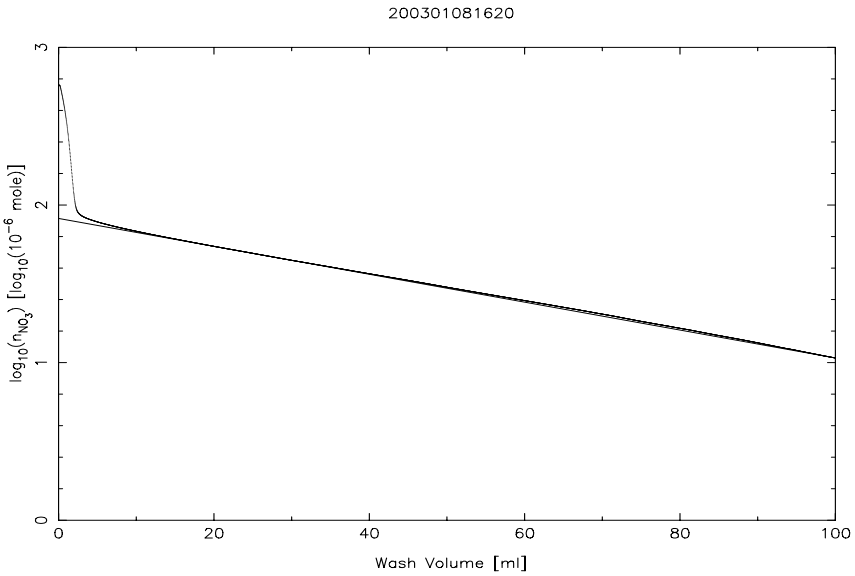

Figure 5.7 Remaining nitrate to be washed out of the column at Q=1 ml/min. The data are corrected by subtracting c_{off} in table 5.3.

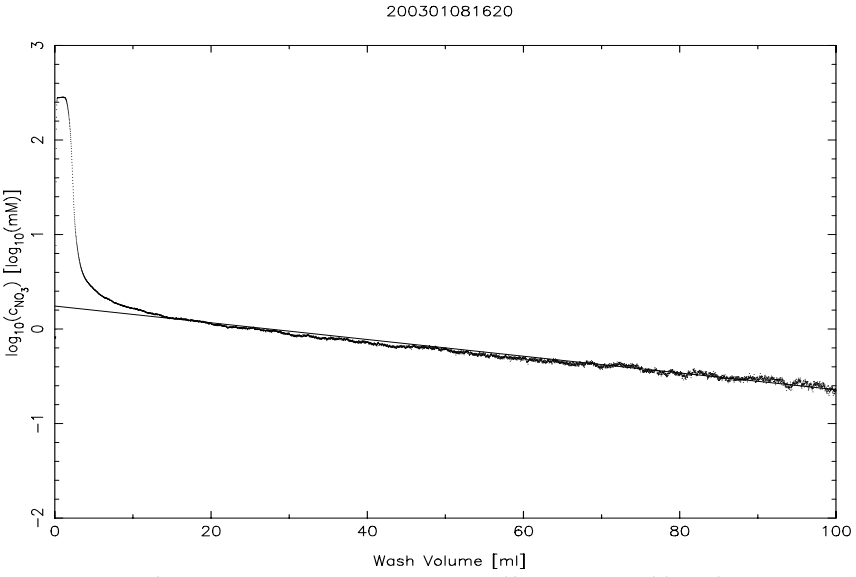

Figure 5.8 Outlet nitrate concentration at Q=1 ml/min corrected by subtracting c_{off}.

5.3 Steric Exclusion Factor

The experiments to determine the steric exclusion factor is similar to the method to determine the retention volumes. The steric exclusion factor is measured at pH 7 and 1 M NaCl where none of the used proteins binds to the ion exchangers.

The retention volume is given as

$$V_R = V_{col}\left(\epsilon + (1-\epsilon)\epsilon_p K_D (1+A)\right) \tag{5-11}$$

At non-binding conditions A is zero and the steric exclusion factor can be calculated as

$$K_D = \frac{\frac{V_R}{V_{col}} - \epsilon}{(1-\epsilon)\epsilon_p} \tag{5-12}$$

5.4 Summary

Only the total porosity can be determined and not the porosities of the two phases individually. One of these parameters has to be guessed and the other can hereafter be calculated.

The hydroxide capacity is always lower than the nitrate capacity due to the weak binding of hydroxide, which makes it difficult to bring the ion exchanger on hydroxide form and it is therefore not trustworthy.

A significant amount of nitrate can be washed out of the column and it can be difficult to determine the amount of resin in the column from nitrate capacity.

Since both the porosity and the nitrate capacity effects the concentration of binding charges, Λ, which is raised to the power of ν even small errors will have a significant effect on the result.

Beside these parameters a number of other parameters must be determined before the process can be modelled, these are the equilibrium parameters and mass transfer parameters inside the particles.

6. Pulse Experiments

Pulse experiments are very valuable for determination of parameters in the linear part of the isotherm. The experiments only require small amounts of protein and are fast to perform. These experiments are used to determine equilibrium parameters and mass transfer parameters. These parameters are all determined from the moments of the fitted peaks, as described in chapter 3.7.2 “Laplace Transform”. Usually peaks are fitted to either a Gaussian peak or an Exponential Modified Gaussian (EMG) function (Jeansonne *et al.*, 1991). Other functions have also been suggested e.g. double modified Gaussian (Lode *et al.*, 1998) and a large number can be found in “PeakFit, User's Manual” (SPSS, 19997).

6.1 Fitting of the Peaks

The first moment of the peak is defined as

$$M'_1 = \frac{\int_{-\infty}^{\infty} t\,F(t)\,dt}{\int_{-\infty}^{\infty} F(t)\,dt} = \frac{\int_{-\infty}^{\infty} t\,F(t)\,dt}{A} \tag{6-1}$$

Where A is the area of the peak. The remaining moments of interest are central moments and denoted as M_n where n indicates the order of the central moment. These moments are given as

$$M_n = \frac{\int_{-\infty}^{\infty} \left(t-\bar{t}\right)^n F(t)\,dt}{A} \tag{6-2}$$

Only the second and third central moments will be considered here.

Four different functions have been implemented to fit the peaks. These are Gaussian without fit of y_{max}, Gaussian with fit of y_{max}, EMG function and fronting EMG function.

6.1.1 Gaussian Function with Fixed y_{max}

$$y = y_{max} \cdot \exp\left(-\frac{(t-\mu)^2}{2\cdot\sigma^2}\right) \tag{6-3}$$

y_{max} is the maximum value of the peak from the chromatogram and μ and σ are fitted parameters.

The first normal moment is given as

$$M'_1 = \mu \tag{6-4}$$

and the second central moment as

$$M_2 = \sigma^2 \tag{6-5}$$

All odd central moments are zero.

The area below the curve is

$$A = y_{max} \cdot \sqrt{2\pi\sigma^2} \tag{6-6}$$

6.1.2 Gaussian Function with Fitted Area

$$y = \frac{A}{\sqrt{2\pi\sigma^2}} \cdot \exp\left(-\frac{(t-\mu)^2}{2\cdot\sigma^2} \right) \tag{6-7}$$

A, μ and σ are fitted parameters. The moments are calculated as above and y_{max} is calculated as

$$y_{max} = \frac{A}{\sqrt{2\pi\sigma^2}} \tag{6-8}$$

6.1.3 EMG Function

The EMG-function is the most widely used chromatographic model to fit asymmetric peaks.

$$z = \frac{t-\mu}{\sigma\sqrt{2}} - \frac{\sigma}{\tau\sqrt{2}} \tag{6-9}$$

$$y = \frac{A}{2\cdot\tau} \exp\left(\frac{\sigma^2}{2\tau^2} - \frac{t-\mu}{\tau} \right) \left(erf(z) + 1 \right) \tag{6-10}$$

Where erf is the error function.

The fitted parameters are A, μ, σ, τ. The first normal moment is given as

$$M'_1 = \mu + \sigma \tag{6-11}$$

the second central moment as

$$M_2 = \sigma^2 + \tau^2 \tag{6-12}$$

and the third central moment as

$$M_3 = 2\cdot\tau^3 \tag{6-13}$$

For positive parameters the EMG function will always be tailing, the function is easily changed to handling fronting peaks by reversing the sign for τ.

6.1.4 Implementation

A number of routines have been made to fit the peaks. The routines can fit both positive and negative peaks (e.g. from nitrate experiments).

First the baseline is subtracted and hereafter the peaks are fitted using a Levenberg-Marquardt routine Dennis *et al.* (1981) where the residuals are the difference between the measured and calculated values.

If the chromatogram contains several peaks and the relative area ratio of the peaks is known, the fit can be improved if the the ratios are inserted, hereby the number of fitted variables is reduced.

Usually when the peak maximum is known and fixed a better fit is obtained.

In the current implementation all parameters must be positive and the EMG-function for fronting peaks is hence a function of its own.

6.2 Results from Isocratic Pulse Experiments

A database containing pulse experiments previously made and pulse experiments made during this project has been made, see chapter 10 “Program”. All chromatograms have been refitted, and the database contains more than 2,300 chromatograms.

6.3 Equilibrium Parameters

Equilibrium data has previously been plotted as the retention volume as a function of the salt concentration. Another approach will be used here. Normally, the column is divided into two phases, a liquid phase where no protein can be adsorbed and a phase where protein can be adsorbed. The properties of the liquid phase is subtracted from the measured data which leaves only the adsorbed phase properties.

For a non-adsorbed component the retention time will be

$$V_{NA} = M'_{NA} - DV_{col} \tag{6-14}$$

Where V_{NA} is the retention volume for a non-adsorbed component, M'_{NA} is the first normal moment of the peak at non-adsorbing conditions, and DV_{col} is the dead volume of the column and HPLC system.

For an adsorbed component the retention time will be

$$V_R = V_{NA} + V_{Ads} \cdot A = M'_R - DV_{col} \tag{6-15}$$

where V_R is the retention volume, M'_R is the first normal moment of the peak, and A=q/y.

Since the desired properties are properties of the stationary phase, subtraction of the non-adsorbed retention volume gives only the properties of the adsorbed phase

$$V_R - V_{NA} = V_{ads} \cdot A \tag{6-16}$$

Using the SMA-formalism and the suggested model gives

$$V_R - V_{NA} = V_{col}(1-\epsilon)\epsilon_p K_D K_{eq} \left(\frac{\Lambda}{C_0} \right)^{\nu_i} \tag{6-17}$$

and

$$\log_{10}(V_R - V_{NA}) = \log_{10}\left(V_{col}(1-\epsilon)\epsilon_p K_D K_{eq} \Lambda^{\nu_i}\right) - \nu_i \log_{10}\left(C_0\right) \quad (6\text{-}18)$$

This approach has a number of advantages compared to plotting the retention volume. Plotting the results gives a straight line in a double logarithmic plot. The dead volume does not have to be determined for the system since this both enters into V_R and V_{NA}. The relationship for the model parameters is seen as a functional relationship and the fitted parameters from the double logarithmic plot can easily be calculated for any other model. This will later be used in chapter 11 “Simulated Moving Bed”.

In all the figures below the following colours are used: pH=6 black, pH=7 red, pH=8 green, and pH=9 blue.

6.3.1 Source 30Q

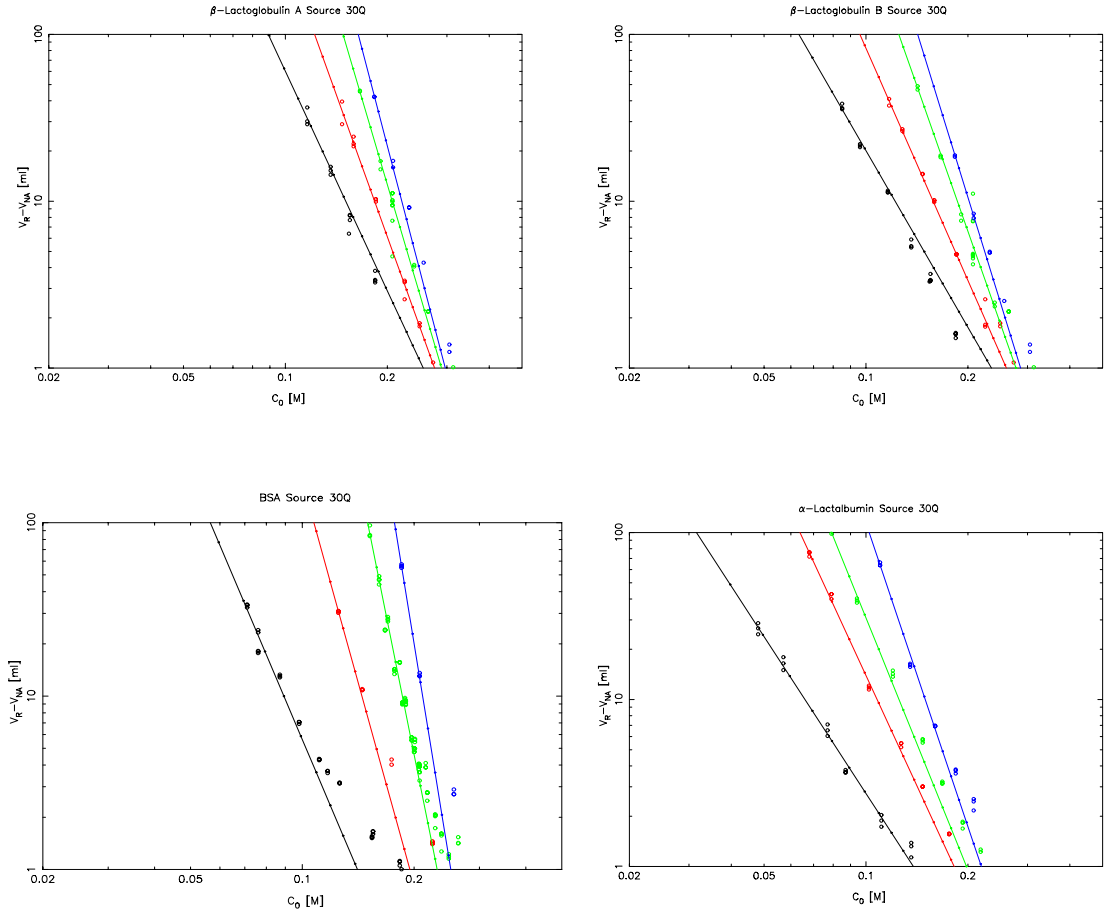

Figure 6.1 Experimental and fitted retention volumes for Source 30Q. The parameters are given in table 6.1.

$\Delta G_0/RT=0.155$

Protein	$\Delta G_p/RT$	ν_6	ν_7	ν_8	ν_9
β-Lactoglobulin A	2.153	4.369	5.643	6.871	7.781
β-Lactoglobulin B	2.157	3.515	4.620	5.777	6.578
BSA	5.252	5.046	7.729	10.676	13.188
α-Lactalbumin	3.702	3.121	4.393	5.014	6.035

Table 6.1 Fitted equilibrium parameters for Source 30 Q data. ν_6 is the binding charge at pH=6 etc.

6.3.2 Q Sepharose XL

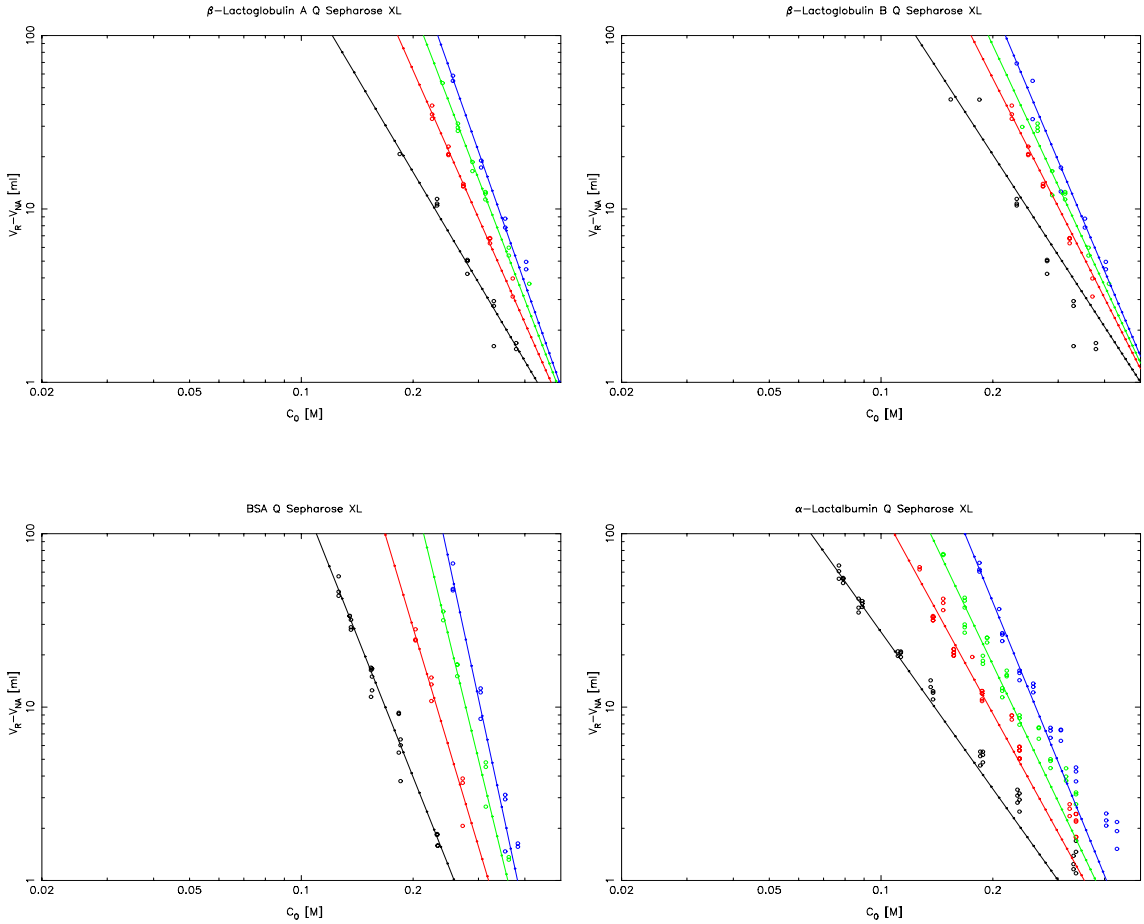

Figure 6.2 Experimental and fitted retention volumes for Q Sepharose XL. The parameters are given in table 6.2.

$\Delta G_0/RT=0.302$

Protein	$\Delta G_p/RT$	ν_6	ν_7	ν_8	ν_9
β-Lactoglobulin A	1.448	3.620	4.839	5.579	6.098
β-Lactoglobulin B	0.857	3.297	4.210	4.607	5.080
BSA	3.957	5.382	7.169	8.811	9.964
α-Lactalbumin	2.907	3.003	3.905	4.490	5.240

Table 6.2 Fitted equilibrium parameters for Q Sepharose XL.

6.3.3 Fractogel EMD TMAE 650(S)

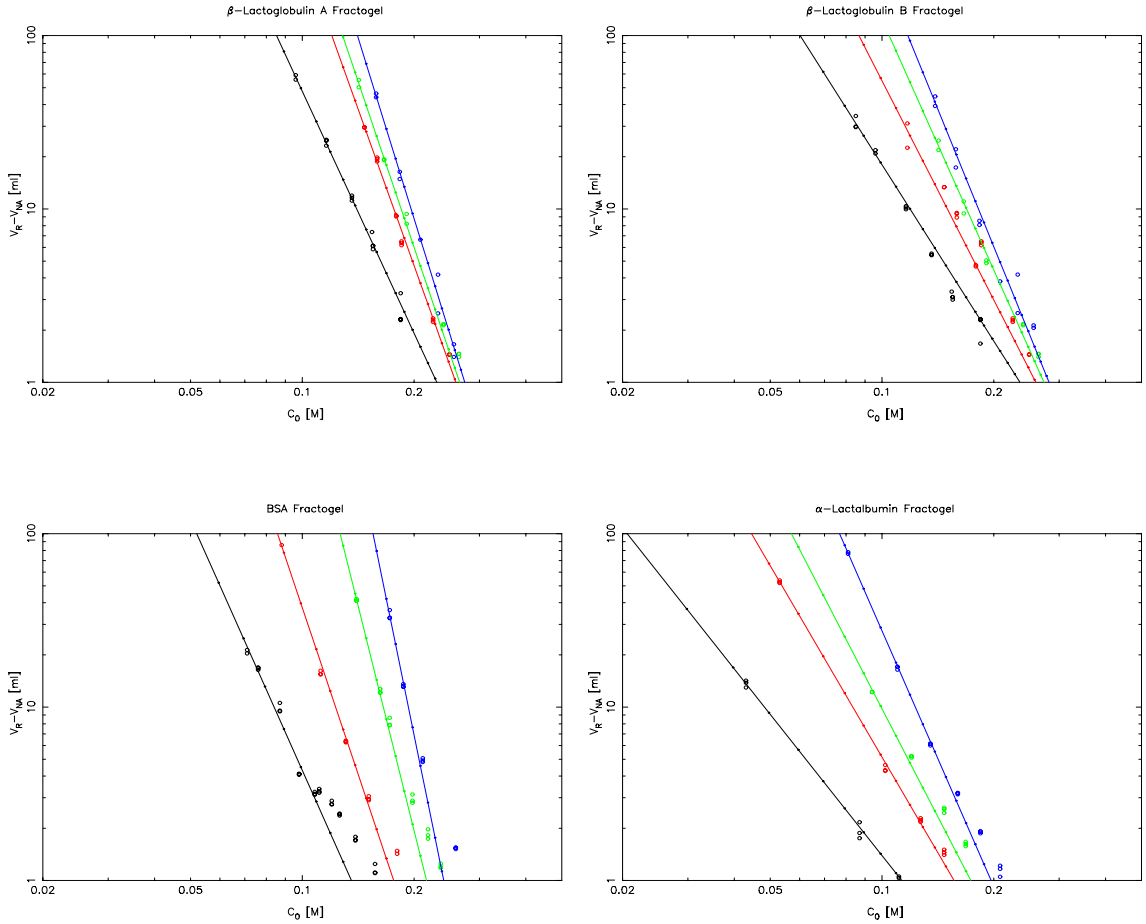

Figure 6.3 Experimental and fitted retention volumes for Fractogel EMD TMAE 650(S). The parameters are given in table 6.3.

$\Delta G_0/RT=1.552$

Protein	$\Delta G_p/RT$	ν_6	ν_7	ν_8	ν_9
β-Lactoglobulin A	2.167	4.632	5.981	6.344	6.917
β-Lactoglobulin B	1.435	3.377	4.197	4.794	5.258
BSA	4.578	4.800	6.388	8.594	10.499
α-Lactalbumin	3.497	2.705	3.666	4.138	4.900

Table 6.3 Fitted equilibrium parameters for Fractogel EMD TMAE 650(S).

6.3.4 Ceramic Q-HyperD F

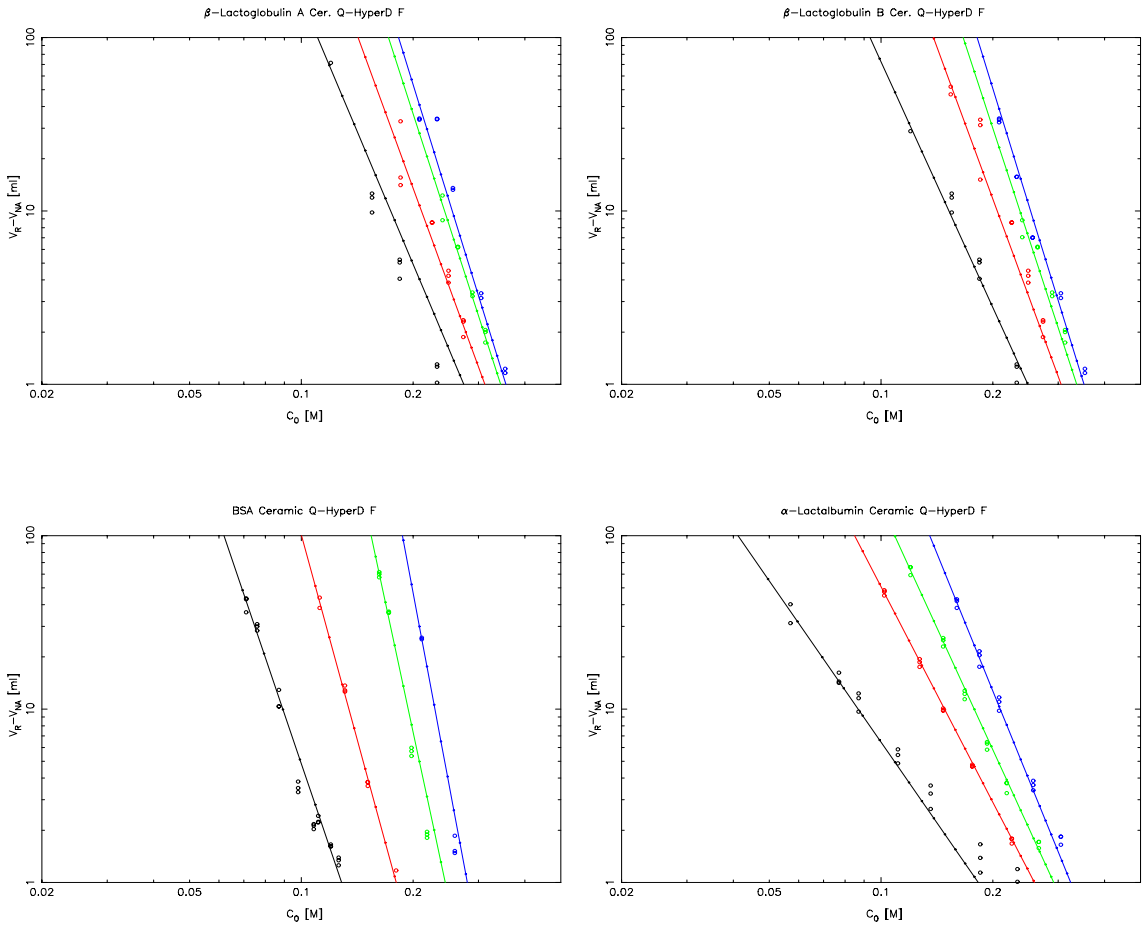

Figure 6.4 Experimental and fitted retention volumes for Ceramic Q-HyperD F the parameters are given in table 6.4.

$\Delta G_0/RT$=-0.060

Protein	$\Delta G_p/RT$	ν_6	ν_7	ν_8	ν_9
β-Lactoglobulin A	4.405	5.078	5.856	6.618	6.917
β-Lactoglobulin B	4.494	4.704	5.815	6.540	6.946
BSA	10.308	6.312	7.838	10.012	11.438
α-Lactalbumin	3.808	3.090	4.128	4.666	5.267

Table 6.4 Fitted equilibrium parameters for Ceramic Q-HyperD F.

As seen in eq. (3-52) the equilibrium parameters only depend on the first normal moment which is usually well determined. The experimental points are therefore in general well determined.

The equilibrium parameters for the four proteins at the four different pH-values on the four different columns are given on the previous pages. As expected the binding charge increases as the pH-value is increased.

α-Lactalbumin is generally the weakest bound of the four proteins and β-Lactoglobulin A is usually the strongest bound protein.

All the proteins bind weakest to Fractogel EMD TMAE 650(S), which has the lowest concentration of binding charges, table 1.4 and strongest to Q Sepharose XL, which is normally used for a capture step.

The largest deviation is usually seen at low binding where the fitted values usually predicts a too low binding.

6.4 Mass Transfer Parameters

Beside the equilibrium parameters the mass transfer parameters can also be calculated from the isocratic experiments using the van Deemter equation, eq. (3-53). The mass transfer parameters are determined from the ratio between the second central moment and the first normal moment squared, and a larger deviation in the data is expected since the second central moment is never as well determined as the first normal moment.

The same line colours are used in all the figures below these are: orange=½ ml/min, black Q=1 ml/min, red Q=2 ml/min, green Q=3 ml/min, blue Q=6 ml/min, magenta Q=7 ml/min, and grey Q=15 ml/min.

All the mass transfer parameters are fitted using the correlation suggested by Wilson and Geankoplis, eq. (4-4), and Pe_d=0.5. The data are plotted as a function of the experimental A-value, A_{exp}, which is calculated by isolating A in eq. (6-16).

6.4.1 Source 30Q

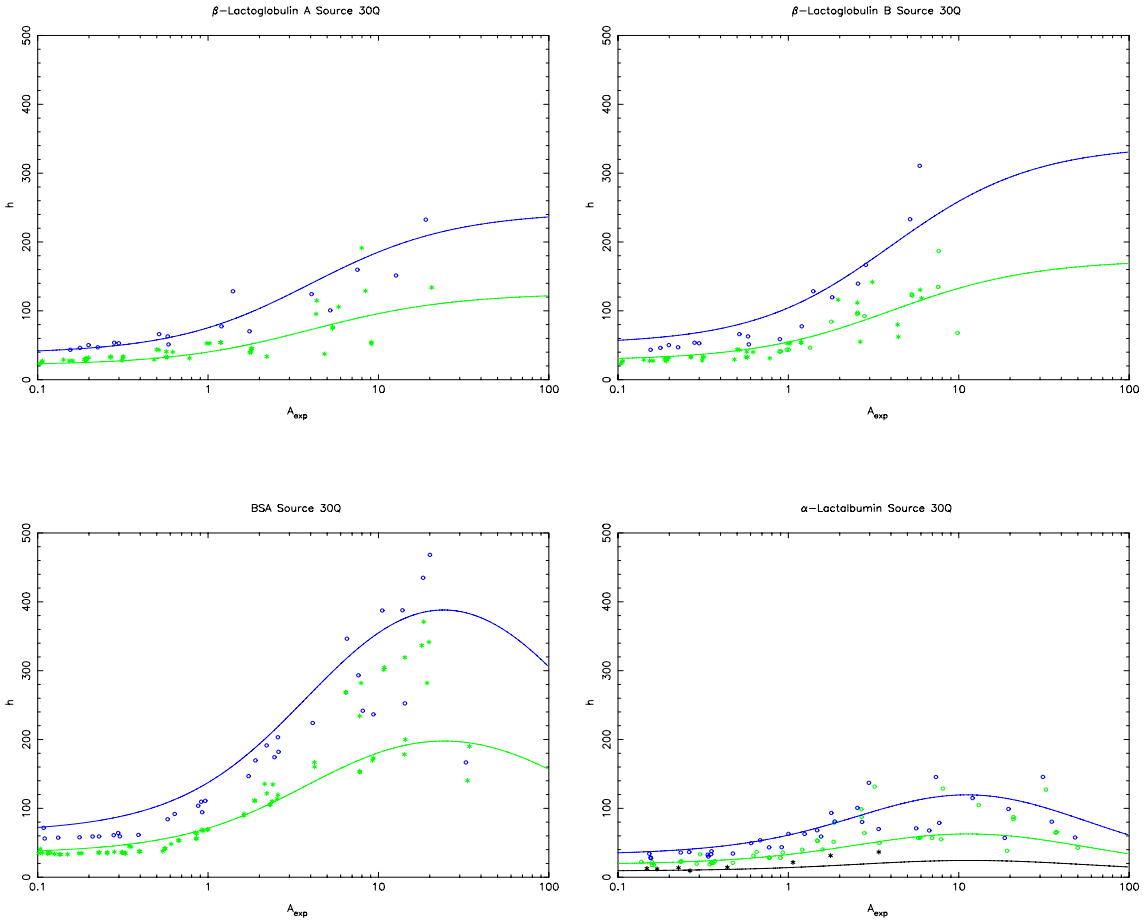

Figure 6.5 Experimental and fitted reduced plate height for Source 30Q. The parameters are given in table 6.5.

		β-Lactoglobulin A	***β-Lactoglobulin B***	***BSA***	***α-Lactalbumin***
k_p	[m/s]	$7.805 \cdot 10^{-06}$	$5.461 \cdot 10^{-06}$	$4.075 \cdot 10^{-06}$	$9.475 \cdot 10^{-06}$
k_q	[m/s]	-	-	$26.881 \cdot 10^{-09}$	$244.040 \cdot 10^{-09}$
k_f(Q=1 ml/min)	[m/s]	-	-	-	$37.706 \cdot 10^{-06}$
k_f(Q=3 ml/min)	[m/s]	$42.564 \cdot 10^{-06}$	$42.564 \cdot 10^{-06}$	$37.829 \cdot 10^{-06}$	$54.381 \cdot 10^{-06}$
k_f(Q=6 ml/min)	[m/s]	$53.627 \cdot 10^{-06}$	$53.627 \cdot 10^{-06}$	$47.662 \cdot 10^{-06}$	$68.516 \cdot 10^{-06}$

Table 6.5 Fitted parameters for mass transport inside the particle and calculated mass transfer parameters for the film layer for Source 30Q.

6.4.2 Q Sepharose XL

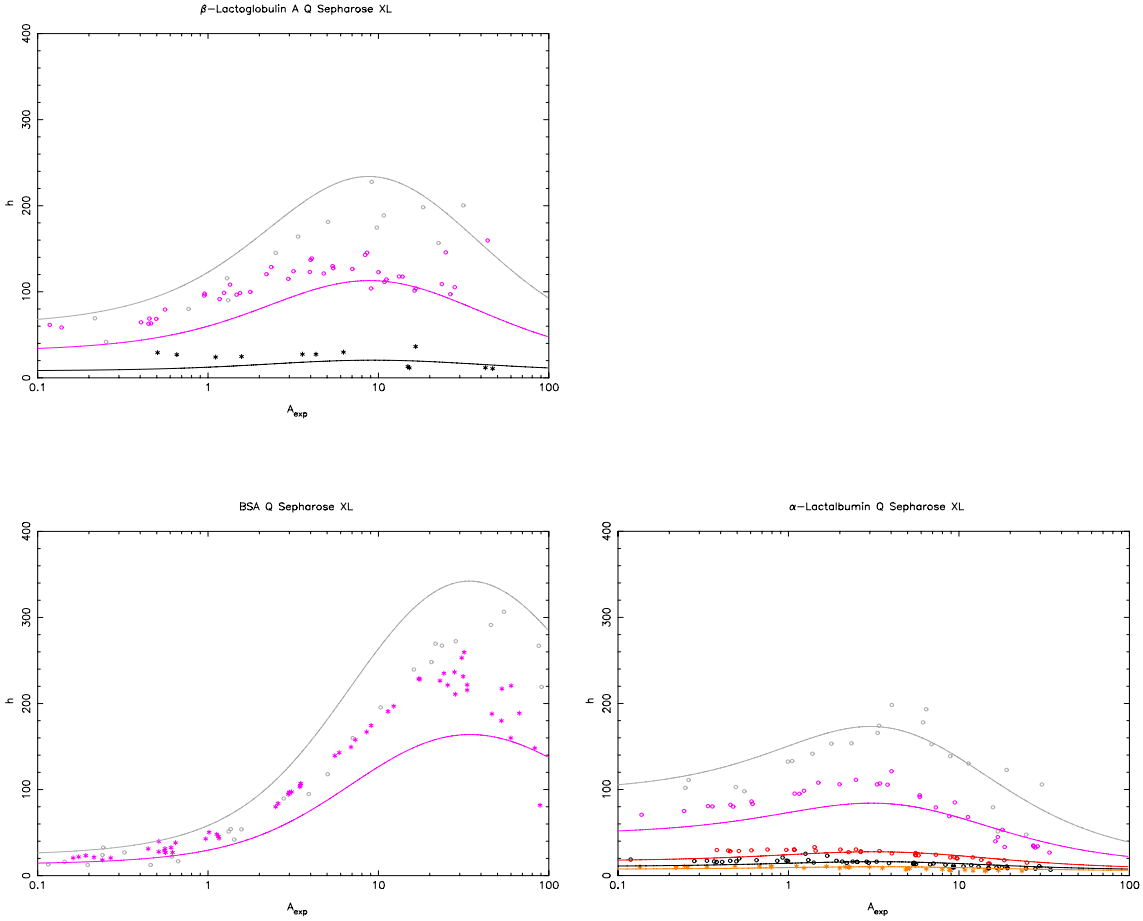

Figure 6.6 Experimental and fitted reduced plate height for Q Sepharose XL. The parameters are given in table 6.6. Only a few experiments differ for β-Lactoglobulin A and B and the plate heights for β-Lactoglobulin B is set to the same as the plate heights for β-Lactoglobulin A.

		β-Lactoglobulin A	***β-Lactoglobulin B***	***BSA***	***α-Lactalbumin***
k_p	[m/s]	$5.785 \cdot 10^{-06}$	$5.785 \cdot 10^{-06}$	$11.418 \cdot 10^{-06}$	$3.817 \cdot 10^{-06}$
k_q	[m/s]	$272.664 \cdot 10^{-09}$	$272.664 \cdot 10^{-09}$	$91.547 \cdot 10^{-09}$	$587.267 \cdot 10^{-06}$
k_f(Q=½ ml/min)	[m/s]	-	-	-	$14.023 \cdot 10^{-06}$
k_f(Q=1 ml/min)	[m/s]	$13.83 \cdot 10^{-06}$	$13.83 \cdot 10^{-06}$	-	$17.668 \cdot 10^{-06}$
k_f(Q=2 ml/min)	[m/s]	-	-	-	$22.260 \cdot 10^{-06}$
k_f(Q=7 ml/min)	[m/s]	$26.453 \cdot 10^{-06}$	$26.453 \cdot 10^{-06}$	$23.511 \cdot 10^{-06}$	$33.798 \cdot 10^{-06}$
k_f(Q=15 ml/min)	[m/s]	$34.104 \cdot 10^{-06}$	$34.104 \cdot 10^{-06}$	$30.311 \cdot 10^{-06}$	$43.573 \cdot 10^{-06}$

Table 6.6 Fitted parameters for mass transport inside the particle and calculated mass transfer parameters for the film layer for Q Sepharose XL.

6.4.3 Fractogel EMD TMAE 650(S)

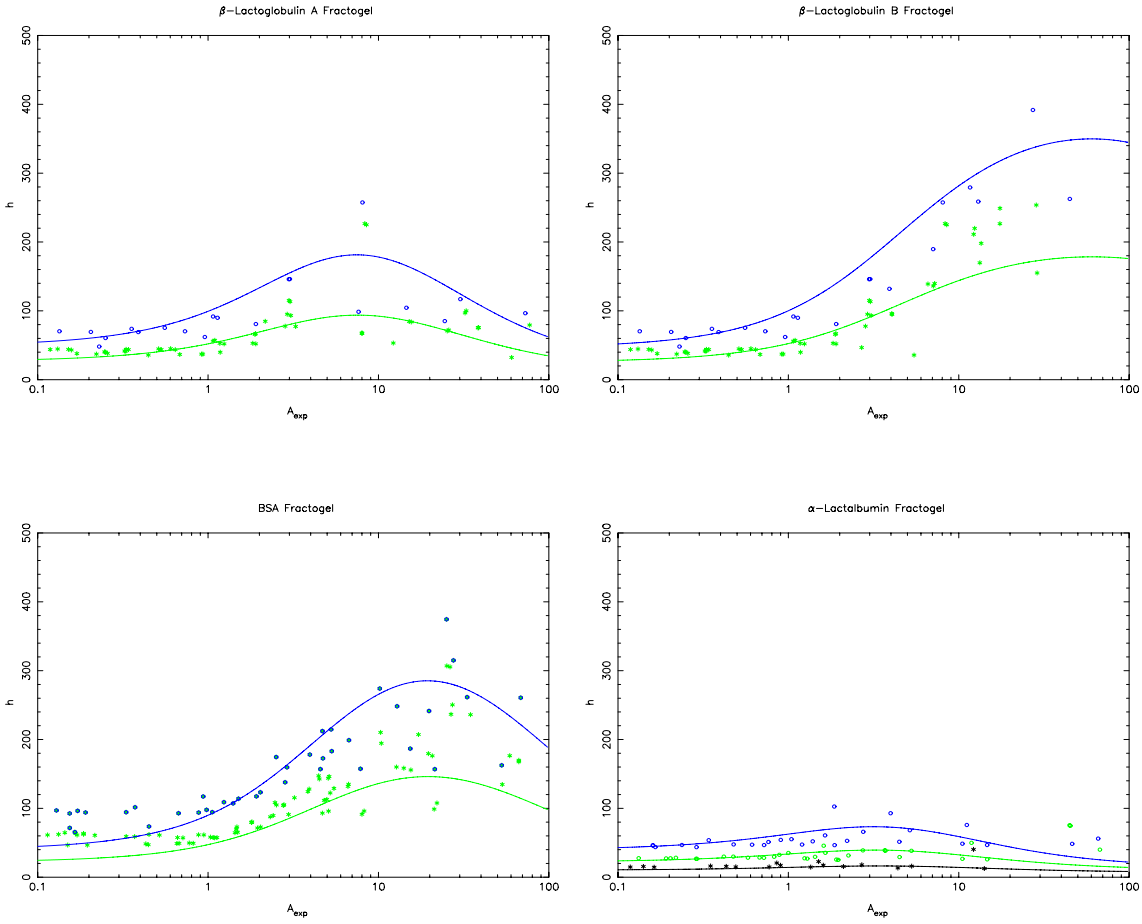

Figure 6.7 Experimental and fitted reduced plate height for Fractogel EMD TMAE 650(S). The parameters are given in table 6.7.

		***β*-Lactoglobulin A**	***β*-Lactoglobulin B**	**BSA**	***α*-Lactalbumin**
k_p	[m/s]	$5.370 \cdot 10^{-06}$	$5.714 \cdot 10^{-06}$	$6.215 \cdot 10^{-06}$	$7.656 \cdot 10^{-06}$
k_q	[m/s]	$398.891 \cdot 10^{-09}$	$6.534 \cdot 10^{-09}$	$88.482 \cdot 10^{-09}$	$1.649 \cdot 10^{-06}$
k_f(Q=1 ml/min)	[m/s]	-	-	-	$37.706 \cdot 10^{-06}$
k_f(Q=3 ml/min)	[m/s]	$42.564 \cdot 10^{-06}$	$42.564 \cdot 10^{-06}$	$37.829 \cdot 10^{-06}$	$54.381 \cdot 10^{-06}$
k_f(Q=6 ml/min)	[m/s]	$53.627 \cdot 10^{-06}$	$53.627 \cdot 10^{-06}$	$47.662 \cdot 10^{-06}$	$68.516 \cdot 10^{-06}$

Table 6.7 Fitted parameters for mass transport inside the particle and calculated mass transfer parameters for the film layer for Fractogel EMD TMAE 650(S).

6.4.4 Ceramic Q-HyperD F

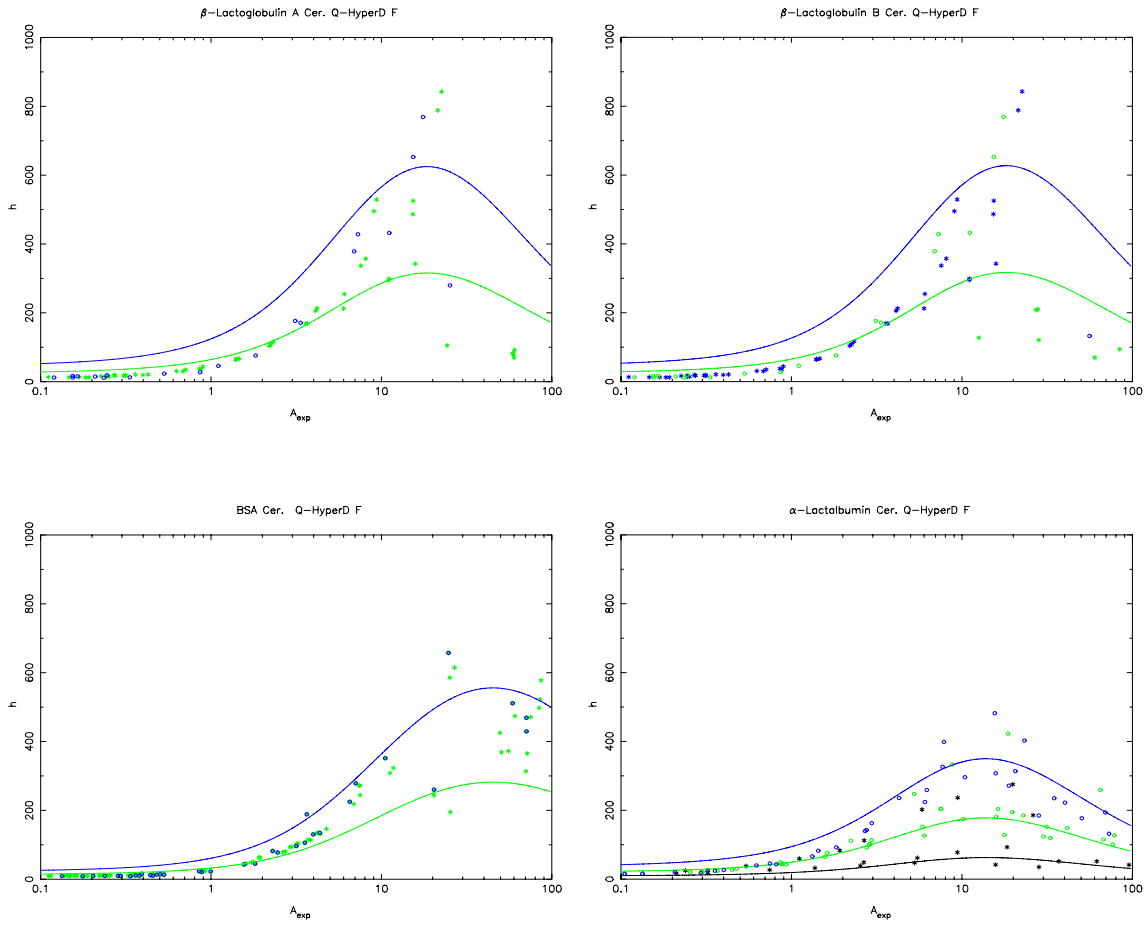

Figure 6.8 Experimental and fitted reduced plate height for Ceramic Q-HyperD F. The parameters are given in table 6.8.

		***β*-Lactoglobulin A**	***β*-Lactoglobulin B**	**BSA**	***α*-Lactalbumin**
k_p	[m/s]	$3.445 \cdot 10^{-06}$	$3.293 \cdot 10^{-06}$	$7.157 \cdot 10^{-06}$	$4.624 \cdot 10^{-06}$
k_q	[m/s]	$123.001 \cdot 10^{-09}$	$133.722 \cdot 10^{-09}$	$45.904 \cdot 10^{-09}$	$292.514 \cdot 10^{-09}$
k_f(Q=1 ml/min)	[m/s]	-	-	-	$26.823 \cdot 10^{-06}$
k_f(Q=3 ml/min)	[m/s]	$30.279 \cdot 10^{-06}$	$30.279 \cdot 10^{-06}$	$26.911 \cdot 10^{-06}$	$38.686 \cdot 10^{-06}$
k_f(Q=6 ml/min)	[m/s]	$38.149 \cdot 10^{-06}$	$38.149 \cdot 10^{-06}$	$33.906 \cdot 10^{-06}$	$48.741 \cdot 10^{-06}$

Table 6.8 Fitted parameters for mass transport inside the particle and calculated mass transfer parameters for the film layer for Ceramic Q-HyperD F.

The reduced plate heights on the y-axis only depend on experimental values, eq. (3-55), whereas the A value is a model parameter. A is, however, for a linear isotherm proportional to V_R-V_{NA}, eq. (6-16), and this could also be plotted on the x-axis. That the reduced plate height starts to decrease at increased binding of the protein can therefore also been shown without any modelling, simply by changing the x-axis. To be able to model this the surface diffusion parameter has been introduced.

Comparing these results with the results obtained from confocal microscopy (Ljunglöf *et al.*, 1998), where very sharp gradients of bound protein are seen, surface diffusion seem to be unlikely. Another more apparent explanation for this result can be the rough approximation made by calculating the liquid phase as an ideal solution, and the surface diffusion parameter, k_q, will therefore only be a convenient modelling parameter to compensate for an error already introduced in the model. As previously mentioned, figure 3.1 p.14, the smallest molecule is also expected to have the fastest mass transport and the lowest plate height. This is also the general trend for all the columns. An exception, however, is the Ceramic Q-HyperD F column where the plate height of the β-Lactoglobulins is higher than the plate height of BSA.

The experiments with β-Lactoglobulin A and B are made with the mixture of the two proteins. In figure 6.10 below the plate heights are plotted for both proteins. At low binding the proteins have the same retention volume and the same zone spreading leading to same binding and the same plate height. When the protein starts to separate initially, the resulting peak in the chromatogram will look as one due to the zone spreading mechanism and the separation, figure 6.9, the chromatogram is therefore fitted as one peak. When the protein binds stronger a better separation is obtained and two peaks are more clearly seen and the chromatogram will be fitted as two peaks. Hereby the peak width of the individual peaks is reduced simply due to the fitting procedure and the plate heights will decrease. This is most pronounced for Ceramic Q-HyperD F since Source 30Q has a very good separation of the proteins and the other two other resins has a very bad separation of the two proteins. Similar results can be expected from impurities in the proteins.

The number of plate heights is also very large for some of the experiments, e.g. a reduced plate height of 800 in the Ceramic Q-HyperD F column corresponds only to 2-3 plates in the column.

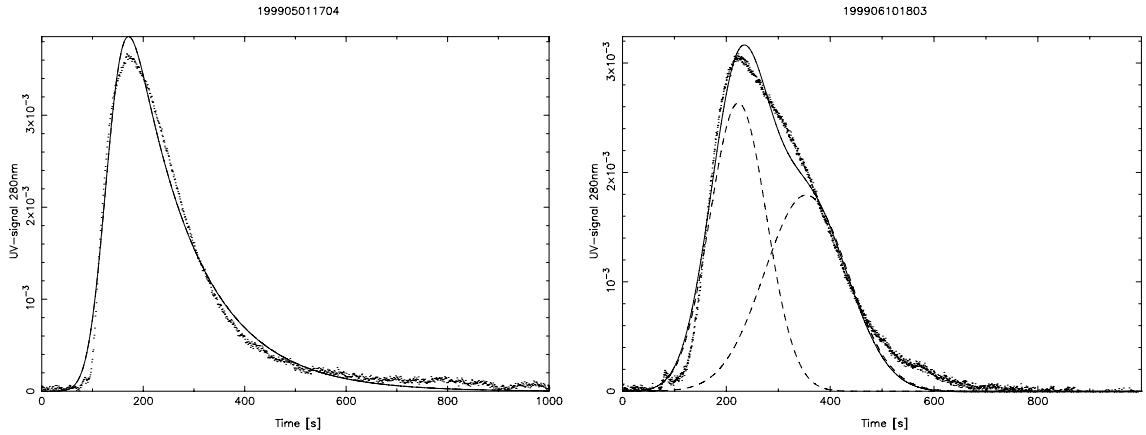

Figure 6.9 Example of two fitted chromatograms both β-Lactoglobulin A and B on Ceramic Q-HyperD F. The curve to the left is fitted with one EMG-function and the reduced plate height is here h(A=15.4, Q=3 ml/min)=525. The curve to the right is fitted with two Gaussian peaks and the reduced plate height for β-Lactoglobulin A is here h(A=24.3, Q=3 ml/min)=105. The dots are the experimental values, the dashed lines are the fitted peaks and the full line is the sum of the fitted peaks.

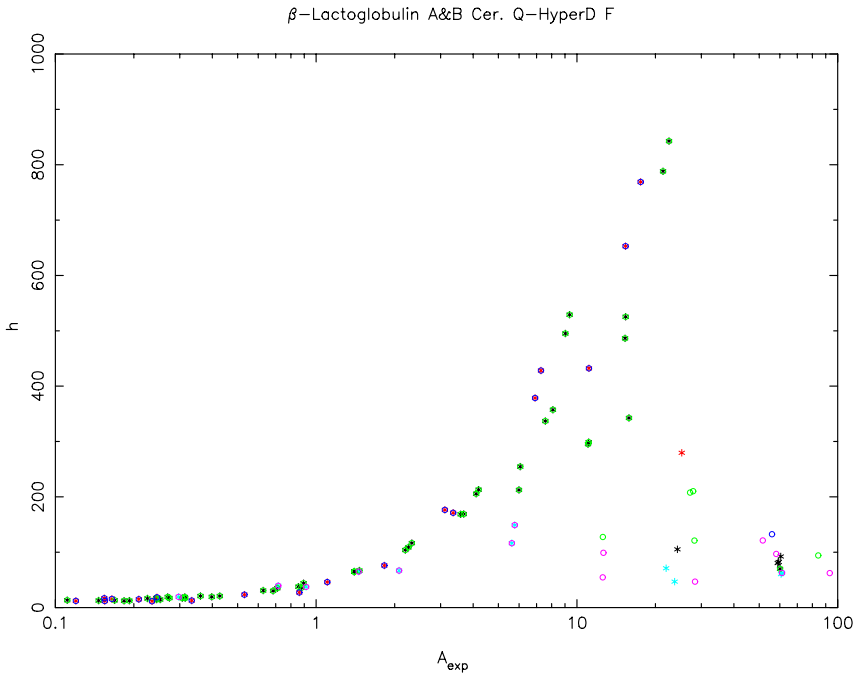

*Figure 6.10 Comparison of plate heights for β-Lactoglobulin A and B on Ceramic Q-HyperD F. If β-Lactoglobulin A and B comes out as one peak the * and o will coinside and visa versa.*

*Legends: * β-Lactoglobulin A, cyan Q= 1 ml/min, black Q= 3 ml/min, and red Q= 6 ml/min. o β-Lactoglobulin B, magenta Q= 1 ml/min, green Q= 3 ml/min, blue Q= 6 ml/min.*

6.5 Results From Gradient Experiments

The retention times from the gradient experiments can be estimated using the approach suggested by Yamamoto *et al.* (1988, p. 226). For this model, it has previously been derived by Pedersen (2003, pp. 34-40). If the protein is eluted at the gradient (if the final salt concentration in the gradient is too low, the protein might be eluted after the gradient) the eluting salt concentration is

$$C_{0,R}=\left(G(1-x_{p,0})(1+\nu)B\left(\frac{\Lambda}{z_0}\right)^{\nu}+C_{0,st}^{\nu+1}\right)^{\frac{1}{1+\nu}} \tag{6-19}$$

where

$$B=V_{col}(1-\epsilon)\epsilon_p K_D K_{eq} \tag{6-20}$$

$$G=\frac{C_{0,end}-C_{0,st}}{V_g} \tag{6-21}$$

and $x_{p,0}$ is the dimensionless axial position of the protein in the column when the gradient starts

$$x_{p,0}=\frac{V_{MC}}{V_{R,0}-V_t} \tag{6-22}$$

$C_{0,st}$ is the initial salt concentration, $C_{0,end}$ is the final salt concentration, V_g is the gradient volume, V_{MC} is the volume from the mixer to the column inlet, $V_{R,0}$ is the retention volume at $C_{0,st}$, and V_t is the total liquid volume.

From the eluting salt concentration the corresponding retention volume can be calculated

$$V_R=\frac{1}{G}\left(G(1-x_{p,0})(1+\nu)B\left(\frac{\Lambda}{z_0}\right)^{\nu}+C_{0,st}^{\nu+1}\right)^{\frac{1}{1+\nu}}-\frac{C_{0,st}}{G}+V_m \tag{6-23}$$

where V_m is the volume the salt travels before it reach the detector.

The data have in previous works been plotted as the retention volume as a function of the salt concentration in a double logarithmic plot. It is suggested instead to plot the eluting salt concentration as a function of the gradient volume. Comparing eq. (6-19) and (6-23) it is seen that the eluting salt concentration is only a weak function of the gradient parameter G (with ν=3 increasing the gradient volume 16 times only leads to approximately half the salt concentration), therefore the eluting salt concentration has a narrow range and can easily be plotted in semi-logarithmic plot.

The retention volume depends strongly on the gradient parameter and therefore this is

normally plotted in a double-logarithmic plot. The retention volume also depends strongly on the initial salt concentration, $C_{0,st}$, which normally has only a marginal effect on the eluting salt concentration.

Both approaches are given in figure 6.11 below. It is seen that the deviation between the predicted and the experimental value is best seen by plotting the eluting salt concentration as a function of the gradient volume. Plotting the elution volume the curves at pH=8 and 9 almost coincide and pH=7 is very close to these lines. Plotting the eluting salt concentration separates the lines much more and any deviation is more easily seen. The largest deviation in the salt concentration is seen at a low gradient volume, where the salt concentration is a steep function of the volume, a small deviation in the retention volume will hence cause a large error in the eluting salt concentration.

The legends in the following figures are the same as for the isocratic experiments. Black pH=6, red pH=7, green pH=8, and blue pH=9.

In all the figures below the eluting salt concentration is only calculated from the gradient (no isocratic part at the end of the gradient). If the peaks are eluted at the isocratic part after the gradient this is seen from the table below the curves, where the final salt concentrations are given.

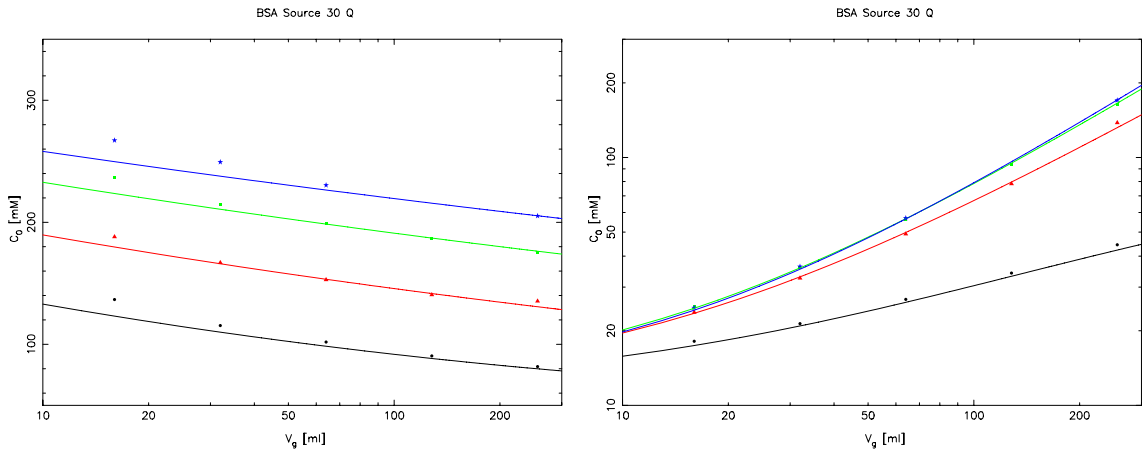

Figure 6.11 Salt concentration at the retention volume and retention volume as a function of the gradient volume. The gradient salt concentrations are given in table 6.9. Legends: black=pH 6, red=pH 7, green=pH 8, and blue=pH 9.

6.5.1 Source 30Q

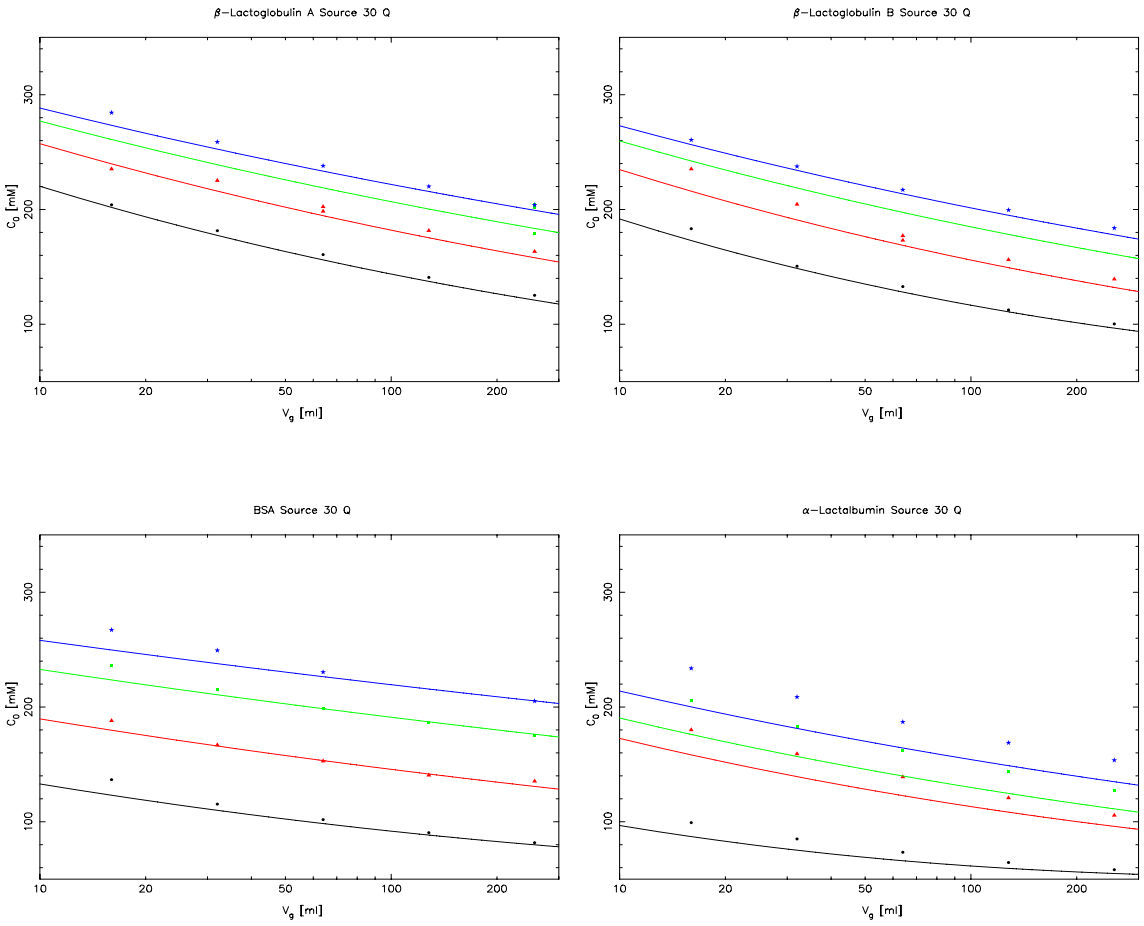

Figure 6.12 Experimental and estimated eluting salt concentration for Source 30Q. The initial and final salt concentrations are given in table 6.9.

	***β*-Lactoglobulin**		***BSA***		***α*-Lactalbumin**	
	$C_{0,st}$ [mM]	$C_{0,end}$ [mM]	$C_{0,st}$ [mM]	$C_{0,end}$ [mM]	$C_{0,st}$ [mM]	$C_{0,end}$ [mM]
pH=6	63	280	59	233	49	136
pH=7	61	323	48	224	60	322
pH=8	51	313	45	263	54	315
pH=9	42	305	43	304	42	305

Table 6.9 Initial and final salt concentrations for the gradient experiments with Source 30Q.

6.5.2 Q Sepharose XL

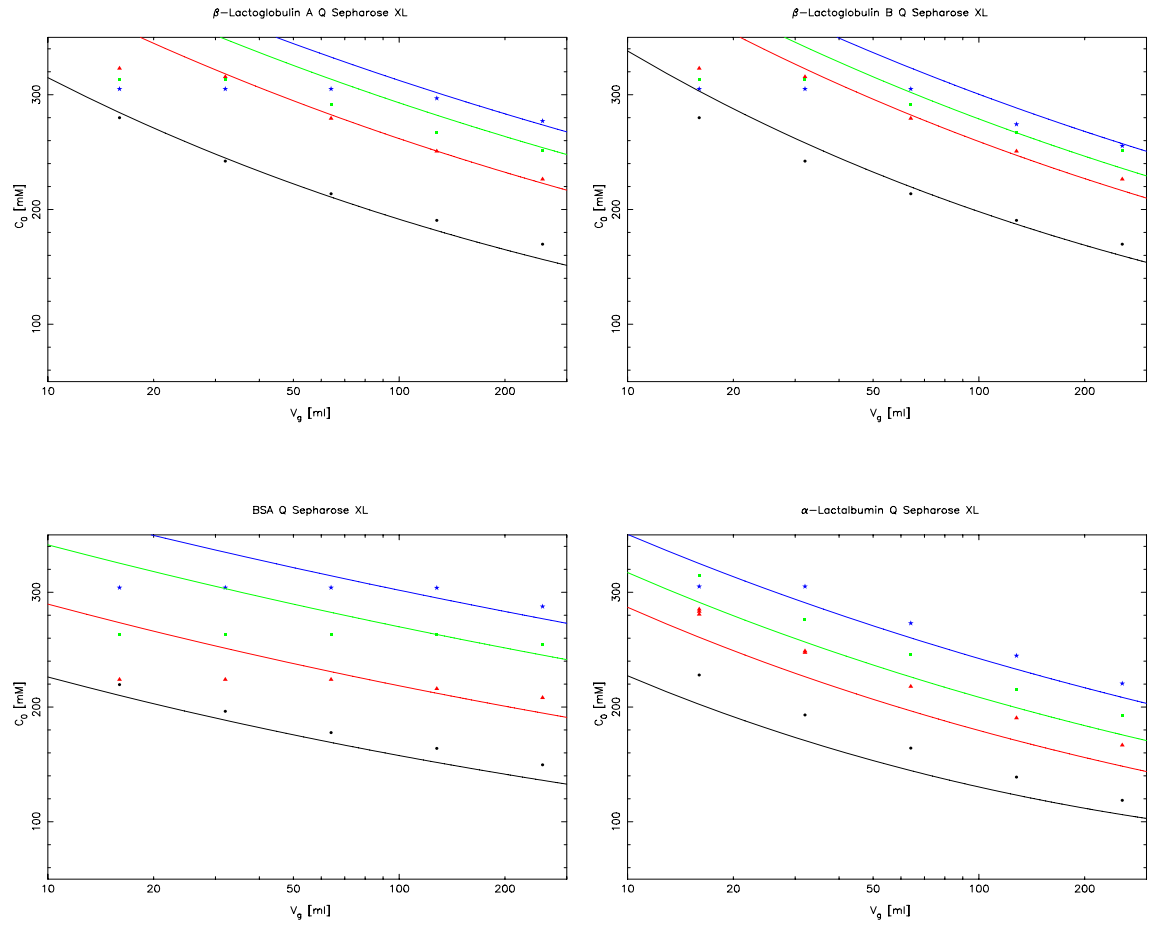

Figure 6.13 Experimental and estimated eluting salt concentration for Q Sepharose XL. The initial and final salt concentrations are given in table 6.10.

	***β*-Lactoglobulin**		***BSA***		***α*-Lactalbumin**	
	$C_{0,st}$ [mM]	$C_{0,end}$ [mM]	$C_{0,st}$ [mM]	$C_{0,end}$ [mM]	$C_{0,st}$ [mM]	$C_{0,end}$ [mM]
pH=6	63	280	58	232	70	330
pH=7	61	323	48	224	60	322
pH=8	51	313	45	263	54	315
pH=9	42	305	43	304	42	305

Table 6.10 Initial and final salt concentrations for the gradient experiments with Q Sepharose XL.

6.5.3 Fractogel EMD TMAE 650(S)

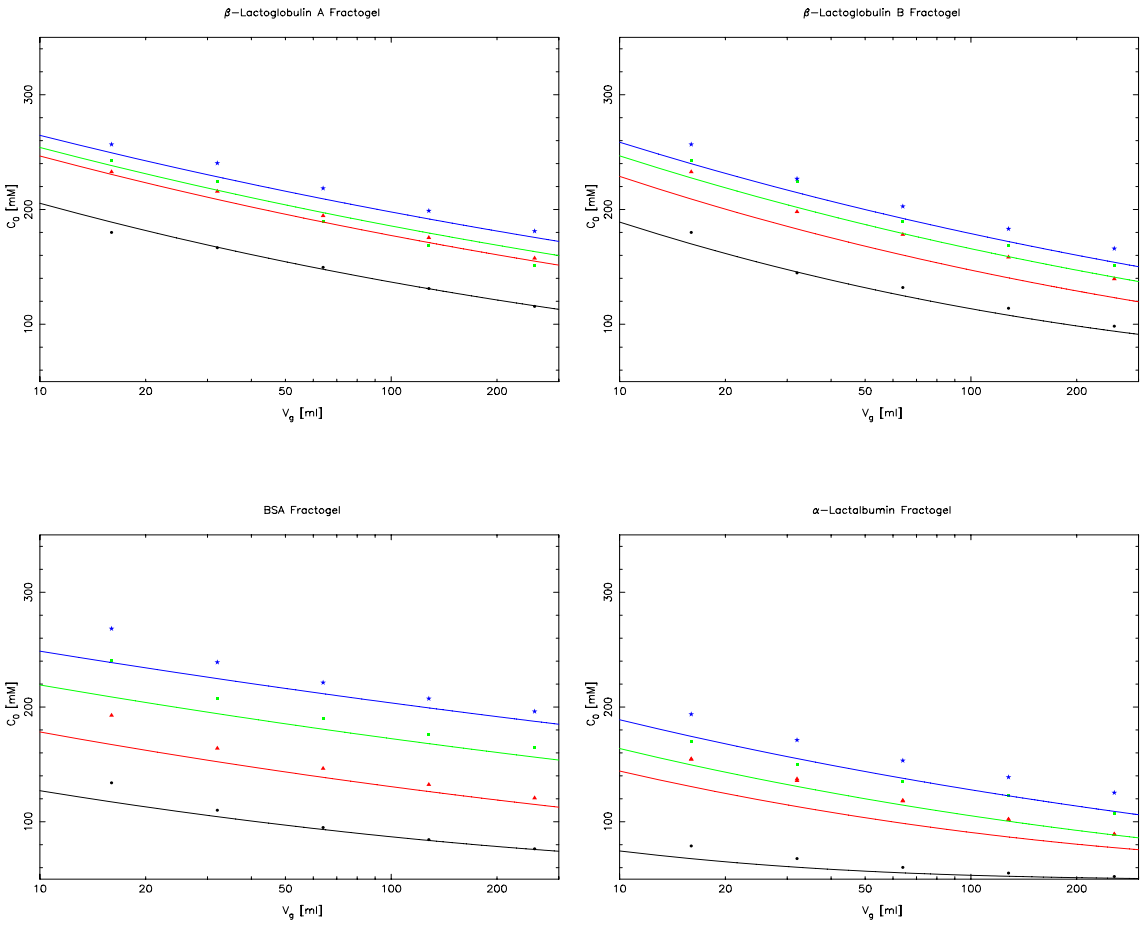

Figure 6.14 Experimental and estimated eluting salt concentration for Fractogel EMD TMAE 650(S). The initial and final salt concentrations are given in table 6.11.

	***β*-Lactoglobulin**		***BSA***		***α*-Lactalbumin**	
	$C_{0,st}$ [mM]	$C_{0,end}$ [mM]	$C_{0,st}$ [mM]	$C_{0,end}$ [mM]	$C_{0,st}$ [mM]	$C_{0,end}$ [mM]
pH=6	63	280	59	233	70	330
pH=7	61	323	64	325	60	322
pH=8	51	313	57	316	54	315
pH=9	42	305	48	356	42	305

Table 6.11 Initial and final salt concentrations for the gradient experiments with Fractogel EMD TMAE 650(S).

6.5.4 Ceramic Q-HyperD F

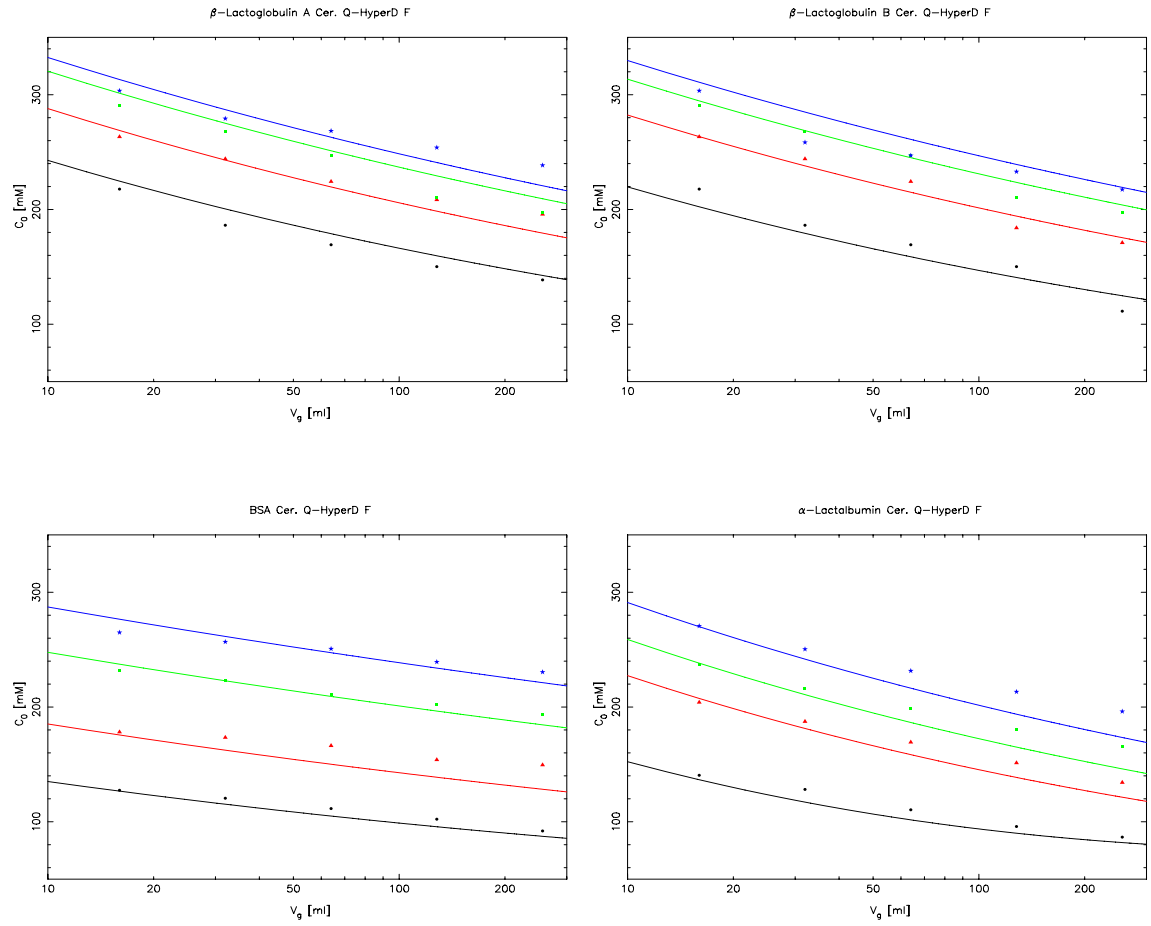

Figure 6.15 Experimental and estimated eluting salt concentration for Ceramic Q-HyperD F. The initial and final salt concentrations are given in table 6.12.

	***β*-Lactoglobulin**		***BSA***		***α*-Lactalbumin**	
	$C_{0,st}$ [mM]	$C_{0,end}$ [mM]	$C_{0,st}$ [mM]	$C_{0,end}$ [mM]	$C_{0,st}$ [mM]	$C_{0,end}$ [mM]
pH=6	63	280	59	233	49	136
pH=7	61	323	64	325	60	322
pH=8	51	313	57	316	54	315
pH=9	42	305	48	356	42	305

Table 6.12 Initial and final salt concentrations for the gradient experiments with Ceramic Q-HyperD F.

From the figures 6.12 to 6.15 is seen that the predicted eluting salt concentration is in general in good agreement with the experimental values.

From experiments is seen that the largest deviation is usually seen for α-Lactalbumin for all the resins. Taking the derivative of $C_{0,R}$, eq. (6-19), with ν gives

$$\frac{\partial C_{0,R}}{\partial \nu} = \left[G(1-x_{p,0})\nu \left(\frac{\Lambda}{z_0} \right)^{\nu} + C_{0,st}^{\nu} \right]^{\frac{1}{\nu}} \tag{6-24}$$

Hereby it is seen that the sensitivity is largest for small values of ν. For all the columns α-Lactalbumin has got the lowest values of ν and the largest deviation could therefore also be expected for this protein.

6.6 Summary

A large part of the data are reported in previous thesis, Hansen (2000) and Pedersen (2003). These data have now been refitted and added to a database where it is possible to find and investigate the data easily.

Some other methods of reporting the result have been suggested. These suggested methods make it easier to change the model parameters to another model. It also makes it easier to see deviations between experimental and fitted/estimated values.

Some reasons for the deviations have also been shown for the mass transfer parameters.

A large number of systems has been presented here. A detailed description of one of these systems, α-Lactalbumin and Q Sepharose XL, is given in the following chapter along with some modelling results.

7. Lactalbumin and Q Sepharose XL

Q Sepharose XL was used for experiments by previous students. However, the data were considered to be difficult to fit into models. New experiments were made with the same column.

The Q Sepharose XL was packed in a column with a diameter of 1.6 cm and a volume of 7.56 ml, table 1.4. Q Sepharose XL is designed for use in a capture steps and has a higher binding capacity, larger particles, and a larger particle size distribution compared to the other resins, produced for the purification steps.

7.1 Experiments

7.1.1 Velocity

In previous experiments the flow rate was scaled to the same superficial velocity for all the columns. The flow rate for the experiments in the columns with d_{col}= 1 cm was typically 3 and 6 ml/min and the flow rate was scaled to 7 and 15 ml/min, for this column.

Yamamoto (1988, p. 63) however, use a reduced velocity, ν, defined as

$$\nu = \frac{v_i \cdot d_p}{D_m} \tag{7-1}$$

where v_i is the interstitial velocity, d_p is the particle diameter and D_m is the diffusion coefficient for the protein, see also equation (4-1).

Using the approach suggested by Yamamoto and requiring the same reduced velocity as for Source 30 Q, d_p=30μm, the velocity should be reduced rather than increased.

A new series of experiments with α-Lactalbumin at pH-values from 6 to 9 but with lower flow rates (½, 1 and 2 ml/min) was made.

7.2 Determination of Equilibrium Parameters

The equilibrium parameters are fitted from the experimental retention volumes.

Since all previous experiments on the Q-Sepharose XL column were run at high velocities, the α-Lactalbumin data have been fitted alone for the present chapter.

The parameters found from the fit of the equilibrium parameters are given in table 7.1 and a plot of the experimental values along with the fitted retention volumes are given in figure 7.1. From eq. (6-18) is seen that plotting V_R-V_{NA} as a function of the salt concentration in a double logarithmic plot ought to give a straight line with the slope -ν, as previously mentioned.

Parameter	*Value*
$\Delta G_0/RT$	0.62
$\Delta G_p/RT$	3.2
ν_6	2.723
ν_7	3.28
ν_8	3.605
ν_9	4.131

Table 7.1 Fitted parameters. The index at ν is the pH-value.

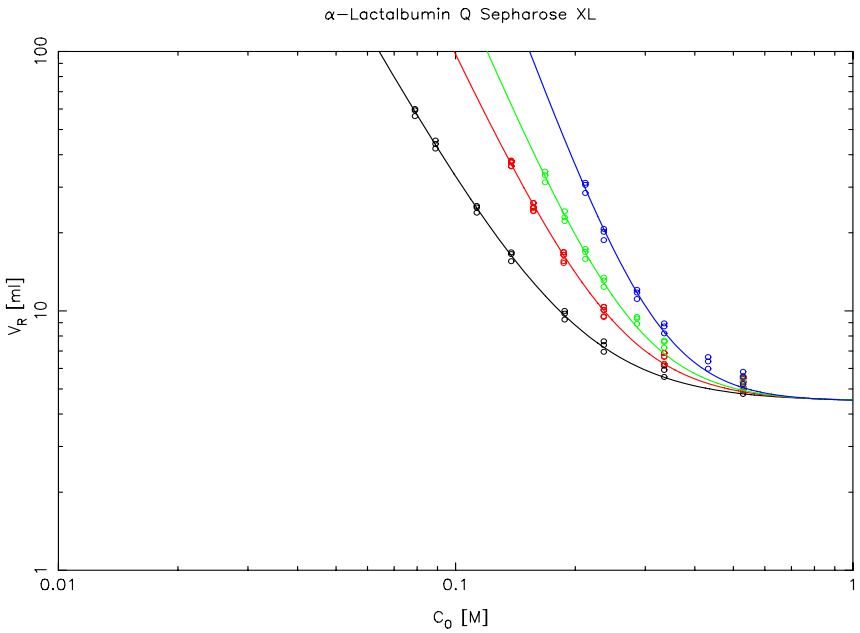

Figure 7.1 Calculated and fitted retention volume. Legends: Black pH=6, red pH=7, green pH=8, and blue pH=9.

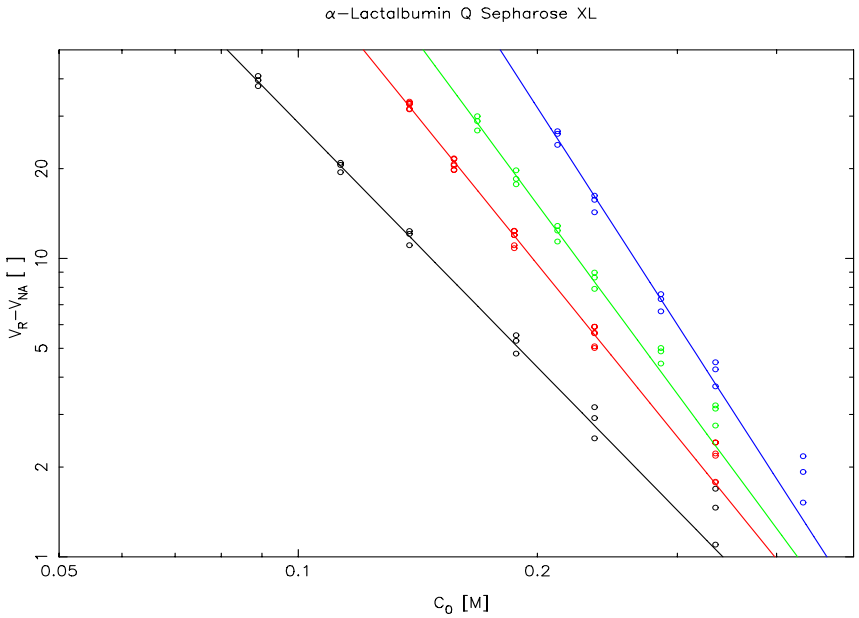

Figure 7.2 Experimental and fitted V_R-V_{NA} as function of the salt concentration. The slope is equal to -ν. Legends as figure 7.1.

7.2.1 Peclet Number

Experiments at pH=7 and $C_{0,nom}$=500 mM (corresponding to non-binding conditions) at different flow rates were made, and the reduced plate height were plotted against the velocity, figure 7.3.

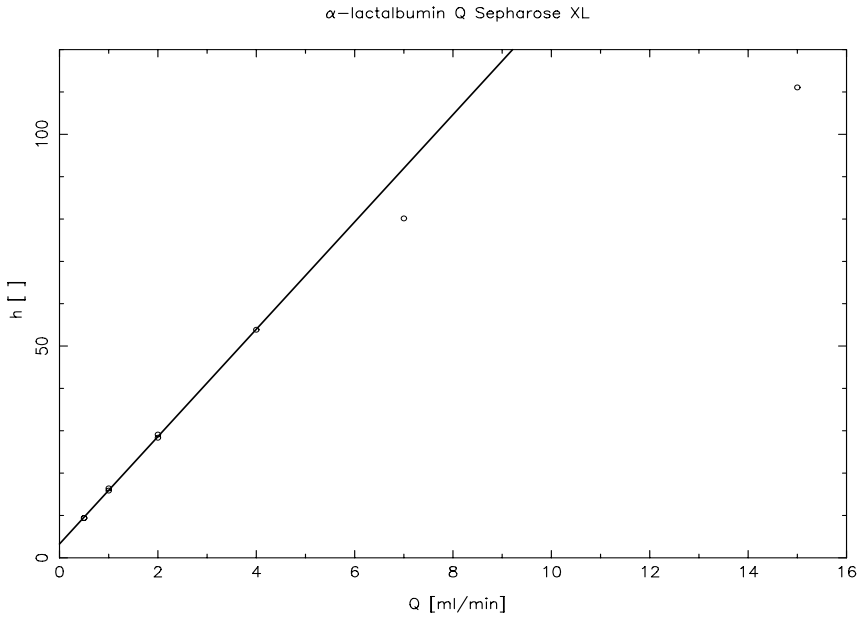

Figure 7.3 Reduces plate height as a function of the flow rate at non-binding conditions. The data are given in table 7.2 below.

runDate	*Flow rate*	*Reduced plate height*
yyyymmddhhmm	[ml/min]	[ ]
200108311446	0.5	9.39
200108311627	0.5	9.44
200108311530	1	15.87
200108311711	1	16.40
200108311555	2	28.35
200108311736	2	29.10
200109040836	4	53.85
200109040845	7	80.14
200109040853	15	111.08

Table 7.2 Parameters for determination of plate height at non-binding conditions and pH=7.

A straight line was fitted to the values with flow rate from 0.5 to 4 ml/min. The fitted line is plotted in figure 7.3. The line is

$$h(Q) = 12.673\left[\frac{min}{ml}\right]\cdot Q + 3.285 \qquad (7\text{-}2)$$

Where Q is the flow rate in ml/min, with R^2=0.9996.

As seen in figure 7.3 the plate heights determined at the two high flow rates are significantly below the calculated plate height, eq. (7-2). Some of the experiments in table 7.2 (one for each flow rate) are modelled in chapter 7.4 "Fast Fourier Transform at Non-Binding Conditions" below.

From the van Deemter equation, eq. (3-53), is seen that the intercept at v_i=0 is equal to $2/Pe_d$. This gives Pe_d=0.6. It should, however, be kept in mind that this values is calculated from a particle diameter of 90 μm.

7.2.2 Transport Parameters

With a Pe_d=0.6 the transport parameters have been fitted to the van Deemter equation, where the film layer coefficient k_f is calculated by the correlation suggested by Wilson and Geankopolis. The fit is given in figure 7.4, and the calculated parameters are given in table 7.3.

From the figures it is seen that k_f is approximately 10 times higher than k_p and k_q indicating that it is the mass transport inside the particles that controls the mass transport.
From the figure it is additionally seen that the plate height is independent of the pH-value as assumed.

Parameter	*Unit*	*Value*
Pe_d	[ ]	0.6
k_p	[m/s]	$2.239 \cdot 10^{-6}$
k_q	[m/s]	$1.009 \cdot 10^{-6}$
k_f(Q=½ ml/min)	[m/s]	$14.023 \cdot 10^{-6}$
k_f(Q=1 ml/min)	[m/s]	$17.668 \cdot 10^{-6}$
k_f(Q=2 ml/min)	[m/s]	$22.260 \cdot 10^{-6}$

Table 7.3 Calculated transport parameters from fitting of van-Deemter equation. The film layer coefficient is calculated from the correlation by Wilson and Geankoplis.

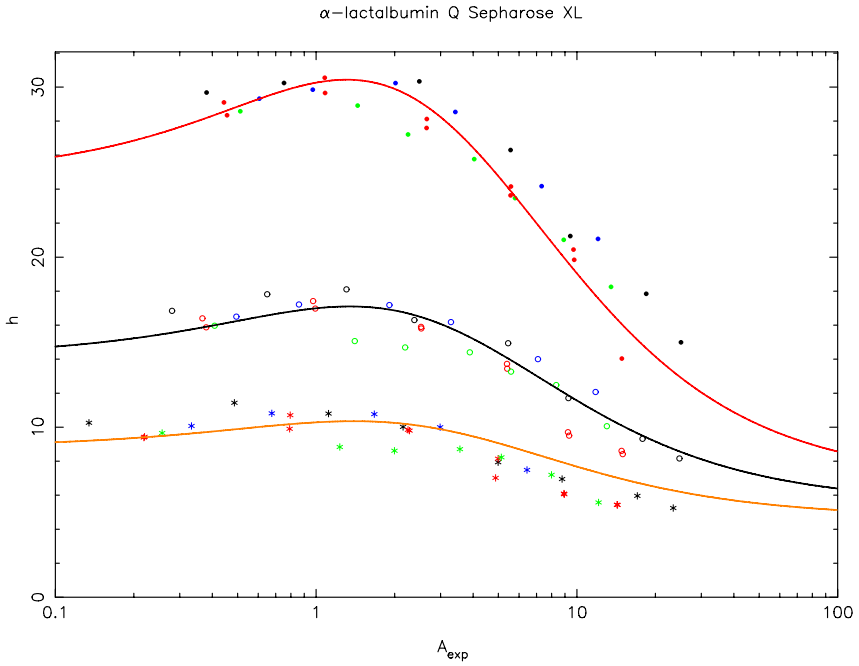

Figure 7.4 Calculated and experimental reduced plate height as a function of the experimental A-value. A_{exp} is calculated by isolating A in equation (6-16).

Legends: Q=½ (orange line), 1 (black line) and 2 ml/min (red line)

** = ½ ml/min, o = 1 ml/min, • = 2 ml/min. Colours: pH 6 = Black, pH 7 = Red, pH 8 = green, pH 9 = blue.*

7.3 Results from Fast Fourier Transform

With the equilibrium parameters and transport parameters determined above, the experiments can be modelled using FFT. Three different cases have been modelled, one at non-binding conditions, one at moderate binding conditions, and one strong binding conditions. The flow rates for the three cases are ½, 1, and 2 ml/min.

All the calculated peaks are scaled to the same height as the experimental peak, to ease comparison of experimental and fitted results.

The easiest way to investigate the approximation of pooling the Pe_d-number with the film layer mass transfer coefficient, k_f, is to plot both simulations in the same diagram. The resulting chromatograms are given below. In all the chromatograms is seen that the lines with pooled Pe_d/k_f coincide with the lines without the pooled parameters. Indicating that the approximation is a good approximation.

From eq. (7-2) is seen that the axial dispersion accounts for approximately 3 particle diameters and at the weak binding conditions the total plate height is approximately 9 particle diameters, and at strong binding the total plate height is approximately 8 particle diameters, figure 7.6. The axial dispersion hence contributes significantly to the total zone spreading. Even under these conditions it is seen that the two calculated chromatograms coincide, justifying the pooling of the axial dispersion with the film layer mass transfer coefficient.

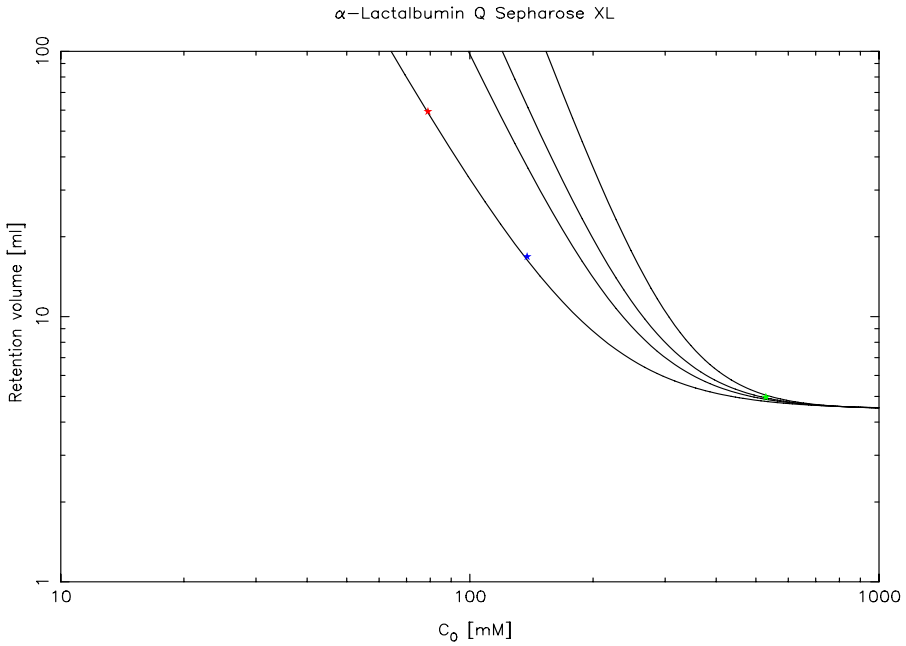

Figure 7.5 Location of retention volume for the modelled experiments. Colours: blue = 200110152105, red = 200110160941, and green = 200108311446.

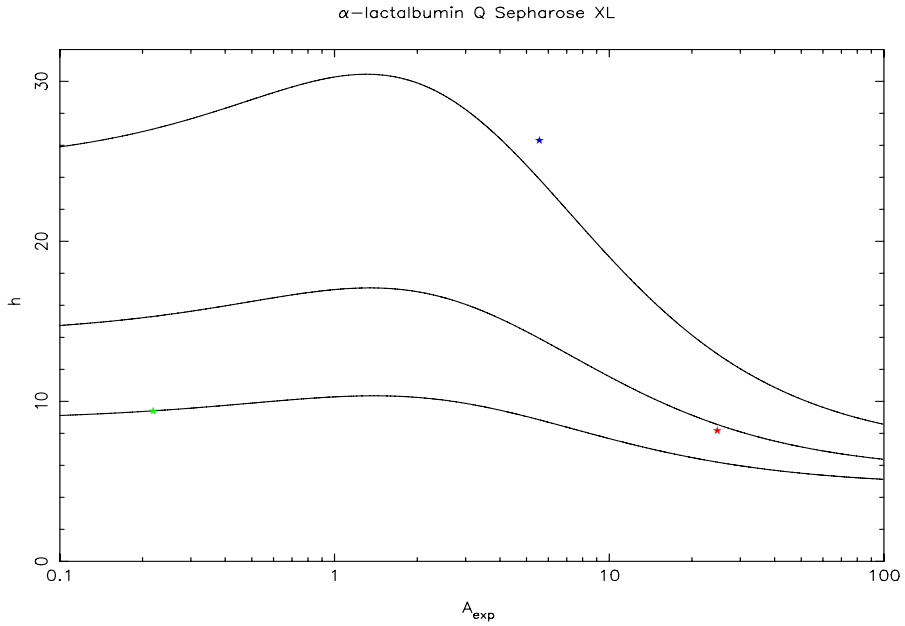

Figure 7.6 Reduced plate height for the modelled experiments. Colours: blue = 200110152105, red = 200110160941, and green = 200108311446.

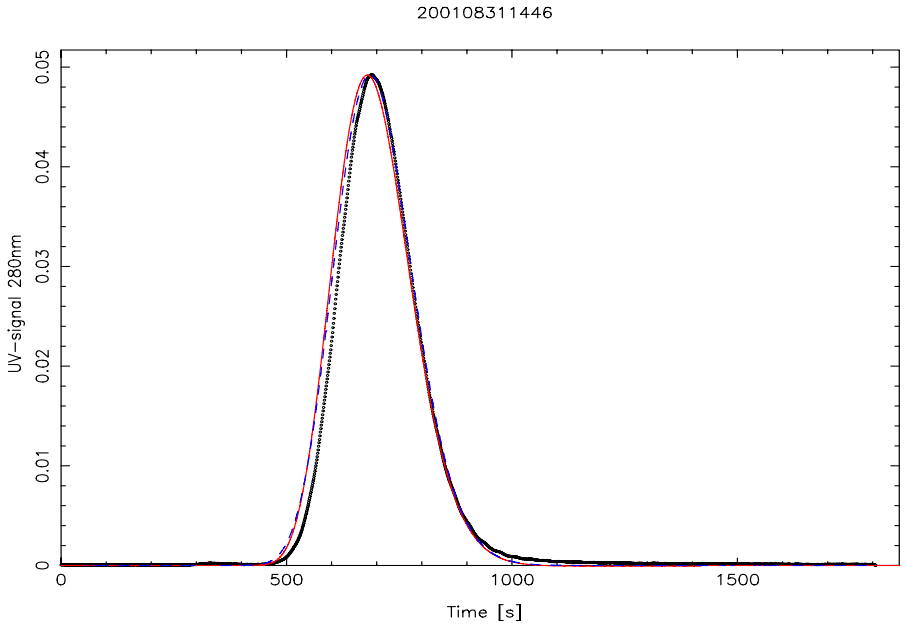

Figure 7.7 Calculated chromatogram at non-binding conditions. Process parameters pH=7, C_0=529 mM, and Q=½ ml/min. Legends: The full red line is the line with the pooled Pe/k_f-numbers. The dashed blue line is without pooling the Pe-number with k_f. The black dots are the the experimental values.

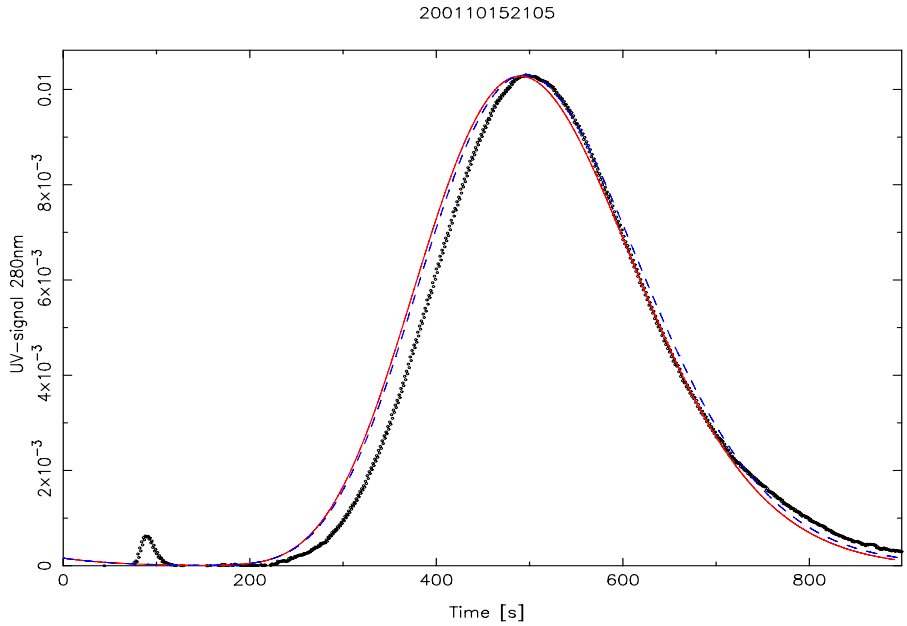

Figure 7.8 Calculated chromatogram at medium-binding conditions. Process parameters pH=6, C_s=138 mM, and Q=2 ml/min. The legends are as given in figure 7.7.

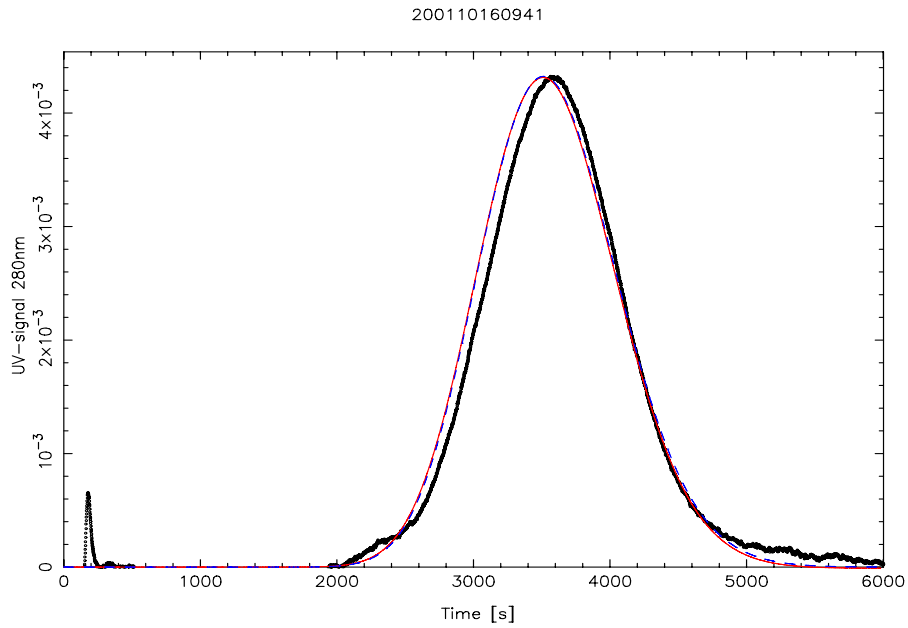

Figure 7.9 Calculated chromatogram at strong-binding conditions. Process parameters pH=6, C_0=79 mM, and Q=1 ml/min. The legends are as given in figure 7.7.

7.4 Fast Fourier Transform at Non-Binding Conditions

Modelling of the chromatograms at pH=7 and C_0=529 mM and for the various flow rates, the experiments given in table 7.2, reveal an interesting result (Q=½ ml/min is already given in figure 7.7). It has previously been shown, eq. (3-63), that the largest deviation between the model including and excluding axial dispersion is expected at low binding. First of all it is noted that the experimental retention volume is above the fitted line, resulting in a too low calculated retention volume which is also seen from the figures below.

From the figures 7.7, 7.10, and 7.11 is seen that the calculated results from pooling Pe_d and k_f coincide.

When the flow rate is increased to 4 ml/min, figure 7.12, a second peak appears at the front. The calculated chromatogram with the pooled Pe_d/k_f parameters shows a sharp peak and a step up in concentration from 0 to app. 0.008 and the two calculated chromatograms no longer coincide.

Increasing the flow rate further to 7 ml/min, figure 7.13, the model including axial dispersion shows a second peak at the front and the step up for the pooled model becomes even more significant.

At 15 ml/min, figure 7.14, the pooled model breaks completely down, and the model including axial dispersion shows a sharp front followed by a long tailing.

This all indicates that at the high flow rates a part of the protein goes straight through the column without even getting in contact with the resin. This is a clear indication of a too high flow rate in these experiments.

It must, however, be expected that this phenomenon is most dominant at non/weak-binding conditions, where the driving force between the particles and the mobile phase is the lowest.

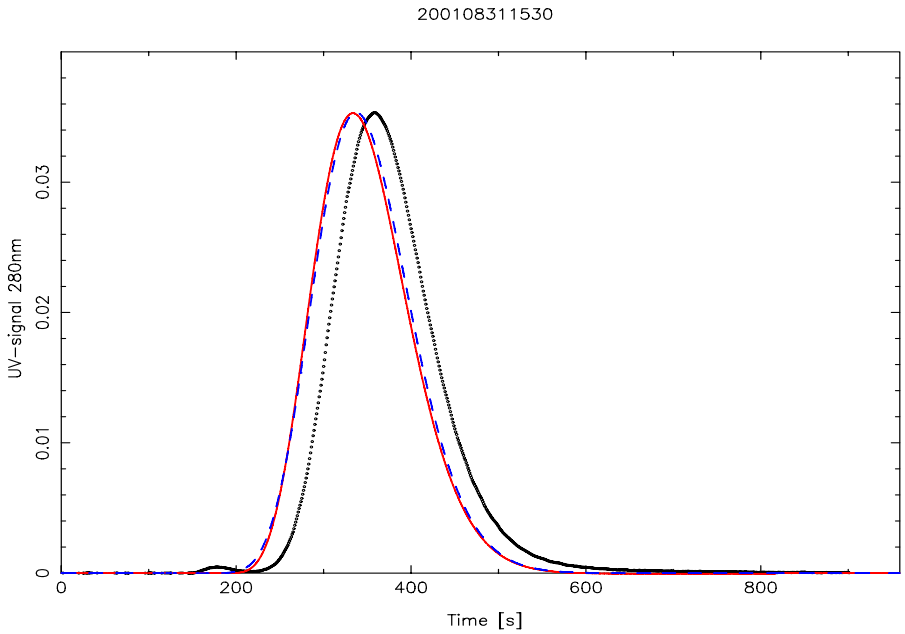

Figure 7.10 Calculated chromatogram at non-binding conditions. Process parameters pH=7, C_0=529 mM, and Q=1 ml/min. The legends are as given in figure 7.7.

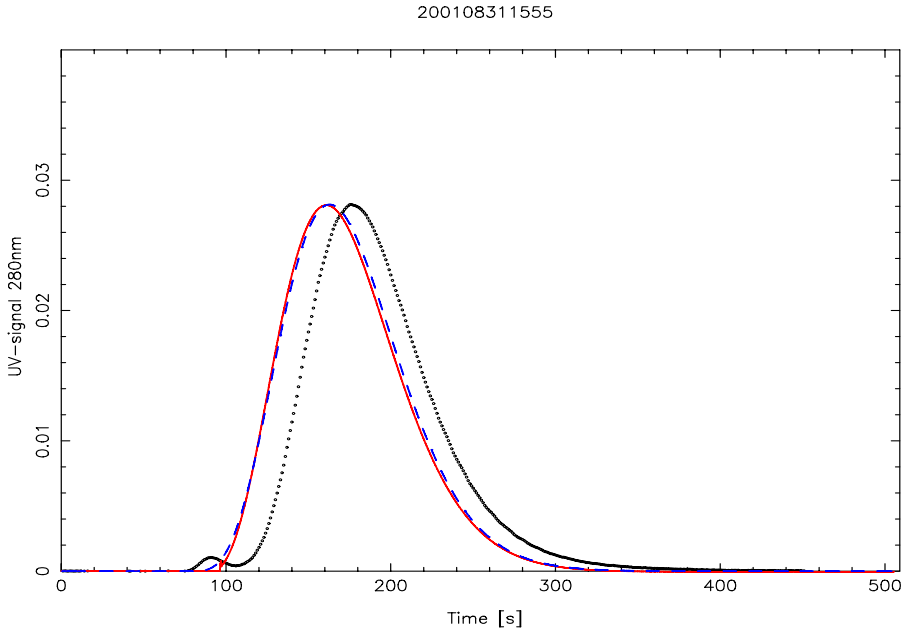

Figure 7.11 Calculated chromatogram at non-binding conditions. Process parameters pH=7, C_0=529 mM, and Q=2 ml/min. The legends are as given in figure 7.7.

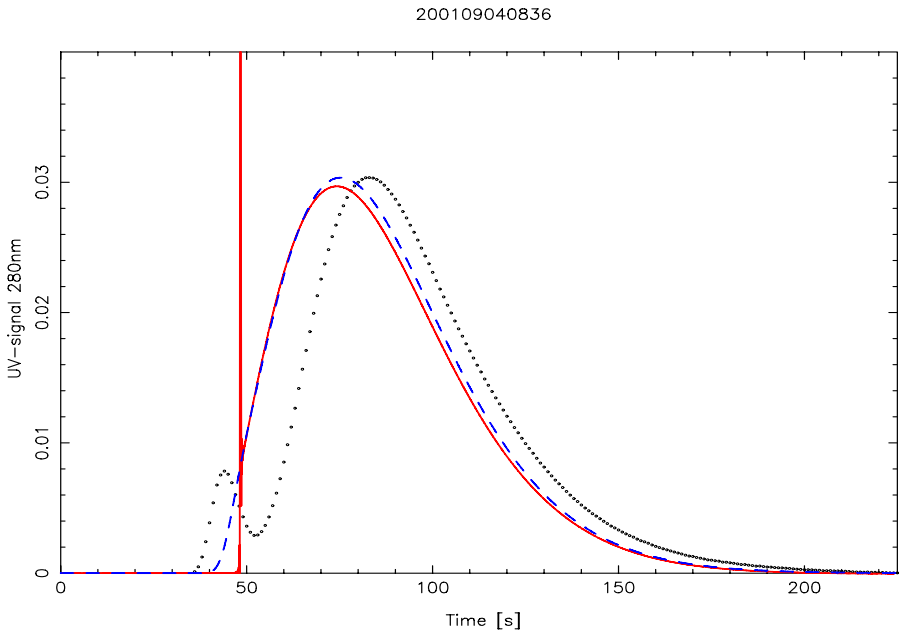

Figure 7.12 Calculated chromatogram at non-binding conditions. Process parameters pH=7, C_0=529 mM, and Q=4 ml/min. The legends are as given in figure 7.7.

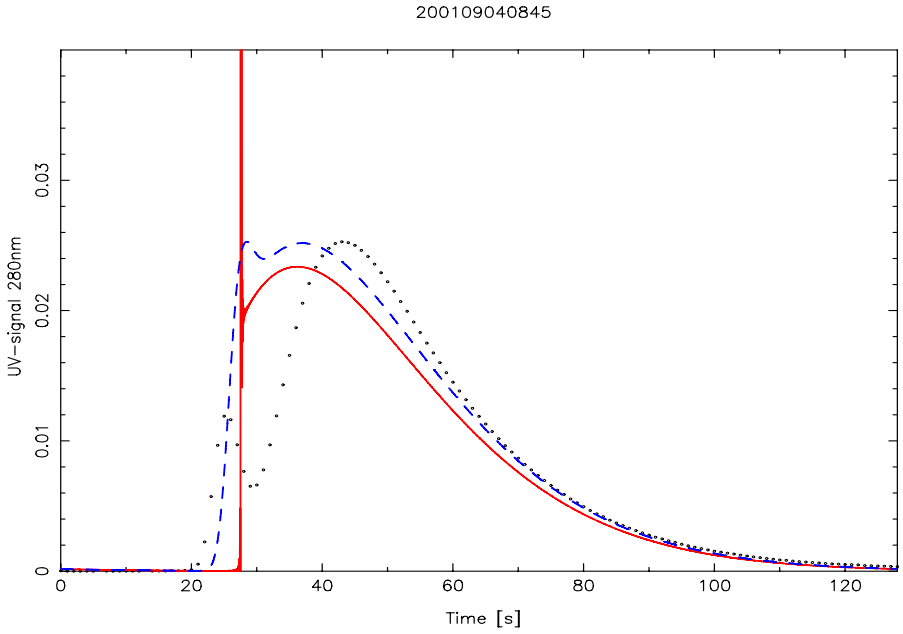

Figure 7.13 Calculated chromatogram at non-binding conditions. Process parameters pH=7, C_0=529 mM, and Q=7 ml/min. The legends are as given in figure 7.7.

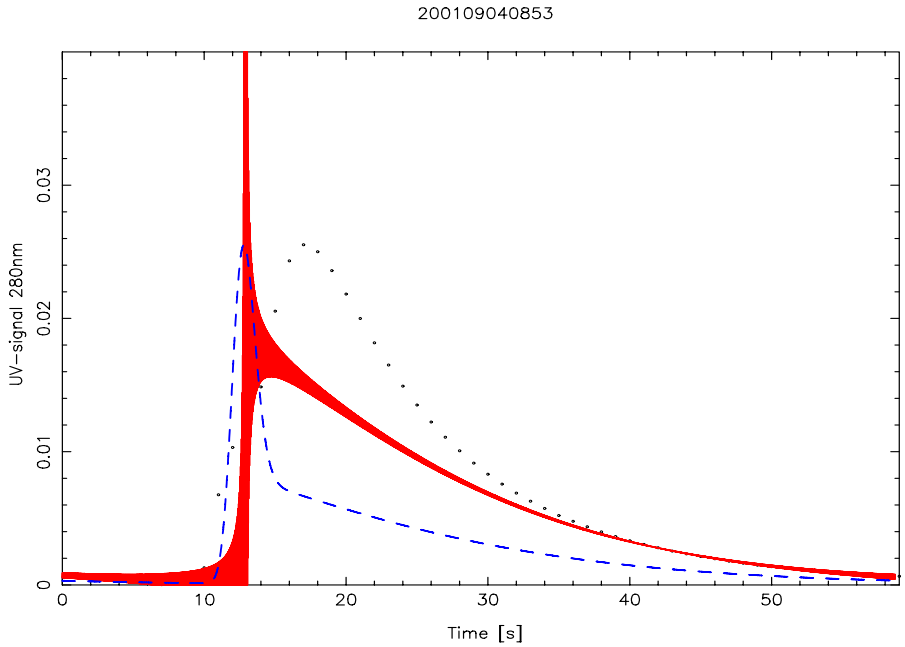

Figure 7.14 Calculated chromatogram at non-binding conditions. Process parameters pH=7, C_0=529 mM, and Q=15 ml/min. The red area is due to oscillations. The legends are as given in figure 7.7.

7.5 Summary

The present chapter gives an example of how to determine the equilibrium and transport parameters for a protein and how these can be used to model the isocratic elution of the linear isotherm.

Flow rates of 7 and 15 ml/min on the Q Sepharose XL column is high and this flow rate can result in a part of the protein never gets in contact with the particles. These high flow rates, however, still gives reasonable results for the first moment. The higher central moments are usually more uncertain. Reducing the flow rate gives excellent results.

The approximation by pooling the Pe_d-number with the St_f-number, chapter 3.7.3 “Eliminating Axial Dispersion“, is also seen to be a good approximation, and for most operating conditions the difference cannot be visually seen on a chromatogram.

The linear part of the isotherm has now been evaluated thoroughly. In preparative chromatography the protein concentrations are normally in the non-linear part of the isotherm and this has to be determined.

8. Breakthrough Experiments

The non-linear part of the isotherm can be determined by either breakthrough experiments or batch experiments. In breakthrough experiments the resin is packed in a column and the column is fed with protein. After breakthrough the protein in the piping and in the interstitial volume is washed out of the column and finally the bound protein is desorbed from the column. A detailed method description is given in appendix I “Breakthrough Experiments”. The breakthrough experiments have been made using the three columns packed with Source 30Q given in table 1.5.

As mentioned in the previous chapter only the non-linear part of the isotherm has to be determined after the pulse experiments. Insertion of eq. (2-3) into (2-2) and introduction the dimensionless variables gives

$$A_i = \frac{q_i}{y_i} = K_{eq,i}\left(\frac{1-\sum_{j=1}^{NP}(\sigma_j+\nu_j)q_j}{y_0}\right)^{\nu_i} \tag{8-1}$$

The only parameter to determine after the pulse experiments is the shielding parameter, σ. Since the protein concentrations are positive, the relative amount of bound protein, A, decrease when the protein concentration is increased, corresponding to a downward curvature of the isotherm.

8.1 Differential Column Breakthrough Curves

The isotherms for BSA on Source 30Q were determined using the differential columns given in table 1.5 named 10 drops and 20 drops.

The capacity of the differential columns were measured with hydroxide and with nitrate. As previously mentioned in chapter 5.2.1 “Hydroxide Capacity” it is difficult to saturate the column with hydroxide due to its very weak binding to the ion exchanger. The nitrate capacity was also measured and the results are given in table 8.1 below. As seen from the table the nitrate capacity varies from 0.0146 mmole to 0.0237 mmole for the column with 20 drops of resin slurry. As mentioned in chapter 5.2.2 “Nitrate Capacity” a large amount of nitrate can be washed out of the column. The dead volume of the differential columns is very small and the amount of washing water is several times the column volume. From this it was concluded that it was not possible to determine the ion exchange capacity of the differential columns.

A number of breakthrough experiments with BSA were made on the differential columns, a typical breakthrough curve is given in figure 8.1 below. As seen from the figure the

breakthrough comes very shortly after the column has been put in line.

When the isotherms were plotted it was noted that the ratio between the adsorbed amount of protein for the two columns was not constant. At strong binding the ratio between the adsorbed amount of protein from the two columns was close to 2.4, figure 8.2. Lowering the pH-value or increasing the salt concentration this ratio was reduced, figure 8.3.

Both a reduction of the pH-value and an increase in the salt concentration reduces the binding. Plotting the ratio between the adsorbed amount of protein for the two columns, figure 8.4, this showed that when the bound amount of protein is reduced the ratio between the adsorbed amount is reduced, too. This means that the small column adsorbes a relative larger amount of protein compared to the larger column.

For (almost) all the experiments 50 ml protein solution was fed to the columns. If a strong bound component is present in the solution the adsorbed amount of this is relatively larger for a small column than for a large column, and therefore also the desorbed amount. When the adsorbance of the weaker bound BSA is reduced this tendency will become more clear, this can be seen from

$$\frac{m_{des,20}^{tot}}{m_{des,10}^{tot}} = \frac{m_{des,20}^{BSA} + m_{des,20}^{SB}}{m_{des,10}^{BSA} + m_{des,10}^{SB}} \tag{8-2}$$

where m_{des} is the desorbed amount, the index 10 and 20 are the column size, and the superscripts tot is total, BSA is for BSA, and SB is Strong Bound. Since the same amount of protein solution is used for both columns m_{des}^{SB} will be constant if the strong bound component is totally adsorbed. At a weaker binding of BSA the adsorbed amount approaches zero and the ratio given in eq. (8-2) will approach unity. At a strong binding of BSA m_{des}^{BSA} will be the dominating term and the true ratio between the column sizes will be approached. This is also the behaviour seen in figure 8.4.

The next question is naturally if BSA contains any strong bound components. In figure 8.5 is shown a chromatogram from a gradient experiment. Beside the BSA peak a second peak is present after the BSA peak corresponding to a stronger bound component.

Q_{load} [ml/min]	V_{load} [ml]	V_{wash} [ml]	λ [mmole]
1.00	30	25	0.0194
5.00	30	25	0.0156
1.00	50	25	0.0237
5.00	30	25	0.0173
1.00	30	25	0.0212
5.00	30	40	0.0146
5.00	50	40	0.0171
5.00	50	50	0.0168
5.00	50	50	0.0164
5.00	50	50	0.0164

Table 8.1 Nitrate capacity measurements packed with 20 drops of Source 30Q. The column was equilibrated with 25 ml 2M NaCl. Hereafter the system was washed with 25 ml 1 M KNO_3 with the column bypassed. and loaded with V_{load} of nitrate, at Q_{load}. The system was washed with 25 ml water, the column put inline for V_{wash} and finally eluted with 25 ml 2 M NaCl.

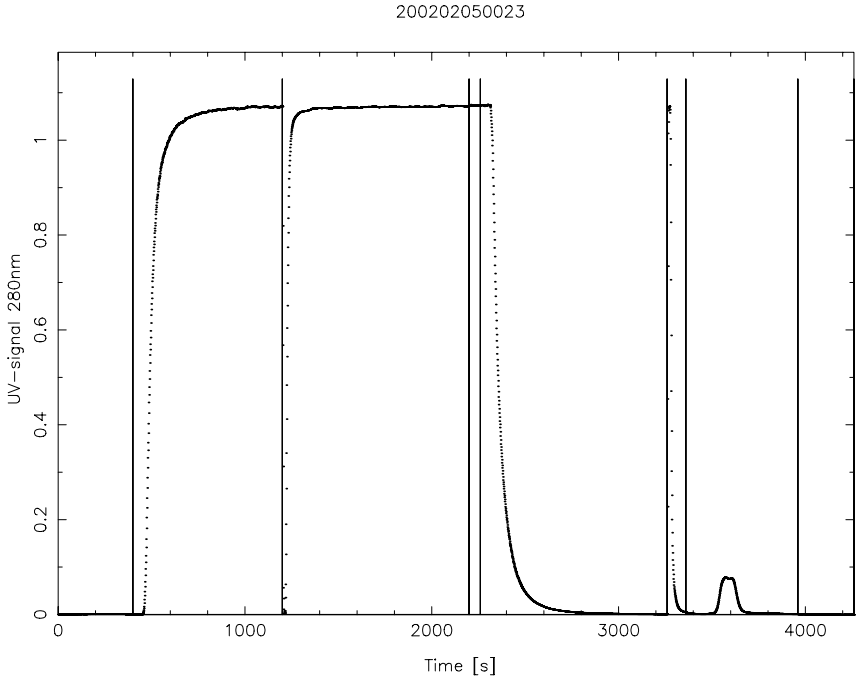

Figure 8.1 Typical breakthrough curve on a differential column Q=3 ml/min.

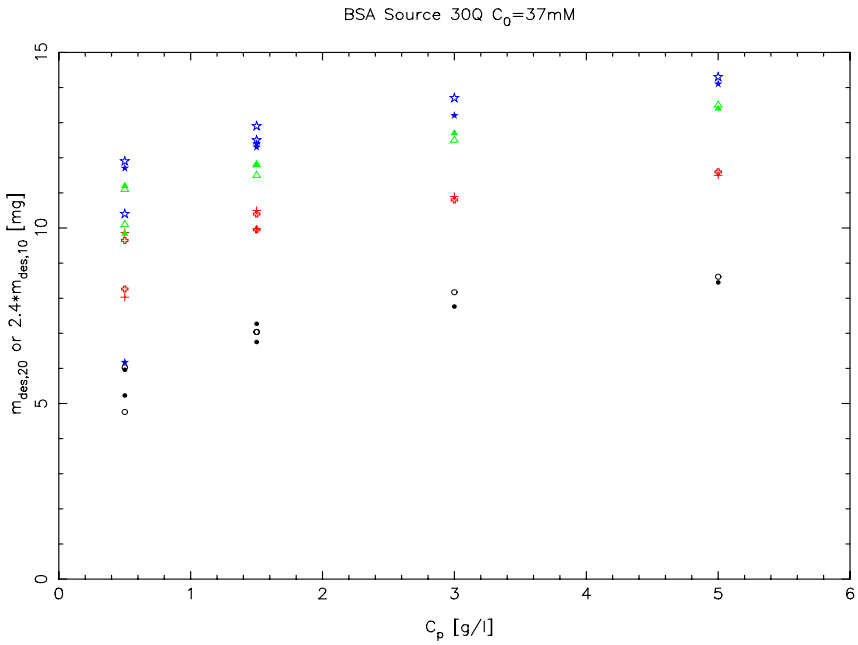

Figure 8.2 Desorbed amount of BSA on the Source 30Q 20 drops and 10 drop columns. Legends: Black pH=6, red pH=7, green pH=8, and blue pH=9. Solid figures 10 drops column, open figures 20 drops column.

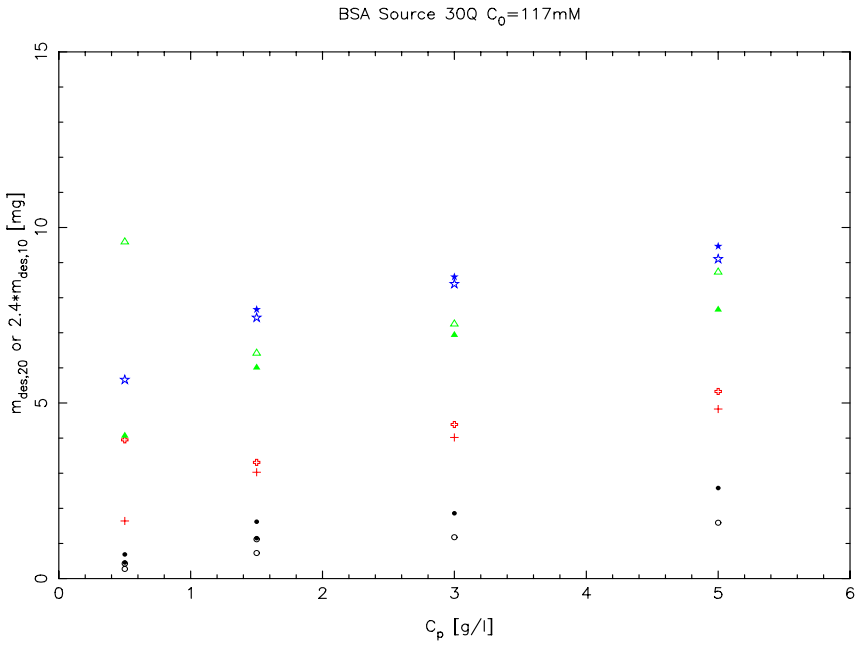

Figure 8.3 Desorbed amount of BSA on the source 20 drops and 10 drop columns. Legends: Black pH=6, red pH=7, green pH=8, and blue pH=9. Solid figures 10 drops column, open figures 20 drops column.

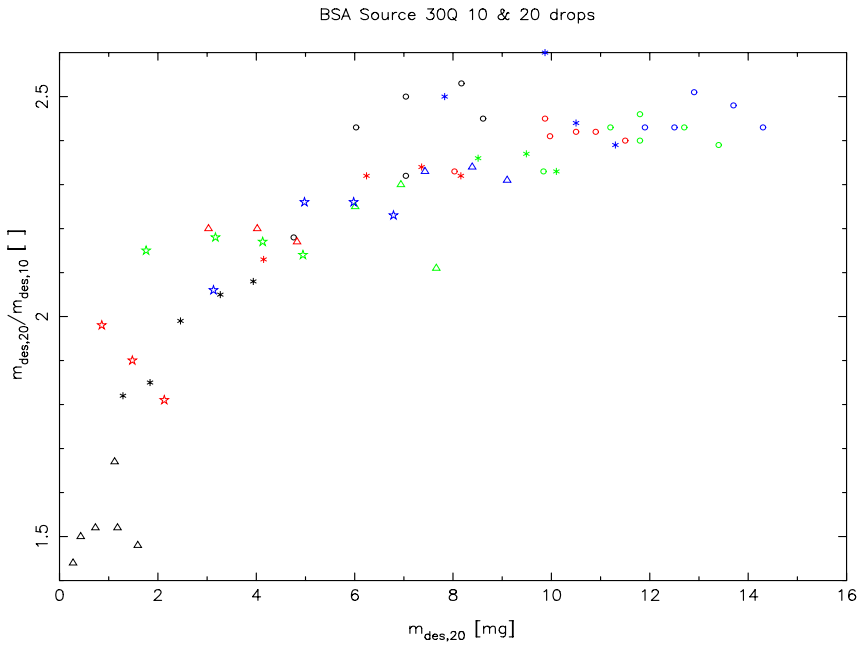

*Figure 8.4 Relative desorbed amount of BSA on the source 20 drops and 10 drop columns. Legends: Black pH=6, red, pH=7, green pH=8, blue pH=9, o C_0=37 mM, * C_0=77 mM, Δ C_0=117 mM, and open stars C_0=157 mM.*

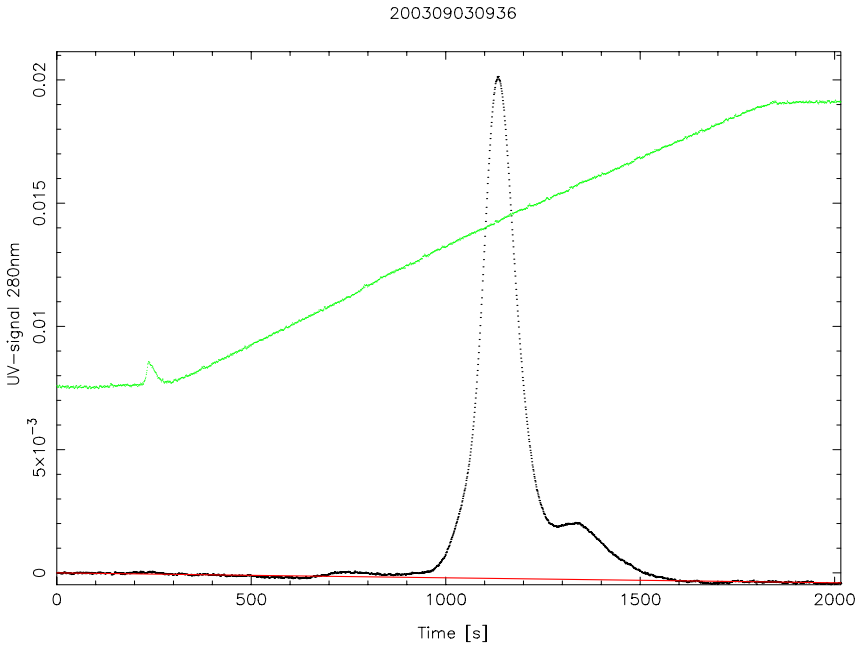

Figure 8.5 Gradient experiment with BSA. A second peak after the BSA peak is observed, this corresponds to a stronger bound component. The red line is the baseline, the green dots are the conductivity (scale not shown) and the black dots are the UV-absorbance.

From the above is seen that the measured capacity can be greatly influenced by stronger bound impurities. A natural question is, why not evaluate the breakthrough curve at half the peak height. In figure 8.1 is seen that for the differential column experiments the breakthrough comes almost immediately after insertion of the column and subtraction of the dead volume from the measured value will introduce a large error.

Another disadvantage of these breakthrough experiments is that the HPLC dead volume from the gradient mixer to the UV-detector is approximately 5.3 ml. Requiring a washing volume four times this volume and for breakthrough etc. the protein consumption easily becomes 50 ml for one data point. The protein consumption therefore cannot be neglected for differential column experiments.

With the many disadvantages of the differential column: Impossible to determine the size, difficult to determine the half breakthrough time, large impact of impurities, and large protein consumption it would be more natural to use a larger column.

8.2 Larger Columns

Pedersen (2003, p. 85) has previously determined the BSA-isotherms at pH=7 and pH=8 using the 1.35 ml column packed with Source 30Q in table 1.5. Pedersen fitted the data in a number of different ways (Pedersen, 2003, pp. 73-88). At weak binding it was observed that the desorbed amount from the breakthrough curves was normally higher than the fitted values, when only the shielding parameter was fitted. In the experiments the same amount of protein was fed to the column. That means $V_{feed} \cdot C_{feed}$ is constant.

Comparing the Source 30Q columns 1.35 ml and 8.07 ml, table 1.4 and 1.5, it is seen that the total porosity is the same for both columns. Fixing the interstitial porosity to the same value leads to the same particle porosity, additionally it is seen that $K_{D,BSA}$ is (almost) the same. Therefore it does not matter whether the data are plotted as a function of the column volume, the available pore volume, or A (=Q/C) when comparing the desorbed amount of protein from the two columns.

However, it is seen that the concentration of binding charges is much lower for the 1.35 ml column compared to the larger 8.07 ml column. This leads to the much different value of Λ_{NO3}. Since Λ in the model is raised to the power of ν it is seen that any deviation in this will have a dramatic effect on the results as previously mentioned. Since the equilibrium constant and the number of binding charges are determined from the 8.07 ml Source 30Q column and

the breakthrough experiments are determined using the 1.35 ml column, Λ for the small column has been set equal to Λ for the 8.07 ml column, when the shielding parameters have been fitted, this therefore corresponds to scaling on the basis of the column volume, eq. (6-18). The results are given in figure 8.6 below.

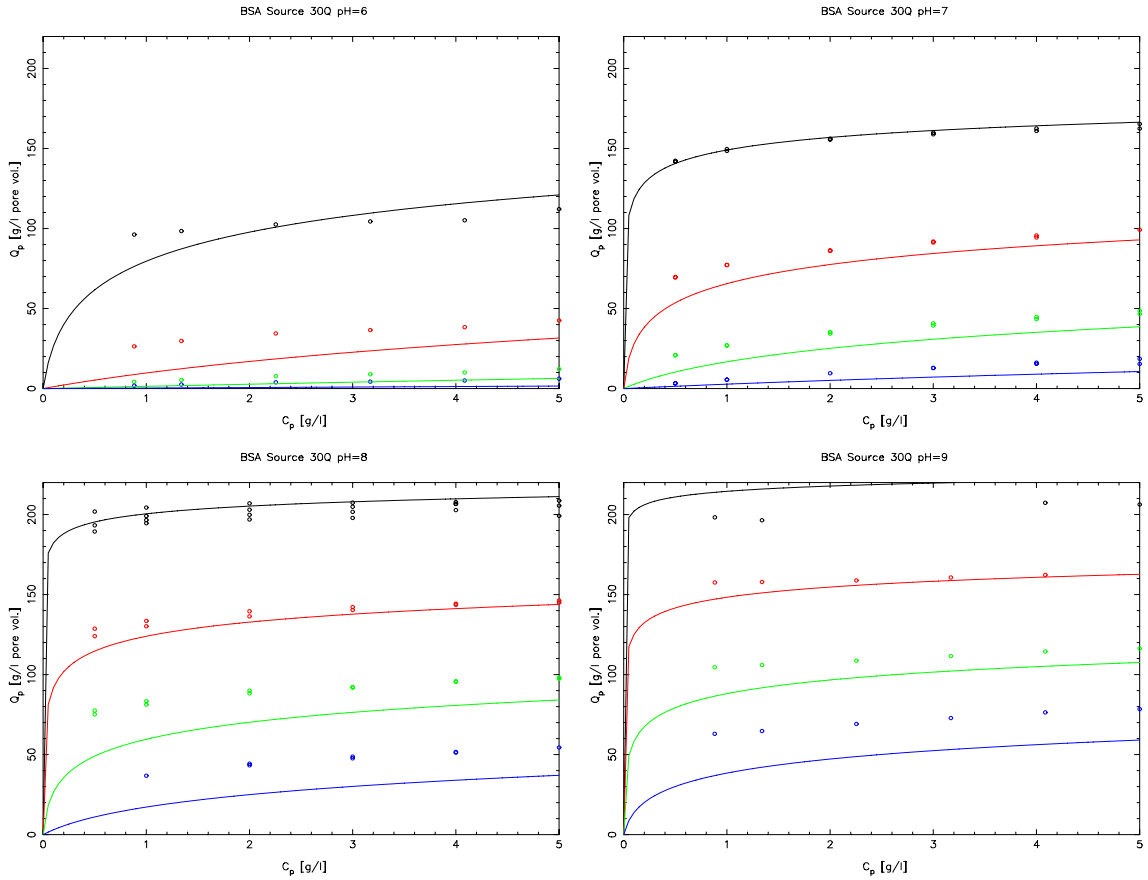

Figure 8.6 Isotherms for BSA and Source 30Q. One shielding parameter for each pH has been fitted. The fitted parameters are: pH=6 σ=67.7, pH=7 σ=73.5, pH=8 σ=61.3, and pH=9 σ=58.5.

Legends: Black C_0=37-38mM, red C_0=77-78mM, green C_0=117-118mM, and blue C_0=157-158mM.

As seen from the isotherms at weak binding the fitted isotherm always underestimates the experimental value. At pH 6 it is seen that not even the initial slope of the isotherm is sufficient to match the experimental points on the isotherms. This has been investigated closer.

The desorbed amount of protein must correspond to the volume of the adsorbed phase times the concentration of bound protein inside this volume.

$$m_{des} = V_{ads} \cdot q \qquad (8\text{-}3)$$

Division by the feed concentration and insertion of the adsorbed volume gives

$$A = \frac{q}{y} = \frac{m_{des}}{V_{col}(1-\epsilon)\epsilon_p K_D y} \tag{8-4}$$

The experiments from the isocratic experiments and the breakthrough experiments can therefore be plotted together, by isolating A in eq. (6-16) and (8-4), and plotting this as a function of the salt concentration. The pulse experiments will form an upper boundary, eq. (8-1), and all breakthrough experiments will lay on or below this line.

At pH 6, figure 8.7 is seen that this is not the case. At weak binding the bound amount of protein from the breakthrough experiments are above the isocratic experiments, when the proteins binds stronger, A from the breakthrough experiments falls below the upper boundary from the isocratic experiments. Therefore it is not possible to use the parameters from the isocratic fit, and only fit a shielding parameter for the breakthrough experiments to match the isocratic experiments.

As previously mentioned for the differential columns a strongly bound component is present in the BSA. This component will have a relative larger effect at weak binding.

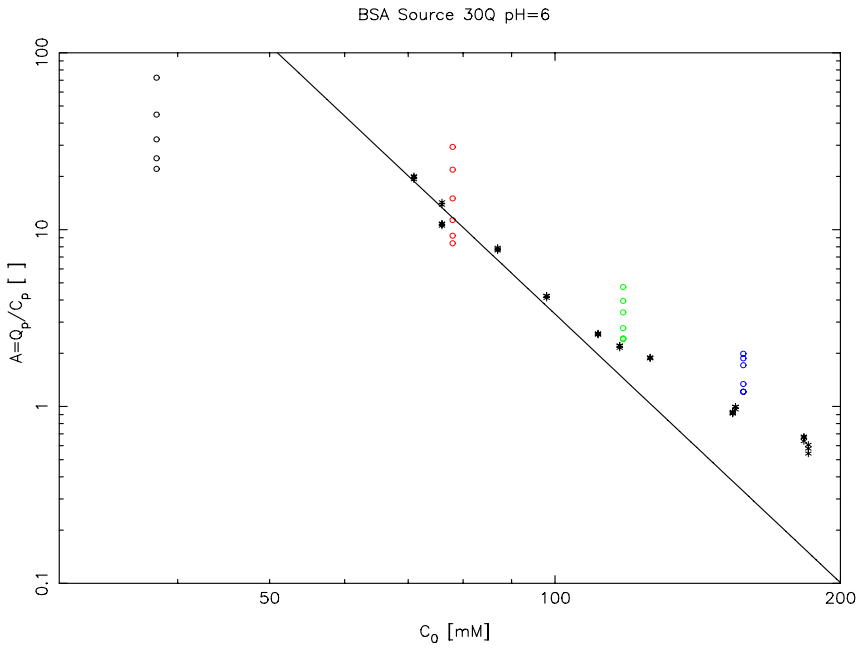

*Figure 8.7 Relative binding of BSA at pH=6 from isocratic and breakthrough experiments. Legends: black * isocratic experiment, black line fitted equilibrium parameters from isocratic experiments. Open circles breakthrough experiments. Black C_0=38 mM, Red C_0=78 mM, green C_0=118 mM, and blue C_0=158 mM.*

At weak binding the breakthrough curve looks very much like the breakthrough curve for the differential column, figure 8.1. And also here it is difficult to determine the breakthrough time at half the breakthrough height. For the experiments at pH=6 this has been done. A is calculated by isolating A in

$$V_{½} - V_{NA} = V_{col}(1-\epsilon)\epsilon_p K_D A \qquad (8\text{-}5)$$

Where $V_{½}$ is the volume from insertion of the column until half of the UV-signal at breakthrough has been reached, figure 8.9.

A more detailed derivation of this is given on page 140. The results are plotted in figure 8.8. It is seen that A from the breakthrough experiments here allways falls below the upper boundary from the isocratic experiments as expected from the SMA-formalism.

A schematic drawing of a breakthrough curve is given in figure 8.9. The volume of a non-adsorbed component is drawn in dark grey. The area of the non-adsorbed component corresponds to the area of the washing peak. When a breakthrough comes almost immediately after insertion of the column, figure 8.1, subtraction of the non-adsorbed volume creates a large error (this is the reason for not including data at the high salt concentration in figure 8.8).

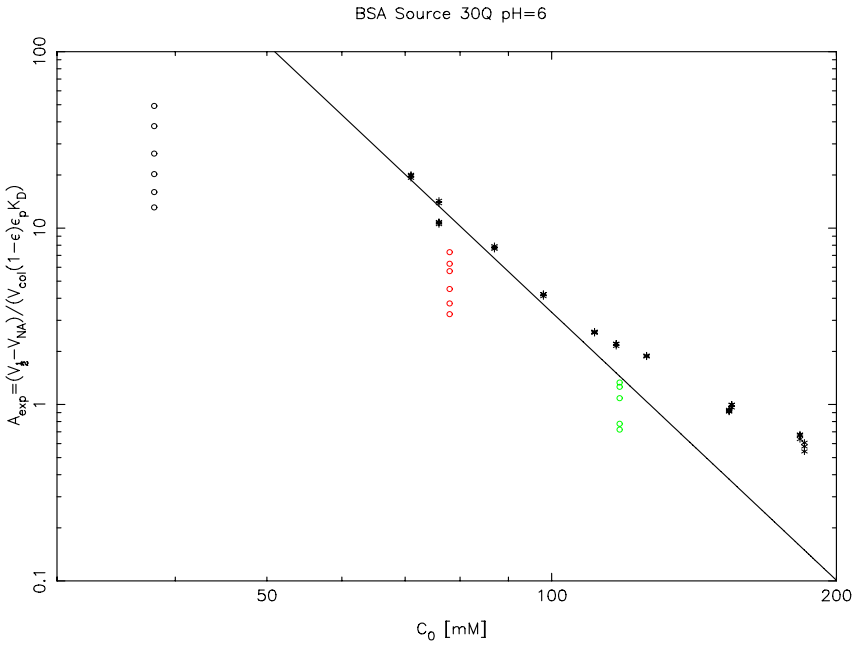

Figure 8.8 Relative binding of BSA at pH=6 from isocratic and breakthrough experiments evaluated at half the breakthrough height. Experiments at C_0=158mM not included due to a too low binding. Legends, see figure 8.7.

For breakthrough experiments on larger columns complete breakthrough is normally not reached, as shown in figure 8.9. Two things can cause this, a slow mass transport or impurities. This is clearly seen from the chromatograms, where a step up is seen when the column is bypassed at the end of the experiment, figure 11.12.

In figure 8.9 a strongly bound component is included, corresponding to e.g. 5% of the total UV-signal. This will be present in the feed stream to the column and will therefore contribute to the total UV-signal when the column is bypassed. When the column is put in-line the strong bound component will be almost completely adsorbed causing a drop in the UV-signal. Increasing the volume where the column is in-line (the volume from 2 to 3 in figure 8.9), the column will be exposed to larger amount of the stronger bound component. At weak binding $V_{½}$ is small and with a large volume where the column is inline ($V_{feed} \cdot C_{feed}$ has been kept constant) the adsorbed amount of BSA will be small and the adsorbed amount of the strong bound component will be large. The stronger bound component will therefore have a significant impact on the desorbed amount. This can cause the large discrepancy between the results in figure 8.7 and 8.8.

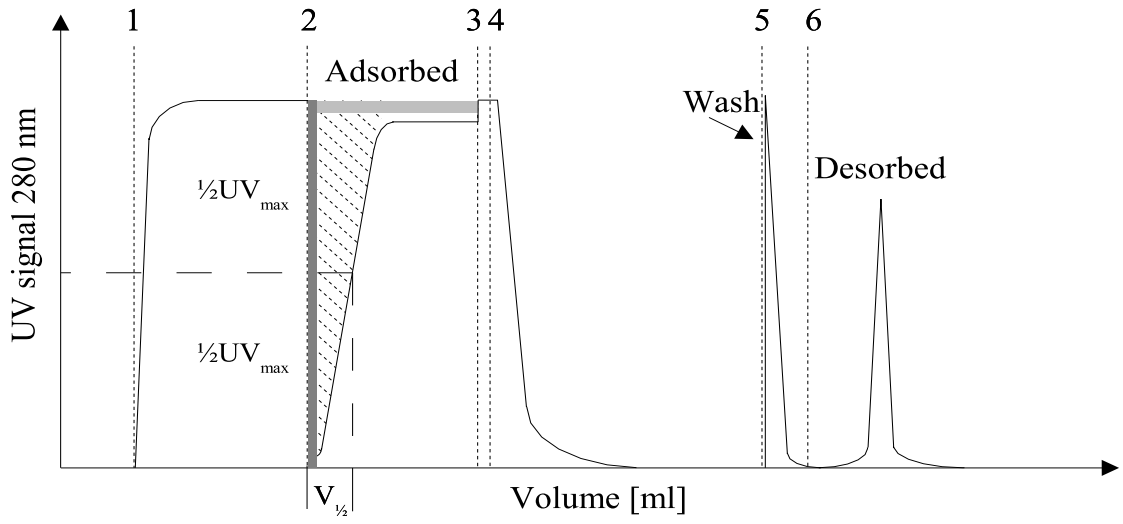

Figure 8.9 Breakthrough curve. The dark grey area after line no. 2 corresponds to the volume of the non-adsorbed phase, V_{NA}. The light grey area between line 2 and 3 corresponds to the UV-signal from a strongly bound component. $V_{½}$ is the volume from insertion of the column to ½ the total UV-signal has been reached.

8.3 Summary

Capacity measurements on differential columns are difficult to analyze, since these are very sensitive to stronger bound impurities in the proteins mixture. In addition to this, it is difficult to determine the size of the column and the protein consumption cannot be neglected for these experiments.

Impurities will have less influence on measured binding capacity when half the breakthrough time is used for capacity measurements rather than the desorbed amount. If a strongly bound component is present this can have a large impact on the desorbed amount of protein.

A more thorough investigation of determining the isotherm from half the breakthrough height, where e.g. flow rates have been changed, has not been made.

Another way to determine the isotherm is from batch experiments, this will be treated in the next chapter.

9. Batch Experiments

Batch methods or static methods has previously been described by Guiochon *et al.* (1994, p. 89) and by Yamamoto *et al.* (1988, p. 121). Bisgaard-Frantzen (1998), has also previously described these methods. However, some findings which have not been reported by these authors will be described here.

In batch experiments resin, buffer and protein is mixed and equilibrated. After equilibration the amount of protein in the liquid phase is determined. The adsorbed amount amount of protein can hereafter be calculated as the difference between the initial and the final concentration in the liquid phase. A detailed method description of the batch experiments is given in appendix J “Batch Experiments”.

The advantage of batch experiments is that only small amounts of protein is required compared to breakthrough curves.

In batch experiments the resin is not packed in a column and a conversion from the capacity measured in the batch experiment to the capacity in a packed column is needed.

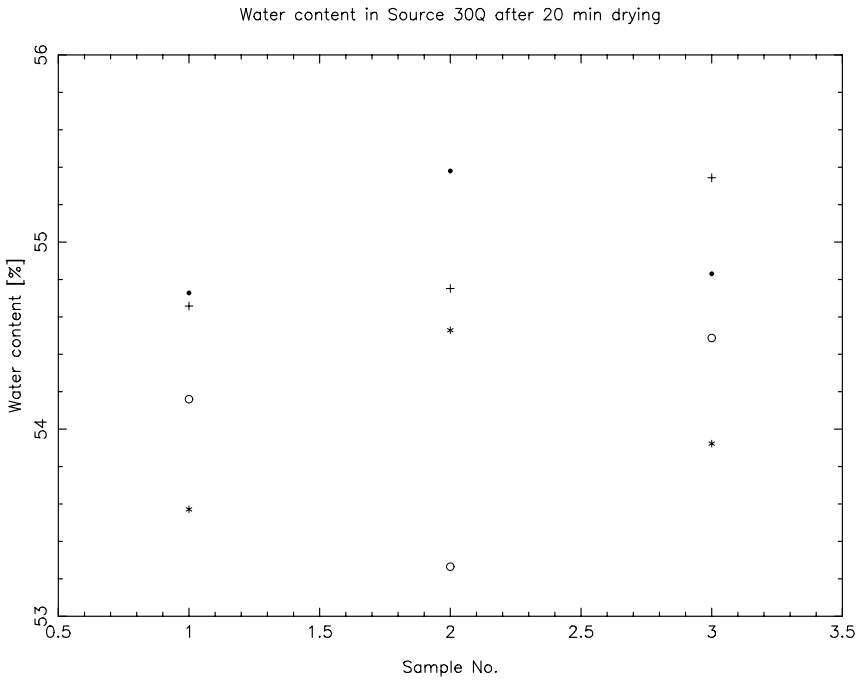

*Figure 9.1 Water content in Source after 20 minutes of drying. • pH 8 C_0=77 mM/1, + pH 8 C_0=77 mM/2, * pH 8 C_0=157 mM/1 and o pH 8 C_0=157 mM/2. Sample no. 1 is taken before the weighting for the experiment, no. 2 in the middle of the experiment and, no. 3 after the experiment.*

Bisgaard-Frantzen (1998) suggested to dry the resin 20 minutes on a glass filter funnel and use this as a reference level. To investigate if this can be used as reference level a number of samples with the mass, m_{res}, were dried in the oven 24 h at 110°C and the dried resin, m_{dry}, was weighed afterwards (the resin is very hygroscopic and a lid must be put on the sample immediately after the resin gets out of the oven). The amount of water was determined as

$$x_{H_2O} = 1 - \frac{m_{dry}}{m_{res}} \tag{9-1}$$

The resin was dried for additional 24 h, to see if the resin was entirely dried. This did not reduce the weight further. The results are given in table 9.1 below and plotted in figure 9.1 above. The variation within each series is low and also the variation among the different series is very limited. From this it was concluded that drying the gel 20 minutes can be used as a reference level. It should be emphasised that the resin after being dried on the filter funnel creates a filter cake. Breaking the filter cake into small pieces before weighing the resin increases the surface and also the evaporation from the surface. Therefore the filter cake was kept as a filter cake during the work and only a small pieces for the sample was “cut” from the filter cake to limit evaporation.

A number of batch experiments were made using the method suggested by Bisgaard-Frantzen. The amount of resin used to determine each point on the isotherm is approximately 200 mg of resin. With 10 points on each isotherm, and four different salt concentration at four different pH-values the required amount of resin cannot be neglected. Additional resin for drying is also required.

One of the benefits of the batch method is the low protein consumption, however, if this is replaced by a large resin consumption the benefits of this method is limited. It was therefore decided to reuse the resin.

At first sight the isotherms were reproducible, figure 9.2 and 9.3. However, after reusing the resin the capacity gradually declined. New experiments starting with new resin were made, where the capacity of the resin was closely followed.

After the resin had been used in a batch experiment it was collected in a bottle. After all resin had been used, the resin from the bottle was packed in a column and regenerated. Then a number of parameters was measured. These were the hydroxide and nitrate capacity, the retention volume at non-adsorbing conditions for BSA, and the nitrate retention volume. The experimental results are tabulated in table 9.2 below.

In figure 9.4 is seen how the isotherm measured June 13th 2003 is lower than the two

isotherms previously measured. Another isotherm using new resin from the same batch was measured the same day. The same buffer and protein solution was used for both isotherms measured June 13th 2002. It is seen that the isotherm with the new resin has a significantly higher binding capacity than the regenerated resin.

Sample no.		m_{res} ***[mg]***	m_{dry} ***[mg]***	m_{H2O} ***[mg]***	H_2O ***[%]***
pH=8, C_0=77/1					
	1	259.1	117.3	141.8	54.73
	2	284.4	126.9	157.5	55.38
	3	427.5	193.1	234.4	54.83
pH=8, C_0=77/2					
	1	250.1	113.4	136.7	54.66
	2	282	127.6	154.4	54.75
	3	350.9	156.7	194.2	55.34
pH=8, C_0=157/1					
	1	168.0	78.0	90.0	53.57
	2	270.5	123.0	147.5	54.53
	3	360.7	166.2	194.5	53.92
pH=8, C_0=157/2					
	1	195.9	89.8	106.1	54.16
	2	372.1	173.9	198.2	53.27
	3	375.5	170.9	204.6	54.49

Table 9.1 Water content in Source 30Q after 20 minuets of drying.

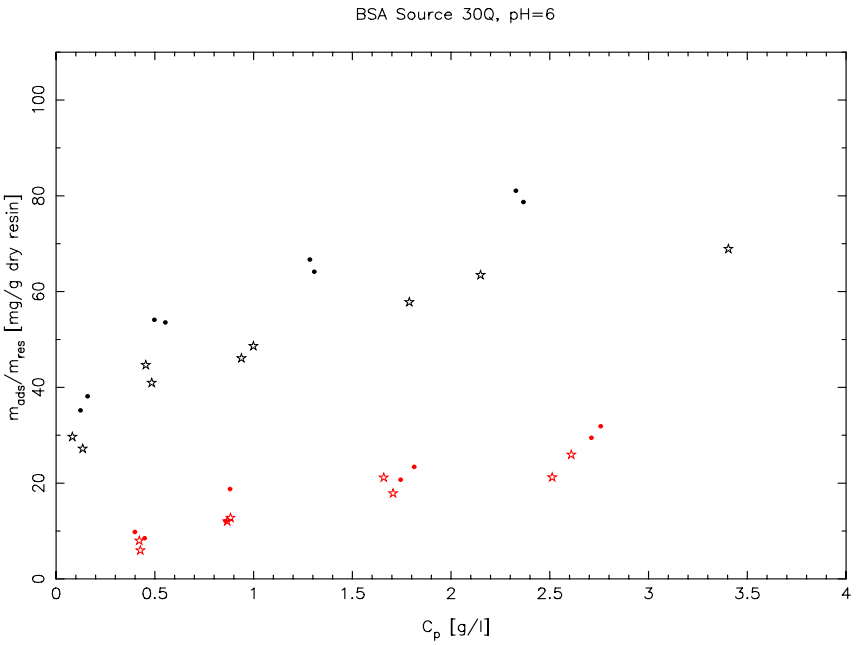

Figure 9.2 Measured isotherms for BSA on Source 30 Q at pH=6.

Legends: black C_0=37 mM, red C_0=77 mM.

Open stars data measured 3/6-2003, and closed circles 23/5-2003.

Date	***YYYYMMDD***	***20020423***	***20020517***	***20030522***	***20020524***	***20020604***	***20020611***	***20020614***
L_{col}	[cm]	10.5	10.5	8.6	7.7	5.7	5.2	3.9
V_{col}	[ml]	21.1	21.1	17.3	15.5	11.5	17.3	7.8
λ_{NO3-}/V_{col}	[mM]	112.8	117.9	107.3	95.7	87.5	85.2	73.5
λ_{OH-}/V_{col}	[mM]	106.9	-	103.6	-	80.6	81.3	79.7
V_{NO3-}/V_{col}	[ ]	-	0.77	0.77	0.77	0.79	0.77	0.81
$V_{NA,BSA}/V_{col}$	[ ]	0.61	0.62	0.62	0.61	0.62	0.62	0.62
$M_{res}/(\rho_{res}V_{col})$	[ ]	0.81	0.72	0.72	0.74	0.73	0.72	-

Table 9.2 Measured parameters for the resin after regeneration in the column.

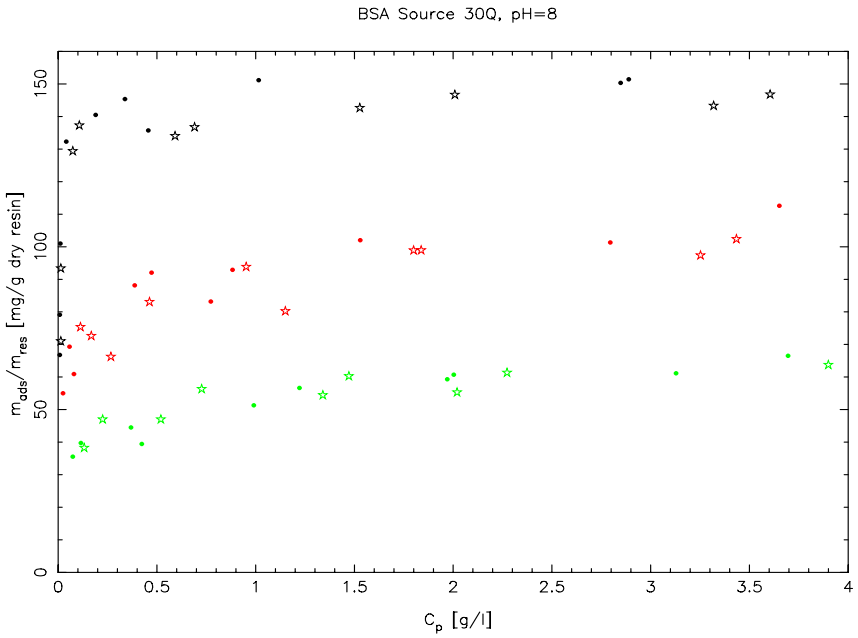

Figure 9.3 Measured isotherms for BSA on Source 30 Q at pH=8. Legends: black C_0=37 mM, red C_0=77 mM, and green C_0=117mM. Open stars data measured 3/6-2003, and closed circles 23/5-2003.

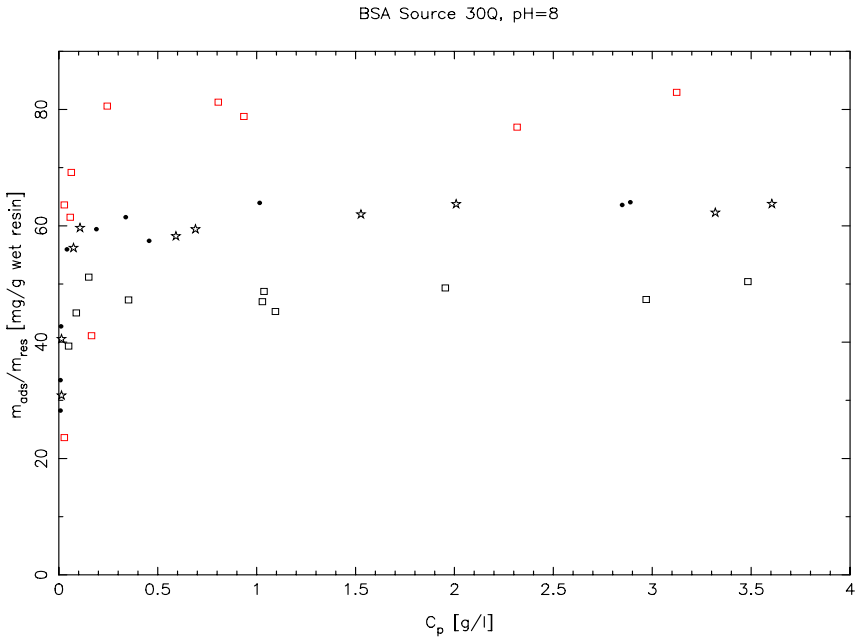

Figure 9.4 Measured isotherms for BSA on Source 30 Q at pH=8 and C_0=37 mM. Legends: Black regenerated Source 30Q, red new Source 30Q. Open stars data measured 3/6-2003, closed circles 23/5-2003, and open squares 13/6-2003. The first two data sets are the same as plotted in figure 9.2. The plotted data are the capacity on a wet resin basis, since the water content of all the samples was not measured.

9.1 Summary

The batch experiments show that the ion exchanger is gradually loosing its capacity. This was not found by Bisgaard-Frantzen, who did not reuse the resin.

When resin is packed in a column this fast loss of capacity is not seen, and it is likely that the treatment for the batch experiments is causing the problems (e.g. water might evaporate from the pores allowing air to enter, and due to the surface tension air remains in the pores).

It is therefore not advisable to regenerate the resin. A natural question is of course if resin looses its capacity even after a few experiments, how much capacity is lost when preparing the resin for the first experiment?

A number of the disadvantages of this methods can be avoided. Another type of batch methods is suggested in chapter 11 “Simulated Moving Bed”. This batch method does not require a long drying time, requires less resin for each sample and reuse of the resin is therefore less important.

10. Program

The previous chapters describe which experiments have been performed and also how the experiments are evaluated afterwards. The amount of data becomes very large and a normal procedure when evaluating the data might be first to export the files containing the chromatogram from the HPLC, fit the data using the program Peakfit, (SPSS, 1997). Hereafter the parameters from the peak fit are entered in the program Sigmaplot and plotted together with a fit of e.g. the retention volume. Other evaluations of the data have been made using Matlab and are stored in spreadsheets. Many programs are involved in this work and changing one parameter e.g. λ_{NO3}, ε or V_{NA} will influence almost all other data in the evaluation. A large part of parameters need to be refitted and many files must be updated. This is a time consuming and tedious work and another approach is needed. Therefore a number of databases has been build. Since the data required for the simulations are already present in the databases, it is desirable that a process simulator communicates with the databases.

To make this possible a program has been constructed, where the export files from the HPLC is imported into the program fitted and stored in the database. It is then possible to search in the databases and find the data needed for a plot. Additionally, it is possible to fit parameters from the experiments and finally simulate the experiments. Since everything is build into the same program, changing a parameter will only cause a minor and fast update of the parameters that are fitted. This chapter describes some of the features in the program.

Graphic capabilities are build into the program to make the desired plots (the majority of the plots in this report have been made by the program).

The program only uses the export file from the HPLC, and can easily be changed to be used with other HPLC-systems[5].

The time for the experiment is stored in the file from the HPLC. Only one experiment can be made at a certain time on the HPLC and this time is therefore a unique identifier of the file. When a file is stored in the program it is stored in the format YYYYMMDDhhmm where YYYY is the year, MM is the month, DD is the day, hh is the hour and mm is the minute, hereby the file can always be found again. Together with this the conditions for the experiment are stored. Hereby it is possible to find, previous data that fulfils certain requirements, and if desired the chromatograms can be retrieved.

System calibrations can be added to the program, too. Only the gradient mixer has been

5 Parts of the program has been modified to evaluate data from the HPLC-system in the SMB work (Merck HPLC).

added, but pump calibration, UV-calibrations, dead volume determinations can be added, too.

1□1 Mixer Calibration

The gradient mixer was calibrated as described in appendix K “Calibration of the Gradient Mixer”, and the evaluation of the calibration mixer was build into the program, too. The dialogue box for this is given in figure 10.1 below.

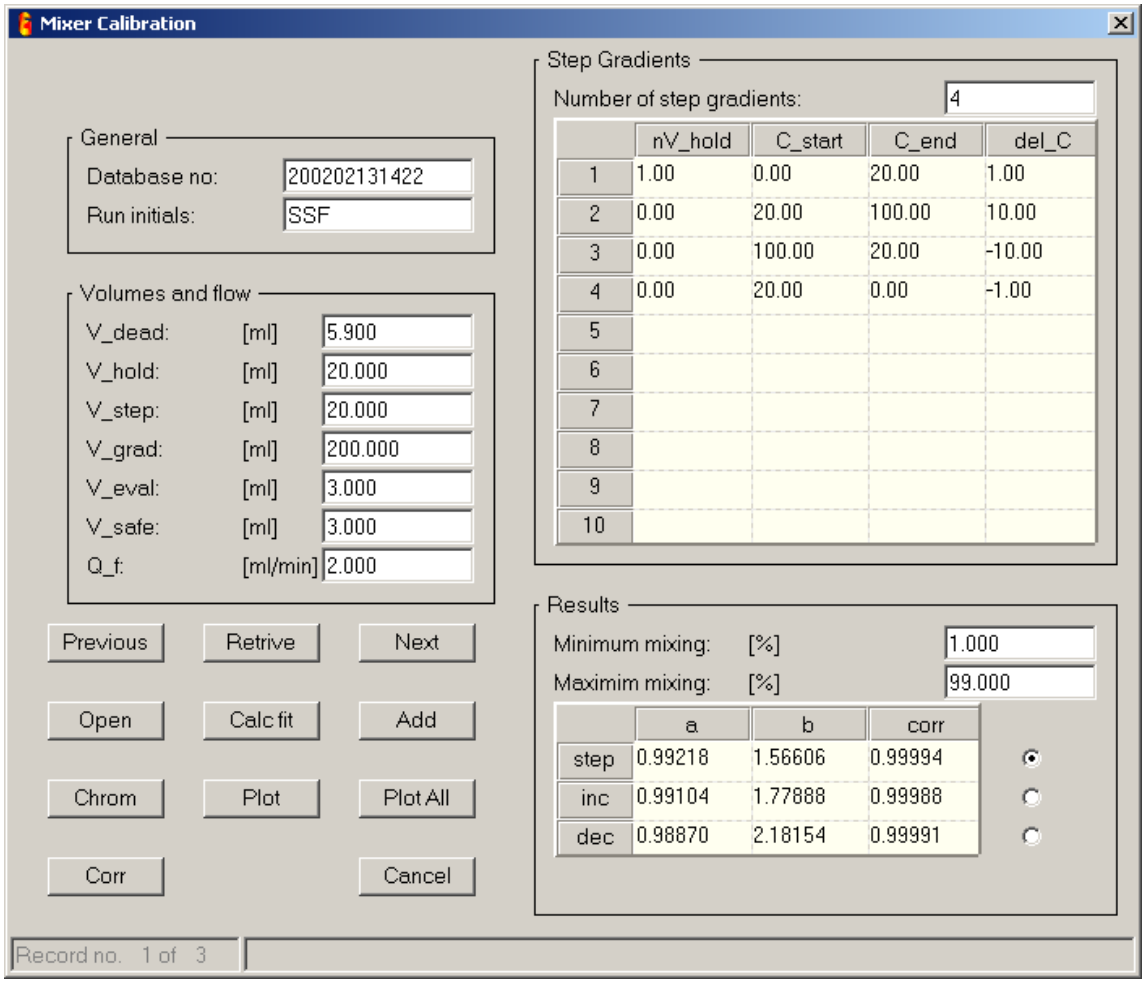

Figure 10.1 Dialogue box for calibration of the mixer. The “database no.” contains the number in the database, the “run initials” the initials of the person who calibrated the mixer. The “Volumes and flow”, “Step Gradients”, and “Results” panels are described in appendix K “Calibration of the Gradient Mixer”. The “Next” and “Previous” buttons jumps to the next or previous record in the database, the record number can be seen at the bottom of the dialogue box “Record no. 1 of 3”. Pushing the “Open” buttons opens a dialogue box for opening a new export file from from the HPLC.

10.2 Column and Component Properties

The most basic properties are the column and the component properties. These can be entered in the “Column and Component data” dialogue box, all these data are stored in a database.

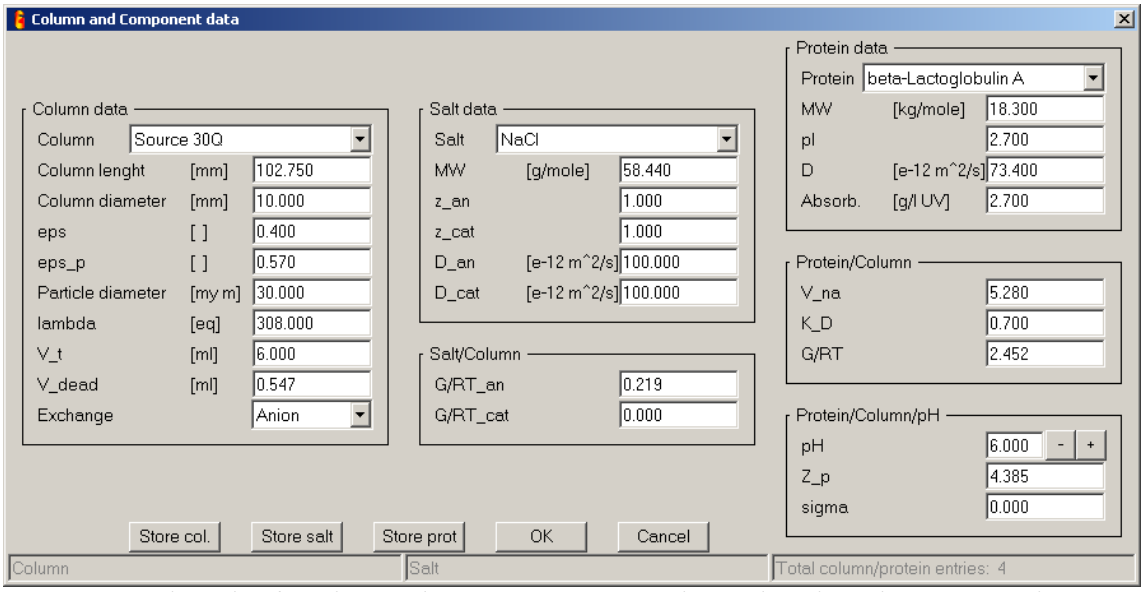

Figure 10.2 Dialogue box for column and component properties. The panel “Column data” contains the pure column data. The panel “Salt data” contains the pure salt data and the panel “Protein data” contains the pure protein data. The “Salt/Column” and the “Protein/Column” contains the data for the interaction between the adsorbed molecule and the ion exchanger. The “Protein/Column/pH” also contains data where protein interaction also depends on the pH-value.

10.3 Isocratic Database

The vast majority of all the experiments are isocratic pulse experiments and the database for isocratic pulse experiments contains more than 2,000 experiments.

Up to four peaks/proteins in one chromatogram can be fitted. The dialogue box for entering isocratic data is given in figure 10.3 below.

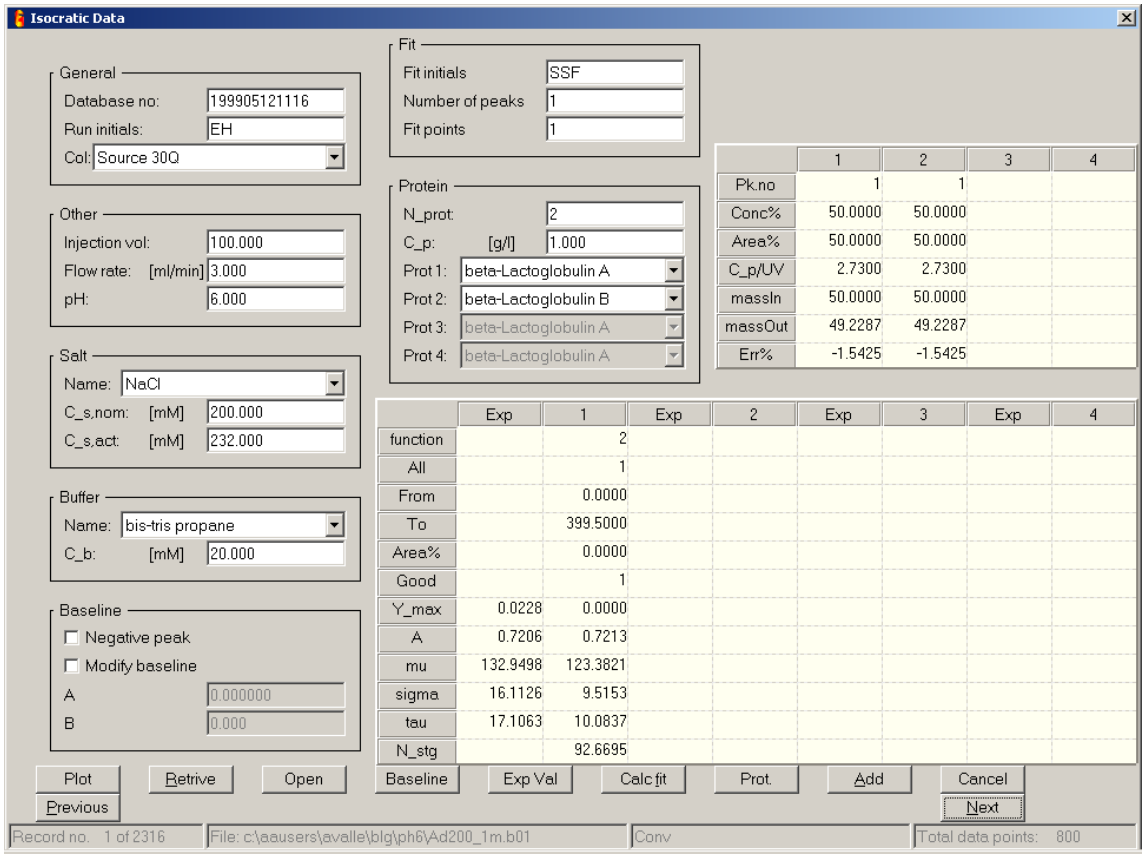

Figure 10.3 The "General" panel contains the database no of the experiment, who made the experiment and which column the experiment was made on. The "Other" panel contains the injected volume the flow rate in the experiment and the pH-value. The "Salt" panel contains the type of salt together with the nominal and actual concentration. The "Buffer" panel contains the type of buffer and the concentration of the buffer. In the "Baseline" panel the baseline can be changed, and it is also possible to fit negative peaks (if nitrate is injected). The "Fit" panel contains information about who fitted the data, how many peaks are in the chromatogram and how many data points should be used when fitting the peaks, e.g. fit points 10 means that only every 10th data point is used when calculating the fitted peaks. The "Protein" panel contains the the number and the names of the proteins together with the total concentration. The small grid links a protein number to a peak number the relative concentration of the protein in the feed, the area percent of the fitted peaks (two proteins can result in only one peak) the UV-absorbance of the protein and a mass balance. The large grid contains two columns for each peak: an experiment, and a fitted column. The row "function" shown which fitting function is used for the peak, "all", "to", and "from" allow to fit the peak to the entire chromatogram or only a range of the chromatogram. The "area%" is used if the relative area of the individual peaks are known. Good=0 indicates a bad experiment or fit and 1 indicates a good fit. Y_max, mu, sigma, and tau are the fitted parameters, see "Pulse Experiments", and N_stg is the number of stages in the column (the dead volume is <u>not</u> subtracted here).

The information bar at the bottom shows the records number in the database, the filename from the HPLC, if the fit converged properly and the number of sample points in the chromatogram.

10.4 Gradient Experiments

The gradient experiments are very similar to the isocratic experiments, the only difference is the proteins are eluted using a salt gradient. The difference is also reflected in the dialogue box where the salt concentrations are entered.

For an isocratic experiment the salt concentration is the same in the entire system, and the dead volume from the mixer to the column is not important. However, for a gradient experiment the dead volume from the gradient mixer to the column inlet depends on the sample loop size. Changing the injection loop to a larger volume increases the dead volume and the gradient enters the column correspondingly later.

300 gradient experiments are added to the database.

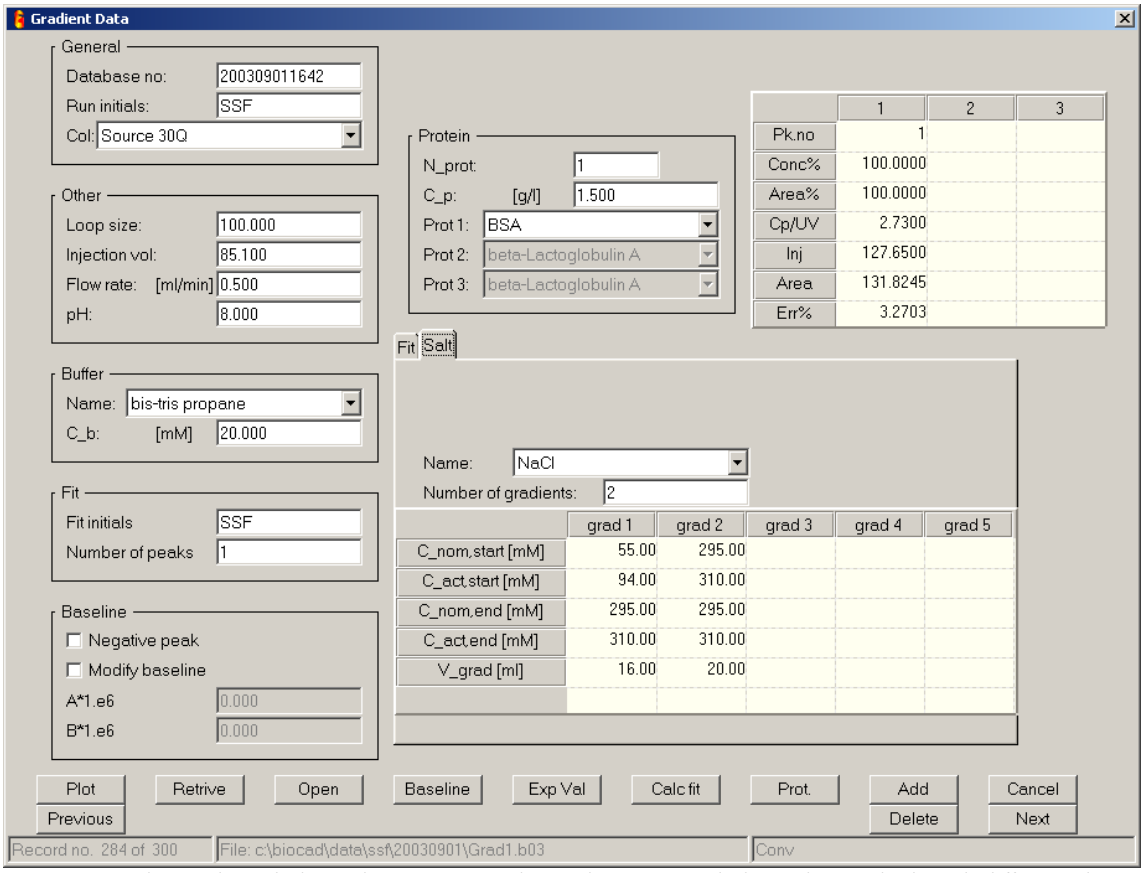

Figure 10.4 The gradient dialogue box is very similar to the isocratic dialogue box, only the salt differs and a tab is created, where the inlet salt gradients are entered.

10.5 Breakthrough Experiments

The Dialogue box for the breakthrough experiments is given in figure 10.5. The data are evaluated as described in appendix I “Breakthrough Experiments”.

Pressing the button “Plot” plots the chromatogram, figure 10.6. The chromatogram is similar to the chromatogram in figure I.1 in appendix I “Breakthrough Experiments”.

More than 400 experiments are stored in the database, all these data are with BSA.

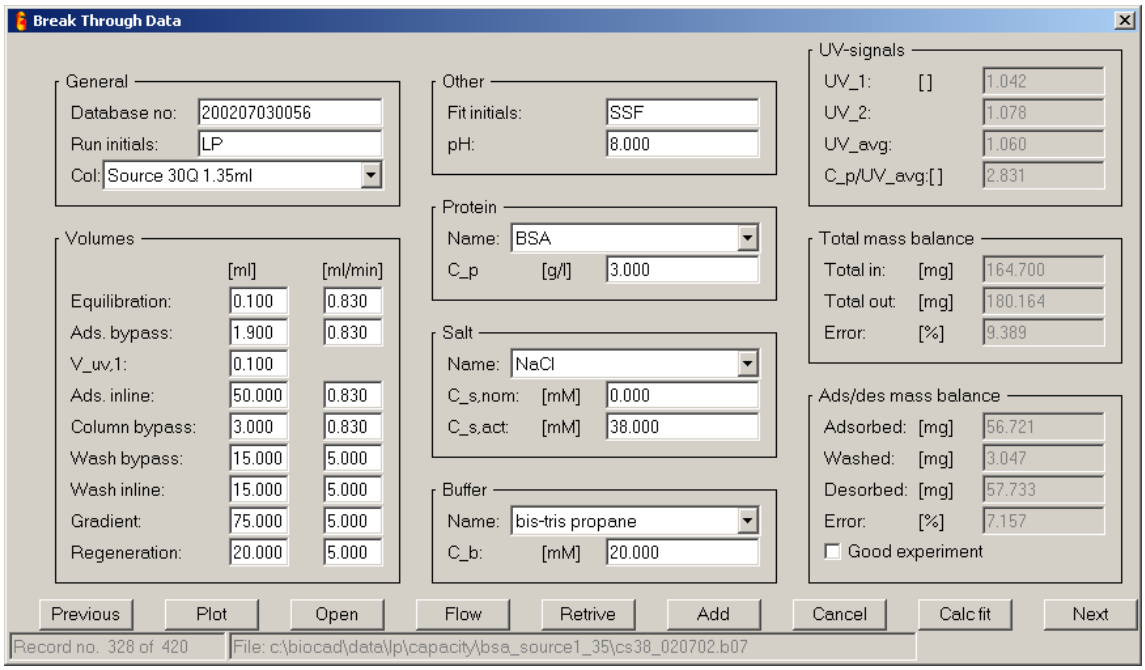

Figure 10.5 Dialogue box for breakthrough experiments. The panel Volumes indicates how long the different times are in the chromatogram. After these volumes have been entered the flow rate in the different periods can be calculated by pushing the “Flow” button. The “UV-signals” panel contains the average UV signal. UV_1 is the average UV-signal in V_uv,1 in the chromatogram, UV_2 is the UV-signal in the column bypass period after the adsorption, and UV_ang is the average of these two values. The inverted absorbance of the protein C_p/UV_avg is calculated from C_p and UV_avg. The “Total mass balance” panel gives the total mass balance for the experiments, due to the large peaks this is normally not the most interesting. A mass balance can also be made as adsorbed=washed +desorbed, this is given in the “Ads/des mass balance” panel, where the error can also be seen.

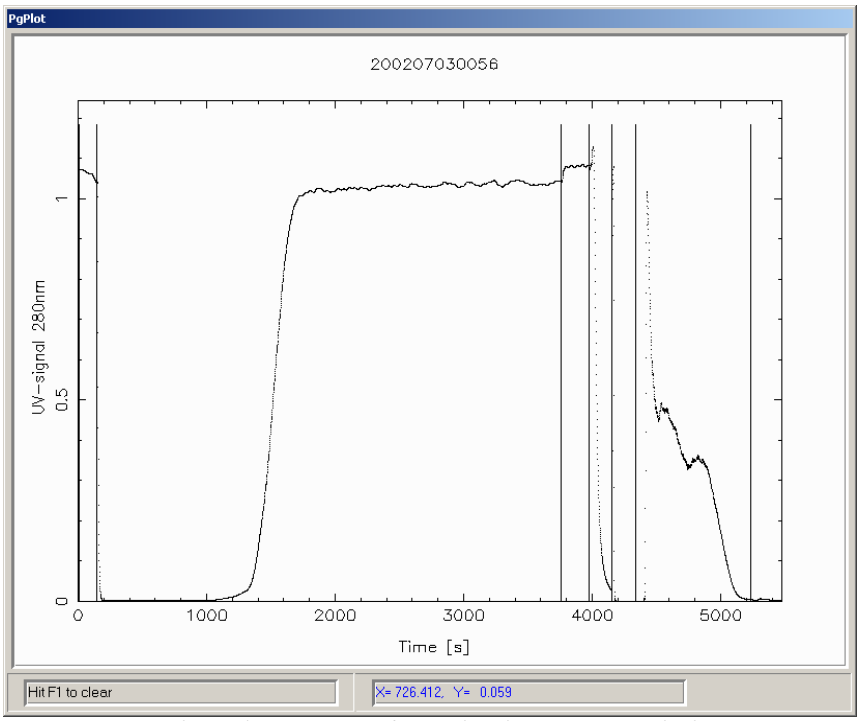

Figure 10.6 Resulting chromatogram from a batch experiment. The lines corresponds to the lines described in appendix I"Breakthrough Experiments".

10.6 Calculation Input

When experimental data have been stored in the database they can be retrieved by the program. This is done in the input file, e.g. “LacTrans.inp” in figure 10.7. An input file is a simple text file that consist of a number of data group, each data group has a name and a number. The name is user specified and the number is an identifier for the type of data group. The first data group, no. 100000, creates a cover page for the output. The second data group, no. 110000, specified the units in the input and output file (e.g. m^3, l, or ml for the volume). The remaining data groups can be chosen freely by the user.

A data group can be

```
=GET1=, 650001, 2, 4, 1, 1, "SSF", "?", "?", ?, ?, ?, ?, 5.9, 6.1, 0.4, 0.6, "SSF", ?, ?, =SERIE1=, 3, 11, *
```

This data groups does not make much sense. The input editor makes it easier to correct the input. In figure 10.8 is given the same data group where the input editor is used to edit the data group. In the left column is given the type of input variable (INT=integer, REAL=real, STR=text string, DGD=data group, BOOL=logical). In the input line to the data group all strings are surrounded by “ “ and all data groups are surrounded by = =, this makes it easier to read the input.

The second column contains the input box. The input box, figure 10.8, is either a text box or a combo box. The third column is the variable name (variables can be references from other data groups) and the rest of the line is a variable description for the user.

Comparing the line in the input file =GET1= with figure 10.7 is seen that the first integer, 2, corresponds to column 2 in the column database, Q-Sepharose XL, the second integer, 4, corresponds to protein four in the protein database, α-Lactalbumin etc. Leaving any text box blank or with a question mark the variable it is not used as a search criteria.

The data group =GET1= therefore search for isocratic experiments with α-Lactalbumin on Q-Sepharose XL and with NaCl as the salt. The pH for the experiments are between 5.9 and 6.1 and the flow rate is between 0.4 and 0.6 ml/min. SSF has both made the experiments and fitted the peaks. From each of the experiments fulfilling these requirements two values are stored and x-value, the experimental A-value, and a y-value, the reduced plate height.

The input file is the file used to create figure 7.4 p. 82. Together with the graphical output, an output file is also created. Each data group creates a small part of the output file. The output from data group 650001 is given in figure 10.9 below. Here the user can see the number of experiments found the search criteria, and a list of the database numbers fulfilling the search criteria together with the x- and y-values from the experiment.

Beside these data groups, other data groups exist to retrieve a single chromatogram, plot it, or calculate it using FFT or orthogonal collocation.

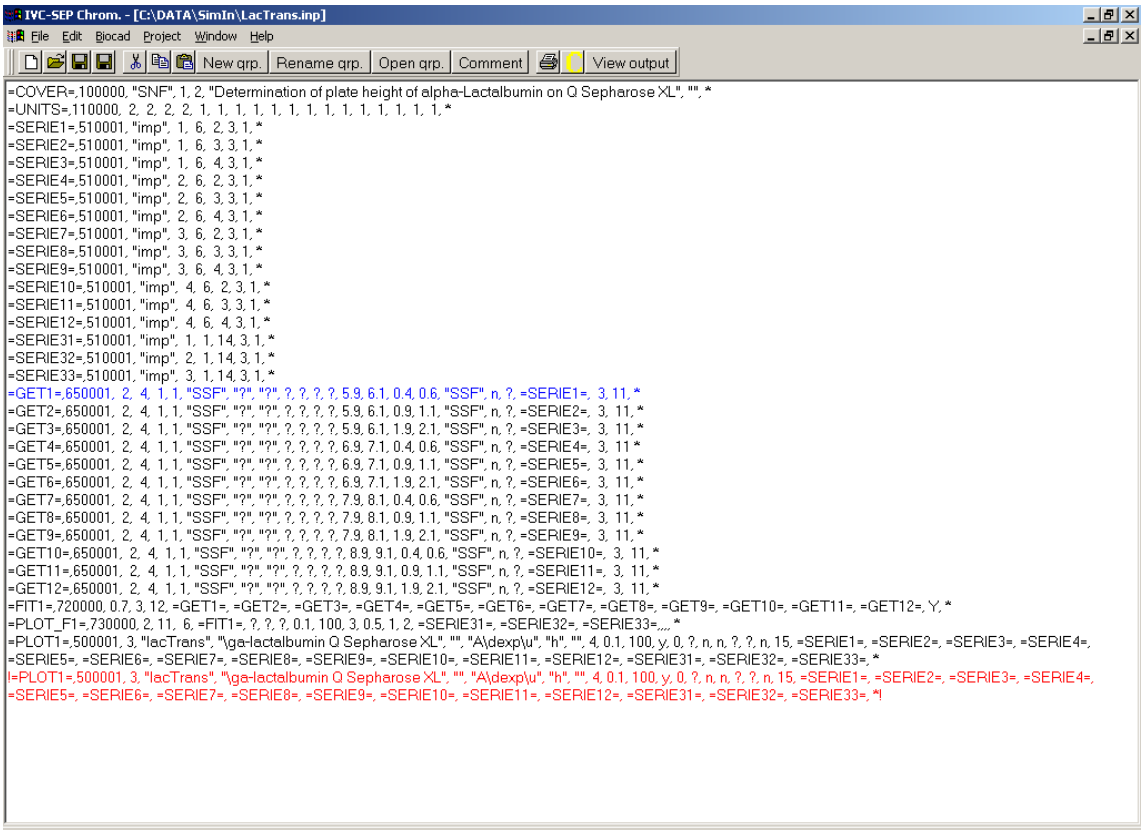

*Figure 10.7 Example of a calculation input. Each data group has a name given in = =, hereafter follows a six digit number, to identify the type of data group, and each data group is terminated by an *. The first data group in a calculation is always a cover data group to create a front page for the output. The second data group is a unit data group, here the user defines the desired units in the input and the output. The input file is a simple text file. The data group where the cursor is located is blue and any data group can be commented out by pressing "Comment", hereafter the the data group is surrounded by ! ! and is shown in red. A calculation is started by pressing the yellow "C" and when the calculation is finished the "View Outlet" button turns green, pressing this button opens the output.*

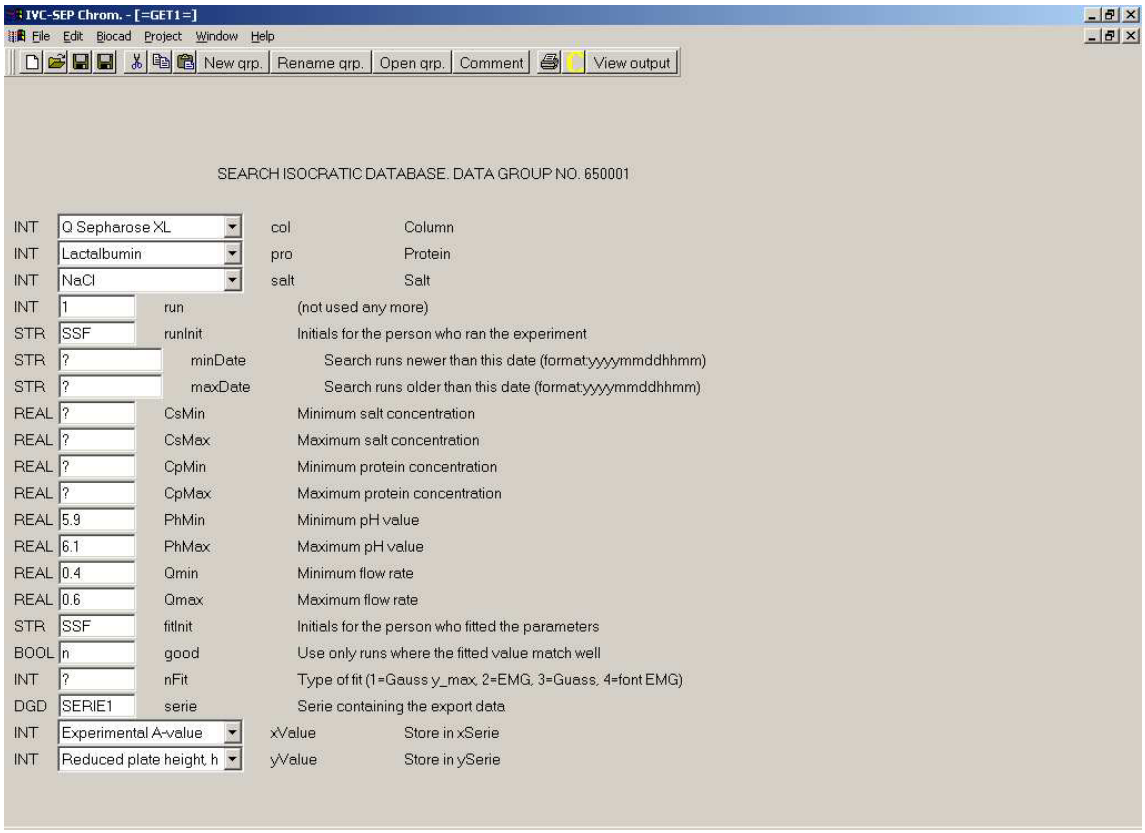

Figure 10.8 A data group can be opened, to edit and view the content of it (here the data group =GET1= in figure 10.7). This data group is for searching data in the isocratic database as seen at the top of the data group, the search criteria are specified in the data group and data for export can selected.

```
 650001 SEARCH ISOCRATIC DATABASE
 --------------------------------
Data group name:                    =GET1=

Number of data set found:          8
Search criteria:
Column name:                   Q Sepharose XL
Protein name:                  Lactalbumin
Salt name:                     NaCl
Run initials:                  SSF
Fit initials:                  SSF
Only good fit
Minimum flow rate:  ml/min      400.000E-03
Maximum flow rate:  ml/min      600.000E-03
Minimum pH:                       5.900E+00
Maximum pH:                       6.100E+00

Data set
YYYYMMDDhhmm
200110151452    134.590E-03       8.794E+00
200110151635    485.832E-03       9.800E+00
200110151824      1.116E+00       9.259E+00
200110152021      2.156E+00       8.589E+00
200110152243      4.990E+00       6.804E+00
200110160148      8.773E+00       5.961E+00
200110160558     17.048E+00       5.111E+00
200110161136     23.417E+00       4.495E+00
```

Figure 10.9 Output from data group =GET1=.

10.7 Summary

A prototype of a program has been created for evaluating the chromatographic data. This can serve as a valuable tool due to the large number of experiments that would be difficult to handle if not stored in the database.

A number of dialogue boxes to edit, evaluate, and store experimental data has also been created.

An input editor that makes it easier to correct the input files, has also been created.

Unfortunately a lot more work is required before the program can be considered to be stable. Errors made by the user, or e.g. taking the logarithm of a negative number can cause the program to crash without any warning to the user. The program should therefore be considered as a prototype and a suggestion of how to handle the large amounts of data.

11. Simulated Moving Bed

The present chapter describes the work done by Klaus Wekenborg and Søren Frederiksen during Søren Frederiksen's stay at Universität Dortmund at the department “Bio- und Chemieingenieurwesen” in the group “Anlagentechnik” during the period February 1st to July 31st 2003. The aim of the work was to separate β-Lactoglobulin A and B by Simulated Moving Bed-chromatography (SMB chromatography) and to model the separation.

The usual chromatographic process can be compared to a batch distillation process without reflux, and suffers from both the drawbacks of the batch process and the lack of reflux. To overcome these drawbacks SMB chromatography can be used. SMB chromatography can be used as a continuous process and with the resin “flow” in the opposite direction of the liquid flow simulates a reflux flow.

β-Lactoglobulin A and B have previously been separated by ion exchange chromatography using the strong anion exchanger Source 30 Q from Amersham Biosciences (Pedersen, 2003). The selectivity between β-lactoglobulin A and B are largest close to the isoelectical point. However, to avoid eventual aggregation and other effects that can take place close to the isoelectical point all experiments have been performed at pH=7.

The chapter describes the experiments performed to determine the equilibrium parameters and the modelling of the SMB-experiments.

The term “steady state” is sometimes seen in SMB literature when one cycle in a run is identical to the following. However, a SMB-process is not steady state and this term is very misleading. Carta (Perry, 1997, p. 16-5) suggest to use the term "periodic state" or "cyclic steady state" and these terms will be used instead.

11.1 Lay-out

A SMB-plant can be considered as a number of columns connected in series. At certain times all columns are shifted to the position upstream its previous position, corresponding to move all the columns one position to the left in figure 11.1, e.g. column no. 2 is moved from position II to position I. Column 1 is moved from position I to the last position, position VIII in figure 11.1. This creates a virtual resin "flow",with the velocity v_r, is in the opposite direction of the mobile phase flow, v_i, figure 11.1.

Normally, the SMB plant is divided into four different sections with a number of columns in each section. Each section serves a specific purpose. In section one all protein must be removed, from the column in position I before it is moved to position VIII. If this procedure is

not followed the protein bound to column one would end up in the raffinate stream. In section two and three the strongest retained protein must have a net transport in the same direction as the resin phase, transporting the strongest retained protein to the extract stream, and the weakest bound protein must have a net transport rate in the same direction as the liquid phase, transporting the weaker retained protein to the raffinate stream. Finally in section four all protein should be retained by the resin, such that a pure mobile phase is leaving the section. This mobile phase can be recycled to section one.

In the general case a split for withdrawal of product as well as a feed point is located between all columns as shown in figure 11.2. However, normally eluent is fed to the first column, and an extract stream containing the strongest bound component is withdrawn after the first section. The feed stream containing the components to be separated is fed between section two and three, and a raffinate stream containing the weaker bound component is withdrawn downstream section three. Finally, the remaining eluent is withdrawn, (or recycled to column one) after section four, see figure 11.1.

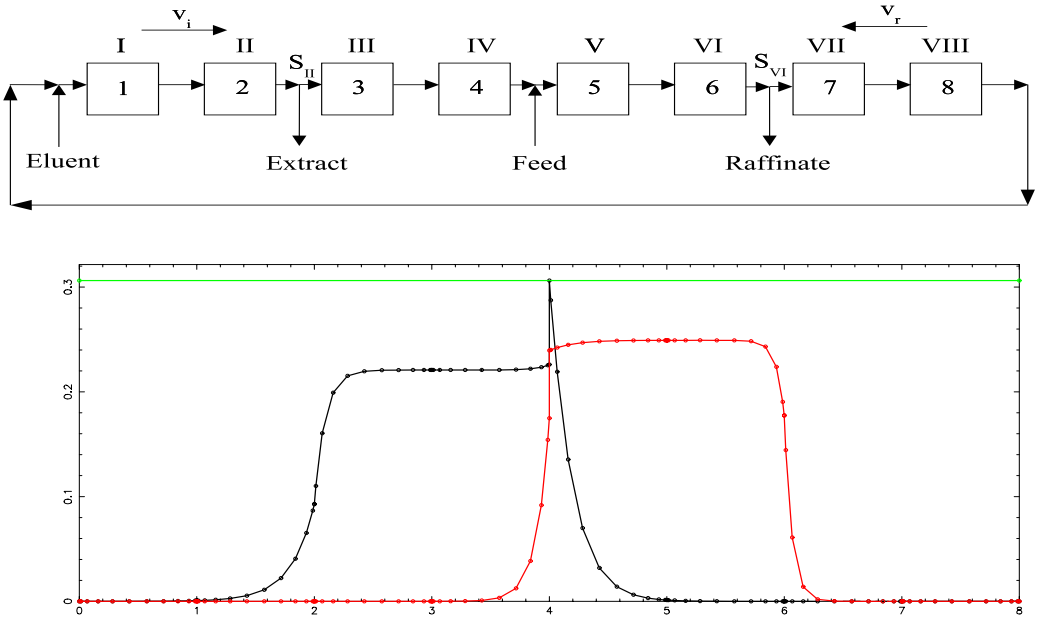

Figure 11.1Top: Schematic drawing of SMB-plant with four sections each containing two columns. The columns are numbered 1,2,...,8 and the positions are numbered I, II,...,VIII.

Bottom: Concentration profile in TCC (True Counter Current) column with two columns in each section and isocratic elution. Legends: Black - stronger bound component, red – weaker bound component, green – salt concentration (scale not shown for salt). x-axis column and y-axis concentration [g/l].

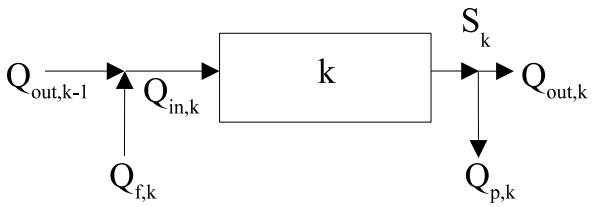

Figure 11.2 Schematic drawing of one section of SMB-plant, indicating the subscripts used for the different positions.

A generalised drawing with feed stream, $Q_{f,k}$, product stream, $Q_{p,k}$, inlet stream, $Q_{in,k}$, outlet stream, $Q_{out,k}$, and product split, S_k, is given in figure 11.2[6]. A product split S_k gives $Q_{p,k}=Q_{in,k}\cdot S_k$ and $Q_{out,k}=(1-S_k)\cdot Q_{in,k}$.

All the columns in the SMB plant are considered to be identical. If the differences of the columns are taken into consideration, things would become very messy, since variations in e.g. L and Λ, would give different dimensionless groups/variables, eq. (2-4), (3-3) and (3-4). A PID of the plant is given in figure O.1 in appendix O "Comment to SMB Plant Lay-Out".

11.2 Ideal TCC Chromatography

A cycle in a SMB plant is the time it takes for a column to move through all the positions in the plant and back to its original position. Therefore a SMB plant with eight columns requires 64 column calculations per cycle. Cyclic steady state is not obtained in the first few cycles and at least three cycles (=192 column calculations) are required to get the cyclic steady state profile. The calculation time for this can be significant, and a process optimization of this might be very time consuming.

Instead of investigating the discontinuous SMB process the continuous True Counter Current process (TCC) can be investigated. In this process a continuous resin flow is considered.

The non-steady state mass balance for the TCC plant for ideal chromatography (no axial dispersion, or resistance against mass transport) is given as

$$\frac{\partial}{\partial t}\left(\epsilon y_j+(1-\epsilon)\epsilon_p K_{D,j}(y_j+q_j)\right)+\frac{\partial}{\partial z}\left(v_i\epsilon y_j-v_r(1-\epsilon)\epsilon_p K_{D,j}(y_j+q_j)\right)=0 \quad \text{j=0,NP} \tag{11-1}$$

where NP is the number of proteins, ε is the column porosity ε_p is the pore porosity and K_D is the fraction of pores large enough for the protein to enter. The interstitial velocity of the

6 Locating the feed stream upstream the column and the product stream downstream later turned out to be a bad idea since an asyncrone shifting time can lead to only one column between a feed stream and a product stream and these are connected to two different columns, see figure 11.6 . A better idea would be to locate both the product split and the feed stream upstream the column since no valve block is used for product withdrawal and feed addition at the same time.

mobile phase is v_i and the velocity of the pore phase is v_r.

Insertion of the dimensionless variables $x=\frac{z}{L}$ and $\tau=\frac{t v_r}{L}$ where v_r is the resin velocity gives

$$\frac{\partial}{\partial \tau}\left(y_j+\psi_j(y_j+q_j)\right)+\frac{\partial}{\partial x}\left(\frac{v_i}{v_r}y_j-\psi_j(y_j+q_j)\right)=0 \qquad \text{j=0,NP} \qquad (11\text{-}2)$$

At steady state the derivatives with respect to τ is zero and the derivative with respect to x must then be 0. From this the function $f'_{j,k}$ is defined for the j'th component in the k'th column. The function f' gives the relative velocity of protein j in column k.

$$f'_{j,k}=\frac{v_{i,k}}{v_r}y_{j,k}-\psi_{j,k}(y_{j,k}+q_{j,k})=\left(\frac{v_{i,k}}{v_r}-\psi_{j,k}\right)y_{j,k}-\psi_{j,k}q_{j,k} \qquad (11\text{-}3)$$

The first term is the flow rate of the protein with the mobile phase and the second term comes from the rate of the particle phase.

Instead of defining the function as described above an analogue function in dimensionless units can be defined by division by $\psi_{j,k}y_{j,k}$

$$f_{j,k}=m_{j,k}-A_{j,k} \qquad (11\text{-}4)$$

Where $A_{j,k}$ is defined as

$$A_{j,k}\equiv\left(\frac{q_j}{y_j}\right)_k \qquad (11\text{-}5)$$

and $m_{j,k}$ is the ratio between the net fluid flow rate and the adsorbed flow rate of protein j in section k, (Storti *et al.* 1993).

$$m_{j,k}=\frac{net\ fluid\ flow\ rate}{adsorbed\ phase\ flow\ rate}=\frac{Q_k-Q_r\epsilon_p K_{D,j}}{Q_r\epsilon_p K_{D,j}}=\frac{\gamma_k-\psi_{j,k}}{\psi_{j,k}} \qquad (11\text{-}6)$$

where the relative volumetric flow rates in the different columns are

$$\gamma_k=\frac{v_{i,k}}{v_r}=\frac{1-\epsilon}{\epsilon}\frac{Q_k}{Q_r} \qquad (11\text{-}7)$$

From this it is seen that if $A_{j,k}>m_{j,k}$, the net flow rate of the protein is in the same direction as the resin flow rate, and vise versa.

Due to the steric exclusion factor, $K_{D,j}$, is normally different for the different components, $m_{j,k}$ will be different for the different components, too. The proteins β-lactoglobulin A and B are of the same size and here m will be the same for all components, which is also assumed in the following.

Index j is omitted in the remaining of the chapter.

The requirements for complete separation of the two proteins in the four sections are summarised in table 11.1 below.

Section	f_A	f_B	m_A	m_B
1	>0	>0	$>A_A$	$>A_B$
2	<0	>0	$<A_A$	$>A_B$
3	<0	>0	$<A_A$	$>A_B$
4	<0	<0	$<A_A$	$<A_B$

Table 11.1 Requirements for the individual sections in the SMB plant. A is the stronger retained component and B is the weaker retained component.

11.3 Complete Separation Region

In the ideal case, a "triangle" diagram showing the region with complete separation can be drawn.

These triangle diagrams are made under the assumption that section one and four work properly, this means that all the protein in the feed stream leaves through one of the two product streams, and nothing through section one and four. In this case the complete separation region can be plotted as a function of m_2 and m_3 only.

The name triangle diagram is somehow misleading since only for a linear isotherm the area of complete separation is a triangle, as shown in figure 11.3, where the lower boundary is given by $m_3=m_2$ corresponding to $Q_f=0$, (Q_f is in the following used for the protein containing feed stream).

The two end points a and b are given as the initial slope of the isotherm for the stronger and the weaker bound component, this can be seen from eq. (11-4) and table 11.1.

Reducing the flow rate in section 2 to $m_2<b$ the weaker bound component will be able to propagate to the extract stream, leading to an impure extract stream. Correspondingly for $m_3>a$ the stronger bound component will pollute the raffinate stream. Therefore only inside the triangle a→b→w→a both the extract and and raffinate streams will be pure.

At increased feed concentration the complete separation region is no longer a triangle, figure 11.4.

Moving from b→w the concentration of $y_{A,2}$ in section two is increasing, thereby also

increasing the denominator in the SMA-isotherm, eq. (2-5). Component B will then be weaker bound and the minimum value of m_2 is decreased.

The line from w→a is now divided into two parts w→r and r→ a. The line from r→a originates from the downward curvature of the SMA-isotherm. A for the stronger bound component in section two, $A_{A,2}$, will decline at increased $y_{A,2}$, thereby also reducing the net transport capabilities of the resin phase of component A in section two.

Finally the line from w→r gives the conditions where breakthrough of component A in section three is possible. This is more complex because it both depends on the concentration of B in the section as well as on the concentration of A at the inlet to column three.

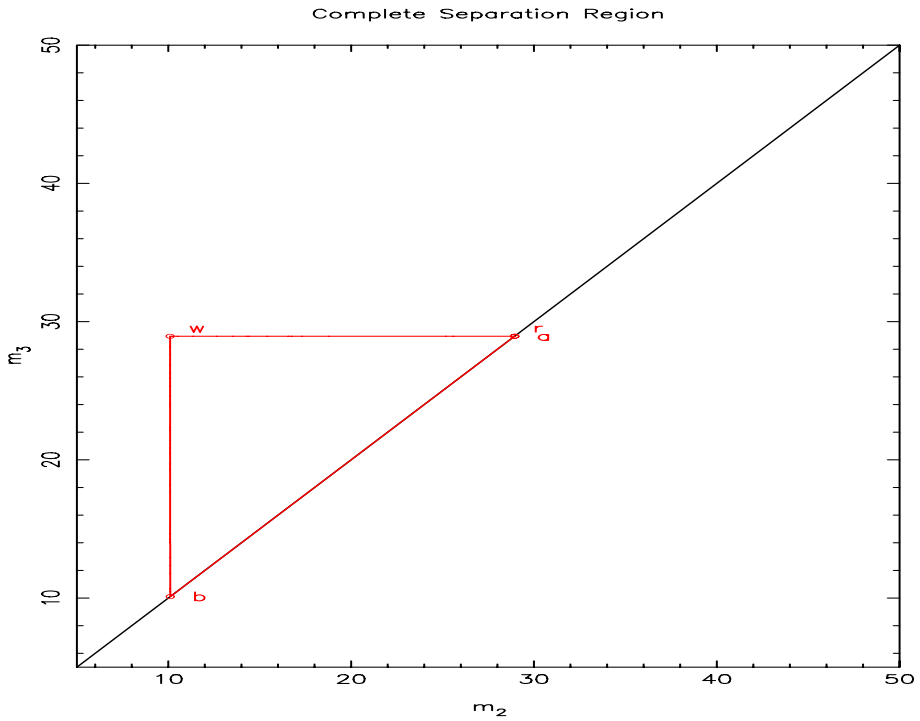

Figure 11.3 Region with complete separation. Parameters are as in figure 11.4 but at infinite dilution.

From figure 11.4 is seen that the upper limit of m_3 for isocratic elution to a large extent is given by the breakthrough of component A in section three (the line w→r is long). That is component A binds too weakly in section three. Since the binding of the components are strongly depending on the salt concentration, lowering the salt concentration in the feed stream will change this boundary upwards. In figure 11.5 below is the region of complete separation given for a gradient elution. The upper boundary is seen to change significantly. It is also seen that the upper boundary to a larger extend is given by the limited transport capabilities in section two (the line r→a is longer).

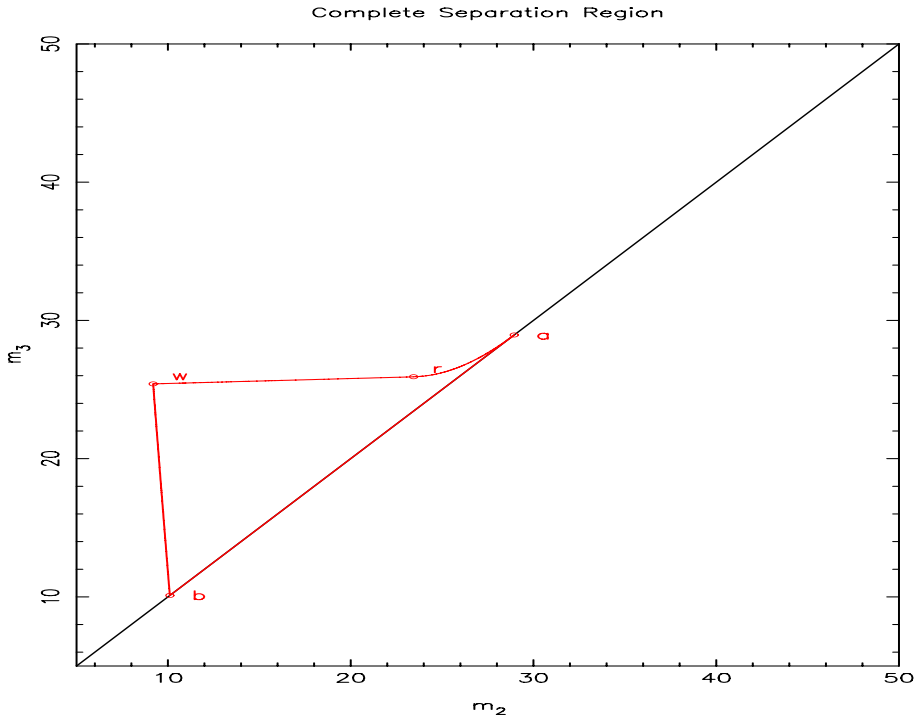

Figure 11.4 Complete separation region. The points a and b corresponds to the retention at infinite dilution. The line from b to w is limited by $m_{2,min}$ the line w to r is limited by $m_{3,max}$ and the line r to a is limited by $m_{2,max}$. Parameters: Λ=300 mM, MW_A=MW_B=18.3kDa, C_0=138 mM, $C_{f,A}$=0.6g/l, $C_{f,B}$=0.4g/l, ν_A=6.21, ν_B=5.5, $\Delta G_s/RT$=0.320, $\Delta G_{p,A}$=3.444, $\Delta G_{p,B}$=3.718, K_D=0.78 ε=0.4, and ε_p=0.57.

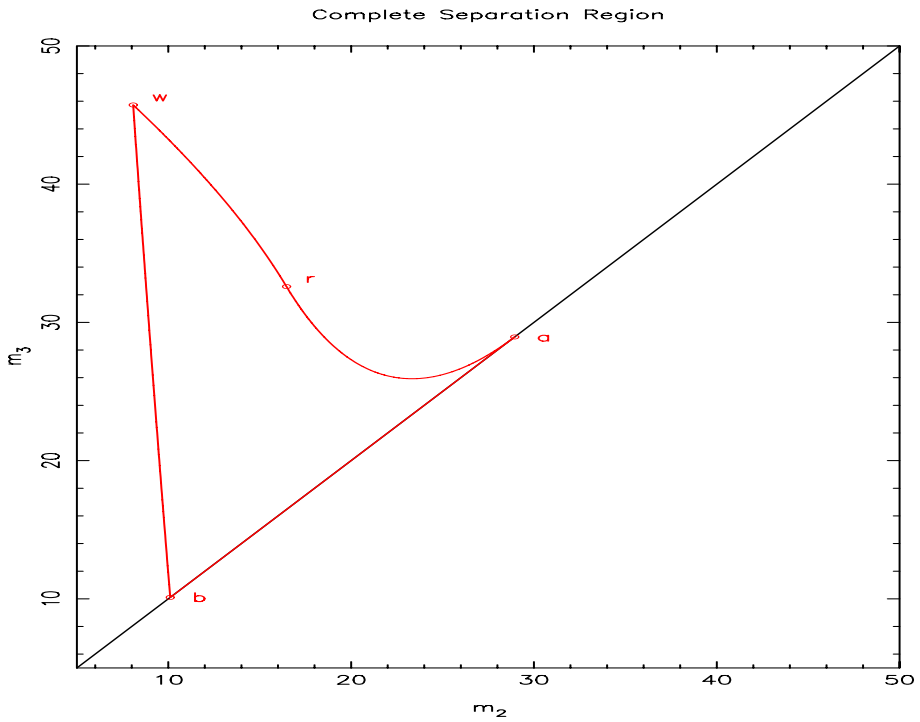

Figure 11.5 Total separation region for gradient operation. Parameters are as in figure 11.4 but with $C_{0,j}$=118 mM.

11.4 Calculation of Triangular Diagrams

A lot of articles have been published for the solution where the selectivity between the two components is constant, e.g. Chiang (1998) and Migliorini *et al.* (2000a). For the SMA formalism the selectivity is, however, not constant and another approach is needed. Migliorini *et al.* (2000b) have suggested a procedure for calculating the total separation region for non-constant selectivity, with favourable, competitive isotherms. The requirements are that the isotherms are purely competitive

$$\frac{\partial q_i}{\partial y_i} > 0 \qquad \text{i=A, B} \tag{11-8}$$

$$\frac{\partial q_i}{\partial y_j} < 0 \qquad \text{i}\neq\text{j} \tag{11-9}$$

The variation of y_i has a stronger influence on the adsorption of component i than on the adsorption of the other components

$$\frac{\partial q_i}{\partial y_i} > \left|\frac{\partial q_j}{\partial y_i}\right| \tag{11-10}$$

These features are shared by all isotherms where two solutes compete for the same sites, Rhee *et al.* (2001b, p. 5).

The procedure suggested by Migliorini is, however, very tedious. To cite Migliorini "*The solution of the four algebraic equations plus the ordinary differential equation, though in principle always feasible, may in practice be rather cumbersome for complex isotherms. This is particularly true because the conditions for the applicability of the method must be controlled during the determination of this portion of the boundary of the complete separation region,...*"

Migliorini has given the following requirements for the total separation of the components.

Break though of component B in section two will occur if

$$m_{2,min} = \left(\frac{\partial q_B}{\partial y_B} \right)_{M_2} \tag{11-11}$$

where the subscript M_2 means evaluated under the conditions in sections two.

The maximum flow rate in section two as a function of the concentration will be

$$m_{2,max} = \left(\frac{\partial q_A}{\partial y_A} \right)_{M_2} \tag{11-12}$$

The minimum flow rate in section three. From flux equation (11-4)

$$m_{3,min} = \frac{q_{B,3}}{y_{B,3}} \tag{11-13}$$

$$m_{3,max} = \frac{q_B^\beta - q_B^3}{y_B^\beta - y_B^3} = \frac{q_A^\beta}{y_A^\beta} \tag{11-14}$$

An alternative approach has been used in the present work. This approach only involves solving two to three algebraic equations. The method has nice convergence properties and is simple to solve, the method is described in appendix L "Alternative Method for Calculation of Complete Separation Region".

11.5 TCC Chromatography

From the calculations of the complete separation region the optimal operating point can be found. However, this does not give insight into pressure drop and zone spreading mechanism from mass transfer resistance and axial dispersion.

As previously mentioned the calculation of a SMB plant can be time consuming and it is desirable to reduce this time. A simple way to obtain the pressure drop and zone spreading is from a steady state TCC calculation since this does not contain any derivatives in τ. The

steady state solution is a double boundary value problem and can be solved by orthogonal collocation. Since the SMB plant consists of a number of columns connected in series, the matrix will be a banded matrix, requiring less resources to solve.

Only the linear driving force approximation is used here and only the model where the axial dispersion is pooled with the film layer mass transfer coefficient.

The equations here are comparable to the equations set up in chapter 3 “Modelling”, the total number of variables are 4·NC·NT·NP, where NC is the number of columns, NT is the total number of collocations points per column, and NP is the number of proteins.

The mobile phase mass balance becomes

$$\frac{dy}{dx}+St_f\phi\left(y-y_s\right)=0 \tag{11-15}$$

and the pore phase and pore surface mass balances becomes

$$\frac{dy_p}{dx}+\frac{LK_{ads}}{v_r}(q_{SMA}(y_p)-q_p)+\gamma St_p\left(y_p-y_s\right)=0 \tag{11-16}$$

$$\frac{dq_p}{dx}-\frac{LK_{ads}}{v_r}(q_{SMA}(y_p)-q_p)+\gamma St_q\left(q_p-q_s\right)=0 \tag{11-17}$$

where K_{ads} is the adsorption rate. The flux equation equations remains the same

$$St_f\phi(y-y_s)-St_p\psi(y_s-y_p)-St_q\psi\left(q_s(y_s)-q(y_p)\right)=0 \tag{11-18}$$

Where the dimensionless Stanton numbers for the columns are

$$St_f=\frac{6L_k k_f}{d_p v_i}\quad,\quad St_p=\frac{6L_k k_p}{d_p v_i}\quad,\quad St_q=\frac{6L_k k_q}{d_p v_i} \tag{11-19}$$

and the dimensionless phase ratios

$$\phi=\frac{1-\epsilon}{\epsilon}\quad\text{and}\quad\psi=\frac{1-\epsilon}{\epsilon}\epsilon_p K_D \tag{11-20}$$

Collocation of these with N inner collocation points the total number of node points are NT=N+2. The mobile phase becomes

$$R_i=\sum_{k=1}^{NT}A_{i,k}y_i+St_f\phi(y_i-y_{s,i})=0 \qquad \text{i=2,NT} \tag{11-21}$$

Where $A_{i,k}$ it the k'th weight of the first derivative in node point i.

The pore phase gives

$$R_{p,i}=\sum_{k=1}^{NT}A_{i,k}y_{p,k}+\frac{LK_{ads}}{v_r}(q_{SMA}(y_p)-q_p)+\gamma St_p\left(y_p-y_s\right)=0 \quad \text{i=1,NT} \tag{11-22}$$

and the pore surface gives

$$R_{q,i}=\sum_{k=1}^{NT} A_{i,k}\, q_{p,k}-\frac{L K_{ads}}{v_r}(q_{SMA}(y_p)-q_p)+\gamma\, St_q\left(q_p-q_s\right)=0 \quad \text{i=1,NT} \tag{11-23}$$

The flux equation remains the same.

These equations all applies to a single column. At the inlet and outlet positions some of these are replaced by the residuals given below.

The inlet concentration to a column depends both on the outlet concentration from the previous column and on the feed stream to the column, figure 11.2.

The fraction of feed from the previous column, α_k, is calculated for the different columns

$$\alpha_k=\frac{Q_{out,k-1}\cdot(1-S_{k-1})}{Q_{out,k-1}\cdot(1-S_{k-1})+Q_{f,k}} \tag{11-24}$$

The salt concentration in section k is then given as

$$y_{k,0}=\alpha_k\cdot y_{k-1,0}+(1-\alpha_k)\, y_{f,k,0} \tag{11-25}$$

The residual for the first mobile phase in x=0 is correspondingly given as

$$R_j=y_{k,j,x=0}-\left(\alpha_k\, y_{k-1,j,x=1}+(1-\alpha_k)\, y_{f,k}\right)=0 \quad \text{j=1,NP} \tag{11-26}$$

where α=0 for the first column and NP is the number of proteins

At the column exit the most obvious boundary condition would be continuity in the pore phase concentrations from the previous column

$$R_{p,j}=y_{p,k,j,x=1}-y_{p,k+1,j,x=0}=0 \qquad \text{j=1,NP} \tag{11-27}$$

and correspondingly for the pore surface. However, when the salt concentration changes e.g. in gradient mode when moving from section three to section two, the salt concentration makes a step change, eq. (11-25). This changes the equilibrium in the pore phase and thereby the pore and pore surface concentrations (K_{ads} is large because equilibrium is assumed). Here the two assumptions, fast mass transfer for salt and equilibrium, create convergence problems. A better residual would originate from the total mass balance inside the particle

$$R_{p,j}=(y_{p,k,j,x=1}+q_{p,k,j,x=1})-(y_{p,k+1,j,x=0}+q_{p,k+1,j,x=0})=0 \quad \text{j=1,NP} \tag{11-28}$$

For the last column the product recycle stream should be pure and the residuals give

$$R_{p,j}=y_{p,k,j,x=1}=0 \qquad \text{j=1,NP} \tag{11-29}$$

$$R_{q,j}=q_{p,k,j,x=1}=0 \qquad \text{j=1,NP} \tag{11-30}$$

An example of a concentration profile is given in figure 11.1 above.

11.6 SMB Solution

As previously mentioned the calculation of the SMB solution requires a large number of column calculations. For the current plant with three cycles, nCyc=3, the total number of column calculations is $nCyc \cdot NC^2$=192 column calculations. A fast column calculation is required to get a reasonable calculation time.

The SMB calculation is calculated without recycle, to convert it to a problem where each column only depends on the outlet composition from the previous column and on the feed stream added, eq. (11-25). If recycle is taken into account (and no dead volume in the recycle stream), all columns had to be solved simultaneously for each time step leading to very large calculation times.

It should be emphasised that the column porosity will effect the net fluid flow rate in the SMB plant. Mobile phase is moved together with the column when the columns are shifted to the upstream position and the net fluid flow rate (corresponding to Q^{TCC} in the TCC process) for the SMB solution is given as

$$Q_k^{TCC} = Q_k^{SMB} - \frac{V_{col}\epsilon}{t_{sft}} \tag{11-31}$$

where Q_k^{SMB} is the actual flow in the SMB plants section , and t_{sft} is the shifting time.

11.7 Dead Volumes Impact on the Operating Point

When moving the columns one position upstream in the SMB plant not only the resin phase but also the mobile phase and the dead volume are moved one position upstream. This reduces the overall net flow and thereby also the relative flow rates, m-values, in the different sections.

$$Q_k^{TCC} = Q_k^{SMB} - \frac{V_{col}\epsilon + V_{dead,k}}{t_{sft}} \tag{11-32}$$

For a SMB plant it is therefore of outmost importance to know the dead volumes in the columns and in the plant. Migliorini *et al.* (1999) have previously reported that the dead volume was 40% of a column volume. These dead volumes were distributed evenly in the plant.

When the dead volumes are evenly distributed in the plant, the m values for the different sections will all be reduced by the same value, eq. (11-32). This can be compensated for by an increase in the flow of the same magnitude through the plant. DV_{col}/t_{sft}.

In the current plant the dead volumes are not distributed evenly but is mainly located downstream column eight, see chapter 11.8 “Measured Dead Volumes”, and appendix M

"Measured Dead Volumes in the SMB-plant". The dead volume downstream column eight is also much larger compared to the dead volumes previously described by Migliorini *et al.* (1999). In the current plant this dead volume accounts for more than 300% of one column volume, and additional precaution must be taken.

The flow rates are different in the different sections of the SMB-plant and the change in the m-values will be different depending on which section column eight is in. Inserting the net fluid flow rate from eq. (11-32) into eq. (11-6) gives

$$m_{DV}=\frac{Q_k-\frac{V_{res}}{t_{sft}+\Delta t_{sft}}\epsilon_p K_D-\frac{V_{col}\epsilon+V_{dead}}{t_{sft}+\Delta t_{sft}}}{\frac{V_{res}}{t_{sft}+\Delta t_{sft}}\epsilon_p K_D}=$$

$$\frac{Q_k(t_{sft}+\Delta t_{sft})-V_{res}\epsilon_p K_D-V_{col}\epsilon-V_{dead}}{V_{res}\epsilon_p K_D}=m_{SMB}+\frac{Q_k\Delta t_{sft}-V_{dead}}{V_{res}\epsilon_p K_D} \quad (11\text{-}33)$$

Here m_{DV} is the m-value including dead volume and m_{SMB} is the m-value for the SMB-plant without dead volume. It is seen that for $\Delta t_{sft}=0$ m_{DV} differs from m_{SMB} only by a constant, and when the dead volumes are the same in all the columns, increasing m_{SMB} with $V_{dead}/(V_{res}\cdot\varepsilon_p\cdot K_D)$ will give the same m-values as for a plant without dead volumes, as mentioned above.

When the dead volumes are not the same for the different columns, another approach is needed. Two columns in the same section have the same Q_k and with different dead volumes the m-values will be different. Two possibilities exist either changing Q_k or Δt_{sft}. Changing Q_k would lead to additional feed streams/product streams thereby increasing the number of pumps and the complexity of the control system. The other possibility is increasing the shifting time for the column with the largest dead volume. The shifting time can be increased by the asynchronous shifting time, $\Delta t_{sft}=V_{dead}/Q_k$.

The column dead volume is the same when it changes position and Δt_{sft} will have different values for the different sections. The total cycle time will correspond to $NC\cdot t_{sft}+\Delta t_{sft}$ and with different values of Δt_{sft} the columns will not all be back at theirs original positions at the same time. A compromise is needed and this is that the average flow rate in the plant is used to calculate the asynchronous shifting time. A detailed scheme showing this strategy is shown in figure 11.6.

The reason for this large dead volume does not come from the detectors. To a large extend it comes from the pump, and with a proper process design this situation can be avoided,

appendix O “Comment to SMB Plant Lay-Out”.

The dead volumes are in the current work calculated as plug flow. Mixing in the dead volume can be taken into account by an axial dispersion term, as previously suggested by Migliorini *et al.* (1999). Migliorini suggests to solve this by a FDTD method and observed the problems when the axial dispersion becomes small, that is the system becomes stiff. However, the problem is a linear partial differential equation with constant coefficients and an obvious method for solving the system would be a Fast Fourier Transform, this is both faster, can handle stiff systems and and is very accurate.

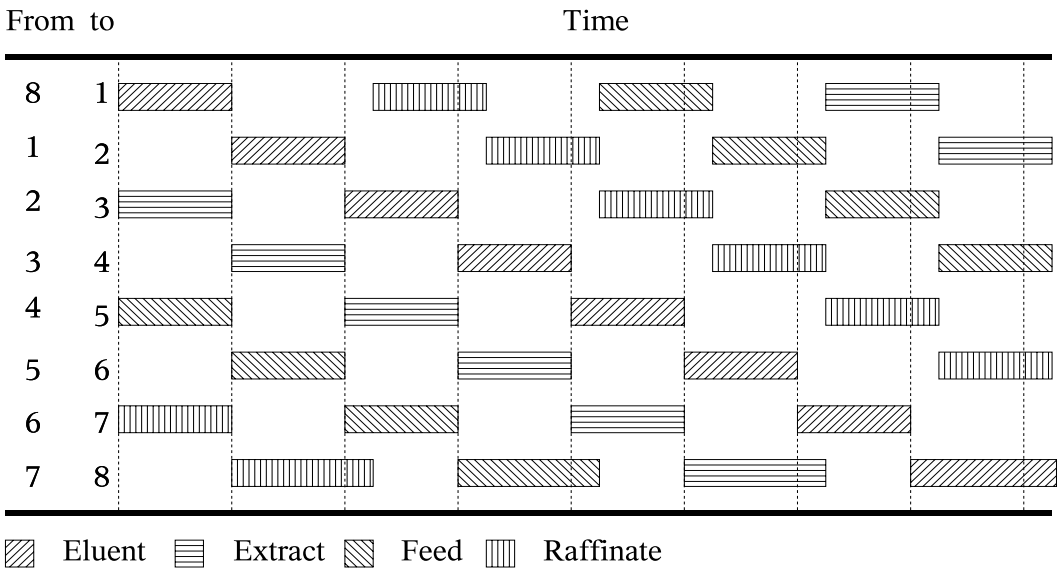

Figure 11.6 Asynchronous shifting for one cycle. The first two columns is the valve position, e.g. from 1 to 2 means the valve block between column 1 and 2. It is seen that whenever a product stream passes column 8 the shifting time of this is delayed compared to the others. The dashed lines shows the end of each shift without the asynchronous shifting time.

11.8 Measured Dead Volumes

As shown above the dead volumes will have an impact on the operating point of the plant and these need to determined. The most important dead volumes are the column dead volume DV_{col}=0.56 ml, the valve block dead volume DV_{val}<0.4 ml and the dead volume in the recycle stream DV_{rec}=23 ml. All these have been measured from pulse experiments and the results are given in appendix M “Measured Dead Volumes in the SMB Plant” and appendix N “Measured Column Dead Volumes”.

	Dead volume
	[ml]
Col. 8 to col. 1	23
Column	0.56
UV detector	0.11
Cond. detector	0.17
Valve block	<0.4

Table 11.2 Used dead volumes for the calculations for the SMB-plant. The valve block dead volume is from the vendor.

11.9 Column Data

A slurry containing approximately 75% resin was used to pack the column[7]. 9.5 g slurry was weighted into each column before packed. After the column was packed the length of the column was measured together with the total binding capacity, λ_{NO3-}, the nitrate retention volume at non-binding conditions and the retention volume of BSA at non-binding conditions.

Column	***No.***	***1***	***2***	***3***	***4***	***5***	***6***	***7***	***8***	***Avg***	***Do***
d_{col}	[cm]	1	1	1	1	1	1	1	1	1	0.5
L	[cm]	8.55	9.00	8.60	8.65	8.55	8.70	8.75	9.00	8.73	9.90
V_{col}	[ml]	6.72	7.07	6.75	6.79	6.72	6.83	6.87	7.07	6.85	1.94
V_{NO3-}	[ml]	4.90	5.30	4.96	5.02	4.95	5.07	5.11	5.30	5.08	1.25
ε_t	[ ]	0.729	0.750	0.734	0.739	0.737	0.743	0.743	0.750	0.741	0.641
ε_p	[ ]	0.549	0.583	0.557	0.564	0.561	0.571	0.572	0.583	0.568	0.402
ε	[ ]	0.40	0.40	0.40	0.40	0.40	0.40	0.40	0.40	0.40	0.40
$V_{NA,BSA}$	[ml]	4.49	4.88	4.33	-	4.45	4.58	4.49	4.79	4.57	1.22
$K_{D,BSA}$	[ ]	0.814	0.829	0.723	-	0.779	0.787	0.737	0.795	0.781	0.941
λ_{NO3-}	[m mole]	0.921	0.907	0.908	0.896	0.892	0.908	0.877	0.887	0.899	0.323
Λ_{NO3-}	[M PV]	0.416	0.367	0.403	0.389	0.394	0.388	0.372	0.359	0.386	0.689

Table 11.3 Measured column parameters. The numbers refers to the the column number in the SMB plant and Do refers to the column previously used in Dortmund.

A summary of the measured data and calculated model parameters are given in table 11.3. It is worth noticing that λ_{NO3-} varies less than Λ_{NO3-} for the different columns, the total capacity of

7 This slurry concentration was higher than suggested by Amersham Biosciences but was used to maximixe the bed volume without use of a packing device (which was not available).

the column λ_{NO3-} seems to be in good agreement with the packed resin amount. Also the total porosity is larger for the long columns than for the shorter columns, which is also expected. From these two observations it is concluded that the resin amount is approximately the same in all the columns but the shorter columns are more dense packed than the longer columns. For the SMB-simulations the column properties in the Avg column in table 11.3 are used. The column designated Do in table 11.3 below is the column previously used for single column experiments in Dortmund, the properties of this column varies more than the properties for column 1 to 8. This column was also used for pulse and breakthrough experiments as described below.

11.1 Determination of Equilibrium Parameters

The parameters for the SMA-formalism have previously been determined by pulse experiments in the linear range. However, for the SMB-experiments the columns are overloaded and the concentration is not in the linear range of the isotherm. The isotherms must therefore be determined up to the maximum concentration of the components in the SMB-plant.

Three different methods have been used to determine the isotherms. Pulse experiments for the linear part of the isotherm and batch and breakthrough curves for the non-linear part of the isotherm. The protein consumption in breakthrough experiments is significant, and the proteins are in general expensive (β-lactoglobulin A or B with a purity above 90 % costs app. 1000 euro/g). It is therefore of great interest to be able to determine the isotherms using pulse experiments and batch experiments.

If the SMA-formalism is applicable, the equilibrium constant and the binding charge ν can be determined from pulse experiments, leaving only the shielding parameter, σ, to be determined from breakthrough curves or batch experiments.

11.10.1 Pulse Experiments

The easiest way to determine the parameters in the linear range of the isotherm as a function of the salt concentration is by pulse experiments as described in chapter 6 “Pulse Experiments”

A linear fit to the double logarithmic plot of the pulse experiments show a good agreement as predicted by the SMA formalism.

This indicates that the SMA formalism is able to model the influence of the salt on the retention volume of the proteins.

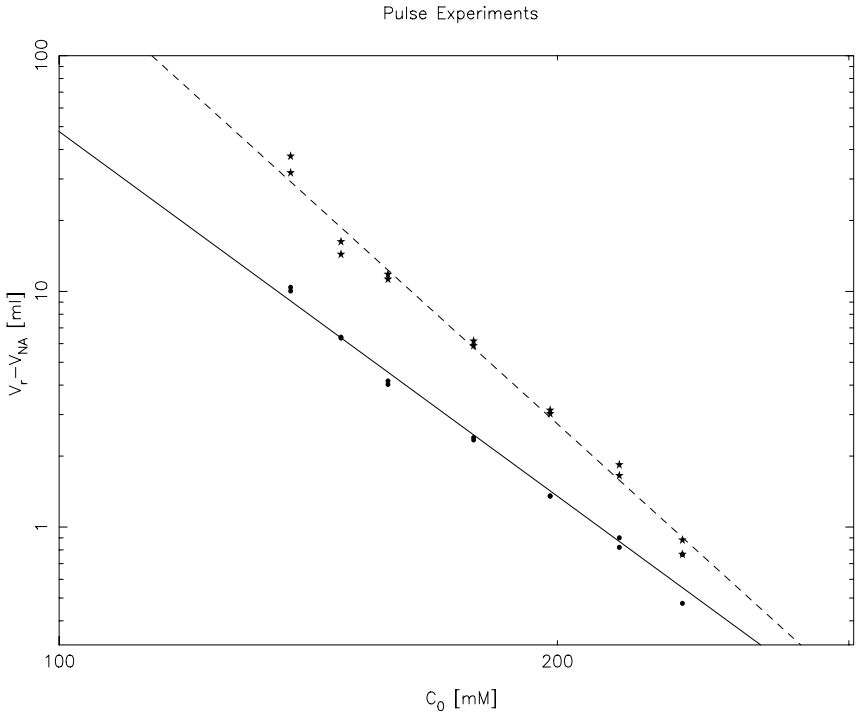

Figure 11.7 Retention volume as a function of the salt concentration. Legends: closed star = β-lactoglobulin A, closed circled = β- lactoglobulin B, dashed line fitted line to β-lactoglobulin A: $\log_{10}((V_r-V_{NA})\ ml^{-1}) = -6.3774 \log_{10}(C_0\ mM^{-1}) + 15.112$, and full line fitted line to β- lactoglobulin B: $\log_{10}(V_r-V_{NA}) = -5.139 \log_{10}((C_0\ mM^{-1}) + 11.956$. Column Do in table 11.3 above.

When fitting these peaks it was observed that the peaks were fronting. To investigate the origin of these fronting peaks a number of pulse experiments at C_p=2 g/l C_0=158 mM and pH=7 were made, where the injected amount was increased. The results of this experiment is given in table 11.4 below. From the table is seen that when the injected amount of protein is increased, the retention volume is increased too. It is further seen that the peaks are fronting when the injected amount of protein is increased ($\tau<0$). Fronting peaks and an increased retention volume at increased injections are both indications of an isotherm of the Freundlich type. The SMA-formalism is not able to describe this type of isotherm and a modified equilibrium expression is needed.

No isotherm can, however, be unlimited in its binding capacity, and this Freundlich-isotherm behaviour is in the best case only at low protein concentrations. The SMA-formalism isotherm

is kept, however bearing in mind, that the K_{eq} and ν cannot be determined from pulse experiments (simply because at the moment no better equilibrium expression has been found for describing the salt dependency).

File name	*DB no.*	V_{inj}	F_B	μ_B	σ_B	τ_B	$M_{1,B}$	F_A	μ_A	σ_A	τ_A	$M_{1,A}$
	[YYYYMMDDhhmm]	[µl]		[min]	[min]	[min]	[min]		[min]	[min]	[min]	[min]
Pulse-5	200306140931	5	G	8.7	1.33	0	8.7	E	14.05	2.34	1.96	16.01
Pulse-10	200306141022	10	E	7.96	1.11	1.2	9.16	E	16.32	2.41	0.52	16.84
Pulse-30	200306141113	30	G	9.71	1.45	0	9.71	E	24.09	1.78	-6.51	17.58
Pulse-60	200306141205	60	E	11.92	1.19	-1.49	10.43	E	29.25	2.37	-8.49	20.76
Pulse-120	200306141256	120	E	13.44	1.2	-1.92	11.52	E	36.02	3.16	-11.37	24.65
Pulse-200	200306140809	200	E	14.3	1.2	-2.14	12.16	E	40.72	3.31	-13.85	26.87

Table 11.4 Fitted parameters from pulse experiments at C_0=158 mM and with varied amount of injected volume. The column F gives the fitting function G=gauss function, E=EMG function. M_1 is the first moment of the peak. The subscript A and B refers to β-lactoglobulin A and B. The experiments were made with column no. 7 in table 11.4 above, and Q=2 ml/min.

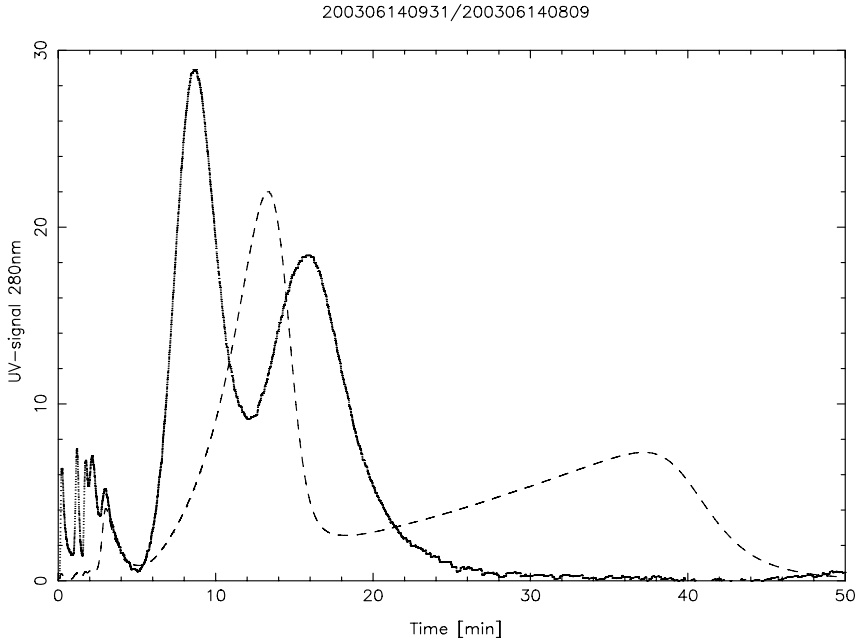

Figure 11.8 Pulse experiments with β-lactoglobulin at C_0=158 mM and pH=7 with 5 and 200 µl injected. The first peak is β-lactoglobulin B and the second peak is β-lactoglobulin A.

Legends: continuous line 5 µl, dashed line 200 µl. The UV-signal for the 5 µl chromatogram has been multiplied by 40.

11.10.2 Breakthrough Experiments

The breakthrough experiments are closest to the conditions in the SMB plant: The contact time between the two phases is comparable in breakthrough experiments and SMB experiments, the protein concentrations are of the same order and the resin is packed in a column in both cases. The breakthrough experiments are therefore of outmost importance when determining the equilibrium parameters. The drawback of breakthrough experiments is, however, the required large amount of protein. All breakthrough experiments are presented here, with a discussion about the results obtained. The first experiments were all made on the Do-column, table 11.3, since the columns for the SMB plant were not available at this time. Three breakthrough experiments were made on the Do-column. The salt concentration for these experiments were C_0=118, 137, and 157 mM. In the break though experiment only the total UV-signal is measured. To determine how much β-lactoglobulin A and B were in the outlet stream a number of samples in each experiment were taken and analysed afterwards, the result of these are shown in the figures below.

The resulting chromatograms are given in the figures 11.9-11.11 below. For all the experiments a breakthrough after a few minutes is seen, this breakthrough is slowly increased up to approximately 0.1 g/l protein. This together with the Freundlich behaviour of the isotherm observed in the pulse experiments leads to the (wrong) conclusion that the concave upwards shape was probably dominating up to approximately 0.1 g/l.

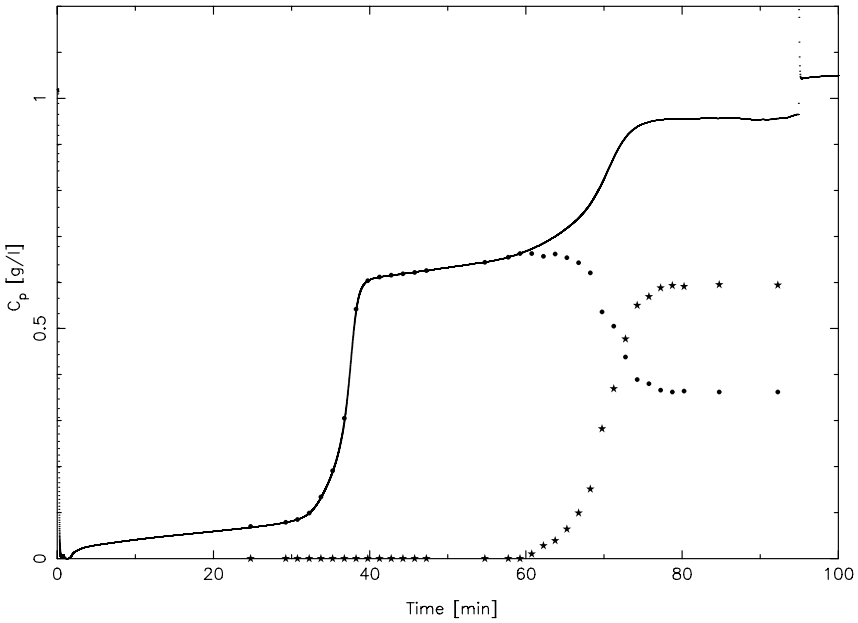

Figure 11.9 Breakthrough Curve with β-Lactoglobulin A and B at C_0=118 mM on Do column. Legends: closed stars: β- lactoglobulin A, closed circles β-lactoglobulin B. Q=1 ml/min.

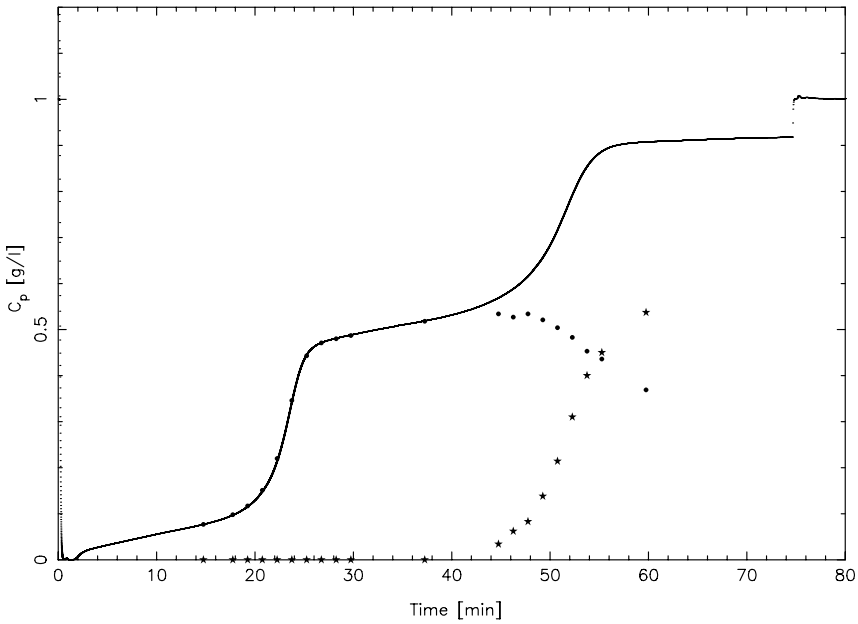

Figure 11.10 Breakthrough Curve with β-Lactoglobulin A and B at C_0=137 mM on Do column. Legends: closed stars: β- lactoglobulin A, closed circles β-lactoglobulin B. Q=1 ml/min.

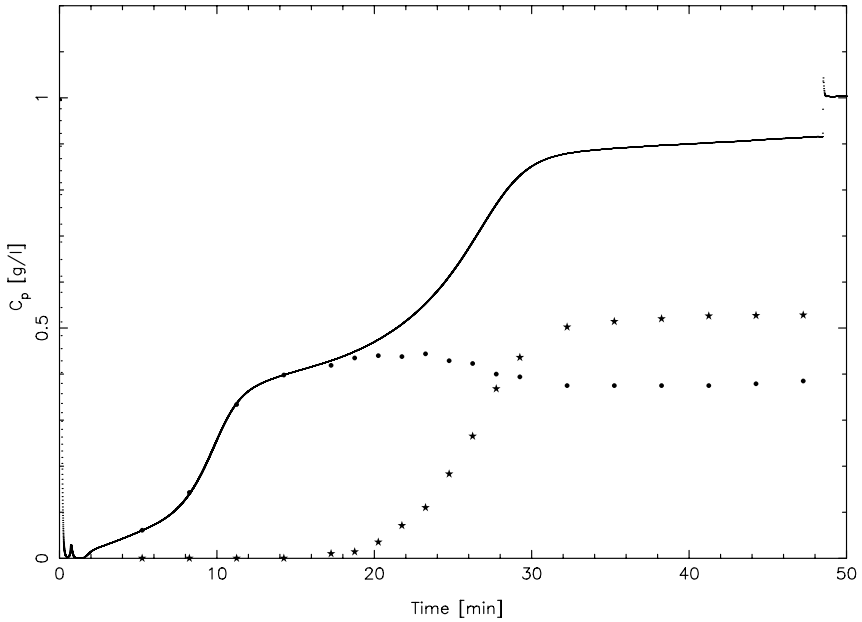

Figure 11.11 Breakthrough Curve with β-Lactoglobulin A and B at C_0=157 mM on Do column. Legends: closed stars: β- lactoglobulin A, closed circles β-lactoglobulin B. Q=1 ml/min.

After the experiments with the Do column the columns for the SMB plant were received the breakthrough experiments at the lowest and the highest salt concentration were repeated. These experiments were made using column no. 7 in table 11.3 since this column was closest to the average column properties for the eight columns in the SMB plant. The superficial velocity in these experiments were the same as for the Do column.

The results of these two experiments are given in figure 11.12 and 11.13 below. Comparing the results at the same salt concentration from the two columns show a clear difference on the breakthrough profile. This is most clearly seen from the C_0=117 mM experiments. Where the breakthrough after approximately 35 min. reaches 0.1 g/l using the Do column, it only reaches 1/4-1/3 of this using column 7. The breakthrough profile of β-lactoglobulin B is also significantly sharper on column 7. Similar results are seen from the experiments at 157 mM, however, here the breakthrough profile is not as sharp as for the 117 mM experiments.

With a concentration of only 0.03 g/l before the β-lactoglobulin B breakthrough on column 7 and not 0.1g/l as for the Do column this concentration must have another reason than equilibrium.

The ratio between the column to particle diameter for the Do column is 0.5cm/30μm = 167 for column 7 this is 333. As mentioned in “Modelling” the ratio should be higher than 200 which

is not the case for the Do column. The non-uniform flow distribution comes from a less dense packing close to the wall, giving a higher flow rate. This will lead to an earlier increase in the UV-signal as seen in the experiments with the Do column. Similar results has previously been observed at DTU.

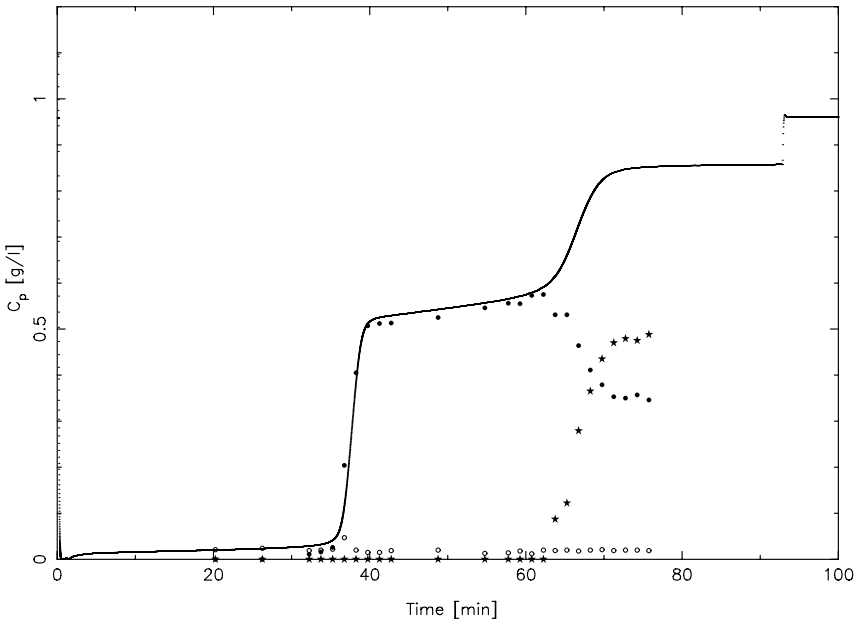

Figure 11.12 Breakthrough Curve with β-Lactoglobulin A and B at C_0=118 mM on column 7. Legends: closed stars: β- lactoglobulin A, closed circles β- lactoglobulin B. Q=4 ml/min.

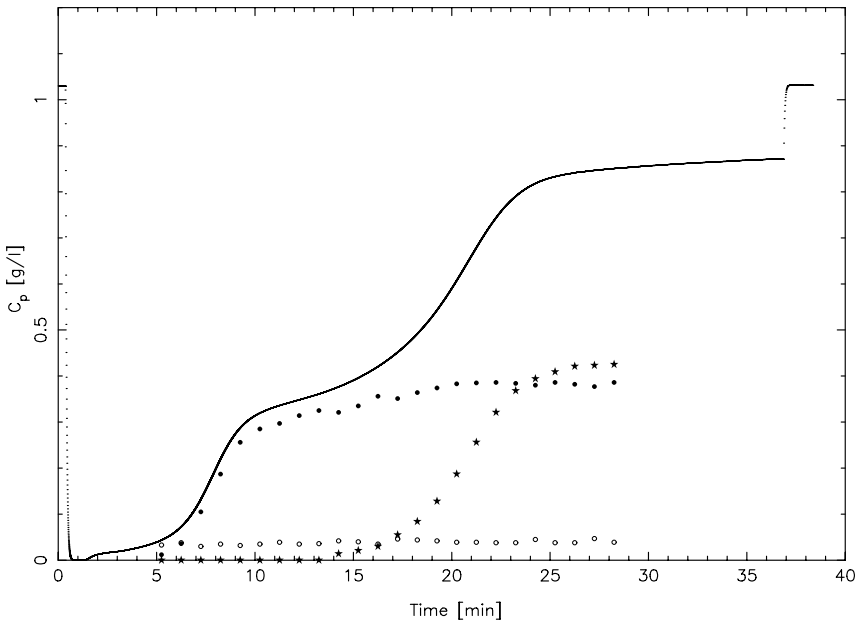

Figure 11.13 Breakthrough Curve with β-Lactoglobulin A and B at C_0=156 mM on column 7. Legends: closed stars: β- lactoglobulin A, closed circles β- lactoglobulin B. Q=4 ml/min.

The adsorbed amount should be calculated from the breakthrough curves. It is desirable to make this in a way similar to the pulse experiments, it means plotting the pure experimental data with a minimum of modelling taken into account.

The total uptake of protein can be found from ideal chromatography

$$m_{uptake} = Q c_f t_{½} = V_{col}\left[\epsilon + (1-\epsilon)\epsilon_p K_D (1+A)\right] c_f + V_{dead} c_f \quad (11\text{-}34)$$

Here $t_{½}$ it the breakthrough time, the subscript ½ emphasises that this in the non-ideal case is evaluated from the time at half the height of the breakthrough curve. Rewriting the equations gives

$$m_{uptake} = V_{col}\left[\epsilon + (1-\epsilon)\epsilon_p K_D\right] c_f + V_{dead} c_f + V_{col}(1-\epsilon)\epsilon_p K_D A\, c_f =$$

$$V_{NA} c_f + V_{col}(1-\epsilon)\epsilon_p K_D A\, c_f \quad (11\text{-}35)$$

And finally

$$V_{½} - V_{NA} = V_{col}(1-\epsilon)\epsilon_p K_D A \quad (11\text{-}36)$$

where $V_{½}=Q\cdot t_{½}$.

The equations (6-16) and (11-36) only contains a non-adsorbed term on the left side and an adsorbed term on the right side. This can be generalised to any model, $V\text{-}V_{NA}=V_{ads}\cdot A$. The right side are identical and plotting the left side as a function of C_0 (all measured data, no modelling data) the measured data from the two approaches can be compared.

The measured data for the breakthrough experiments are given below in table 11.5.

Filename	***Rundate no***	***column***	***Q***	***C_B***	***$t_{½,B}$***	***$V_{½,B}$***	***$t_{½,A}$***	***$V_{½,A}$***
	[YYYYMMDDhhmm]		[ml/min]	[g/l]	[min]	[ml]	[min]	[ml]
DBK-BETA-80-1	200302271715	Do	1	0.57	37.0	37	70.0	70
DBK-BETA-100-1	200303201450	Do	1	0.48	23.0	23	51.0	51
DBK-BETA-120-1	200303101446	Do	1	0.40	9.0	9	26.0	26
BTC-Lg 80mM	200305261425	7	4	0.53	37.0	148	67.0	268
Brk_Cs120_pH7	200306161059	7	4	0.39	8.3	33	21.3	85

Table 11.5 Breakthrough experiments. C_B in column five is the concentration at breakthrough of β-lactoglobulin B.

The first breakthrough is of the weaker binding β-lactoglobulin B, and the point therefore corresponds to a point on the pure component isotherm. The next breakthrough is β-lactoglobulin A and here both β-lactoglobulins are present and this point therefore corresponds to a point on a competitive isotherm.

11.10.3 Batch Experiments

The isotherms can also be determined from batch experiments, where resin and protein solution is equilibrated overnight. From the remaining protein concentration in the liquid phase the adsorbed amount of protein can be calculated. The composition in the initial solution and in the equilibrated solution can be determined by determining the peak areas from pulse experiments. Due to the fronting of the peaks, no method has been found where β-lactoglobulin A and B have a baseline separation. This adds to the uncertainty in determining the concentrations of the individual components. Since the isotherms are determined from the difference in the initial and final composition, even small errors in the determined concentrations can have a large impact on the results and these pure component isotherms reflect this uncertainty.

A detailed method description, of the currently used method is given in appendix J “Batch Experiments”. This method is similar to the method used in “Forschungszentrum Jülich, Institute of Biotechnology” and differs from the method previously suggested (Bisgaard-Frantzen, 1998). The main differences are that resin is handled as a slurry and not as a dried phase and the sample size is smaller. This reduces the amount of resin used in each experiment and also reduces any risk of a long drying time of the resin on the filter funnel.

Protein	C_0 [mM]	$C_{p,max}$ [g/l]	V_{res} [µl]	*Date*	*Comments*
β-Lg A	118	2	50	26/5 2003	Pure component isotherm
β-Lg A	157	1	50 and 100	28/3 2003	Pure component isotherm
β-Lg B	118	2	50	26/5 2003	Pure component isotherm
β-Lg B	157	1	100 and 150	28/3 2003	Pure component isotherm
β-Lg A and B	118	3	50	21/2 2003	Pipette error
β-Lg A and B	118	3	50	22/2 2003	
β-Lg A and B	118	1	50	6/3 2003	
β-Lg A and B	118	2	50 and 100	25/5 2003	Two complete series with 50 and 100 µl
β-Lg A and B	136	2	50	9/4 2003	
β-Lg A and B	136	2	100	9/4 2003	
β-Lg A and B	157	1	50 and 100	10/3 2003	
β-Lg A and B	157	3	50	7/3 2003	Something wrong with experiments
β-Lg A and B	157	2	50 and 100	1/4 2003	Dortmund resin, only total capacity
β-Lg A and B	157	2	50 and 100	1/4 2003	Copenhagen resin, only total capacity
β-Lg A and B	157	2	50 and 100	15/6 2003	Two complete series with 50 and 100 µl
BSA	88	2	50	10/4 2003	
BSA	88	2	100	10/4 2003	

Table 11.6 Batch experiments.

A large number of batch experiments were made, these are tabulated in table 11.6. However, no clear conclusion was drawn from the experiments but a number of problems were addressed during the period. A summary of the experience obtained with the batch experiments are therefore given.

As seen in the method description, appendix J “Batch Experiment”, the resin from the glass filter funnel is mixed with a corresponding amount of buffer. Reducing the amount of buffer added increases the resin content but also makes it impossible to pipette the resin slurry. The dry resin concentration is normally roughly 20% in the slurry phase. It is therefore important that the resin content is accurately determined, since any error will be multiplied by a factor of 5. When packing the columns for the SMB-plant five experiments were made to determine the dry content of resin in the resin slurry, these are tabulated in table 11.7 below.

There is a good agreement for the resin content in the different samples above. The average resin concentration is x_{res}=22.49 mass%. Having used 9.5 g resin slurry for each column. The

	Unit	*1*	*2*	*3*	*4*	*5*
m_{glass}	[g]	10.8445	10.8656	10.8720	10.9918	11.0881
V_{res}	[ml]	1	1	1	1	1
$m_{g,wet}$	[g]	11.8598	11.8815	11.8976	12.0129	12.1133
m_{tot}	[g]	11.8330	11.8330	11.8943	11.9892	12.0625
m_{cap}	[g]	0.7616	0.7400	0.7910	0.7671	0.7425
$m_{t,g}$	[g]	11.0763	11.0980	11.1074	11.2270	11.3232
m_{wet}	[g]	1015.3	1015.9	1025.6	1021.1	1025.2
m_{t0}	[mg]	226.9	227.4	231.3	230.3	231.9
m_{t1}	[mg]	231.8	232.4	235.4	235.2	235.1
ρ	[g/ml]	1.0153	1.0159	1.0256	1.0211	1.0252
x_{res}	[mass %]	22.35	22.38	22.55	22.55	22.62

Table 11.7 Determination of dry resin amount in resin slurry.

dry resin content in the columns is 2.14 g. The backbone density of the resin is 1.08 g/ml, leading to 1.98 ml dry resin in the column, or with an average column volume of 6.85 ml the total porosity of the columns is ε_t=0.71, this is in reasonable agreement with the 0.741 found, table 11.3. Another important value is V_{col}/m_{res}=3.21 ml/g resin since this value is used when converting the isotherm from batch experiments to the corresponding isotherm measured for the columns.

From this it was concluded that the dry resin amount in the slurry can be accurately determined.

The total amount of protein after equilibration was determined from the absorbance at 280 nm. To avoid getting out of the linear region of the photometer, samples at high concentrations were diluted. A photometer was not available at first in the department and all samples were diluted before analysing these in another department. Diluting a sample to 1/10 of its original concentration any uncertainty in the measurement will give rise to a 10 times higher uncertainty in the result. Drift of the baseline was observed and a better approach is to dilute the samples to utilise the linear range of the photometer. This was done by starting with the highest concentration and from the result evaluate the minimum dilution for the following sample. This approach was used in samples dated after April 2nd.

Not enough resin of the batch used to pack the Do[8] column was available to pack the columns

8 Do is the resin used to pack the Do column in table 11.3 with lot no. 285818 the resin named Cph is the resin from Copenhagen with lot no. 276819

for the SMB plant. To compare the capacities of the two resins two experiments were made April 1st. All the isotherms measured at 157 mM are given in figure 11.10 below (except the data March 3rd with an error). The two isotherms measured April 1st use the same buffer and protein solution, however, a clear discrepancy between the data is seen, the capacity of the Cph resin is higher than the Do resin. For comparison the experiments with the Do resin dated March the 10th are shown in the figure and with the Cph resin dated June the 15th. A good agreement between data set with the same resin batch and resin amount is found, even though different buffers and protein solutions are used in these experiments. From this it is concluded that the batch variations cause the differences in the isotherms, even though the impact seems to be small in a packed column, table 11.5.

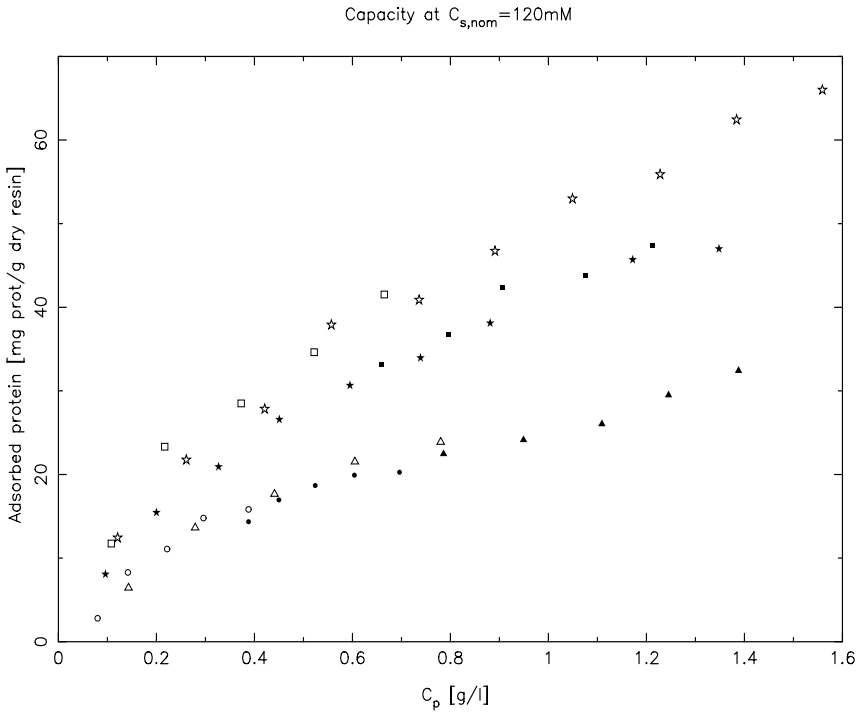

Figure 11.14 Measured total capacity at C_0=157 mM.

Legends: Circles data measured 10/3 (Do resin), triangles data measured 1/4 (Do resin), squares data measured 1/4 (Cph resin), stars data measured 15/6 (Cph resin). Open figures 50 µl resin, closed 100 µl resin.

Another interesting observation from the isotherms in figure 11.10 is that the isotherms measured using 100 µl resin has a lower capacity than isotherms measured using 50 µl of resin. At low protein concentrations the isotherm ought to be linear since no competitive effects are expected. However, the two series measured June the 15th also shows a lower

capacity for isotherm with 100 µl resin even at low protein concentrations.
Finally it is observed that all the measured isotherms do not seem to have a shape leading to fronting peaks, a Freundlich type isotherms.
Comparing experiments with the same type and amount of resin used there is a good agreement between the experiments. It is therefore likely that a systematic error is causing the discrepancy.
The purity of the protein is according to specifications >95 wt%, a few pulse experiments showed that the protein did not only contain β-lactoglobulin A and B but at least four components, figure 11.16. The four peak are:

1) a very weak/non-binding component (3.3%)
2) β-lactoglobulin B (38%)
3) β-lactoglobulin A (51%)
4) a strong bound component (7.7%)

The area below each peak was determined from the fit shown left figure in 11.16, and the fitted areas in percent of the total UV-signal is given the parenthesis. Even though the purity is >95% wt the impurities contributes to approximately 11% of the total UV-signal (the UV-absorbance of the impurities must be higher than for the β-lactoglobulins).
Comparing these impurity levels with the break-through curves above, figure 11.9-11.13, it is seen that none of the breakthrough curves reach complete breakthrough, a step up is seen when the column is by-passed at the end of each experiment. The strong bound component binds very strongly to the column and a break though of this component is unlikely under the conditions in the break-through experiments. The strongly bound component only elutes at very high salt concentrations and for the analysis of the samples this peak was normally not seen.
The weakly bound component can also be seen as an early break-through in the experiments, most clearly at C_0=118 mM with column 7 (less wall effects), figure 11.12. Naturally both these impurities must be taken into account when evaluating the batch experiments.
Taking these two components into account and consider them as being non-bound and entirely bound changes the isotherm from the ones given in figure 11.15 to the ones given in figure 11.17. It is seen that the bound amount is significantly reduced and it is crucial to take these components into account.

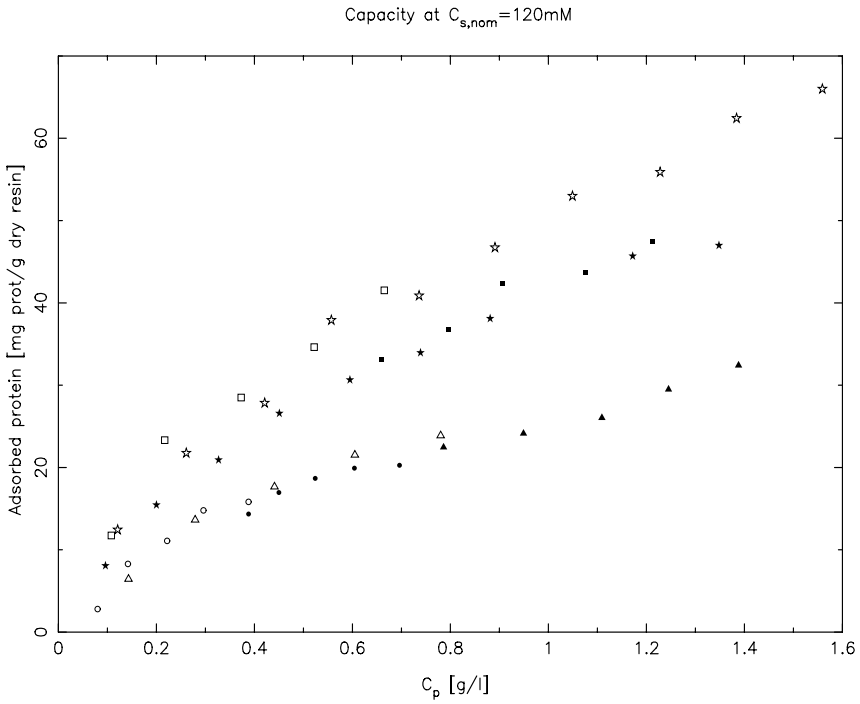

Figure 11.15 Measured total capacity at C_0=157 mM.

Legends: Circles data measured 10/3 (Do resin), triangles data measured 1/4 (Do resin), squares data measured 1/4 (Cph resin), stars data measured 15/6 (Cph resin). Open figures 50 µl resin, closed 100 µl resin.

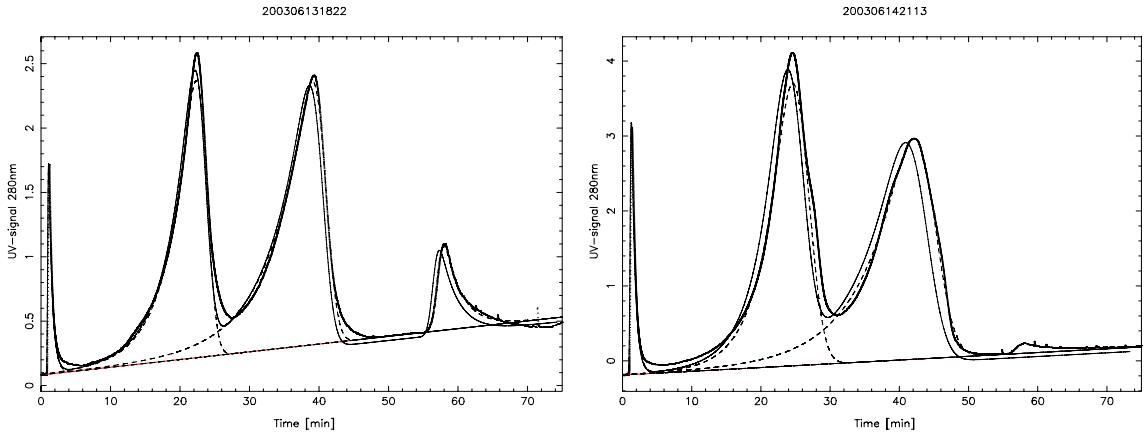

Figure 11.16 Left: Chromatogram of β-lactoglobulin A and B solution. Right: Chromatogram of liquid phase from batch experiment after equilibration.

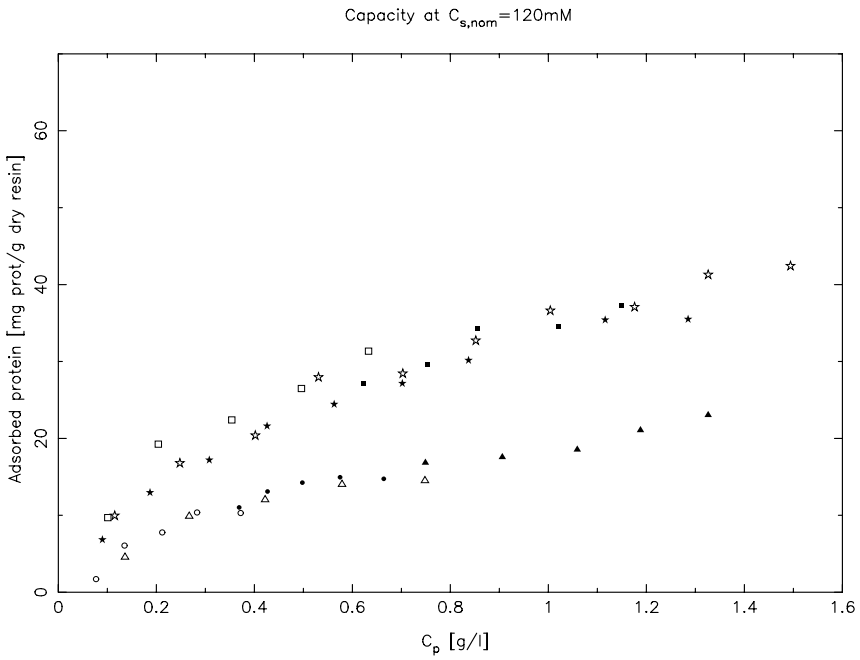

Figure 11.17 Measured total capacity at C_0=157 mM. Legends: see figure 11.10.

11.10.4 Used Equilibrium Parameters

The determination of the equilibrium parameters did not lead to a clear conclusion. Due to time limitations it was required to make a judgement which parameters to use. With the many problems found in the batch experiments these were not considered to form a trustworthy basis for a set of equilibrium parameters, and these were given a low weight.

Furthermore it was known that the current equilibrium expression was not able to take the isotherms upward curvature into account. This increased protein uptake was considered to be at low protein concentrations only, based on the shape of the front for the breakthrough curve at 118 mM on column no. 7. The SMA formalism were kept and the parameters for this model had to be determined. ν is of course a very important parameter for a gradient experiment since this gives the salt dependence of adsorbed protein. From the pulse experiments ν for the two proteins were found as 5.139 and 6.377 and these were used as the binding charge of the two proteins. It should be noted that these were determined at low protein concentrations and it would probably be better to determine these at higher protein injections if a Freundlich type isotherm is valid at low protein concentrations.

Using only ν from the isocratic experiments, two more parameters have to be determined: K_{eq} and σ, from the breakthrough curves. These are determined from the break though times given

in table 11.5. The first breakthrough is a pure component breakthrough and depends only on the adsorbance of β-lactoglobulin B. Both β-lactoglobulin A and B are present at the second breakthrough and both components must be taken into account, therefore this point corresponds to a point on a competitive isotherm.

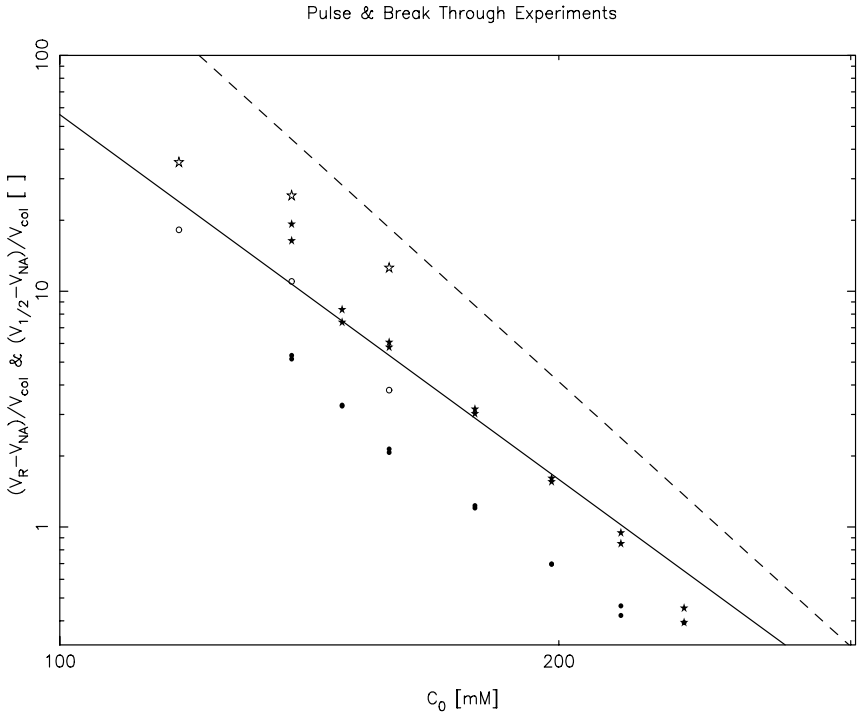

Figure 11.18 Breakthrough experiments and pulse experiment together with the values used for the SMB calculations. Legends: star = β- lactoglobulin A, circled = β- lactoglobulin B, open figures breakthrough experiments, closed figures pulse experiments. Dashed line used parameters for β-lactoglobulin A: $log_{10}((V_r-V_{NA})$ $ml^{-1})=-6.3774\ log_{10}(C_0\ mM^{-1}) + 15.36$, and full line used parameters for β-lactoglobulin B: $log_{10}((V_r-V_{NA})\ ml^{-1})= -5.139\ log_{10}(C_0\ mM^{-1}) + 12.09$. Column Do in table 11.3 above.

11.11 SMB Simulations

The recycle of the salt has not been taken into account and the SMB-plant has been calculated using the process simulator gPROMS and the model used in Dortmund. This model is given as

$$\frac{\partial C_j}{\partial t}=(D_m+E_D)\frac{\partial^2 C_j}{\partial z^2}-v_i\frac{\partial C_j}{\partial x}-\frac{1-\epsilon}{\epsilon}\frac{6}{d_p}k_{eff,j}(C_j-C_{p,j}) \tag{11-37}$$

$$(1-\epsilon_p)\frac{\partial Q_j}{\partial t}+\epsilon_p K_D\frac{\partial C_{p,j}}{\partial t}=k_{eff,j}\frac{6}{d_p}(C_j-C_{p,j}) \tag{11-38}$$

Equilibrium inside the particles is assumed. From the equations is seen that the bound amount of protein refers to the backbone volume of the ion exchanger.

It is therefore necessary to calculate the equilibrium parameters for this model. The equilibrium parameters can be calculated by requiring

$$K_{eq}(1-\epsilon)\epsilon_p K_D \bar{Q}_0^{\nu} = (1-\tilde{\epsilon})(1-\tilde{\epsilon_p})\tilde{\bar{Q}}_0^{\tilde{\nu}}\tilde{K}_{eq} \tag{11-39}$$

Where the parameters with ~ refers to the model used in Dortmund.

As mentioned in chapter 6.3 “Equilibrium Parameters” the relationship between the model parameter is easily seen by the formulation used in equation (6-18), where only the experimental results are plotted. Setting V_{col} equal for the two models equation (11-39) is obtained. The benefit of using the formulation suggested in equation (6-18) is here seen.

Λ can have different values in the two model and a second requirement is that the same uptake of protein must lead to the same relative reduction in Λ since $\bar{Q}_0$ is raised to the power of ν. This gives

$$\Lambda - \sum(\sigma+\nu) = \tilde{\Lambda} - \sum(\tilde{\sigma}+\nu) \Leftrightarrow \frac{n_p}{V_{col}(1-\epsilon)\epsilon_p K_D} = \frac{n_p}{V_{col}(1-\tilde{\epsilon})(1-\tilde{\epsilon_p})} \tag{11-40}$$

The following parameters have been used for the simulation, Λ=883mM, $C_{f,A}$= 0.45 g/l, ν_A=6.377, σ_A=40, $K_{eq,A}$=1.45·10^{-3}, $K_{D,A}$=0.67, $K_{eff,A}$=3·10^{-6}m/s, $C_{f,B}$= 0.41 g/l, ν_B=5.139, σ_B=40, $K_{eq,B}$=3.5·10^{-3}, $K_{D,B}$=0.67, and $K_{eff,B}$=3·10^{-6}m/s[9].

With these equilibrium parameters inserted into the right hand side of equation (11-39) and taking the logarithm is found

$$\log_{10}\left((1-0.4)(1-0.57)883^{6.377}1.45\cdot10^{-3}\right) = 15.36 \tag{11-41}$$

$$\log_{10}\left((1-0.4)(1-0.57)883^{5.139}3.5\cdot10^{-3}\right) = 12.09 \tag{11-42}$$

Hereby it is shown how with relative ease the model parameters can be calculated, and the advantage of plotting V_R-V_{NA}.

11.12 Gradient SMB Experiment

A gradient experiment were made on the SMB plant where the salt concentration in the feed stream was 116 mM and in the eluent stream 156 mM.

The shifting time was t_{sft}=25 min and with and average liquid velocity in the plant of 3.14 ml/min the asynchronous shifting time was 7 min.

9 These values differs slightly from the values using the approach suggested above. This is however not considered to have a large impact on the results.

Stream	*Flow rate* [ml/min]
Eluent	4.04
Extract	3.69
Feed	2.17
Raffinate	2.52

Table 11.8 External flow rates.

Zone	*Flow rate* [ml/min]
1	5.45
2	1.76
3	3.93
4	1.41

Table 11.9 Internal flow rates.

The results from the experiment and the simulation of the experiment are given in figure 11.19 below. The data presented are the concentration profiles outlet column 8. At every shift the column is moved one position upstream in the plant. The first 25 minutes, therefore, corresponds to the outlet concentration from position VIII, the following 25 minutes to the outlet concentration from position VII etc.
The strong influence of the salt on the protein adsorption is clearly seen in the figure.

11.12.1 Salt Concentration

The chloride concentration in the feed stream was 116 mM and the in eluent stream 156 mM. From this the salt concentrations can be calculated for the TCC solution in the different zones. It is given that $C_V=\alpha_V C_{f,V}+(1-\alpha_V)C_{IV}$ and $C_I=\alpha_I C_{f,I}+(1-\alpha_I)C_{VIII}$ where the index refers to the column position, figure 11.1. The salt concentrations in position I to IV are the same and the salt concentration in position V to VIII are the same therefore

$C_I\left[1-(1-\alpha_I)(1-\alpha_V)\right]=\alpha_I C_{f,I}+\alpha_V(1-\alpha_I)C_{f,V}$. With α_I=4.04/5.45 and α_V=2.17/3.93 the salt concentration in the first two zones will be 149.5 mM and in the last two zones 131.0 mM.

At every shift, the columns are shifted one position upstream its previous position. The column moved from position V to position IV contains after the shift the lower salt concentration from position five. The mixing ratio α is the same and a lower salt concentration is expected after the shift. With the salt concentration calculated above this initially lower salt concentration is

$$c_{in,V}(t)=\alpha_V c_{f,V}+(1-\alpha_V)c_V^{TCC}=\frac{2.17}{3.93}116mM+\left(1-\frac{2.17}{3.93}\right)131.0\,mM=122.7\,mM$$

$$\text{for}\quad 0\le t\le\frac{V_{col}\epsilon_t+V_{dead}}{Q_{IV}}$$

For a closed loop, where the liquid phase is recycled from the last position to the first position the same thing happens. The column in position VIII now contains the high salt concentration from position I and is mixed with the feed stream to position I.

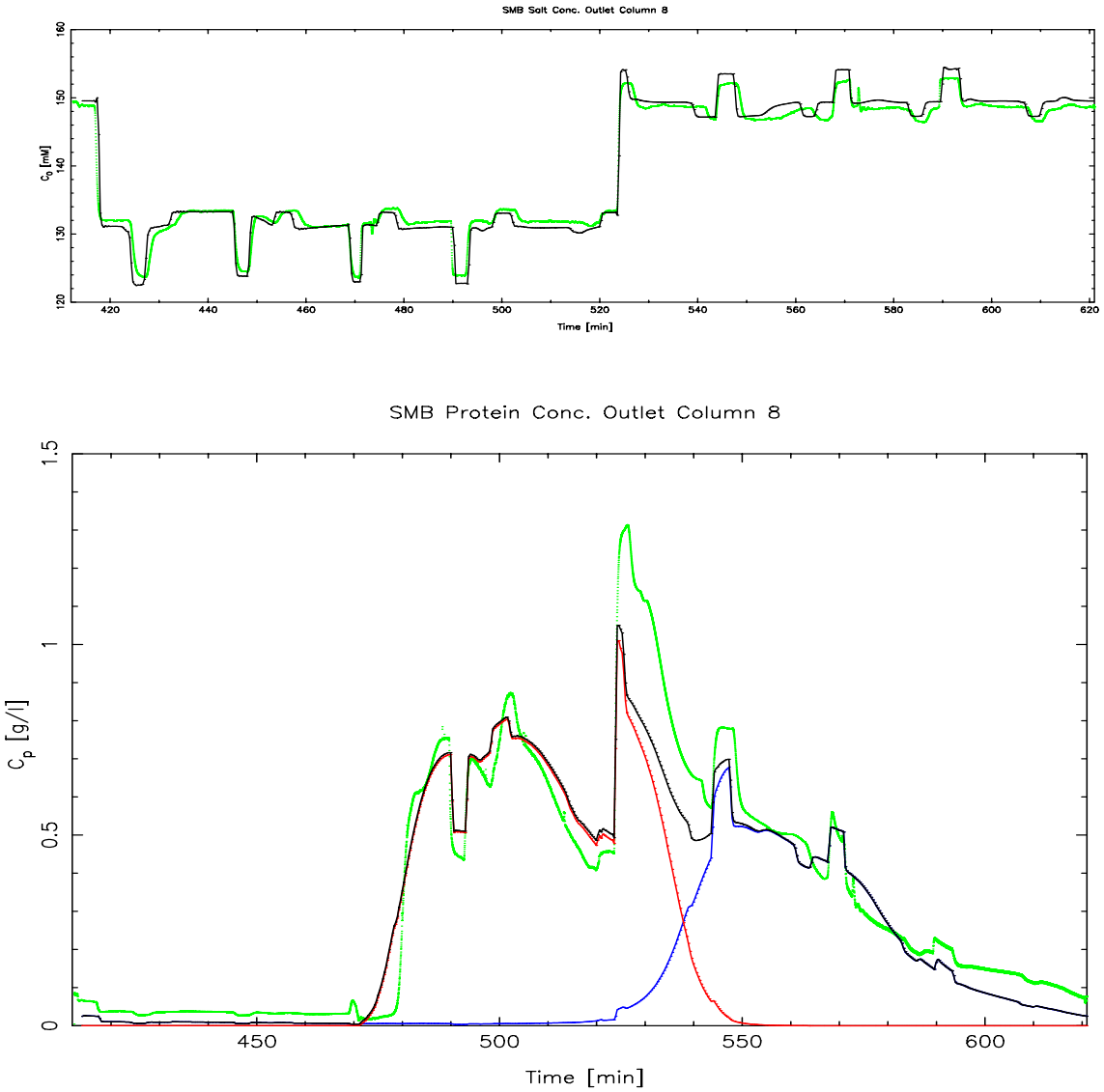

Figure 11.19 Experimental and simulated salt and protein concentration outlet column 8. Legends: Green experimental data, black simulated data (sum curve for the proteins), blue β-Lactoglobulin A, red β-Lactoglobulin A.

Initially the concentration inlet position I will be

$$c_{in,I}(t)=\alpha_I c_{f,I}+(1-\alpha_I)c_I^{TCC}=\frac{4.04}{5.45}156mM+\left(1-\frac{4.04}{5.45}\right)149.5\,mM=154.3\,mM$$

These two salt concentrations will travel through the SMB plant, however at every feed point the peak will be diluted.

The measured and simulated salt concentration are given in figure 11.19 above, the four salt concentration calculated above can all be found in this figure.

It is interesting to know how these salt peaks will effect the performance of the SMB plant. When a low salt concentration peak is travelling through section three and four of the system the proteins will bind stronger and a breakthrough of the strongly retained component is reduced. Similarly a high salt concentration peak travelling through section one and two will reduce the binding and the weaker bound component will not be able to pollute the extract stream. The peaks are usually diluted significantly when passing a feed position and the effect hereafter on the equilibrium is correspondingly reduced. From an overall operating point of view these peaks will, therefore, have a minor effect on the purity of the products.

11.13 Summary

In the current work β-lactoglobulin A and B has been separated into two pure product streams using simulated moving bed technology. In connection with this a number of tools has been developed.

From the ideal chromatography model an alternative method has been suggested to calculate the region of complete separation. This method seems simpler than the method previously suggested by Migliorini *et al.* (2000b) and convergence problems has not been observed.

A true counter current method taking mass transfer resistance into account has also been suggested. Axial dispersion can be included in this model by pooling it with the film layer mass transfer coefficient k_f, as previously suggested. This method serves as a fast method to calculate the profile inside the SMB plant. Convergence problems are still seen and it probably will be advantageous to use more elements in each column to cope with steep profiles.

Equilibrium parameters for the β-lactoglobulin A and B have been determined, however, these are only based on a few measurements and more experiments are needed.

With the equilibrium parameters determined from the batch and breakthrough experiments the SMB process has been modelled and a good agreement between the modelled and simulated

profile is found.

A lot of work still has to be done. The equilibrium parameters should be better determined. Breakthrough curves has this far been considered to be the best basis to determine the equilibrium parameters. The breakthrough experiments on the Do column all suffered from a too small column to particle diameter ratio. Only two experiments have been made with column seven, containing the same resin used for the SMB experiments. Both these experiments were made with a concentration of 1 g/l. Competitive effects are seen at the low salt concentration and more experimental data are required to improve the parameters for the isotherms.

A functional relationship for the concentrations and retention time for the breakthrough curves has previously been derived for a Langmuir isotherm, Guiochon *et al.* (1994, pp. 248-298). Using a similar approach and the SMA-formalism a relationship between the SMA-parameters can possibly be obtained and more information can be gained from each experiment.

The batch experiments have not been very successful. The method has, however, been improved and a number of problems has been solved. The method is, however, very attractive due to the low amount of resin and protein required to determine an isotherm. It seem difficult to determine how well the method works with the current four component mixture. A better starting point could be using a single component known to be pure and try with different amount of resin.

The SMA-formalism is not able to describe the Freundlich type behaviour of the isotherm. An equilibrium expression being able to do this and including the influence of the salt could be suggested.

No process optimization has been done, however, this cannot be done before better equilibrium parameters are found.

12. Conclusion

A model has been derived for modelling of ion-exchange chromatography of proteins. The suggested model is capable of using either diffusion of the proteins inside the particle, or a linear driving force approximation. For a linear isotherm the model can be solved by Fast Fourier Transformation, a rapid method to solve the system of equation. When the isotherm is non-linear the calculation time can be dramatically reduced by using orthogonal collocation on finite elements, and solving one element at a time. The resulting calculated chromatogram is not notably influenced by the used numerical method.

The measured ion-exchange capacity of hydroxide is lower than the measured ion-exchange capacity using nitrate due to the weak binding of the hydroxide. Also the nitrate capacity is difficult to determine, since nitrate can be washed out of the column. No method has been found four scaling better than scaling on the column volume.

A more robust method to determine the mass transfer parameters inside the particles using a correlation to calculate the film-layer mass transfer coefficient, and only fit the parameters for the particle is used. The two remaining parameters are fitted and these are not strongly correlated. Both a pore diffusion and a surface diffusion parameter is required to be able to model the observations from the laboratory.

Equilibrium and mass transport parameters can be fitted from isocratic experiments. From these it is possible to model the isocratic experiments and also to predict the retention volume for gradient experiments. The retention volume is best predicted for high values of the binding charge. By modelling α-Lactalbumin it has been shown how model parameters can be determined from isocratic experiments and how the parameters can be used to model the experiments and explain results observed in the laboratory.

For breakthrough experiments the influence of stronger bound impurities is shown to have a large influence on the determined isotherms for the differential columns. Also for larger columns impurities will have a large impact on the measured isotherms. The influence is seen to be largest at weak binding of the measured component. Impurities in the proteins will also have a large influence on the measured capacity from batch experiments. A gradual decline of the ion-exchange capacity for the batch experiments was found when the ion-exchanger was reused.

Plotting pure experimental values efficiently separates experiments and modelling. From the experimental values parameters for a model can be determined. Using this approach a

functional relationship between the model parameters are easily seen. This method also makes it possible to convert model parameters from one model to another model.

It is shown that the β-Lactoglobulins cannot be modelled using the SMA-formalism at low concentrations where the proteins behave more like a Freundlich type isotherm with an upward curvature. The SMA-formalism has, however, been used to describe the equilibrium between β-Lactoglobulin A and B and Source 30Q. The results at low concentrations have been neglected. The fronting is, however, considered to be at low concentrations, and will have only a marginal effect at higher concentrations.

A method to calculate the total separation region for components with a non-constant selectivity has been suggested. The method is easier to solve than the previously suggested method.

β-Lactoglobulin A and B has been successfully separated in a SMB-plant with a salt gradient. The Separation of the two proteins has been modelled taking a large dead volume in the recycle stream into account. Good agreement between the experimental and the simulated results has been found.

13. Discussion and Future Work

The SMA-formalism is not able to take the fronting of the β-Lactoglobulins into account. The SMA-formalism must be modified to be able to do this or another equilibrium expression must be derived, which is able to take fronting peaks into account and the influence of salt.
The linear part of the isotherm has been thoroughly investigated. For the non-linear part of the isotherm breakthrough experiments have been made using BSA and Source 30Q. The results however have not been used for any modelling and this still needs to be done. This will also give additional insight into whether it is best to use half the breakthrough height or the desorbed amount of protein for modelling.
For protein mixtures the approach suggested by Guiochon *et al.* (1994, pp. 248-266) can possibly be derived for the SMA-formalism and used to gain additional insight into the chromatographic separation and to evaluate breakthrough curves from the experimental chromatograms with more proteins.
The batch method still need to be evaluated further. Due to the problems associated with impurities in the proteins, it is suggested to start with a pure protein and make sure that the problems are associated with impurities in the protein solutions.
The program can in its current version not be considered to be anything but a prototype. If the program is to be used it must be improved to be more stable. It would be an advantage to split the program into two parts, a program written in standard fortran 90, which can be compiled using all standard fortran compiler. This part contains all calculation, evaluation, and simulation routines, and functions. The second part of the program contains the user interface, this part can be written in non-standard fortran or another appropriate language.
In the SMB-model the salt concentration in the different sections is calculated from the TCC-model. Salt still needs to be implemented in this models differential mass balance including the influence from the recycle stream, this can be done by either calculating salt as plug flow whereby one column can be calculated at a time or by use of a Predictor-Corrector method.
More experiments are needed to determine the equilibrium parameters for β-Lactoglobulin A and B.
An optimization of the chromatographic separation of the proteins on a single column or in a SMB-plant has not yet been made.

References

Bisgaard-Frantzen Hans, "Characterization of Column Packings for Chromatography of Proteins", Master-thesis IVC-SEP, DTU, (1998)

Brooks Clayton A., Steven M. Cramer, "Steric Mass-Action Ion Exchange: Displacement Profiles and Induced Salt Gradients", *AIChE Journal*, pp. 1969-1978, vol. 38, (1992)

Carberry James J., "A Boundary-Layer Model of Fluid-Particle Mass Transfer in Fixed Beds", *AIChE Journal*, pp. 460-463, vol. 6, (1960)

Carta Giorgio, Alberto Cincotti, "Film Model Approximation for Non-Linear Adsorption and Diffusion in Spherical Particles", *Chemical Engineering Science*, pp. 3483-3488, vol. 53, (1998)

Chiang Anthony S. T., "Equilibrium Theory for Simulated Moving Bed Adsorption Processes", *AIChE Journal*, pp. 2431-2441, vol. 44, (1998)

Chung S. F., C. Y. Wen, "Longitudinal Dispersion of Liquid Flowing Through Fixed and Fluidized Beds", *AIChE Journal*, pp. 857-866, vol. 14, (1968)

Cluff John R., Stephen J. Hawkes, "Zone Dispersion in Packings of Impermeable Spheres", *Journal of Chromatographic Science*, pp. 248-255, vol. 14, (1976)

Danckwerts P. V., "Continuous Flow Systems, Distribution of Residence Times", *Chemical Engineering Science*, pp. 1-13, vol. 2, (1953)

Dennis John E., David M. Gay, Roy E. Welsch, "Algorithm 573, NL2SOL-An Adaptive Nonlinear Least Square Algorithm [E4]", *ACM Transactions on Mathematical Software*, pp. 369-383, vol. 7, (1981)

Do D. D., R. G. Rice, "On the Relative Importance of Pore and Surface Diffusion in Non-Equilibrium Adsorption Rate Processes", *Chemical Engineering Science*, pp. 2269-2284, vol. 42, (1987)

Gerstner Joseph A., Jeffrey A. Bell, Steven M. Cramer, "Gibbs Free Energy of Adsorption for Biomolecules in Ion-Exchange Systems", *Biophysical Chemistry*, pp. 97-106, vol. 52, (1994)

Glueckauf E., "Formulæ for Diffusion into Spheres and their Application to Chromatography", *Trans. Faraday Soc.*, pp. 1540-1551, vol. 51, (1955)

Guiochon Georges, Sadrottin Golshan Shirazi, Anita M. Katti, "Fundamentals of Preparative and Nonlinear Chromatography", Academic Press Inc., Boston, (1994), ISBN: 0-12-305530-X

Hansen Ernst, "Application of the Linear Driving Force Approcimation to the Study of Mass Transfer in Ion-exchange Chromatography", Ph.D.-thesis IVC-SEP, DTU, /2000)

Helfferich Friedrich, "Ion Exchange", Dover Publications, New York, (1995), ISBN: 0-486-68784-8

Intel, "Intel Math Kernel Library, Reference Manual, document no. 630813-011", http://developer.intel.com, pp. 1029, vol. , (2001)

Iserles Arieh, "A First Course in the Numerical Analysis of Differential Equations", Cambridge University Press, Cambridge, (1996), ISBN: 0-521-55376-4

Jansen Marcel L., G. W. Hofland, J. Houwers, A. J. J. Straathof, L. A. M. van der Wielen, K. C. A. M Luyben, W. J. J. Tweel, "Effect of pH and Concentration on Column Dynamics of Weak Electrolyte Ion Exchange", *AIChE Journal*, pp. 1925-1937, vol. 42, (1996)

Jeasnsonne Mark S., Joe P. Foley, "Review of the Exponentially Modified Gaussian (EMG) Function since 1983", *Journal of Chromatographic Science*, pp. 258-266, vol. 29, (1991)

Kataoka Takeshi, Hiroyuki Yoshida, Koretsune Ueyama, "Mass Transfer in Laminar Region Between Liquid and Packing Material Surface in Packed Bed", *Journal of Chemical Engineering of Japan*, pp. 132-136, vol. 5, (1972)

Kidal Steffen, "Metoder til karakterisering af ionbytningskromatografi", Master-thesis IVC-SEP, DTU, (2001)

Kreyszig Erwin, "Advanced Engineering Mathematics, eighth edition", John Wiley & Sons, New York, (1999), ISBN: 0-471-33328-X

Lambert J. D., "Numerical Methods for Ordinary Differential Systems. The Initial Value Problem", John Wiley & Sons, New York, (1991), ISBN: 0-471-92990-5

Lide David R. (editor), "CRC Handbook of Chemistry and Physics, 83rd edition", CRC Press, New York, (1998), ISBN: 0-8493-0483-0

Ljunglöf Anders, Jörg Thömmes, "Visualising Intraparticle Protein Transport in Porous Adsorbents by Confocal Microscopy", *Journal of Chromatography A*, pp. 387-395, vol. 813, (1998)

Lode F.G., A. Rosenfeld, Q.S. Yuan, T.W. Root, E.N. Lightfoot, "Refining the Scale-Up of Chromatographic Separations", *Journal of Chromatography A*, pp. 3-14, vol. 796, (1998)

Ma Z., G. Guiochon, "Application of Orthogonal Collocation on Finite Elements in the Simulation of Non-Linear Chromatography", *Computers and Chemical Engineering*, pp. 415-426, vol. 15, (1991)

Michelsen Michael L., "The Axial Dispersion Model and Orthogonal Collocation", *Chemical Engineering Science*, pp. 3675-3676, vol. 49, (1994)

Migliorini Christiano, Marco Mazzotti, Massimo Morbidelli, "Robust Design of Countercurrent Adsorption Separation Processes: 5. Nonconstant Selectivity", *AIChE Journal*,

pp. 1384-1399, vol. 46, (2000b)

Migliorini Christiano, Marco Mazzotti, Massimo Morbidelli, "Robust Design of Countercurrent Adsorption Separation Processes: 5. Nonconstant Selectivity", *AIChE Journal*, pp. 1384-1399, vol. 46, (2000b)

Migliorini Christiano, Marco Mazzotti, Massimo Morbidelli, "Design of Simulated Moving Bed Multicomponent Separations, Langmuir Systems", *Separation and Purification Technology*, pp. 79-96, vol. 20, (2000a)

Migliorini Christiano, Marco Mazzotti, Massimo Morbidelli, "Simulated Moving-Bed Units with Extra-Column Dead Volume", *AIChE Journal*, pp. 1411-1421, vol. 45, (1999)

Molekylærbiologisk Institut, Københavns Universitet, "Vejledning til Øvelser i Proteinkemi", , pp. 23-25, vol. , (2001)

Mollerup Jørgen, Ernst Hansen, "Kromatografisk teori, metoder og teknikker", IVC-SEP, DTU, Lyngby, (2000), ISBN:

Ohashi Hiroyasu, Takuo Sugawara, Ken-Ichi Kikuchi, Kiroshi Konno, "Correlation of Liquid-Side Mass Transfer Coefficients for Single Particles and Fixed Beds", *Journal of Chemical Engineering of Japan*, pp. 433-438, vol. 14, (1981)

Pedersen, Linda, "Modeling Retention Volumes, Isotherms and Plate Heights for Whey Proteins in Anion-Exchange Chromatography", Ph.D.-thesis IVC-SEP, DTU, /2003)

Perry Robert H. (editor), "Perry's Chemical Engineers' Handbook, Seventh Edition", McGraw-Hill, New York, (1997), ISBN: 0-07-049841-5

Rhee Hyun-Ku, Rutherford Aris, Neal R. Amundson, "First Order Differential Equations, vol. 2", Dover Publications, New York, (2001b), ISBN: 0-486-41994-0

Rhee Hyun-Ku, Rutherford Aris, Neal R. Amundson, "First Order Differential Equations, vol. 1", Dover Publications, New York, (2001a), ISBN: 0-486-41993-2

Rice R. G., Do D. D., "Applied Mathematics and Modeling for Chemical Engineers", John Wiley & Sons, New York, (1995), ISBN: 0-471-11156-2

Righetti Pier Giorgio, Gabriela Tudor, "Isoelectric Points and Molecular Weights of Proteins, a New Table", *Journal of Chromatography*, pp. 115-194, vol. 220, (1981)

Righetti Pier Giorgio, Tiziana Caravaggio, "Isoelectric Points and Molecular Weights of Proteins", *Journal of Chromatography*, pp. 1-28, vol. 127, (1976)

Roche, "Aprotinin data sheet cat. no. 236 624..., Version 6, February 2003", (2003)

Schramm Henning, Stefan Grüner,, "Optimal Operation of Simulated Moving Bed Chromatographic Process by means of Simple Feedback Control", *Journal of*

Chromatography A, pp. 3-13, vol. 1006, (2003)

Schweitzer Philip A. (editor), "Handbook of Separation Techniques for Chemical Engineers", McGraw Hill, , (1979), ISBN: 0-07-055790-X

Sober Herbert A. (editor), "Handbook of Biochemistry, Selected Data for Molecular Biology", Chemical Rubber Company Co., Ohio, (1968)

SPSS Science, "PeakFit, Peak Separation and Analysis Software, Manual", SSPS Inc., Chicago, (1997), ISBN: 1-56827-183-2

Storti Giuseppe, Marco Mazzotti, Massimo Morbidelli, Sergio Carrà, "Robust Design of Binary Countercurrent Adsorption Separation Processes", AIChE Journal, pp. 471-492, vol. 39, (1993)

Søndergaard Carl Christian, "Kalibrering af lineær gradientmixer på BioCAD'en", unpublished, (1999)

van Deemter J. J., F. J. Zuiderweg, A. Klinkenberg, "Longitudinal Diffusion an Resistance to Mass Transfer as Causes of Nonideality in Chromatography", *Chemical Engineering Science*, pp. 271-289, vol. 5, (1956)

Villadsen John, Michael L. Michelsen, "Solution of Differential Equations by Polynomial Approximation", Prentice Hall, Englewood Cliffs, (1978), ISBN: 0-13-822205-3

Wilson E. J., C. J. Geankoplis, "Liquid Mass Transfer at Very Low Reynolds Numbers in Packed Beds", *Industrial and Engineering Chemistry Fundamentals*, pp. 9-14, vol. 5, (1966)

Yamamoto Shuichi, Kazuhiro Nakanishi, Ryuichi Matsuno, "Ion-Exchange Chromatography of Proteins", Marcel Dekker, New York, (1988), ISBN: 0-8247-7903-7

Yoshida Hiroyuki, Motonobu Yoshikawa, Takeshi Kataoka, "Parallel Transport of BSA by Surface and Pore Diffusion in Strongly Basic Chitosan", *AIChE Journal*, pp. 2034-2044, vol. 40, (1994)

Young M. E., P. A. Carroad, R. L. Bell, "Estimation of Diffusion Coefficients of Proteins", *Biotechnology and Bioengineering*, pp. 947-955, vol. , (1980)

Østergaard K, M. L.. Michelsen, "On the Use of the Imperfect Tracer Pulse Method for Determination of Hold-Up and Axial Mixing", *The Canadian Journal of Chemical Engineering*, pp. 107-112, vol. 47, (1969)

Appendix

Table of Appendices

Appendix A: Calculation of SMA-formalism

A.I SMA-formalism for Positive Concentrations

The easiest way to solve the Steric Mass Action-formalism (SMA-formalism) is to determine the free salt, $\bar{q}_0$, first since this is given as one (implicit) equation in one variable.

The free salt on the pore surface can be found from

$$\bar{q}_0 = \frac{y_0}{G(\boldsymbol{y})} \tag{A-1}$$

Where the denominator is given as

$$G(\boldsymbol{y}) = y_0 + \sum_{j=1}^{NP} (\sigma_j + \nu_j) K_{eq,j} \left(\frac{\bar{q}_0}{y_0} \right)^{\nu_j - 1} y_j = y_0 + \sum_{j=1}^{NP} L_j y_j \tag{A-2}$$

with

$$L_j = (\sigma_j + \nu_j) K_{eq,j} \left(\frac{\bar{q}_0}{y_0} \right)^{\nu_j - 1} \tag{A-3}$$

From eq. (A-1) the free salt can easily be determined by a Newton iteration defining the function

$$F_1 = -y_0 + \bar{q}_0 G(\boldsymbol{y}) = 0 \tag{A-4}$$

and

$$F_2 = \frac{dF_1}{d\bar{q}_0} = G(\boldsymbol{y}) = y_0 + \sum_{j=1}^{NP} L_j \nu_j y_j \tag{A-5}$$

After the free salt has been found the protein bound to the ion exchanger can be found from

$$q_i = \frac{K_{eq,i} \left(\frac{\bar{q}_0}{y_0} \right)^{\nu_i - 1}}{G(\boldsymbol{y})} = \frac{L_i}{(\sigma_i + \nu_i) G(\boldsymbol{y})} \qquad \text{i=1,NP} \tag{A-6}$$

And the total amount of salt bound to the ion exchanger is then given as

$$q_0 = \bar{q}_0 + \sum_{j=1}^{NP} \sigma_j y_j \tag{A-7}$$

The Jacobian matrix can be efficiently calculated by first defining the auxiliary function

$$S_1 = \sum_{j=1}^{NP} L_j y_j (\nu_j - 1) \tag{A-8}$$

and then calculating the derivative of F_1 with respect to y_0.

$$\frac{dF_1}{dy_0} = \bar{q}_0 - 1 - S_1 \frac{\bar{q}_0}{y_0} \tag{A-9}$$

$$\frac{dF_1}{dy_i} = \bar{q}_0 L_i \qquad \text{i=1,NP} \qquad \text{(A-10)}$$

$$\frac{d\bar{q}_0}{dy_i} = -\frac{\frac{\partial F_1}{\partial y_i}}{\frac{\partial F_1}{\partial \bar{q}_0}} \qquad \text{i=0,NP} \qquad \text{(A-11)}$$

The derivatives of the denominator is given as

$$\frac{dG(\boldsymbol{y})}{dy_0} = 1 + S_1\left(\frac{1}{\bar{q}_0}\frac{d\bar{q}_0}{dy_0} - \frac{1}{y_0}\right) \qquad \text{(A-12)}$$

$$\frac{dG(\boldsymbol{y})}{dy_i} = S_1\frac{1}{\bar{q}_0}\frac{d\bar{q}_0}{dy_i} + L_i \qquad \text{i=1,NP} \qquad \text{(A-13)}$$

Having calculated the derivatives of the denominator, the derivatives of protein concentrations are given as

$$\frac{dq_i}{dy_0} = L_i y_i \frac{(\nu_i - 1)\left(\frac{1}{\bar{q}_0}\frac{d\bar{q}_0}{dy_0} - \frac{1}{y_0}\right)G(\boldsymbol{y}) - \frac{dG(\boldsymbol{y})}{dy_0}}{(\sigma_i + \nu_i)G(\boldsymbol{y})^2} \qquad \text{i=1,NP} \qquad \text{(A-14)}$$

$$\frac{dq_i}{dy_j} = L_i y_i \frac{(\nu_i - 1)\frac{1}{\bar{q}_0}\frac{d\bar{q}_0}{dy_j}G(\boldsymbol{y}) - \frac{dG(\boldsymbol{y})}{dy_j}}{(\sigma_i + \nu_i)G(\boldsymbol{y})^2} \qquad \text{i=1,NP; j=1,NP; i}\neq\text{j} \qquad \text{(A-15)}$$

$$\frac{dq_i}{dy_i} = L_i \frac{1 + \left((\nu_i - 1)\frac{1}{\bar{q}_0}\frac{d\bar{q}_0}{dy_i}G(\boldsymbol{y}) - \frac{dG(\boldsymbol{y})}{dy_i}\right)y_i}{(\sigma_i + \nu_i)G(\boldsymbol{y})^2} \qquad \text{i=1,NP} \qquad \text{(A-16)}$$

and the derivatives of q_0 is

$$\frac{dq_0}{dy_j} = \frac{d\bar{q}_0}{dy_j} + \sum_{i=1}^{NP}\sigma_i\frac{dq_i}{dy_j} \qquad \text{j=0, NP} \qquad \text{(A-17)}$$

In order to have an efficient calculation and avoid numerous calculations of the same value the following variables are stored in a user vector. These values are stored in the function evaluation and used in the jacobi evaluation. It must therefore be ensured that the function evaluation has been called before the jacobi evaluation.

Variable	*Position*	*Calculated in*
ν	1:NP	User specified
σ	NP+1:2·NP	User specified
K_{eq}	2·NP+1:3· NP	User specified
L	3·NP+1:4·NP	F_1
$\bar{q}_0$	4·NP+1	F_1
$G(\underline{y})$	4·NP+2	F_1
F_2	4·NP+3	F_2

Table A.1 Parameters stored in the user vector for the ordinary SMA-formalism.

A.II Handling Negative Concentrations

For orthogonal collocation negative concentrations can occur. It is therefore crucial to have an equilibrium expression which can handle negative concentrations in a proper manner.

In the SMA-formalism the ratio between the free salt, $\bar{q}_0$, and the salt concentration in the solution, y_0, is raised to a normally non-integer power. If the ratio $\frac{\bar{q}_0}{y_0}$ becomes negative, any non-integer charge, ν_i, will lead to a complex value. However, salt is a small molecule and the diffusion of this is much faster than for the proteins. Assuming plug flow for the salt is then considered to be a reasonable assumption and this will guarantee non-negative values of y_0.

Furthermore it must be guaranteed that the free salt concentration is non-negative. In dimensionless units $0<\bar{q}_0\leq 1$ for positive protein concentrations. Negative protein concentrations can lead to values outside this range.

The amount of free salt is normally given by eq. (A-1), however, to be able to handle negative concentrations the denominator is replaced by

$$G(\boldsymbol{y})= y_0+\sum_{y\geq y_c} L_i\, y_i+\sum_{0<y<y_c} P_i(\boldsymbol{y}) \qquad \text{(A-18)}$$

In this expression only positive protein concentrations will contribute to the denominator. y_c is the critical protein concentration, below which the protein contribution is replaced by a polynomial approximation.

The critical protein contribution is defined as

$$y_{c,i}=\frac{\beta\, y_0}{(\sigma+\nu)K_{eq}\left(\frac{\bar{q}_0}{y_0}\right)^{\nu-1}}=\frac{\beta\, y_0}{L_i} \tag{A-19}$$

β is a small value e.g. 10^{-6}.

The polynomial approximation must ensure that the denominator is continues and differentiable in the two endpoints y=0 and y=y_c. And the requirements to the polynomial are

$$P_i(y_i=0)=0 \tag{A-20}$$

$$\left(\frac{\partial P_i}{\partial y_i}\right)_{y_i=0}=0 \tag{A-21}$$

$$P_i(y_i=y_{c,i})=(\sigma_i+\nu_i)K_{eq,i}\left(\frac{\bar{q}_0}{y_0}\right)^{\nu_i-1} y_{c,i}=L_i\, y_{c,i} \tag{A-22}$$

$$\left(\frac{\partial P_i}{\partial y_i}\right)_{y_i=y_{c,i}}=L_i+\beta\frac{y_0}{\bar{q}_0}(\nu_i-1)\frac{\partial \bar{q}_0}{\partial y_i} \tag{A-23}$$

$$\left(\frac{\partial P_i}{\partial y_0}\right)_{y_i=y_{c,i}}=\left(L_i(\nu_i-1)\frac{1}{\bar{q}_0}\frac{\partial \bar{q}_0}{\partial y_0}+L_i(1-\nu_i)\frac{1}{y_0}\right)y_{c,i}=$$

$$L_i(\nu_i-1)\left(\frac{1}{\bar{q}_0}\frac{\partial \bar{q}_0}{\partial y_0}-\frac{1}{y_0}\right)y_{c,i} \tag{A-24}$$

$$\left(\frac{\partial P_i}{\partial y_j}\right)_{y_i=y_{c,i}}=\beta\frac{y_0}{\bar{q}_0}(\nu_i-1)\frac{\partial \bar{q}_0}{\partial y_j} \tag{A-25}$$

In general the last term involving derivatives of $\bar{q}_0$ origins from (smaller) secondary effects from the change in “free” salt when molecules are exchanged, and these terms are neglected (for a time). The four major requirements to the polynomial,with respect to y_i, is then given by the equations (A-20-A-23) neglecting the last term in eq. (A-23) the polynomial

$$P_i(y)=\Big(\big(A\, y_i+B\big)\, y_i+C\Big)\, y_i+D \tag{A-26}$$

is used

The two requirements in y=0 requires that C=D=0, and the two requirements in y=$y_{c,i}$ gives

$$P_i(y_i=y_{c,i})=(A\, y_{c,i}+B)\, y_{c,i}^2=L_i\, y_{c,i} \tag{A-27}$$

$$\left(\frac{\partial P_i(y)}{\partial y_i}\right)_{y_i=y_{c,i}}=(3A\, y_{c,i}+2B)\, y_{c,i}=L_i \tag{A-28}$$

From which it is seen that $3A\, y_{c,i}+2B=A\, y_{c,i}+B \Leftrightarrow A\, y_{c,i}+B=-A\, y_{c,i}$ where insertion into (A-27) and isolation of A gives

$$A=-\frac{\beta\, y_0}{y_{ic}^3}=-\frac{L_i^3}{\beta^2\, y_0^2} \tag{A-29}$$

$$B=-2\,A\,y_{c,i}=\frac{2\beta\, y_0}{y_{c,i}^2}=\frac{2\,L_i^2}{\beta\, y_0} \tag{A-30}$$

The polynomial then becomes

$$P_i(y)=\beta\, y_0\left[2-\left(\frac{y_i}{y_{c,i}}\right)\right]\left(\frac{y_i}{y_{c,i}}\right)^2 \tag{A-31}$$

It should be noted that $y_{c,i}$ and L_i are functions of y.

The approximation given by eq. (A-31) and the corresponding term from the SMA-law is given in figure 2.2. It is seen from the figure that the biggest error between the true value and the approximated value is at low $\frac{y_i}{y_{c,i}}$.

The derivative of L_i are

$$\frac{\partial L_i}{\partial y_j}=L_i(\nu_i-1)\frac{1}{\bar{q}_0}\frac{\partial \bar{q}_0}{\partial y_j} \tag{A-32}$$

$$\frac{\partial L_i}{\partial y_0}=L_i(1-\nu_i)\frac{1}{y_0}+L_i(\nu_i-1)\frac{1}{\bar{q}_0}\frac{\partial \bar{q}_0}{\partial y_0}=L_i(\nu_i-1)\left(\frac{1}{\bar{q}_0}\frac{\partial \bar{q}_0}{\partial y_0}-\frac{1}{y_0}\right) \tag{A-33}$$

giving the derivatives of A and B

$$\frac{\partial A_i}{\partial y_j}=-\frac{1}{\beta^2\, y_0^2}3L^3\frac{\partial L_i}{\partial y_j}=3\,A_i(\nu_i-1)\frac{1}{\bar{q}_0}\frac{\partial \bar{q}_0}{\partial y_j}=-3\frac{\beta\, y_0}{y_{c,i}^3}(\nu_i-1)\frac{1}{\bar{q}_0}\frac{\partial \bar{q}_0}{\partial y_j} \tag{A-34}$$

$$\frac{\partial B_i}{\partial y_j}=2\,B_i(\nu_i-1)\frac{1}{\bar{q}_0}\frac{\partial \bar{q}_0}{\partial y_j}=4\frac{\beta\, y_0}{y_{c,i}^2}(\nu_i-1)\frac{1}{\bar{q}_0}\frac{\partial \bar{q}_0}{\partial y_j} \tag{A-35}$$

$$\frac{\partial A_i}{\partial y_0}=-\frac{3L_i^2\beta^2\, y_0^2\frac{\partial L_i}{\partial y_0}-2L_i^3\beta^2\, y_0}{\beta^4\, y_0^4}=3\,A_i(\nu_i-1)\left(\frac{1}{\bar{q}_0}\frac{\partial \bar{q}_0}{\partial y_0}-\frac{1}{y_0}\right)-\frac{2\,A_i}{y_0} \tag{A-36}$$

$$\frac{\partial B_i}{\partial y_0}=2\,B_i(\nu_i-1)\left(\frac{1}{\bar{q}_0}\frac{\partial \bar{q}_0}{\partial y_0}-\frac{1}{y_0}\right)-\frac{B_i}{y_0} \tag{A-37}$$

Leading to

$$\frac{\partial P_i}{\partial y_0}=\beta\, y_0(\nu_i-1)\left(\frac{1}{\bar{q}_0}\frac{\partial \bar{q}_0}{\partial y_0}-\frac{1}{y_0}\right)\left(4-3\frac{y_i}{y_{c,i}}\right)\left(\frac{y_i}{y_{c,i}}\right)^2+\beta\left(2\frac{y_i}{y_{c,i}}-2\right)\left(\frac{y_i}{y_{c,i}}\right)^2 \tag{A-38}$$

$$\frac{\partial P_i}{\partial y_i}=(3A_i y_i+2B_i)y_i+\beta\left(4-3\frac{y_i}{y_{c,i}}\right)\left(\frac{y_i}{y_{c,i}}\right)^2(\nu_i-1)\frac{y_0}{\bar{q}_0}\frac{\partial \bar{q}_0}{\partial y_i} \tag{A-39}$$

and

$$\frac{\partial P_i}{\partial y_j}=\beta\left(4-3\frac{y_i}{y_{c,i}}\right)\left(\frac{y_i}{y_{c,i}}\right)^2(\nu_i-1)\frac{y_0}{\bar{q}_0}\frac{\partial \bar{q}_0}{\partial y_j} \tag{A-40}$$

These equations sees to fulfil the requirement of equations (A-20-A-40) exactly, though an approximation was made when deriving the solution. The approximation will then ensure continuity and continuous partial derivatives.

In order to avoid unnecessary calculations in the evaluation of $\bar{q}_0$ (evaluation of y_c, A and B), the iterations evaluating the "free" salt uses the simpler denominator

$$G=y_0+\sum_{y>0}(\sigma_i+\nu_i)K_{eq,i}\left(\frac{\bar{q}_0}{y_0}\right)^{\nu_i-1}y_i \tag{A-41}$$

$\bar{q}_0$ calculated from this approximation has an error of $\approx\beta$. The correct $\bar{q}_0$ calculated using the denominator in (A-18) then only requires one or two iterations.

When $\bar{q}_0$ has been calculated the bound protein concentrations are calculated from

$$q_i=\frac{K_{eq,i}\left(\frac{\bar{q}_0}{y_0}\right)^{\nu_i-1}y_i}{G(\bar{y})} \qquad \text{i=1,NP} \tag{A-42}$$

As can be seen the from above the bound protein concentrations can be negative but the concentrations will always be real numbers.

A larger number of variables to be stored in the user variable is required for an optimal calculation of this version of the SMA-law, these are given in table A.2 below. As for the ordinary SMA implementation the function evaluation must be called before the jacobi evaluation.

Variable	*Position*	*Calculated in*
ν	1:NP	User
σ	NP+1:2·NP	User
K_{eq}	2·NP+1:3·NP	User
L	3·NP+1:4·NP	F1
y_c	4·NP+1:5·NP	F1
A	5·NP+1:6·NP	F1
B	6·NP+1:7·NP	F1
$\bar{q}_0$	7·NP+1	F1
G	7·NP+2	F1
$\partial G/\partial \bar{q}_0$	7·NP+3	F2
β	7·NP+4	User

Table A.2 Parameters stored in the user vector for the SMA-formalism handling negative concentrations.

A.III Alternative Variables

An attractive implementation of the SMA-formalism is possible, where all the equations are explicitly given. This can be obtained if the chosen variables are the salt concentration in the liquid phase, y_0, and the bound amount of proteins, q_p. The calculated concentrations are then the bound salt amount, q_0, and the liquid protein concentrations y_p.

The bound salt concentration is simply given as

$$q_0 = 1 - \sum_{i=1}^{NP} \nu_i q_{p,i} \tag{A-43}$$

To avoid negative concentrations $\hat{q}_0$ is introduced

$$\hat{q}_0 = q_0 - \sum_{i=1}^{NP} \sigma_i q_{p,i} \tag{A-44}$$

From this the free salt is given as

$$\bar{q}_0 = \hat{q}_0 \quad \text{for} \quad \hat{q}_0 \geq \beta$$

and

$$\bar{q}_0 = \beta \exp\left(\frac{\hat{q}_0}{\beta} - 1\right) \quad \text{for} \quad \hat{q}_0 < \beta \tag{A-45}$$

This ensures that the function is continues and has continues derivatives in the point $\hat{q}_0 = \bar{q}_0$

From this the free salt concentrations are given as

$$c_{p,i} = \frac{q_{p,i}}{K_{eq,i}} \left(\frac{y_0}{\bar{q}_0} \right)^{\nu_i} = L_i q_{p,i} \qquad \text{i=1,NP} \qquad \text{(A-46)}$$

Where the parameter L here is given as

$$L_i = \frac{1}{K_{eq,i}} \left(\frac{y_0}{\bar{q}_0} \right)^{\nu_i} \qquad \text{i=1,NP} \qquad \text{(A-47)}$$

The derivatives are

$$\frac{\partial q_0}{\partial y_0} = 0 \qquad \text{(A-48)}$$

$$\frac{\partial q_0}{\partial q_{p,i}} = -\nu_i \qquad \text{i=1,NP} \qquad \text{(A-49)}$$

$$\frac{\partial \bar{q}_0}{\partial y_0} = 0 \qquad \text{(A-50)}$$

$$\frac{\partial \bar{q}_0}{\partial q_{p,i}} = -(\nu_i + \sigma) \qquad \bar{q}_0 \geq \beta \text{ , i=1,NP} \qquad \text{(A-51)}$$

$$\frac{\partial \bar{q}_0}{\partial q_{p,i}} = -(\nu_i + \sigma) \exp\left(\frac{\hat{q}_0}{\beta} - 1 \right) \qquad \bar{q}_0 < \beta \text{ , i=1,NP} \qquad \text{(A-52)}$$

$$\frac{\partial y_{p,i}}{\partial y_0} = \frac{q_{p,i} \nu_i}{y_0} L_i \qquad \text{i=1,NP} \qquad \text{(A-53)}$$

$$\frac{\partial y_{p,i}}{\partial q_{p,i}} = L_i - \frac{\nu_i q_{p,i}}{\bar{q}_0} L_i \frac{\partial \bar{q}_0}{\partial q_{p,i}} \qquad \text{i=1,NP} \qquad \text{(A-54)}$$

$$\frac{\partial y_{p,i}}{\partial q_{p,j}} = -\frac{\nu_i q_{p,i}}{\bar{q}_0} L_i \frac{\partial \bar{q}_0}{\partial q_{p,j}} \qquad \text{i=1,NP, j=1,NP, i≠j} \qquad \text{(A-55)}$$

The parameters stored in ur are the same as the first 4NP+1 parameters given in table A.1 above, and in 4NP+2 is stored the user defined value β.

A requirement for this method, as for the other methods above, is that $\bar{q}_0 > 0$. Also if $\bar{q}_0$ is approaching 0 this must result in a very steep increase in y_p.

In this approach the isotherm is modified at high concentrations, whereas the approach described in appendix A.II “Handling Negative Concentrations“ modified the isotherm at low concentrations.

Appendix B: Laplace Transform

An easy way to handled the system is to solve the mobile phase first and find an expression for the flux term between the two phases from the particle phase mass balance equation and the flux equation and inserting this into the mobile phase mass balance equation. This also facilitates the evaluation of the other models for the two phases.

B.I Mobile Phase with Axial Dispersion

The mobile phase balance equation including axial dispersion is given in eq. (3-5). The Laplace transform of this equation with initial concentration of 0 gives

$$s\cdot Y-0=\frac{1}{Pe_L}\frac{\partial^2 Y}{\partial x^2}-\frac{\partial Y}{\partial x}-St_f\phi(Y-Y_s) \qquad \Leftrightarrow$$

$$-\frac{1}{Pe_L}\frac{\partial^2 Y}{\partial x^2}+\frac{\partial Y}{\partial x}+\left(s+St_f\phi\left(1-\frac{Y_s}{Y}\right)\right)\cdot Y=0$$

$$-\frac{1}{Pe_L}\frac{\partial^2 Y}{\partial x^2}+\frac{\partial Y}{\partial x}+\left(s+F(s)\right)\cdot Y=0 \tag{B-1}$$

where the flux term between the two phases is written as F(s).

The roots of this ordinary differential equation will be real and distinct when s+F(s)>0.

$$x=\frac{Pe_L}{2}\left(1\pm\sqrt{1+\frac{4}{Pe_L}\left(s+F(s)\right)}\right) \tag{B-2}$$

And the solution to the differential eq. (B-1) is

$$Y(s,x)=C_1\cdot\exp\left(\frac{Pe_L}{2}\left(1-\sqrt{1+\frac{4}{Pe_L}\left(s+F(s)\right)}\right)x\right)+$$

$$C_2\cdot\exp\left(\frac{Pe_L}{2}\left(1+\sqrt{1+\frac{4}{Pe_L}\left(s+F(s)\right)}\right)x\right) \tag{B-3}$$

Using the open boundary condition (3-11) gives $C_2=0$.

The boundary condition $Y(x=0,s)=Y_{in}$, eq. (3-12), gives $C_1=Y_{in}$, and the outlet concentration becomes

$$Y_{out}(x=1,s)=Y_{in}\cdot\exp\left(\frac{Pe_L}{2}\left(1-\sqrt{1+\frac{4}{Pe_L}\left(s+F(s)\right)}\right)\right) \tag{B-4}$$

Alternatively the inlet condition (3-8) can be used, but the derivation will be more troublesome and the impact on the result will be minor as previously mentioned.

The moment generating function will then be

$$h(s)=\ln\left(\frac{Y_{out}}{Y_{in}}\right)=\frac{Pe_L}{2}\left(1-\sqrt{1+\frac{4}{Pe_L}\left(s+F(s)\right)}\right) \tag{B-5}$$

With the derivatives

$$h'(s)=-\left(1+\frac{4}{Pe_L}\left(s+F(s)\right)\right)^{-1/2}\left(1+F'(s)\right) \tag{B-6}$$

$$h''(s)=\frac{2}{Pe_L}\left(1+\frac{4}{Pe_L}\left(s+F(s)\right)\right)^{-3/2}\left(1+F'(s)\right)^2- F''(s)\left(1+\frac{4}{Pe_L}\left(s+F(s)\right)\right)^{-1/2} \tag{B-7}$$

$$h'''(s)=-\frac{12}{Pe_L^2}\left(1+\frac{4}{Pe_L}\left(s+F(s)\right)\right)^{-5/2}(1+F'(s))^3+ \frac{6}{Pe_L}\left(1+\frac{4}{Pe_L}\left(sF(s)\right)\right)^{-3/2}\left(1+F'(s)\right)F''(s)- \left(1+\frac{4}{Pe_L}\left(s+F(s)\right)\right)^{-1/2}F'''(s) \tag{B-8}$$

B.II Mobile Phase Without Axial Dispersion

The mobile phase mass balance without axial dispersion is given by equation (3-13) with the Laplace transform

$$Y\cdot s-0+\frac{\partial Y}{\partial x}+St_f\phi(Y-Y_s)=0 \tag{B-9}$$

Rewriting this and using F(s) as given above gives

$$\frac{\partial Y}{\partial x}+\left(s+St_f\phi\left(s+\frac{Y_s}{Y}\right)\right)Y=\frac{\partial Y}{\partial x}+\left(s+F(s)\right)Y=0 \tag{B-10}$$

With the solution

$$Y(s,x)=C_1\exp\left(-\left(s+F(s)\right)x\right) \tag{B-11}$$

With the inlet condition $C_1=Y_{in}$ and the outlet concentration

$$Y_{out}(s,x=1)=Y_{in}(s)\exp\left(-\left(s+F(s)\right)\right) \tag{B-12}$$

This ought to be the same as the equation above for $Pe_L\rightarrow\infty$. The Taylor series for a square root is

$$\sqrt{1+x}=1+\frac{1}{2}x-\frac{1}{2\cdot4}x^2+\cdots \qquad -1\le x\le 1 \tag{B-13}$$

Inserting this into equation (B-5) and letting $Pe_L \to \infty$ equation (B-12) is found. An easier way to find the moments for the model without axial dispersion is then to take the results from the model including axial dispersion and letting $Pe_L \to \infty$.

B.III Particle Phase with Linear Driving Force

The surface concentration when applying the linear driving force can be isolated from the flux equation as given is eq. (3-48). Together with the Laplace transform of eq. (3-50) gives

$$s \cdot Y_p - 0 = \frac{1}{1+A} \cdot \gamma \cdot Y - \frac{1}{1+A} \cdot \gamma \cdot Y_p \tag{B-14}$$

isolating Y_p gives

$$Y_p = \frac{\gamma}{\gamma + (1+A)s} \cdot Y \tag{B-15}$$

Inserting this into the the expression for F(s) gives

$$F(s) = St_f \cdot \phi \cdot \left[1 - \frac{Y_s}{Y} \right] = \psi \gamma - \psi \frac{\gamma^2}{\gamma + (1+A)s} \tag{B-16}$$

With the derivatives and boundary conditions for $s \to 0$

$$\lim_{s \to 0} F(s) = 0 \tag{B-17}$$

$$F'(s) = \psi \frac{\gamma^2 (1+A)}{(\gamma + (1+A)s)^2} \qquad \lim_{s \to 0} F'(s) = \psi (1+A) \tag{B-18}$$

$$F''(s) = -\psi \frac{2\gamma^2 (1+A)^2}{(\gamma + (1+A)s)^3} \qquad \lim_{s \to 0} F''(s) = -\frac{2\psi}{\gamma} (1+A)^2 \tag{B-19}$$

$$F'''(s) = \psi \frac{6\gamma^2 (1+A)^3}{(\gamma + (1+A)s)^4} \qquad \lim_{s \to 0} F'''(s) = \frac{6\psi}{\gamma^2} (1+A)^3 \tag{B-20}$$

It is noted that F(s)>0 for s>0 as assumed for equation (B-2).

B.IV Particle Phase with Diffusion Model

The diffusion model for the particle phase is given in eq. (3-14) with the boundary conditions (3-20) and (3-22) for the centre and surface of the particle.

Instead of the previous suggested dimensionless variables the used variable transform is

$$C_p = \frac{y_p}{r} \tag{B-21}$$

with the derivative in r

$$\frac{\partial C_p}{\partial r} = \frac{1}{r} \frac{\partial y_p}{\partial r} - \frac{1}{r^2} \frac{\partial y_p}{\partial r} \tag{B-22}$$

After this variable transform the normal variable transforms in time eq. (3-3) and in radial position

$$u=\frac{r}{R_p} \tag{B-23}$$

can be inserted into the result of adding the equations (3-15) and (3-16). The equation to be solved is

$$(1+A)\frac{v_i}{L}\frac{\partial y_p}{\partial \tau}=(D_p+A\,D_q)\frac{1}{R_p^2}\frac{\partial^2 y_p}{\partial u^2} \tag{B-24}$$

with the boundary conditions at the centre

$$\lim_{u\to 0} y_p=0 \tag{B-25}$$

and at the surface

$$k_f(y-y_p)_{u=1}=K_D\epsilon_p(D_p+A\,D_q)\frac{1}{R_p}\left(\frac{\partial y_p}{\partial u}-y_p\right)_{u=1} \tag{B-26}$$

The solution to the Laplace transform of (B-24) is

$$Y_p=C_1\cosh\left(p(s)\,u\right)+C_2\sinh\left(p(s)\,u\right) \tag{B-27}$$

where $$p(s)=\sqrt{\frac{(1+A)\,v_i\,R_p^2}{(D_p+A\,D_q)L}\,s} \tag{B-28}$$

C_1 will be 0 due to the first boundary condition and the second one gives

$$C_2=\frac{Y(s,u)}{K_D\epsilon_p\left(\frac{1}{Bi_p}+\frac{A}{Bi_q}\right)p(s)\cosh\left(p(s)\right)+\left(1-K_D\epsilon_p\left(\frac{1}{Bi_p}+\frac{A}{Bi_q}\right)\right)\sinh\left(p(s)\right)} \tag{B-29}$$

From this Y_s/Y can be isolated and inserted into equation (B-16) with the boundary of the first and second derivative

$$\lim_{s\to 0} F(s)=0 \tag{B-30}$$

$$\lim_{s\to 0} F'(s)=\psi(1+A) \tag{B-31}$$

$$\lim_{s\to 0} F''(s)=-2\frac{\psi}{St_f}(1+A)^2\left(K_D\epsilon_p+\frac{Bi_p\,Bi_q}{Bi_q+A\,Bi_p}\right) \tag{B-32}$$

Again the first derivative is identical to the model for ideal chromatography.

B.V Moment Analysis

The first moment and the second and third central moments are required in the moment analysis here. As described by Østergaard *et al.* (1969) the first moment is $M'_1= -h'(s)$.

Inserting the derivatives of F(s) into the derivatives of h(s), eq. (B-6) to (B-8), and finding the boundary condition s→0 gives

The first normal moment M'_1 is given as[10]

$$M'_1 = \tau_r = -\lim_{s\to 0} h'(s) = 1+\psi(1+A) \tag{B-33}$$

Insertion of the value for τ and ψ gives

$$t_r = \frac{L}{v_i}\left(1+\frac{1-\epsilon}{\epsilon}\epsilon_p K_D(1+A)\right) \tag{B-34}$$

which is the same result as found from ideal chromatography.

The second central moment is

$$M_2 = \lim_{s\to 0} h''(s) = \frac{2}{Pe_L}\left(1+\psi(1+A)\right)^2 + 2\frac{\psi}{\gamma}(1+A)^2 \tag{B-35}$$

and the reduced plate height is

$$h = \frac{HETP}{d_p} = \frac{L}{d_p}\cdot\frac{M_2}{M'^2_1} = \frac{\frac{2}{Pe_L}\left(1+\psi(1+A)\right)+2\frac{\psi}{\gamma}(1+A)^2}{(1+\psi(1+A))^2} =$$

$$\frac{2}{Pe_d} + 2\frac{L}{d_p}\frac{\frac{\psi}{\gamma}(1+A)^2}{(1+\psi(1+A))^2} \tag{B-36}$$

Inserting γ in the last term gives

$$2\frac{L}{d_p}\frac{\frac{\psi}{\gamma}(1+A)^2}{(1+\psi(1+A))^2} = 2\left(\frac{1+A}{1+\psi(1+A)}\right)^2\psi\cdot\frac{v_i}{6}\cdot\frac{k_f+\epsilon_p K_D(k_p+Ak_q)}{k_f(k_p+Ak_q)} =$$

$$2\left(\frac{1+A}{1+\psi(1+A)}\right)^2\psi\cdot\frac{v_i}{6}\cdot\frac{k_f+\epsilon_p K_D(k_p+Ak_q)}{k_f(k_p+Ak_q)} =$$

$$2\left(\frac{1+A}{1+\psi(1+A)}\right)^2\psi\cdot\frac{v_i}{6}\cdot\epsilon_p\cdot K_D\cdot\left(\frac{1}{k_f}+\frac{1}{\epsilon_p K_D(k_p+Ak_q)}\right) =$$

$$2\left(\frac{1+A}{\frac{1}{\psi}+1+A}\right)^2\frac{\epsilon v_i}{6(1-\epsilon)}\cdot\left(\frac{1}{k_f}+\frac{1}{\epsilon_p K_D(k_p+Ak_q)}\right) \tag{B-37}$$

10 The first moment is marked with ' since this is not a central moment as the two other moments used here

Inserting this into eq. (B-36) the reduced plate height can be calculated as

$$h=\frac{2}{Pe_d}+2\left(\frac{1+A}{\frac{1}{\psi}+1+A}\right)^2\frac{\epsilon\,\nu_i}{6(1-\epsilon)}\cdot\left(\frac{1}{k_f}+\frac{1}{\epsilon_p K_D(k_p+A\,k_q)}\right) \tag{B-38}$$

This equation is also known as the van Deemter equation.

The third central moment and the skewness is given as

$$M_3=-\lim_{s\to 0}h'''(s)=\frac{12}{Pe_L^2}\left(1+\psi(1+A)\right)^3+\frac{12}{Pe_L}\frac{\psi}{\gamma}\left(1+\psi(1+A)\right)(1+A)^2+6\frac{\psi}{\gamma^2}(1+A)^3 \tag{B-39}$$

$$Skew=\frac{M_3}{M_2^{3/2}}=\frac{\frac{12}{Pe_L^2}\left(1+\psi(1+A)\right)^3+\frac{12}{Pe_L}\frac{\psi}{\gamma}\left(1+\psi(1+A)\right)(1+A)^2+6\frac{\psi}{\gamma^2}(1+A)^3}{\left(\frac{2}{Pe_L}\left(1+\psi(1+A)\right)^2+2\frac{\psi}{\gamma}(1+A)^2\right)^{3/2}} \tag{B-40}$$

It is seen that both the numerator and the denominator is positive leading to a positive skewness. This means that a linear isotherm always will be tailing (never fronting).

In a similar fashion the van Deemter equation can be derived for the model including axial dispersion inside the particle by inserting (B-30)-(B-32) into (B-33), (B-35), and (B-37).

For the model with diffusion inside the particle the van Deemter equation reads

$$h=\frac{2}{Pe_d}+2\left(\frac{1+A}{\frac{1}{\psi}+1+A}\right)^2\frac{\epsilon\,\nu_i}{6(1-\epsilon)}\cdot\left(\frac{1}{k_f}+\frac{1}{5}\cdot\frac{R_p}{\epsilon_p K_D(D_p+A\,D_q)}\right) \tag{B-41}$$

Appendix C: Fast Fourier Transform

For the linear isotherms the resulting chromatogram can be calculated using Fast Fourier transform (FFT).

The injection of the sample can be considered to be periodic in time, with a periodicity of t_{end}. Due to the periodicity of the Fourier transform it will be more convenient to scale the dimensionless time using

$$\tau = \frac{2\pi}{t_{end}} t \tag{C-1}$$

C.I Mobile Phase with Axial Dispersion

The mobile phase mass balance in dimensionless units then reads

$$\frac{L}{v_i}\frac{2\pi}{t_{end}}\frac{\partial y}{\partial \tau} + \frac{\partial y}{\partial x} + \phi St_f (y - y_s) - \frac{1}{Pe_L}\frac{\partial^2 y}{\partial x^2} = 0 \tag{C-2}$$

With the Fourier transform

$$-\frac{1}{Pe_L}\frac{\partial^2 \hat{y}_m}{\partial x^2} + \frac{\partial \hat{y}_m}{\partial x} + \left(\frac{L}{v_i}\frac{2\pi}{t_{end}} im + \phi St_f \left(1 - \frac{\hat{y}_{s,m}}{\hat{y}_m} \right) \right) \hat{y}_m = 0 \tag{C-3}$$

where $\hat{y}_m$ is a short notation of y(m,x) which is the Fourier transform of y(τ,x).

This equation is seen to be almost identical to the similar Laplace transformed equation (B-1).

C.II Mobile Phase without Axial Dispersion

Similarly the mobile phase mass balance without axial dispersion is given as

$$\frac{\partial \hat{y}_m}{\partial x} + \left(\frac{L}{v_i}\frac{2\pi}{t_{end}} im + \phi St_f \left(1 - \frac{\hat{y}_{s,m}}{\hat{y}_m} \right) \right) \hat{y}_m = 0 \tag{C-4}$$

With the solution

$$\hat{y}_m(x) = C_1 \exp\left(-\left(\frac{L}{v_i}\frac{2\pi}{t_{end}} im + F_m \right) x \right) \tag{C-5}$$

where

$$F_m(x) = \phi St_f \left(1 - \frac{\hat{y}_{s,m}}{\hat{y}_m} \right) \tag{C-6}$$

C.III Particle Phase with Linear Driving Force

As for the mobile phase the particle phase mass balance is Fourier transformed

$$(1 + A)\frac{2\pi}{t_{end}}\frac{\partial y_p}{\partial \tau} = a_p (k_p + A k_q) \cdot (y_s - y_p) \tag{C-7}$$

with the Fourier transform (and after multiplying both sides by L/v_i)

$$(1+A)\frac{L}{v_i}\frac{2\pi}{t_{end}} i m\, \hat{y}_{m,p} = (St_p + A\,St_q)\cdot(\hat{y}_{m,s} - \hat{y}_{m,p}) \tag{C-8}$$

Isolation of y_s/y as in the Laplace transform and insertion into equation (C-6) gives

$$F_m = St_f \cdot \phi \cdot \left[1 - \frac{\hat{y}_{m,s}}{\hat{y}_m} \right] = \psi\gamma - \psi \frac{\gamma^2}{\gamma + (1+A)\frac{L}{v_i}\frac{2\pi}{t_{end}} i m} \tag{C-9}$$

which is similar to equation (B-16) in the Laplace domain.

The different functions of $\hat{y}_m$ are orthogonal and the functions can be solved individually.

C.IV Result for Model with Axial Dispersion

Insertion of equation (C-9) into (C-3) and using the same boundary conditions as for the Laplace transform the m'th Fourier transform is similar to (B-4) namely

$$\hat{y}_m(x) = C_m \exp\left(\frac{Pe_L}{2} \left(1 - \sqrt{1 + \frac{4}{Pe_L}\left(\frac{L}{v_i}\frac{2\pi}{t_{end}} i m + \psi\gamma - \psi \frac{\gamma^2}{\gamma + (1+A)\frac{L}{v_i}\frac{2\pi}{t_{end}} i m} \right)} \right) x \right) \tag{C-10}$$

The constants C_m can be found from the inlet composition, x=0, and the outlet composition can be calculated at x=1.

Result for Model Without Axial Dispersion

Insertion of (C-9) into the mobile phase equation without axial dispersion (C-5) gives

$$\hat{y}_m(x) = C_m \exp\left(-\left(\frac{L}{v_i}\frac{2\pi}{t_{end}} i m + \psi\gamma - \psi \frac{\gamma^2}{\gamma + (1+A)\frac{L}{v_i}\frac{2\pi}{t_{end}} i m} \right) x \right) \tag{C-11}$$

As above the constants are found from the inlet composition and the outlet composition can be calculated from this.

C.V Particle Phase with Diffusion Model

Similar to the linear driving force model the FFT of the diffusion model is similar to the Laplace transform of the model. With this model

$$F_m = St_f \phi \left[1 - \frac{\sinh(p_m)}{K_D \epsilon_p \left(\frac{1}{Bi_p} + \frac{A}{Bi_q} \right) p_m \cosh(p_m) + \left(1 - K_D \epsilon_p \left(\frac{1}{Bi_p} + \frac{A}{Bi_q} \right) \right) \sinh(p_m)} \right] \tag{C-12}$$

where $p_m = \sqrt{\frac{(1+A)R_p^2}{(D_p + A D_q)} \frac{2\pi}{t_{end}} i m}$ (C-13)

This can be inserted into the Fourier transform of the two mobile phase models.

C.VI Implementation

The fast Fourier transform is calculated using the "The Intel Math Kernel Library"-routine (MKL) optimized for Intels processors (Intel, 2001). The forward transform is calculated as

$$\hat{y}_m = \sum_{k=-2^{NP-1}}^{2^{NP-1}-1} y_k \exp\left(-\frac{2\pi i}{2^{NP}} m k\right) \qquad -2^{NP-1} \le m \le 2^{NP-1}-1 \qquad \text{(C-14)}$$

The inverse FFT is calculated as

$$y_m = \frac{1}{2^{NP-1}} \sum_{k=0}^{2^{NP-1}-1} \hat{y}_k \exp\left(\frac{2\pi i}{2^{NP}} m k\right) \qquad -2^{NP-1} \le m \le 2^{NP-1}-1 \qquad \text{(C-15)}$$

The MKL routines use normal ordering, meaning that when the number of sampling points are 2^{NP}, the first 2^{NP-1} elements in the vector y corresponds to $0 \le m \le 2^{NP-1}-1$ and the elements from $2^{NP-1}+1$ to 2^{NP} corresponds to $-2^{NP-1} \le m \le -1$ when solving the differential equations. Usually the loaded amount of protein (20-100µl) is very small compared to the total volume in a run (10-100 ml) and NP≤10 could easily lead to no sampling points at the initial peak. To avoid this NP must be set sufficiently large. The maximum values of NP is 15 corresponding to 32,768 sampling points which requires a lot of memory.

Appendix D: Orthogonal Collocation

D.I Collocation of the Mobile Phase with Axial Dispersion

For the model including axial dispersion the outlet concentration from element ne is used as inlet concentration to element ne+1. This corresponds to using equation (3-8) as inlet condition and the open boundary as outlet condition (3-11).

The mobile phase is solved with the node points $x(1-x)P_N(x)$, where $P_N(x)$ is the Legendre polynomial of degree N. The number of inner collocation points is N and the total number of node points is NT=N+2.

The concentration for the first node point, $y_1=y(x=0)$, is given by equation (3-8)

$$y_{in} = y_{x=0} - \frac{1}{Pe_L}\left(\frac{\partial y}{\partial x}\right)_{x=0} \tag{D-1}$$

Introducing the Lagrange interpolation $y_N(x)=\sum_{k=1}^{N} y_k l_k(x)$ (D-1) is rewritten as

$$y_{in}(\tau) - y_1 = -\frac{1}{Pe_L}\sum_{k=1}^{NT} A_{1,k}\, y_k = -\frac{A_{1,1}}{Pe_L} y_1 - \frac{1}{Pe_L}\sum_{k=2}^{NT} A_{1,k}\, y_k \tag{D-2}$$

Where $A_{1,k}$ is the first derivative of $l_k(x=0)$. Isolating y_1 gives

$$y_1 = \frac{Pe_L}{Pe_L - A_{1,1}}\, y_{in}(\tau) + \sum_{k=2}^{NT} \frac{A_{1,k}}{Pe_L - A_{1,1}}\, y_k \tag{D-3}$$

Collocation of the mobile phase (2-12) gives

$$\left(\frac{\partial y}{\partial \tau}\right)_{x=x_i} = \sum_{k=1}^{NT}\left(\frac{B_{i,k}}{Pe_L} - A_{i,k}\right) y_k - St_f\, \phi\,(y_i - y_{s,i}) \qquad \text{i=2,...,NT} \tag{D-4}$$

$A_{i,k}$ and $B_{i,k}$ are the weights of the first and second derivatives respectively. The expression of y_1, eq. (D-3), is inserted and gives

$$\left(\frac{\partial y}{\partial \tau}\right)_{x=x_i} = -St_f\,\phi\left(y_i - y_{s,i}\right) + \frac{B_{i,1} - A_{i,1} Pe_L}{Pe_L - A_{1,1}}\, y_{in}(\tau) + \sum_{k=2}^{NT}\left(\frac{(B_{i,1} - A_{i,1} Pe_L) A_{1,k}}{(Pe_L - A_{1,1}) Pe_L} + \frac{B_{i,k}}{Pe_L} - A_{i,k}\right) y_k \qquad \text{i=2,...,NT} \tag{D-5}$$

After convergence the outlet concentration from the element can be calculated as

$$y_{out} = y_{NT} - \frac{1}{Pe_L}\left(\frac{\partial y}{\partial x}\right)_{NT} \tag{D-6}$$

Where the subscript NT denotes the concentration in the last node point. Collocation of this equation gives

$$y_{out} = y_{NT} - \sum_{k=1}^{NT} \frac{A_{NT,k}}{Pe_L}\, y_k \tag{D-7}$$

Insertion of y_1, eq.(D-3), gives

$$y_{out} = -\frac{A_{NT,1}}{Pe_L - A_{1,1}} y_{in}(\tau) - \sum_{k=2}^{N+1} \left(\frac{A_{NT,1} A_{1,k}}{(Pe_L - A_{1,1}) Pe_L} + \frac{A_{NT,k}}{Pe_L} \right) y_k +$$

$$\left(1 - \frac{A_{NT,1} A_{1,NT}}{(Pe_L - A_{1,1}) Pe_L} - \frac{A_{NT,NT}}{Pe_L} \right) y_{NT} \quad \text{(D-8)}$$

D.II Collocation of the Mobile Phase without Axial Dispersion

For the model without axial dispersion the equations to be solved correspond to the model above when $Pe_L \rightarrow \infty$. This gives

$$y_{x=x_1} = y_{in}(\tau) \quad \text{(D-9)}$$

$$\left(\frac{\partial y}{\partial \tau} \right)_{x=x_i} = -St_f \phi (y_i - y_{s,i}) - A_{i,1} y_{in}(\tau) - \sum_{k=2}^{NT} A_{i,k} y_k \qquad \text{i=2,...,NT} \quad \text{(D-10)}$$

And the outlet concentration from the element is simply given as

$$y_{out} = y_{NT} \quad \text{(D-11)}$$

D.III Collocation of the Diffusion Model

The equations for the particle is collocated using the collocation points from $(1-u)P_N^{(0,½)}$, where $P_N^{(0,½)}$ is the Jacobi polynomial of degree N. NR is the number of inner collocation points in the particle and NTR=NR+1 is the total number of collocation points in the particle. It is noted that the surface concentration, y_s, above corresponds to $y_{p,NTR}$. The pore surface mass balance (3-19) gives

$$\left(\frac{\partial q_p}{\partial \tau} \right)_{u=u_i} = \frac{L K_{ads}}{v_i} (q_{SMA} - q_p) + \frac{St_f}{Bi_q} \sum_{m=1}^{NTR} \left(2 A_{l,m} + \frac{4}{3} u_l B_{l,m} \right) q_{p,m} \quad \text{(D-12)}$$

the pore phase mass balance (3-18) gives

$$\left(\frac{\partial y_p}{\partial \tau} \right)_{u=u_i} = -\frac{L K_{ads}}{v_i} (q_{SMA} - q_p) + \frac{St_f}{Bi_p} \sum_{m=1}^{NTR} \left(2 A_{l,m} + \frac{4}{3} u_l B_{l,m} \right) y_{p,m} \quad \text{(D-13)}$$

The mass balance for the particle surface (3-30) gives

$$\left(\frac{\partial y_s}{\partial \tau} \right)_{u=1} = \frac{St_f}{\Theta} \phi (y - y_s) - \frac{2 \psi St_f}{\Theta Bi_p} \sum_{m=1}^{NTR} A_{NT_R,m} y_{p,m} + \frac{2 \psi St_f}{\Theta Bi_q} \sum_{m=1}^{NTR} A_{NT_R,m} q_{p,m} \quad \text{(D-14)}$$

D.IV Solving the System

The particle model for the linear driving force approximation (3-35), (3-36) and its flux equation (3-37) does not contain derivatives other variables than τ and these are not collocated.

D.IV.a Mobile Phase

The two mobile phase models can be written in a general form

$$\left(\frac{\partial y}{\partial \tau}\right)_{x=x_i} = -St_f \phi (y - y_s) + D_{i,1} y_{in}(\tau) + \sum_{k=2}^{NT} D_{i,k} y_k \qquad \text{i=2,...,NT} \qquad \text{(D-15)}$$

Where the values of the matrix **D** for the model including axial dispersion can be found by comparing with equation (D-5) and for the model without axial dispersion it is equal to -**A**. The outlet concentration in the general case is written as

$$y_{out}(\tau) = D_{1,NT} y_i(\tau) + \sum_{k=2}^{N+1} D_{1,k} y_k + D_{1,NT} y_{NT} \qquad \text{(D-16)}$$

Here the first index (=1) indicates the position in the matrix D, the values for the axial dispersion model can be found by comparing the expression with equation (D-8) and for the model without axial dispersion $D_{1,k}=0$ k=1,2,...,N+1 and $D_{1,NT}=1$.

D.IV.b Pore Phase

In a similar way the generalised pore phase equations can be written as

$$\left(\frac{\partial q_p}{\partial \tau}\right)_{u=u_l} = \frac{L K_{ads}}{v_i}(q_{SMA,l}(y_{p,l}) - q_{p,l}) + EF_{1,j} \sum_{m=1}^{NTR} E_{l,m} q_{p,m} \qquad \text{l=1,...,NR} \qquad \text{(D-17)}$$

$$\left(\frac{\partial y_p}{\partial \tau}\right)_{u=u_l} = -\frac{L K_{ads}}{v_i}(q_{SMA,l}(y_{p,l}) - q_{p,l}) + EF_{2,j} \sum_{m=1}^{NTR} E_{l,m} y_{p,m} \qquad \text{l=1,...,NR} \qquad \text{(D-18)}$$

and for the surface

$$\frac{\partial y_s}{\partial \tau} = \left(\frac{\partial y_p}{\partial \tau}\right)_{u=1} = \frac{St_f}{\Theta}\phi (y - y_{NTR}) + EF_{3,j} \sum_{m=1}^{NTR} E_{NTR,m} y_{NTR,m} + EF_{4,j} \sum_{m=1}^{NTR} E_{NTR,m} q_m \qquad \text{(D-19)}$$

Here the matrix EF has the dimensions 4×NC and contains the resistance against mass transfer for component j, j=1,...,NC. The values of EF, and E for the diffusion model can be found by comparing with equation (D-17), (D-18) and (D-19). The linear driving force model

corresponds to NTR=2 and model corresponds to NTR=2 and $EF_{1,j} = \frac{\psi_j St_{q,j}}{\Theta}$,

$EF_{2,j} = \frac{\psi_j St_{p,j}}{\Theta}$, $EF_{3,j} = St_{p,j}$, and $EF_{4,j} = St_{q,j}$ with $E = \begin{bmatrix} -1 & 1 \\ 1 & -1 \end{bmatrix}$

Appendix E: Determination of Total Column Porosity

Injection of a nitrate pulse in a highly concentrated sodium chloride solution corresponding to non-binding conditions ought to give the total porosity of the column, ε_t, however, even at a high sodium chloride concentration, 1-2 M, the total porosity has been found to be much too high. This is most likely due to the strong binding of nitrate to the ion exchanger, eq. (5-4). A way to overcome this problem is by saturating the column with e.g. 1 M KNO_3, resetting the UV-signal at these conditions and injecting a nitrate pulse with a lower nitrate concentration e.g. 0.5-0.75 M. The lower nitrate concentration will appear as a negative pulse in the chromatogram, and the retention time for this can be determined. The program for this measurement is given in program E.1 below.

```
Elapsed          Block    Event
-------------------------------------------------------------------------------------------------------

General Settings: Set Detectors Inline
General Settings: Set Column 2 Inline
General Settings: UV Detector Wavelength = 254 nM and 280 nM
General Settings: Flow Rate = 1.00 ml/min
General Settings: Turn UV Detector Lamp On
Pump On
 0.00    min      Method Start
 0.00    min      [01] Equil Block
 0.00    min              (A) Step Segment
 0.00    min                   0.00 ml  Set Solvent Blend  100% A:KNO3 1.0 M
 0.50    min                   0.50 ml  Zero UV Detector*
 1.00    min                   1.00 ml  End Solvent Blend  100% A:KNO3 1.0 M
 1.00    min
 1.00    min      ---------------------------------------------------------------------------
 1.00    min      [02] Load Block
 1.00    min              (A) Sample Loader Inject Segment
 1.00    min                   0.00 min  Load Sample into Loop: 100.0 µl: 1: KNO3
 1.17    min                   0.17 min  Inject Sample
 1.17    min
 1.17    min      ---------------------------------------------------------------------------
 1.17    min      [03] Elute Block
 1.17    min              (A) Step Segment
 1.17    min                   0.00 ml  Set Solvent Blend  100% A:KNO3 1.0 M
 1.17    min                   0.00 ml  Data Collection Start*
16.17    min                   15.00 ml  Pump Off*
16.17    min                   15.00 ml  End Solvent Blend  100% A:KNO3 1.0 M
16.17    min
16.17    min      ---------------------------------------------------------------------------
-------------------------------------------------------------------------------------------------------
```

Program E.1 Program to determine total column porosity.

Appendix F: Column Capacity

Programs for nitrate capacity measurements.

```
Elapsed         Block     Event
-------------------------------------------------------------------------------------------------------
General Settings: Set Detectors Inline
General Settings: Set Column Offline
General Settings: UV Detector Wavelength = 254 nM and 280 nM
General Settings: Flow Rate = 10.00 ml/min
Pump On
 0.00  min Method Start
 0.00  min [01] Equil Block
 0.00   min              (A) Cl-
 0.00   min                        0.00 ml  Set Solvent Blend  100% E:NaCl
 2.50   min                        25.00 ml  Set Column 1 Inline*
 3.20   min                        25.00 ml  Set Flow Rate = 1.00 ml/min*
 4.20   min                        33.00 ml  Zero UV Detector*
 6.20   min                        35.00 ml  End Solvent Blend  100% E:NaCl
 6.20   min              (B) NO3-
 6.20   min                        0.00 ml  Set Solvent Blend  100% E:KNO3 0.5M
 6.20   min                        0.00 ml  Set Column Offline*
31.20  min                        25.00 ml  Set Column 1 inline*
41.20  min                        35.00 ml  End Solvent Blend  100% E:KNO3 0.5M
41.20  min              (C) Wash
41.20  min                        0.00 ml  Set Solvent Blend  100% F:H2O
41.20  min                        0.00 ml  Set Column Offline*
66.20  min                        25.00 ml  Set Column 1 inline*
76.20  min                        35.00 ml  End Solvent Blend  100% F:H2O
76.20  min              (D) OH-
76.20  min                        0.00 ml  Set Solvent Blend  100% E:NaOH  1M
76.20  min                        0.00 ml  Set Column Offline*
101.20  min                       25.00 ml  Set Column 1 inline*
201.20  min                       125.00 ml  End Solvent Blend  100% E:NaOH  1M
201.20  min              (E) Cl-
201.20  min                       0.00 ml  Set Solvent Blend  100% F:NaCl  1M
201.20  min                       0.00 ml  Set Column Offline*
226.20  min                       25.00 ml  Set Column 1 inline*
236.20  min                       35.00 ml  End Solvent Blend  100% F:NaCl  1M
236.20  min
236.20  min ---------------------------------------------------------------------------
-------------------------------------------------------------------------------------------------------
```

Program F.1 Program to investigate hydroxide saturation of the column.

```
Elapsed         Block     Event
-------------------------------------------------------------------------------------------------------

General Settings: Set Detectors Inline
General Settings: Set Column 1 Inline
General Settings: UV Detector Wavelength = 254 nM and 280 nM
General Settings: Flow Rate = 5.00 ml/min
General Settings: Turn UV Detector Lamp On
Pump On
 0.00  min Method Start
 0.00  min [01] Equil Block
 0.00   min          (A) Load Column with NaCl
 0.00   min                        0.00 ml  Load through Pump  100% E:NaCl
 5.00   min                        25.00 ml  Divert to Waste*
 5.00   min                        25.00 ml  Zero UV Detector*
 6.00   min                        30.00 ml  Load through Pump  100% E:NaCl
 6.00   min ---------------------------------------------------------------------------
 6.00  min [02] Elute Block
 6.00   min          (A) Replace Cl- with NO3-
 6.00   min                        0.00 ml  Set Solvent Blend  10.0% A:KNO3 90.0% F:H2O
 6.00   min                        0.00 ml  Set Column Offline*
12.00  min                        30.00 ml  Set Column 1 Inline*
20.00  min                        70.00 ml  Set Column Offline*
21.00  min                        75.00 ml  Set Solvent Blend  10.0% A:KNO3 90.0% F:H2O
21.00  min ---------------------------------------------------------------------------
21.00 min [03] Wash Block
21.00  min          (A) Wash Column
21.00  min                        0.00 ml  Set Solvent Blend  100% F:H2O
27.00  min                        30.00 ml  Set Column 1 Inline*
30.00  min                        45.00 ml  End Solvent Blend  100% F:H2O
30.00  min ---------------------------------------------------------------------------
30.00 min [04] Elute Block
30.00  min           (A) Elute NO3-
30.00  min                        0.00 ml  Set Solvent Blend  100% E:NaCl
38.00  min                        40.00 ml  Pump Off*
38.00  min                        40.00 ml  End Solvent Blend  100% E:NaCl
38.00  min
38.00  min ---------------------------------------------------------------------------
-------------------------------------------------------------------------------------------------------
```

Program F.2 Program to measure the nitrate capacity.

Appendix G: Buffers and Protein Solutions

Chemicals	*Number*	*Vendor*
NaCl	1.06404-1000	Merck
NaCl	0231	J.T. Baker
$NaNO_3$	1.06537.1000	Merck
KNO_3	0277	J.T. Baker
Bis-Tris Propane	B-6755	Sigma
5M HCl	LAB00440	Bie & Berntsen
5M NaOH	LAB000334	Bie & Berntsen
Aprotinin	Batch no. A38H42112	Novo Nordisk A/S
BSA	A-6918	Sigma
Tyrosin	T-5754	Sigma
α-Lactalbumin	L-5385	Sigma
β-Lactoglobulin A	L-7880	Sigma
β-Lactoglobulin B	L-8005	Sigma
β-Lactoglobulin A and B	L-0130	Sigma

Table G.1 List of Chemicals

G.I Chemicals

The chemicals for the solutions are given in table G.1. H_2O used for the experiments are ultra pure water produced on a Maxima Ultra Pure Water (MAF 09130) from Holm & Halby. Initially the sodium chloride was from Merck, this was later replaced by sodium chloride from J.T. Baker, since this was considerably cheaper. Similarly the $NaNO_3$ from Merck was replaced by KNO_3 from J.T. Baker.

G.II Buffer

The buffer solution contains buffer, salt + HCl and NaOH to adjust the pH. Often 5 litre of buffer is made. The volumes given below corresponds to 5 l of buffer solution.

- The amount of buffer is weighted (20 mM of Bis-Tris Propane[11] is used as buffer) in a pyrex glass.
- Salt is weighted and mixed with the buffer.

11 Bis-Tris Propane is 1,3-bis[tris(Hydroxymethyl)-methylamino]propane), $C_{11}H_{26}N_2O_6$, MW=282.3g/mole, pK_{a1}=6.8, pK_{a2}=9.0. 20 mM is recommended by Amersham Biosciences.

- 5 litres of water are measured and the 4 litres are added directly to the 5 litre bluecap bottle. The remaining 1 litre of water is used for dissolving salt and buffer as described below.
- Adequate water is added to the salt and buffer to ensure that all is dissolved.
- The solution of salt, buffer, and water is filtered using a 0.45 µm filter paper (Millipore "Durapore membrane filters" HVLP04700).
- The filtered buffer solution is added to the 5 litre blue cap bottle, and the filter is washed with the remaining of the 1 litre water.
- The remaining of the water is added to the 5 litre blue cap bottle.
- The buffer is mixed and the pH is titrated to pH 6 with 5 M HCl. This ensures that the same amount of anion is added to the solution irrespectively of the final pH-value.
- The pH is adjusted to the desired value using 5 M NaOH.

G.III Salt Concentration

Two different chloride concentrations have previously been used for the buffers the nominal salt concentration and the actual salt concentration. The nominal salt concentration is given as

$$C_{0,nom} = \frac{m_{NaCl}}{MW_{NaCl} V_{H_2O}} \tag{G-1}$$

Where m_{NaCl} is the mass of the water, MW is the chloride concentration and V is the volume of water added. This does not take the volume change from mixing water and salt into account. Assuming a density of pure water of 1 kg/l, the nominal salt concentration in molar corresponds to the molality in mole/kg H_2O, $\bar{m}_{NaCl}$

$$\bar{m}_{NaCl} = \frac{m_{NaCl}}{MW_{NaCl} m_{H_2O}} \tag{G-2}$$

The specific volume as a function of the salt molality is plotted in figure G.1 together with the fitted specific volume for the NaCl-solutions. Where the fitted value is given as

$$\nu = \frac{1}{\rho} = 10^{-3}\left[\frac{m^3}{kg}\right] - \alpha \cdot \bar{m}_{NaCl} \tag{G-3}$$

where $\alpha = 35.1 \cdot 10^{-3}\left[\frac{m^3}{mole}\right]$ (G-4)

The actual concentration takes the volume change into account and also the chloride added for titration of the buffer, (the hydroxide volume added is not taken into account), this is given as

$$C_0 = \frac{V_{H_2O} \cdot \rho_{H_2O} \cdot m_{NaCl} + V_{HCl} C_{HCl}}{\nu \cdot V_{H_2O} \cdot \rho_{H_2O} \left(1 + m_{NaCl} MW_{NaCl}\right) + V_{HCl}} \quad \text{(G-5)}$$

Where n_{NaCl} is the number of moles of NaCl, V_{H2O} and ρ_{H2O} is the volume and density (used 1000 kg/m^3) of the pure water (without salt) and V_{HCl} and C_{HCl} is the concentration and volume of the HCl used for titration. The volume of NaOH used for titration is not taken into account.

Molality	***Specific volume***
[mole/kg H_2O]	[10^{-3}m^3/kg]
0	1.001797
0.1	0.997620
0.2	0.991564
0.5	0.981833
0.75	0.972505
1	0.963544
2	0.930909

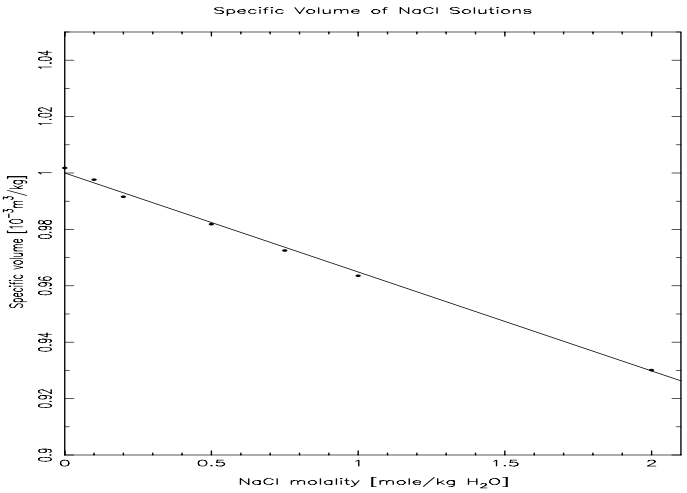

Table G.2 Specific volume of NaCl solutions at 20°C (Lide, 1998, p. 6-5).

Figure G.1 Molality of NaCl solutions as a function of molality. and the fitted function with α=35.1·10^{-3} m^3/mole.

Normally only a few salt concentrations are mixed. The mixing to the desired salt concentration in the particular run is done by the BioCad's mixer.

G.IV Protein Solutions

The protein solutions are prepared by measuring the amount of protein and adding this to the buffer with the desired salt concentrations.

For pulse experiments the protein consumption is very modest and the solution is not filtered.

For breakthrough experiments the protein consumption is a significant amount of the feed to the column and the protein solutions are filtered, using a 0.45 µm filter (Millipore "Durapore membrane filters" HVLP04700).

Appendix H: Pulse Experiments

The UV-lamp is always turned on one hour before the experiments are started to warm up the UV-lamp, this applies for all types of experiments.

H.I Isocratic Pulse Experiments

When running the pulse experiments, it is desirable to know approximately the proteins retention volume at the given pH and salt concentration in order to avoid too long experiments. This can be estimated from a few initial isocratic and gradient experiments.
When a series of pulse experiments with different salt concentrations are made, the proteins solutions in the injection loop is mixed from the buffer with the lowest salt concentrations.
Program H.1 shows an example of a program for an isocratic experiment. In this example the gradient mixer is not used for mixing the salt concentration. If the gradient mixer is used for mixing the desired salt concentration, the non-linearity of the gradient mixer must be taken into account, appendix K “Calibration of Gradient Mixer”.
An extra step can be added to the end of the method where remaining protein is washed out by e.g. a 1 M salt solution.

H.II Gradient Pulse Experiments

Beside the isocratic pulse experiment also experiments where the salt concentration in increased linearly is used. In these experiments the gradient mixer is always used to make the gradient and it is important when calculating the salt concentration to take the calibration of the gradient mixer into account, see appendix K “Calibration of Gradient Mixer”.
An example of a program for a pulse experiment is given in program H.2. An isocratic step is always used at the end of these experiments to make sure that protein is eluted from the column.

```
Elapsed          Block     Event
-------------------------------------------------------------------------------------------------------

General Settings: Set Detectors Inline
General Settings: Set Column 1 Inline
General Settings: UV Detector Wavelength = 254 nM and 280 nM
General Settings: Flow Rate = 2.00 ml/min
General Settings: Turn UV Detector Lamp On
Pump On
 0.00    min      Method Start
 0.00    min      [01] Equil Block
 0.00     min             (A) Step Segment
 0.00     min                 0.00 ml  Set Solvent Blend  100% A:NaCl 200 mM
 2.33     min                 7.00 ml  Zero UV Detector*
 2.67     min                 8.00 ml  End Solvent Blend  100% A:NaCl 200 mM
 2.67     min
 2.67     min     ---------------------------------------------------------------------------
 2.67     min     [02] Load Block
 2.67     min             (A) Sample Loader Inject Segment
 2.67     min                 0.00 min  Load Sample into Loop: 100.0 µl: 1: Lactalbumin 1 g/l
 2.77     min                 0.10 min  Inject Sample
 2.77     min
 2.77     min     ---------------------------------------------------------------------------
 2.77     min     [03] Elute Block
 2.77     min             (A) Step Segment
 2.77     min                 0.00 ml  Set Solvent Blend  100% A:NaCl 200 mM
 2.77     min                 0.00 ml  Data Collection Start*
11.10     min                 25.00 ml  Pump Off*
11.10     min                 25.00 ml  End Solvent Blend  100% A:NaCl 200 mM
11.10     min
11.10     min     ---------------------------------------------------------------------------
-------------------------------------------------------------------------------------------------------
```

Program H.1 Program for isocratic pulse experiment.

```
Elapsed          Block     Event
-------------------------------------------------------------------------------------------------------

General Settings: Set Detectors Inline
General Settings: Set Column 1 Inline
General Settings: UV Detector Wavelength = 254 nM and 280 nM
General Settings: Flow Rate = 6.00 ml/min
General Settings: Turn UV Detector Lamp On
Pump On
 0.00    min      Method Start
 0.00    min      [01] Equil Block
 0.00     min             (A) Step Segment
 0.00     min                 0.00 ml  Set Solvent Blend  98.0% A:NaCl 0 M 2.0% B: NaCl 300 mM
 6.50     min                 39.00 ml  Zero UV Detector*
 6.67     min                 40.00 ml  End Solvent Blend  98.0% A:NaCl 0 M 2.0% B: NaCl 300 mM
 6.67     min
 6.67     min     ---------------------------------------------------------------------------
 6.67     min     [02] Load Block
 6.67     min             (A) Sample Loader Inject Segment
 6.67     min                 0.00 min  Load Sample into Loop: 100.0 µl: 1: Lactalbumin 1 g/l
 6.77     min                 0.10 min  Inject Sample
 6.77     min
 6.77     min     ---------------------------------------------------------------------------
 6.77     min     [03] Elute Block
 6.77     min             (A) Gradient Segment
 6.77     min                 0.00 ml  Start Gradient  98.0% A:NaCl 0 M 2.0% B: NaCl 300 mM
 6.77     min                 0.00 ml  Data Collection Start*
 9.43     min                 16.00 ml  End Gradient  100% B: NaCl 300 mM
 9.43     min
 9.43     min             (A) Step Segment
 9.43     min                 0.00 ml  Set Solvent Blend  100% B: NaCl 300 mM
16.10     min                 40.00 ml  Pump Off*
16.10     min                 40.00 ml  End Solvent Blend  100% B: NaCl 300 mM
16.10     min
16.10     min     ---------------------------------------------------------------------------
-------------------------------------------------------------------------------------------------------
```

Program H.2 Program for gradient pulse experiment.

Appendix I: Breakthrough Experiment

A typical capacity measurement is described in table I.2 and the resulting chromatogram is given in figure I.1. The steps are the following, first the column is equilibrated with buffer. After this column is bypassed and the protein solution replace the buffer in all the piping upstream and downstream of the column. Furthermore the UV-signal at the feed protein concentration can be determined. The column is put inline and the buffer in the piping to/from the column itself and in the column is replaced by the protein solution and protein is adsorbed to the ion exchanger in the column. The amount of protein adsorbed to the column and in the piping/mobile phase corresponds to the hatched area in figure I.1.

At the end of the adsorption the column is bypassed and the UV-signal corresponding to the feed protein concentration is again determined.

To replace the protein in the piping upstream and downstream of the column water is fed to the system while the column is bypassed. Putting the column inline while feeding the system with water the protein solution in the piping to/from the column and the in the mobile phase, is removed. The corresponding peak is seen in figure I.1 between line five and six. Finally the adsorbed protein is desorbed from the column resulting in the peak seen after line six in figure I.1. The program is similar to the program for nitrate capacity measurements, program F.2.

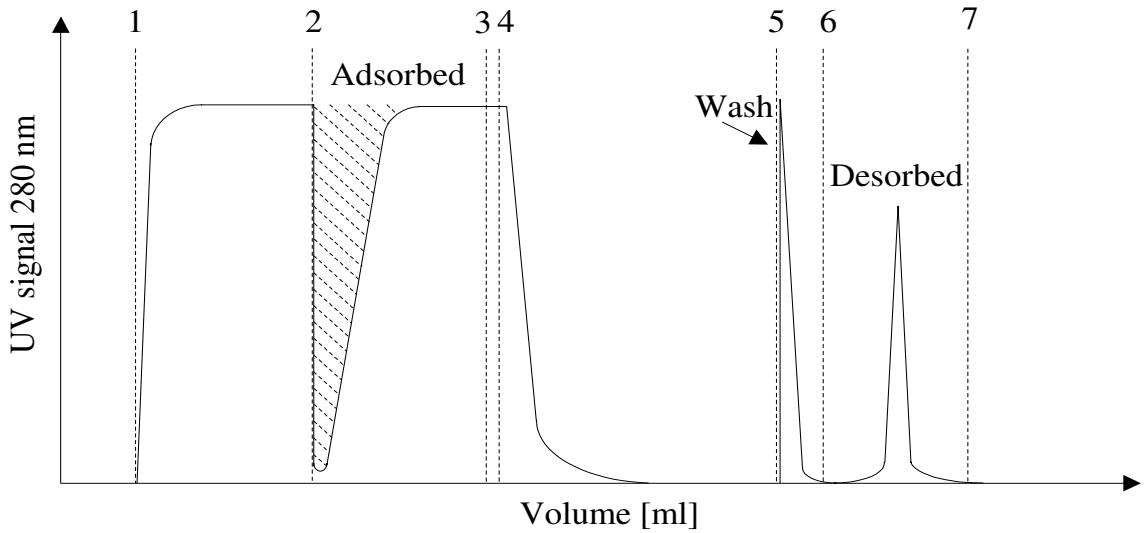

Figure I.1 Schematic drawing of chromatogram for capacity measurement on a differential column. The vertical lines indicate an event in the experiment, see table I.2.

Solution	*Name*	*BSA [g/l]*	*NaCl [mM]*
A	protein	5	C_0
B	Buffer	0	C_0
C	Salt	0	1000
D	Water	0	0

Table I.1 Solutions for capacity measurements. C_0 is the salt concentration for the experiment.

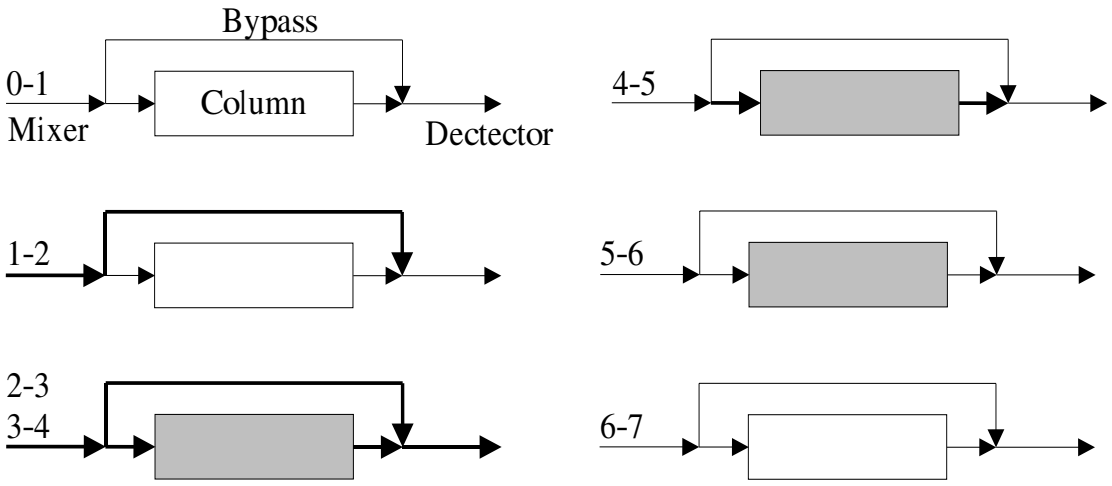

Figure I.2 Schematic drawing of breakthrough experiments. The numbers to the left of the figure corresponds to the numbers in figure I.1. Thick lines indicate that protein is present in the piping at the end of the period and thin lines indicate that protein is not present. Correspondingly a white column indicate that no protein is present in the column and a grey column indicates that protein is present in the column.

Typical vol. [ml]	*From*	*To*	*Column*	*Feed*	*Purpose*
20	start	1	inline	B	Equilibration of the column.
40	1	2	bypass	A+B	Make sure the protein is in all the piping upstream and downstream of the column. The last 5 ml before event 2 is used to determine the UV-signal at the feed concentration.
50	2	3	inline	A+B	Adsorption of protein.
3	3	4	bypass	A+B	Determine the UV-signal at the feed concentration.
			bypass	D	Washing of all the piping upstream and downstream of
50	4	5			the column.
5	5	6	inline	D	Remove protein not bound to the column.
30	6	7	inline	C+D	Salt gradient to remove protein from the column
20	7	end	inline	C	Remove remaining protein from the column

Table I.2 The typical steps in a capacity measurement. The to/from numbers refer to figure I.1 and the feed corresponds to the solutions given in table I.1. The typical volumes are for a run with C_p=5g/l and Source 30Q using a differential column.

Appendix J: Batch Experiments

Two different types of batch experiments have been made. The two types are the one suggested by Bisgaard-Frantzen (1998), J.II "Dry Resin", and the second method is the one used at Dortmund University, J.I "Resin Slurry". The main difference between the two methods is that the method suggested by Bisgaard-Frantzen handles the ion exchanger as a dried phase whereas the method used in Dortmund handles it as a slurry phase.

J.I Resin Slurry

Name	*Number*	*Vendor*
Micro test tubes 2 ml	0030 120.094	Eppendorf
Glass filter funnel	1-P-5840-4	Bie & Berntsen
Vacuum erlenmayer flask	1170413	Buch og Holm
Eppendorf Centrifuge MiniSpin	5452 000.018	Eppendorf
UV-detector, Shimadzu UV mini 1240		Shimadzu
Merck HPLC[12]		Merck
Transfer pipette	1-P-0056C	Bie & Berntsen
Eppendorf pipette 100-1000 µl	3111 000.165	Eppendorf
Eppendorf pipette 20-200 µl	3111 000.157	Eppendorf
Eppendorf pipette tips 2-200µl	0030 000.870	Eppendorf
Eppendorf pipette tips 50-1000 µl	0030 000.919	Eppendorf
1.5 ml HPLC-glass vials bottles	548-0028	VWR International
HPLC 200 µl sample flask	300405	GC-Chromatographie Service GmbH

Table J.1 List of equipment

Resin purification and equilibration

1) App. 2 ml of resin slurry is transferred to a glass filter funnel, placed on a vacuum Erlenmayer flask.
2) The resin is equilibrated with 1 M NaCl solution to remove any unwanted component adsorbed to the resin.
3) The NaCl solution is removed from the glass filter funnel by vacuum, and vacuum is turned off again, when the liquid has been removed.
4) The resin is equilibrated with buffer at the desired salt concentration for five minutes and the buffer is removed by vacuum. The vacuum is turned off when the buffer has been

12 The Merck HPLC is equipped with L-7250 sampling table, L-7100 pump, L-7360 Column oven and L-7400 UV detector.

removed.

5) Step 4 is repeated.
6) The resin is equilibrated with buffer at the desired salt concentration for ten minuets and the buffer is removed by vacuum.
7) The resin is removed from the glass filter funnel and transferred to an micro test tube, the mass of resin transferred to the micro test tube is noted.
8) An equivalent amount of buffer (e.g. 800 µl buffer to 800 mg resin) is added to the micro test tube with an pipette.

The above procedure is very much the same as the procedure previously suggested by Bissgaard-Frantzen (1998). However, a reference level after 20 min of vacuum drying is not used and resin is handled as a slurry.

Samples:

1) A standard solution containing pure protein solution (1½-2 ml) is transferred to an micro test tube.
2) With a pipette the desired amount of buffer is transferred to an micro test tube.
3) With another pipette the desired amount of proteins solution is added to the micro test tube.
4) The desired amount of resin slurry is added to micro test tube with a pipette
5) The samples are equilibrated over night.

Analyzing the samples:

1) The photometer is turned on app. 1 hour before use.
2) The samples are centrifuged at 10,000 rpm in 30 seconds to separate and mobile phase and resin.
3) The cuvette is washed with ½ ml of buffer solution.
4) The cuvette is filled with ½ ml of buffer solution and the photometer is reset to determine the baseline.
5) ½ ml of undiluted standard solution is transferred to a HPLC-glass vial bottle (only if mixture of proteins).
6) The cuvette is washed with ½ ml of diluted standard protein solution.
7) The cuvette is filled with diluted standard protein solution (to be in the linear range of the UV-detector) and the absorbance at 280 nm is determined.
8) 200 µl of undiluted protein solutions is transferred to a 200 µl sample flask (only if mixture of proteins).

9) The cuvette is washed with the sample containing the diluted highest protein concentration.
10) The cuvette is filled with diluted sample solution and the absorbance at 280 nm is determined.
11) Step 8 to 10 is repeated for the remaining samples going from the highest protein solution and downwards. For every five samples the baseline is checked acc. 4 and 5.

Starting from the highest protein concentration and moving downwards the appropriate dilution of the following sample can estimated. Normally a low dilution (being in the linear range) is most beneficial since any effect from a baseline drift is avoided. All the samples for the HPLC is analysed (only if mixture of proteins).

Determination resin in resin slurry:

1) A small glass is weighted, m_g.
2) ½-1 ml of resin slurry, V_{wet}, is added to the glass and the weight is noted, $m_{g,wet}$.
3) The resin is dried in an oven at 60 ºC over night.
4) Immediately after the resin comes out of the oven the glass is closed with a cap (the resin is very hygroscopic).
5) The close glass is weighted, m_{total}.
6) The cap is taken off the glass and weighted, m_{cap}.
7) After one hour the resin in the glass is weighted, $m_{t1,g}$.

The one hour measurement is only used for control.

J.II Dry Resin

	Number	***Vendor***
Glass filter funnel Ø 60mm porosity #4	1-P-5844-4	Bie & Berntsen
Centrifuge glass 100·13 mm	1-C-265471	Bie & Berntsen
Stopper 10·3.8/11.8 mm	1-P-2053	Bie & Berntsen
Vacuum Pyrex BS 1739		
Movil-tub/P-Selectra blood mixer		Buck & Holm
Pasteur Pipette 202 macro-pet	1-P-0056C	Bie & Berntsen
Centromix/P-Selectra centrifuge		Buck & Holm

Table J.2 List of equipment.

1. Approximately 5 g of new or regenerated resin is added to a glass filter funnel mounted on top of a vacuum Pyrex.

2. Excess liquid is removed by vacuum.
3. The filter funnel is filled with water and stirred to mix water and resin.
4. After 5-10 minutes the water is removed by vacuum.
5. Step 3 and 4 is repeated.
6. The filter funnel is filled with buffer and stirred gently.
7. After 5-10 minutes the buffer is removed by vacuum.
8. Step 6 and 7 is repeated.
9. Water is removed by applying vacuum for 20 min to remove as much buffer as possible.
10. In each centrifuge glass app. 2-300 mg of resin is added (this can be less for strongly binding conditions and more for weakly binding conditions). It is important that the filter cake is not broken into small pieces before the weighting of the resin, the increased surface will increase the evaporation of water from the resin.
11. Protein solution (e.g. C_p=5g/l) is added with a pipette, buffer solution is added with a pipette up to 8 ml.
12. The centrifuge glasses are closed and transferred to a blood mixer and equilibrated over night at room temperature.
13. The remaining resin from the filter funnel is added to the blue cap bottle containing regenerated resin.

Measurement of remaining protein in the mobile phase.

After equilibration the samples are centrifuged for 5 min at 5000 rpm.

The BioCad is mounted with the 5 ml syringe and the 5 ml injection loop. The dead volume from the injection loop to the UV-detector is very small when bypassing both columns, and the resulting peaks have a flat plateau from which the protein concentration can be determined, see appendix K “Calibration of the Gradient Mixer”.

Usually when measuring a series of samples, the first centrifuge glasses contains the low protein concentrations and the protein concentration is gradually increased to cover the whole isotherm. This means that the last injection from the previous run was a high protein concentration. To avoid contamination from the previous run all the four injection ports in the BioCad are injected with 5 ml water before the method is started. The four first samples are connected to the four sample loops for the BioCad and the program is started. It is VERY important that the tube from the injection port is above the resin in the bottom of the

centrifuge glass, to avoid resin in the BioCad.

An example of a program with 10 measurements is given in program J.1 below. As can be seen from the program the sample port is flushed (with 500 µl sample) before each injection to ensure that the previous sample is removed from the tubing. The steps 2 and 3 are repeated corresponding to the number of samples, except the injection port in always switched from 1, 2, 3, 4, 1, 2, ...

The samples can be changed while the HPLC is loading, however, it is safest to replace the samples while the BioCad is not loading a sample, to avoid the tube loading being pushed into the resin or above the surface of the sample.

```
Elapsed          Block     Event
-------------------------------------------------------------------------------------------------------------

General Settings: Set Detectors Inline
General Settings: Set Column Offline
General Settings: UV Detector Wavelength = 254 nM and 280 nM
General Settings: Flow Rate = 3.00 ml/min
General Settings: Turn UV Detector Lamp On
Pump On
 0.00    min      Method Start
 0.00    min      [01] Wash Block
 0.00     min             (A) Step Segment
 0.00     min                  0.00 ml  Set Solvent Blend  100% F:H2O
 3.33     min                  10.00 ml  Zero UV Detector*
 4.00     min                  12.00 ml  End Solvent Blend  100% F:H2O
 4.00     min
 4.00     min      ------------------------------------------------------------------------------
 4.00     min      [02] Load Block
 4.00     min             (A) Sample Loader Inject Segment
 4.00     min                  0.00 min  Flush Sample Loader:  1:
 4.58     min                  0.58 min  Load Sample into Loop: 5000.0 \265l: 1:
 6.77     min                  2.77 min  Inject Sample
 6.77     min
 6.77     min      ------------------------------------------------------------------------------
 6.77     min      [03] Wash Block
 6.77     min             (A) Step Segment
 6.77     min                  0.00 ml  Set Solvent Blend  100% F:H2O
10.10     min                  10.00 ml  End Solvent Blend  100% F:H2O
10.10     min
10.10     min      ------------------------------------------------------------------------------
61.67     min      [21] Wash Block
61.67     min             (A) Step Segment
61.67     min                  0.00 ml  Set Solvent Blend  100% F:H2O
71.67     min                  30.00 ml  End Solvent Blend  100% F:H2O
71.67     min
71.67     min      ------------------------------------------------------------------------------
-------------------------------------------------------------------------------------------------------------
```

Program J.1 Example of BioCad program for batch experiments to measure 10 samples. The blocks [2] and [3] are repeated 10 times, except the last wash block (block [21]) which is increased to 30 ml.

Appendix K: Calibration of Gradient Mixer

The gradient mixer in the BioCad has previously been calibrated by Søndergaard (1999). Søndergaard found that the actual mixing was given by $y=a \cdot x+1-a$, where a= 0.89925, x is the set point of the mixer in % and y is the actual mixing in %.

The old computer in the BioCad was in January 2000 replaced by a new computer with an updated version of the software. Experiments made using the new computer and the gradient mixer deviated from previous results and a more thorough calibration of the gradient mixer was necessary.

However, the new computer broke down august 2002. Service technicians were unable to repair the computer and the old computer was reinserted October 2002.

Two different tests have been made to test the mixer. In the first test a number of steps in the mixing have been made and in the second test a linear gradient has been applied to the mixer. Pure water is connected to one of the inlets of the BioCad and nitrate solution is connected to another inlet.

For the experiments it is important that the UV-signal is in the linear range.

K.I Step Test

To check the mixer a number of steps have been made first in ascending order from 0 to 100% and hereafter in descending order from 100 to 0%. A higher number of sample points are desired at the limits of the mixer to check it at its boundaries. A typical example of a step procedure are given in table K.1 below.

Close to 0 and 100 % the mixing is only increased 1 % but in the range 10-90% the step size is increased to 5%. In each step 20 ml is pumped into the BioCad, V_{step}, however, at 0 and 100% mixing the volume is increased to 40 ml, V_{hold}, since these act as reference levels.

From [%]	*To [%]*	*Increase [%]*
0	10	1
10	90	5
90	100	1
100	90	-1
90	10	-5
10	0	-1

Table K.1 Typical steps for calibration of the mixer. All the steps are 20 ml except at 0 and 100% mixing.

K.II Linear Gradient Test

A linear gradient from 0 to 100 % both in ascending and in descending order is applied to the BioCad, the typical gradient volume, V_{grad}, is 200 ml. In between the two gradients a volume of 40 ml with 100 % KNO_3 is inserted, and after the last gradient 40 ml of 100 % H_2O is added.

An example of a program to check the mixer is given in program K.1 and the resulting chromatogram is seen in figure K.2.

K.III Evaluation of Calibration Chromatogram

The evaluation of the chromatograms is build into the program.

Step test

In the step test the UV-signal is calculated as an average around the end of each step, figure K.1.

The dead volume from the mixer to the UV-detector has been measured to, (V_{dead} = 5.9 ml. To be certain that measurements around a step change do not influence the measurement a safety margin,V_{safe}, around 3 ml is subtracted

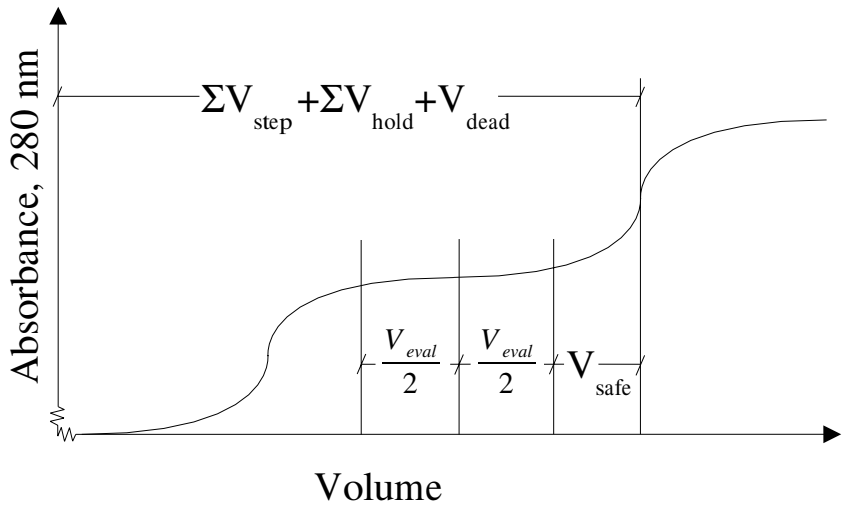

Figure K.1 Evaluation of absorbance in step test.

In step segment m the UV-signal is calculated as the average in the range

$$\left[V_m - \frac{V_{eval}}{2}, V_m + \frac{V_{eval}}{2} \right] \tag{K-1}$$

where

$$V_m = \sum_{i=1}^{m} V_{step} + \sum V_{hold} + V_{dead} - V_{safe} \tag{K-2}$$

Linear Gradient Test

The linear gradient starts after

$$V_{g1} = \sum V_{step} + \sum V_{hold} + V_{dead} \tag{K-3}$$

and ends after

$$V_{g2} = V_{g1} + V_{grad} \tag{K-4}$$

The second gradient starts at

$$V_{g3} = V_{g2} + V_{hold} \tag{K-5}$$

and ends at

$$V_{g4} = V_{g3} + V_{grad} \tag{K-6}$$

For all the experiments the actual mixing is calculated as the measured absorbance relative to the absorbance with 100% KNO_3 at 280 nm.

```
Elapsed         Block     Event
-------------------------------------------------------------------------------------------------------------

General Settings: Set Detectors Inline
General Settings: Set Column Offline
General Settings: UV Detector Wavelength = 254 nM and 280 nM
General Settings: Flow Rate = 4.00 ml/min
General Settings: Turn UV Detector Lamp On
Pump On
 0.00  min Method Start
 0.00  min [01] Load Block
 0.00   min        (A) Step Segment
 0.00   min                    0.00 ml  Load through Pump  100% A:H2O
 8.75   min                    35.00 ml  Zero UV Detector*
10.00  min                    40.00 ml  Load through Pump  100% A:H2O
10.00  min
10.00  min        (B) Step Segment
10.00  min                    0.00 ml  Load through Pump  99.0% A:H2O  1.0% F:KNO3 ?M
15.00  min                    20.00 ml  Load through Pump  99.0% A:H2O  1.0% F:KNO3 ?M
15.00  min
15.00  min        (K) Step Segment
185.00  min                   0.00 ml  Load through Pump  100% F:KNO3 ?M
195.00  min                   40.00 ml  Load through Pump  100% F:KNO3 ?M
195.00  min
195.00  min       (L) Step Segment
195.00  min                   0.00 ml  Load through Pump  1.0% A:H2O  99.0% F:KNO3 ?M
200.00  min                   20.00 ml  Load through Pump  1.0% A:H2O  99.0% F:KNO3 ?M
365.00  min
365.00  min       (T) Step Segment
365.00  min                   0.00 ml  Load through Pump  99.0% A:H2O  1.0% F:KNO3 ?M
370.00  min                   20.00 ml  Load through Pump  99.0% A:H2O  1.0% F:KNO3 ?M
370.00  min
370.00  min       (U) Step Segment
370.00  min                   0.00 ml  Load through Pump  100% A:H2O
380.00  min                   40.00 ml  Load through Pump  100% A:H2O
380.00  min ----------------------------------------------------------------------------
380.00  min [02] Elute Block
380.00  min       (A) Gradient Segment
380.00  min                   0.00 ml  Load through Pump  100% A:H2O
430.00  min                   200.00 ml  Load through Pump  100% F:KNO3 ?M
```

```
430.00  min
430.00  min       (B) Step Segment
430.00  min                   0.00 ml  Load through Pump  100% F:KNO3 ?M
440.00  min                   40.00 ml  Load through Pump  100% F:KNO3 ?M
440.00  min
440.00  min       (A) Gradient Segment
440.00  min                   0.00 ml  Load through Pump  100% F:KNO3 ?M
490.00  min                   200.00 ml  Load through Pump  100% A:H2O
490.00  min
490.00  min       (B) Step Segment
490.00  min                   0.00 ml  Load through Pump  100% A:H2O
500.00  min                   40.00 ml  Load through Pump  100% A:H2O
500.00  min
500.00  min ---------------------------------------------------------------------------
-------------------------------------------------------------------------------------------------------------
```

Program K.1 Example of BioCad program for calibration of the mixer. Only a limited number of the steps has been inserted in "[01] Load Block". The steps and times corresponds to the values in table K.1.

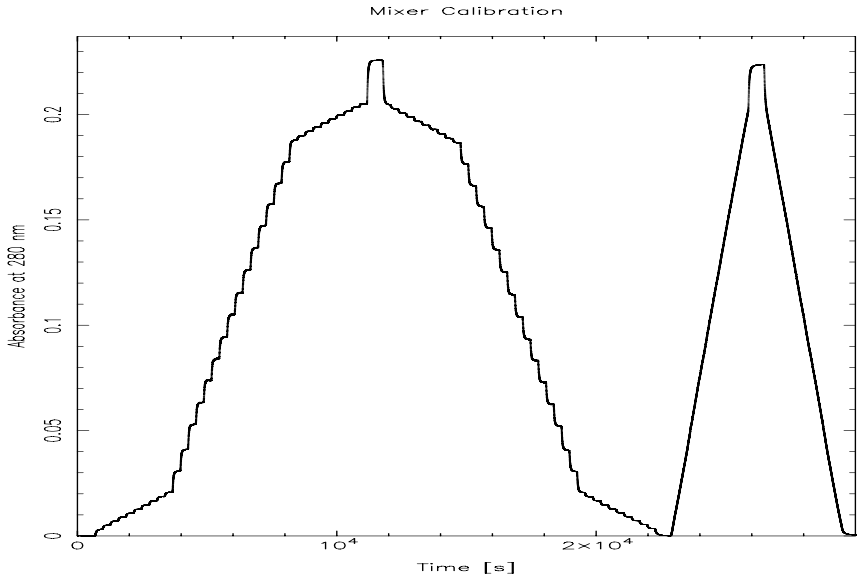

Figure K.2 Resulting chromatogram from mixer calibration. The first "peak" is the step calibration the second "peak" is the linear gradient calibration.

K.IV Results

For all the experiments three lines were fitted. These fits are based on the step experiment, the increasing gradient and the decreasing gradient. The data points are fitted to y=ax+b, where a and b are given the the tables below.

To avoid the influence of pure solvent results (0 and 100%) affecting the fit, only values in a certain mixer set point interval are used, e.g. 3-97 %.

To give an indication of the offset close to 100 % mixing a column "offset 100%" is added to the tables this result is calculated as 100-(a·100+b).

K.V New Computer

Only one experiment were made on the new computer, rundate 200202131422. The method was not carried out exactly as described above since only small step changes were made from 0 to 20% and not at the other boundary, 80-100%. The values are fitted in the range 1-99 % mixing.

From the correlation coefficient in table K.2 it is seen that the mixing is very close to linear in the range 1-99 %. Additionally it is seen that the new computer only has a relative small offset at both ends of the mixing. The resulting figures are given in figure K.3.

Experiment	***a***	***b***	***corr***	***offset 100%***
Step	0.9922	1.5661	0.99994	-0,78610
Increasing gradient	0.9910	1.7789	0.99988	-0,87890
Decreasing gradient	0.9887	2.1815	0.99991	-1,05150

Table K.2 Calculated values from line fit with new computer, rundate 200202131422 .

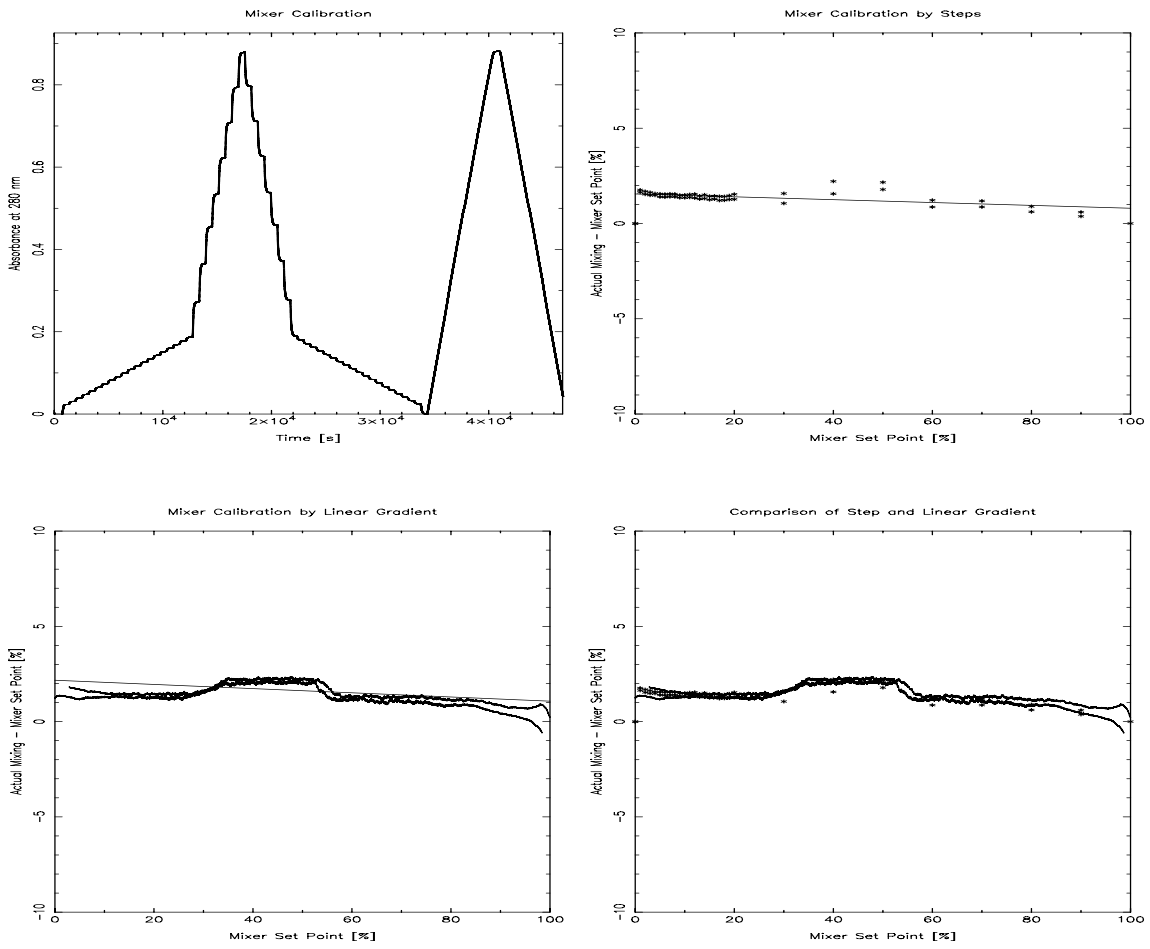

Figure K.3 top left: Resulting chromatogram from step experiments and gradient experiment.

Top right: Measured points from step experiment and fitted line.

Bottom left: Linear gradients from increasing and decreasing experiments and fitted line for decreasing gradient.

Bottom right: Comparison between experiments from step experiment and linear gradient experiments.

K.VI Old Computer

Using the old computer an experiment was made with water on entry F (pure water is usually connected to F) and nitrate on entry A, 200212061030. As for the new computer the data fits very well to a straight line. However, a significant offset is seen at 100 % mixing. At 0 % mixing only a very small offset was found, see table K.3. This is in contradiction to the previous findings of Søndergaard, who found a significant offset close to 0% mixing. Offset in one end of the mixing but not in the other is a clear indication of the lack of symmetry. The data was fitted in the range 3-97 % mixing, to avoid boundary effects.

The offset is also clearly seen on the jump in the chromatogram for the step experiment, when the mixing is increased from 99 to 100% mixing.

Experiment	***a***	***b***	***corr***	***offset 100%***
Step	0.9205	0.1485	0.99996	7.80150
Increasing gradient	0.9113	0.1534	0.99996	8.71660
Decreasing gradient	0.9146	0.1431	0.99997	8,39690

Table K.3 Calculated values from line fit on old computer, rundate 200212061030 .

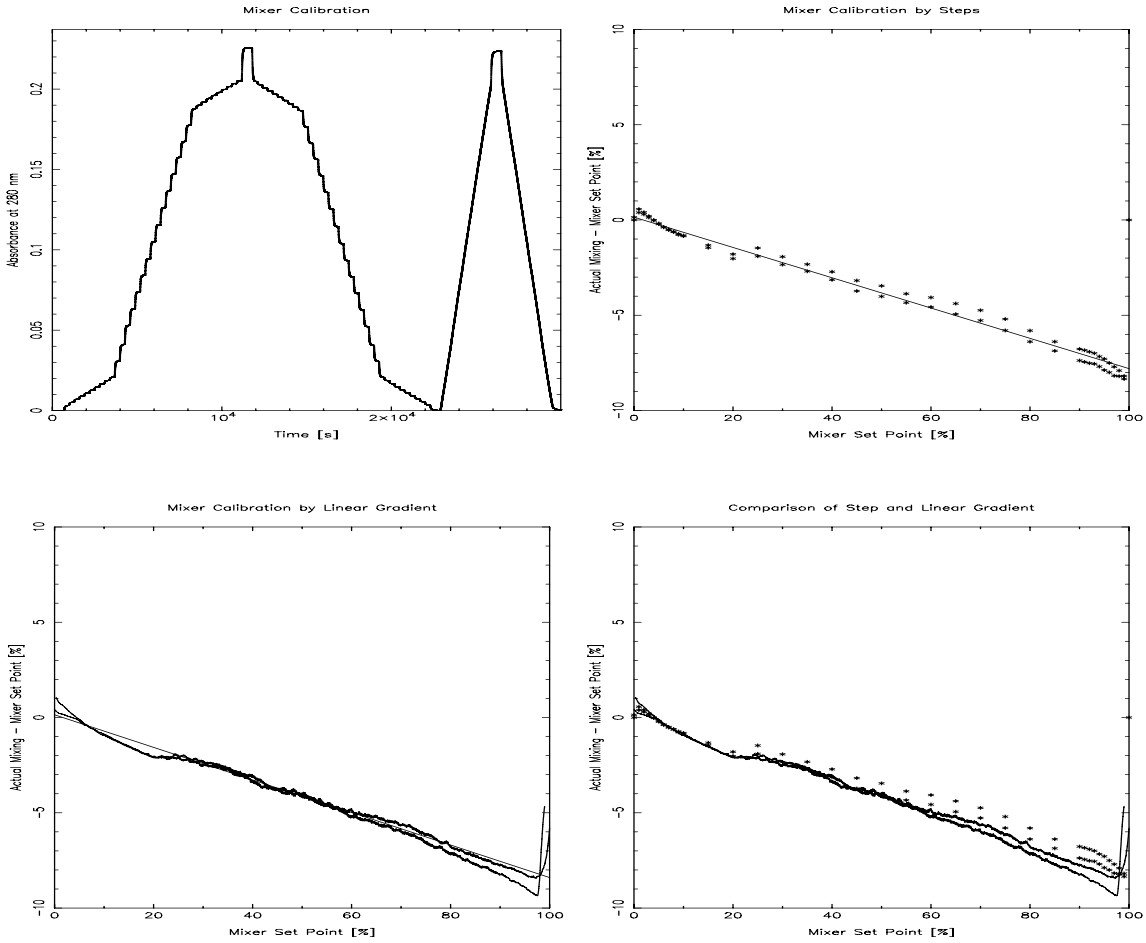

Figure K.4 Comments see figure K.3.

A second experiment was made, where water was connected to entrance A and nitrate was connected to entrance F, 200212031549. The results from this experiment is given in table

K.4 and figure K.5. The data was again fitted in the interval 3-97 %. In the table it is seen that the large offset is now close to 0 % mixing, as found by Søndergaard.

Experiment	***a***	***b***	***corr***	***offset 100%***
Step	0.9171	8.9131	0.99993	-0,62310
Increasing gradient	0.9144	8.6707	0.99994	-0,11070
Decreasing gradient	0.9078	8.9053	0.99997	0,31470

Table K.4 Calculated values from line fit. Rundate 200212031549 .

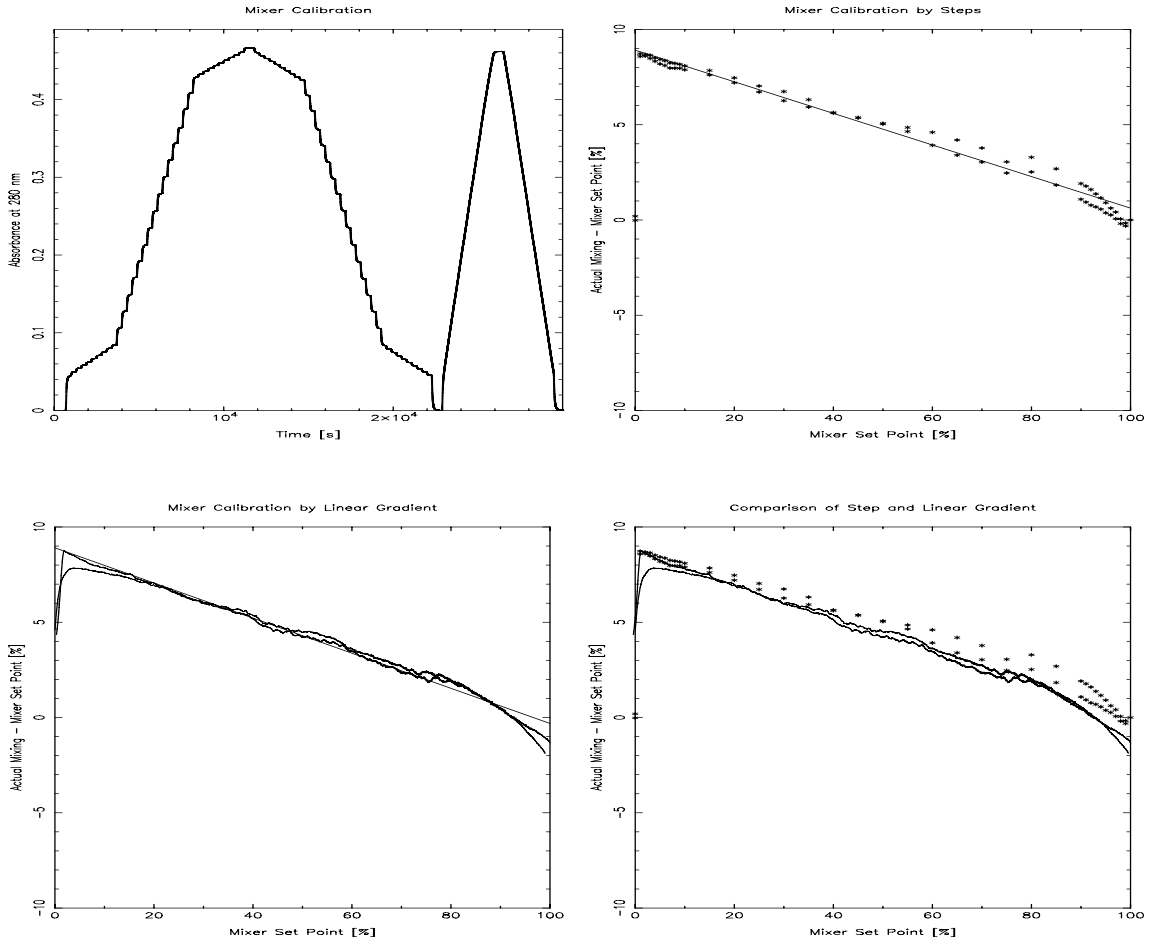

Figure K.5 See figure K.3.

K.VII Step Gradients Deviation

In the above figures from the step gradients it is seen that the step gradients do not fit exactly from the increasing and the decreasing gradient. If the step volume, V_{step}, is too small the concentration will not have reached a steady level, and this may result in the deviation in the results. A simple indication showing if a steady level has been reached is to check the correlation coefficient in each of the evaluated intervals. If the correlation coefficient is ~1 in the increasing steps and ~ -1 in the decreasing steps the step volume is too small and has to be increased. In figure K.6 below is plotted the correlation coefficient for all the steps in experiment 200212061030. The first half of these points is the increasing gradient and the last half is the decreasing gradient. From the figure no clear tendency of an increase/decrease in the gradient is found and that the step volume is considered to be adequate.

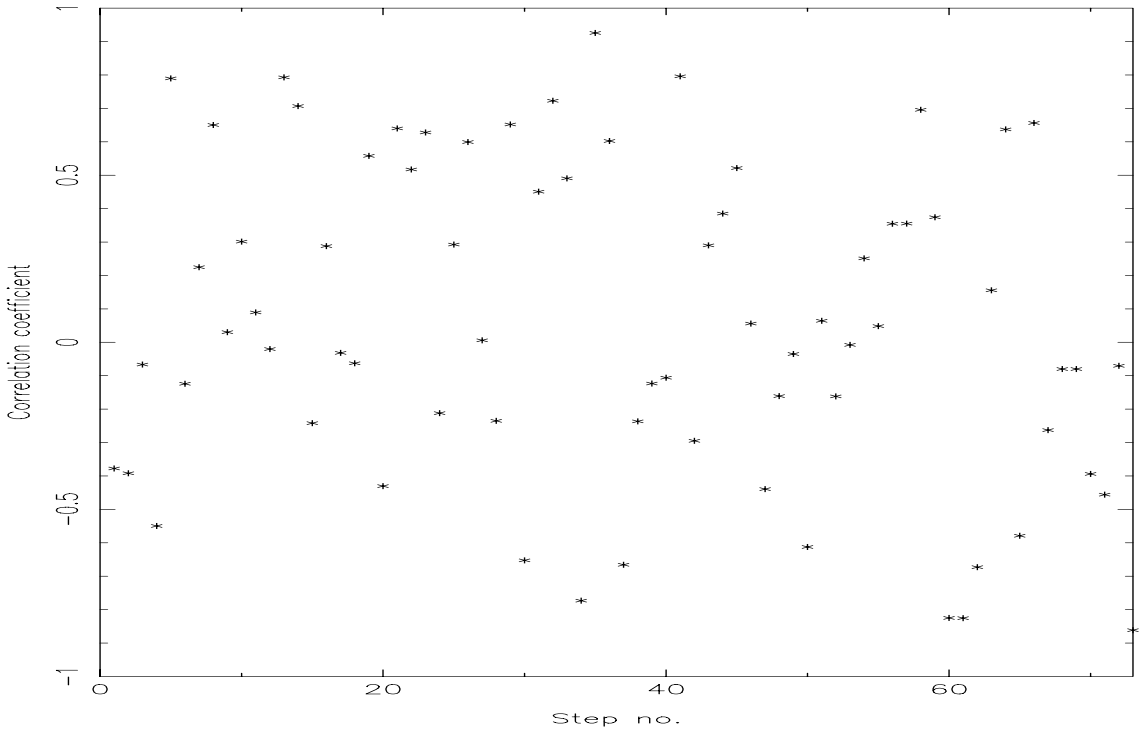

Figure K.6 Correlation coefficients for the evaluation of the steps in the steps gradient.

K.VIII Offset

From the experiments with the old computer it is seen that the mixing has an offset in one end but not in the other end. From this it is then clear that the mixer is not symmetrical, meaning e.g. that mixing 40 % 100 mM NaCl from inlet A with 60 % 300 mM NaCl from inlet C, will lead to a different concentration than mixing 60 % 300 mM NaCl from inlet A with 40 % 100

mM NaCl from inlet C.

An experiment was made to find out in which part of the mixer the offset occurred.

The set-up of the experiment was as follows:

1. Water is connected to inlet position A, the remaining inlet positions, B-F, are connected to a bottle with nitrate.
2. The system is purged to ensure that all tubing up to the mixer is filled with the desired solvent.
3. Pure water is pumped through the BioCad, with Q=20 ml/min.
4. The UV-detector is reset when a steady state is reached.
5. The mixing is changed to 99 % water and 1 % nitrate from inlet B.
6. After 1 minute the UV-signal is read and the nitrate inlet is changed to inlet C.
7. Points 5 and 6 are repeated with the remaining ports, D-F.

The experiments are repeated with inlet B-F connected to the water one at a time.

Results

The results from the experiments are given in table K.5 below. As seen from the table the offset occurs when water is mixed with nitrate from a port with a letter occurring later in the alphabet than the port with the water, e.g. CD, AE, but not CA.

One should therefore be very cautious when using the gradient mixer on the old computer.

These findings are in direct contradiction to the findings of Søndergaard (1999, p.5) who writes "*Af figur 3 ses det, at hverken valg af mobilfaseindgang eller flow har nogen nævneværdig indflydelse på UV-signalet*" ("*From figure 3 is seen that neither the chosen inlet port nor the flow has any significant influence on the UV-signal*")

H_2O	KNO_3	A	B	C	D	E	F
A	B-F	99%	0.047	0.047	0.047	0.047	0.045
B	A, C-F	0.0015	99%	0.043	0.045	0.044	0.044
C	A-B, D-F	0.0003	0.0009	99%	0.047	0.046	0.046
D	A-C, E-F	0.0003	0.0005	0.0000	99%	0.045	0.044
E	A-D, F	0.0001	0.0009	0.0000	0.0000	99%	0.041
F	A-E	0.0002	0.0015	0.0003	0.0006	0.0023	99%

Table K.5 The first column shows the inlet position with water, the second column gives the inlet positions with nitrate. The last six columns shows which inlet the water is mixed with, 99% on the diagonal indicates a mixing with 99% H_2O and 1% KNO_3.The values around the diagonal is the absorbance at 280 nm after 1 min.

K.IX Summary

The gradient mixer seem to be linear in almost the entire range (3 – 97 %), where it operates, the correlation coefficient is close to 1.

The results from a step experiment correspond very well with the result obtained from both an ascending and a descending linear gradient.

With the new computer the offset is nearly 0 resulting in a slope close to 1, and there seems to be no reason to make any corrections for the mixer with the new computer.

With the old computer the offset is considerably either close to 0 % or close to 100 % mixing, this should be taken into account when making experiments on the old computer.

The old computer and the new computer runs different versions of the software and it is likely that the offset is a due to an error in the software, since the offset is not connected to a specific hardware port but depends on the letters for the individual inlet ports.

An offset higher than 10% as previously found by Søndergaard (1999) is seems to be high compared with the present findings and a correction of $y_B = 0.915 \cdot x_B$ or $y_A = 0.915 \cdot x_A + 8.5$ depending on the selected entrances is suggested (x is set points of the mixer in % and y is the actual mixing in %).

Appendix L: Alternative Method for Calculation of Complete Separation Region

The conditions with complete separation can be calculated by using the following strategy.

The total mass balance gives

$$Q_f = Q_3 - Q_2 = \left(Q_3 - Q_r \epsilon_p K_D\right) - \left(Q_2 - Q_r \epsilon_p K_D\right) = (m_3 - m_2) \cdot Q_r \epsilon_p K_D \quad \text{(L-1)}$$

Where the index 2 and 3 refers to the section.

If complete separation is obtained, the feed flow of the strongest bound component, subscript A, must equal the net flow of this component in segment 2. That is

$$Q_f c_{f,A} = -f'_{A,2} = Q_r \epsilon_p K_D q_A - \left(Q_f - Q_r \epsilon_p K_D\right) y_A \quad \text{(L-2)}$$

The sign is due to the net flow is in the in the opposite direction of the liquid flow rate.

Insertion of the feed flow, equation (L-1), and division with $Q_r \epsilon_p K_D$ gives

$$(m_3 - m_2)\, y_{f,A} = q_{A,2} - m_2\, y_{A,2} \quad \text{(L-3)}$$

Correspondingly the flow of component B, the weaker bound, is given by

$$(m_3 - m_2)\, y_{f,B} = m_3\, y_{B,3} - q_{B,3} \quad \text{(L-4)}$$

Compared to the article by Migliorini *et. al.* (2000b) m_3 is in the following replaced by

$$m_3 = (1+\alpha)\, m_2 \qquad \alpha > 0 \quad \text{(L-5)}$$

This changes the constraint from the linear constraint $m_3 > m_2$ to the simple constraint $\alpha > 0$. The feed flow is then proportional to α and using m_2 as a variable is equivalent to a line search along the line given by equation (L-5).

First the point w is calculated, this is the end point of the line b→w. m_2 is given by eq. (L-10). Additionally at the point w the requirement is that the net flux of A in section 3 is 0. From equation (11-4) this gives

$$f_{A,3} = m_3 - A_{A,3} = 0 \quad \text{(L-6)}$$

$y_{A,2}$ and $y_{B,3}$ are used as variables. $m_{2,min}$ and $m_{3,min}$ can be calculated from $y_{A,2}$ using equation (L-10) and (L-11). From this α can be calculated.

A material balance for component A in the mixing point to column 3 gives

$$y_A^{in} = \frac{Q_2\, y_{A,2} + Q_f\, y_{A,f}}{Q_2 + Q_f} = \frac{(m_2+1)\, y_{A,2} + \alpha\, m_2\, y_{A,f}}{(1+\alpha)\, m_2 + 1} \quad \text{(L-7)}$$

The salt concentration inlet column 3 is calculated similarly to y_A^{in}

If the protein concentration from the mixing point, y_A^{in} is large enough to create a chock wave into section three where $y_B = y_{B,3}$, breakthrough of component A will occur.

With the guessed concentration of component B in column 3, $A_{B,3}$ and the residual can be

calculated

$$R_1=(1+\alpha)\,m_2-A_{A,3}=(1+\alpha)\,m_2-\frac{q(y_s^{in},y_A^{in},y_{B,3})}{y_A^{\beta}} \tag{L-8}$$

The concentration of component B in section 3 must fulfil the mass balance requirement

$$R_2=m_2\alpha\,y_{B,f}-m_2(1+\alpha)\,y_{B,3}+q_{B,3} \tag{L-9}$$

By this procedure it is easy to ensure that y_A and y_B corresponds to the same α and m_2. Once the point w is calculated the line b→w is calculated in the same way as suggested by Migliorini *et al* (2000b) that is fulfilling the mass balance for section two where $m_2=m_{2,min}$ given by equation (11-11), and use y_A as the running parameter. Giving the line

$$m_{2,min}=\left(\frac{\partial q_B}{\partial c_B}\right)_{y_A} \tag{L-10}$$

$$m_{3,min}=\frac{1}{y_{f,A}}\left[\left(\frac{\partial q_B}{\partial c_B}\right)_{y_A}\left(y_{f,A}-y_A\right)+q_A\right] \tag{L-11}$$

From the point w the upper boundary of α, α_{max} can be calculated. From the previous calculation of w the composition $y_{A,2}$, $y_{B,3}$ and m_2 is known. Gradually reducing α from α_{max} to 0 the line w→r can be calculated. The three residuals are defined from the flux equations of component A in section 2 and B in 3 and finally from equation (L-8). The variables are $y_{A,2}$, $y_{B,3}$ and m_2.

$$R_1=\alpha\,m_2\,y_{A,f}+m_2\,y_{A,2}-q_{A,2} \tag{L-12}$$

$$R_2=m_2\alpha\,y_{B,f}-m_2(1+\alpha)\,y_{B,3}+q_{B,3} \tag{L-13}$$

This is a simple system with three simple ordinary algebraic equations in three unknowns, which is considerably easier to solve than the system of equations suggested by Migliorini. Having solved this system $y_{A,2}$ is now known, this can be used to calculate the the location on the line defined by $m_{2,max}$.

$$m_{2,A}=\left(\frac{\partial q_A}{\partial y_A}\right)_{y_{A,2}} \tag{L-14}$$

$$m_{3,A}=m_2+\frac{1}{y_{A,2}}\left(q_{A,2}-\frac{\partial q}{\partial y}\,y_{A,2}\right) \tag{L-15}$$

With the calculated values of $m_{2,A}$ and $m_{3,A}$ from the line w→r and r→a, the squared distance between these two points can be calculated

$$err=(m_2-m_{2,A})^2+(m_3-m_{3,A})^2 \tag{L-16}$$

where $m_{2,A}$ and $m_{3,A}$ indicates the line is calculated from the r→a line, equation (L-14) and (L-15).

The two lines w→r and r→a intersect at r. Monitoring the error, the minimum error corresponds to the point r, and from this point m_2 and m_3 can be calculated from equations with $y_{A,2}$ as the running parameter

$$m_2=\left(\frac{\partial q}{\partial y}\right)_{y_{A,2}} \tag{L-17}$$

and from eq. (L-3) and (L-17)

$$m_3=m_2+\left(q_{A,2}-\left(\frac{\partial q}{\partial y}\right)_{y_{A,2}} y_{A,2}\right)\frac{1}{y_{f,2}} \tag{L-18}$$

Appendix M: Measured Dead Volumes in the SMB Plant

The dead volumes for the SMB-plant have been measured by pulse experiments. A number of set-ups have been used to determine the dead volumes in the plant. The dead volumes in the table below have been used for the calculations.

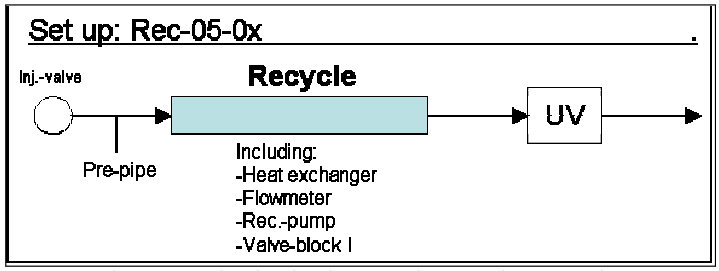

Set-up to determine the dead volume in the recycle stream between column 8 and column 1.

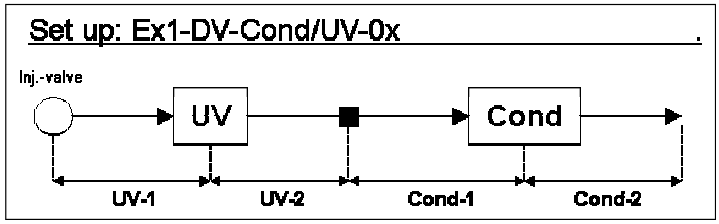

Set-up to determine the dead volume of detectors.

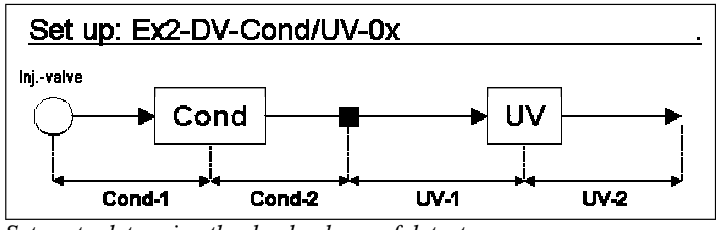

Set-up to determine the dead volume of detectors.

File	***Q*** [ml/min]	t_r [s]	***DV*** [ml]
Pre-pipe			0.124
Rec-5-02	5	276.5	22.921
Rec-5-03	5	276.1	22.884
Rec-5-04	2	699.1	23.181
Rec-5-05	2	691.5	22.927
		Average	22.978
UV-1 + UV-2 + Cond-1			
Ex1-DV-Con-01	0.265	62.54	0.276
Ex1-DV-Con-02	0.265	57.84	0.255
Ex1-DV-Con-03	0.5	31.81	0.265
Ex1-DV-Con-04	0.5	31.55	0.263
		Average	
UV-1			
Ex1-DV-UV-01	0.265	29.03	0.128
Ex1-DV-UV-02	0.265	23.11	0.102
Ex1-DV-UV-03	0.5	12.77	0.106
Ex1-DV-UV-04	0.5	12.81	0.107
		Average	0.111
Cond-1			
Ex2-DV-Con-01	0.265	35.38	0.156
Ex2-DV-Con-02	0.265	34.77	0.154
Ex2-DV-Con-03	0.5	20.53	0.171
Ex2-DV-Con-04	0.5	22.20	0.185
		Average	0.166
Cond-1 + Cond-2 + UV-1			
Ex2-DV-UV-01	0.265	63.96	0.283
Ex2-DV-UV-02	0.265	62.64	0.277
Ex2-DV-UV-03	0.5	35.86	0.299
Ex2-DV-UV-04	0.5	36.56	0.305
		Average	0.291

Table M.1 Measured dead volumes in the SMB-plant for the recycle stream from column 8 to column 1 and the dead volumes for the detectors.

Appendix N: Measured Column Dead Volumes

The following dead volumes have been measured for the HPCL and the columns by pulse experiments. From this it is concluded that the dead volume of the column is 0.56 ml (=1.455-0.893 ml).

Filename	***Database no.*** [YYYYMMDDhhmm]	***Q*** [ml/min]	t_r [min]	V_r [ml]
HPLC DV, I				
SMB-COL-DV-1a	200304291335	0.5	1.786	0.893
SMB-COL-DV-1b	200304291343	0.5	1.787	0.894
SMB-COL-DV-1c	200304291350	0.5	1.786	0.893
			Average	0.893
HPLC+col. DV, I				
SMB-COL-DV-2a	200304291406	0.5	2.911	1.456
SMB-COL-DV-2b	200304291414	0.5	2.909	1.455
SMB-COL-DV-2c	200304291421	0.5	2.911	1.456
			Average	1.455
HPLC DV, II				
DV_05a	200305151144	0.5	1.819	0.910
DV_1a	200305151208	1	0.953	0.953
DV_2a	200305151221	2	0.514	1.028
DV_05b	200305151331	0.5	1.800	0.900
DV_1b	200305151343	1	0.953	0.953
DV_2b	200305151350	2	0.514	1.028
			Average	0.962

Table 14.1 The HPLC got new piping May15th and the experiments "HPLC DV, I" is the dead volumes of the HPLC before this date and "HPLC DV,II" is the measured dead volumes after this date.

Appendix O: Comments to SMB Plant Lay-Out

In the current lay-out of the SMB-plant the recycling pump is located downstream column 8, figure O.1. With a location between column 8 and column 1 the recycling pump must always match the flow through column 8. When column 8 changes position from VIII to VII and further downwards to position VI, V,...,I in each cycle, the set point (SP) to the pump changes every time the pump moves into a new section. The SP-change have an immediate effect on the pump flow. This flow change affects the PIC located upstream the pump and controlling the extract pump. It was observed that this PIC-regulation had problems with these sudden flow changes and a period with high fluctuations after a SP change at the PI was observed. Even vacuum (if the PI gives correct results at low pressures) was observed for a short period, which is critical for operating the plant.

When a product stream is withdrawn downstream column 7, the pressure difference to the surroundings is the lowest possible since product is withdrawn only one column upstream the recycle pump. At the next column shift the same product stream is withdrawn downstream column 8, meaning downstream the recycle pump. The pressure drop to the surroundings is now much higher almost Δp_{SMB} higher, where Δp_{SMB} is the total pressure drop in the plant. Using a control valve for product redraw, this would be disturbed by this significant and sudden pressure change. This might be the reason for the current lay-out with product redraw using reciprocating pumps. Using reciprocating pumps also requires back-pressure values downstream the product withdrawal pumps to avoid the product from running directly through the pumps. The set-point of these back-pressure values must be higher than the highest possible pressure upstream the product pump, approximately Δp_{SMB}.

The current design of the SMB-plant has a large dead volume downstream column 8, and a compensation for this dead volume can be made. However, the compensation will not be able to operate the plant with the desired m-values in the different sections, see chapter 11.7 “Dead Volumes Impact on the Operating Point“ p. 129. This dead volume does to a large extent not come from the detectors, see “Measured Dead Volumes“. Additionally the stream composition outlet column 8 is time dependent, figure 11.19, and the dead volume will remix the components desired to separated.

With the current design five pumps are required in total, all pumping liquid (a non-compressible fluid) into a constant volume. Naturally, this gives large pressure fluctuations in the plant which was also observed. The plant was not equipped with any pulsation dampers,

and these would also act as added dead volume and possibly also as a mixer.
The current design with the recycle pump outlet column 8 has got a number of draw-backs, and a better plant lay-out is desirable.
In figure O.2 an alternative lay-out of the SMB-plant is shown. In this lay-out the recycling pump is removed from column 8 outlet and replaced in a separate recycle stream. This requires one or two extra valves for each column.
However, the dead volume downstream column 8 is significantly reduced, since only detectors and sample loop is now located here. Locating the recycle stream in an separate stream, the composition is (almost) time independent, and remixing of the two components to be separated is avoided (since none of these are present in the recycle stream), a pulsation damper can be used to reduce the strong pressure changes from the pump (Pulsation dampers can also be used for the feed pumps, also for the original lay-out), since the composition of these streams are time independent.
The upstream pressure for the product streams with this lay-out are much more constant and the product pumps could be replaced by control valves.
Possibly the recycle stream could be recycled to a position upstream the eluent pump, figure O.3.

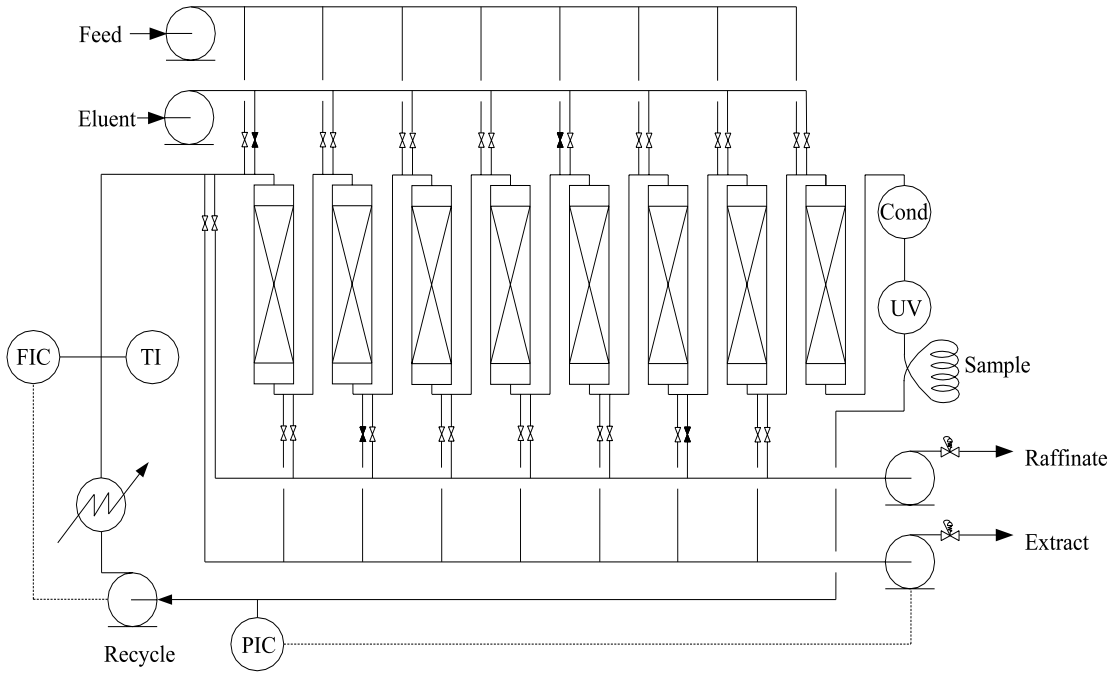

Figure O.1 Flow sheet of SMB plant in Dortmund. The black valves indicates an open valve. In this situation eluent is fed to column one and flows through column one and two. A part of the stream is split outlet column two and goes to the extract pump, and the remaining part flows through column three and four. At the inlet of column five the stream is mixed with the protein containing feed stream and flows through column five and six. At the outlet of column six the stream is split and a part of it goes through the raffinate stream. The remaining part flows through column seven and eight. From column eight the stream goes through the conductivity measurement and the UV-detector. A sample can be taken out for analysis in the sample loop before the it is pumped through the recycle pump. A heat exchanger (not used) can cool down the stream before it is returned to column one together with eluent from the eluent pump.

The recycle flow is controlled by a FIC and the pressure on the inlet side of the recycle pump is controlled by FIC controlling the extract stream flow.

Since the pressure in the plant is higher than the ambient pressure back-pressure valves are needed at the outlet of the extract and raffinate pumps.

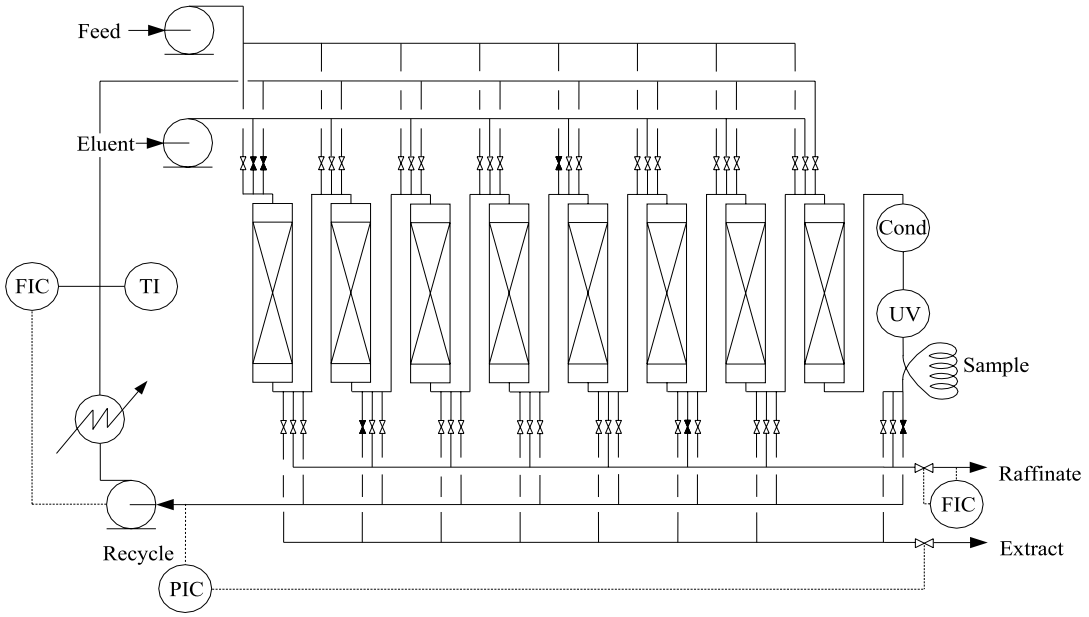

Figure O.2 Alternative lay-out of SMB-plant. The recycle stream has now been removed from the outlet position of column 8 and inserted into its own recycle line. This will dramatically reduce the dead volume downstream column 8 and fluctuations in the flow. The fluctuations in the raffinate and extract stream will be significantly reduced.

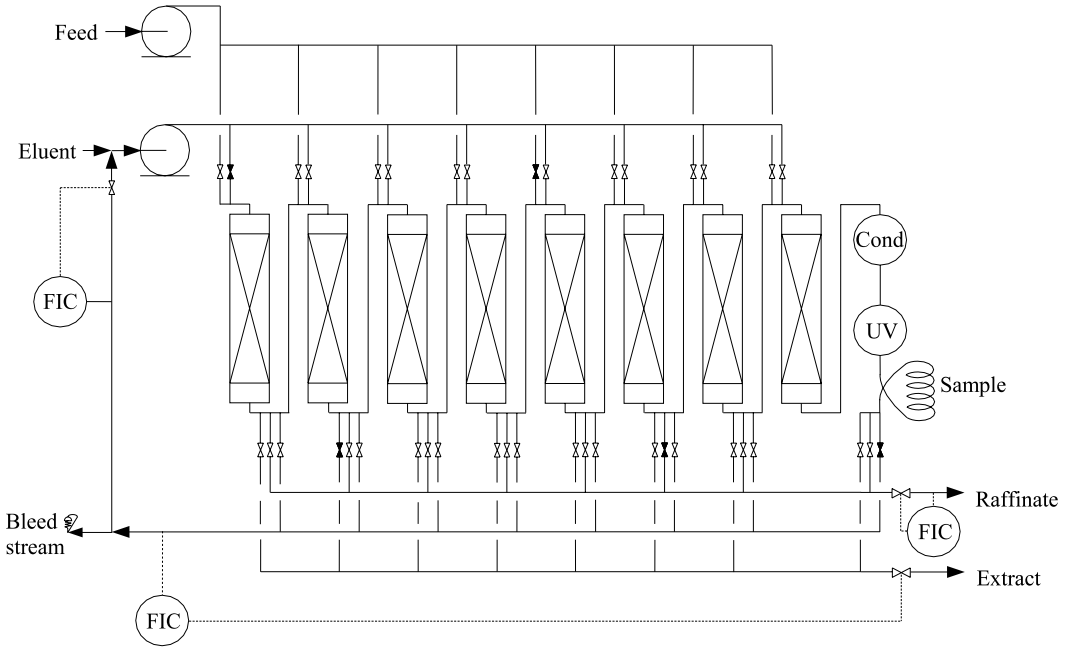

Figure O.3 Alternative lay-out of SMB-plant. The recycle stream is recycled to upstream the eluent pump and a small bleed stream is perhaps required for control. Alternatively one of the product streams can be controlled.